

**EGRU** 

## **Sn-W-Critical Metals & Associated Magmatic Systems**

**An International Geological Conference**

**24<sup>th</sup> - 28<sup>th</sup> June 2019**  
**Tinaroo Lake Resort**  
**Atherton Tablelands**  
**Queensland, Australia**

### **EXTENDED ABSTRACTS**

Edited by:  
Kaylene Camuti, Jan Marten Huizenga, Carl Spandler, Yanbo Cheng



# **Sn-W-Critical Metals & Associated Magmatic Systems**

An International Geological Conference

## **EXTENDED ABSTRACTS**

Edited by:

Kaylene Camuti, Jan Marten Huizenga, Carl Spandler, Yanbo Cheng

Hosted by:

Economic Geology Research Centre (EGRU)

James Cook University

Townsville, Queensland



## **EGRU Contribution 70**

24 - 28 June 2019

Atherton Tablelands, Queensland

Australia

James Cook University

## **Sn-W-Critical Metals & Associated Magmatic Systems Conference**

Atherton Tablelands, Queensland, Australia  
24 - 28 June 2019

### **Conference Organising Committee**

Judy Botting  
Kaylene Camuti  
Yanbo Cheng  
Jan Marten Huizenga  
Carl Spandler

### **Conference Editorial Committee**

Kaylene Camuti  
Jan Marten Huizenga  
Carl Spandler

### **Abstract Volume**

Kaylene Camuti

### **Published by:**

Economic Geology Research Centre (EGRU)  
James Cook University  
Townsville, QLD 4811  
Australia

### **Enquiries**

[egru@jcu.edu.au](mailto:egru@jcu.edu.au)

ISSN 0816 780 X

ISBN 978-0-6485037-3-6

© James Cook University

Front cover designed by Kaylene Camuti.  
Images courtesy of Tourism and Events Queensland.

# Introduction

Our world will be a different place by 2040. Electric vehicles will dominate the roads, and clean renewable sources will provide most of our energy needs. The internal combustion engine will be headed for the history books to join the computer floppy disc and the Walkman. Smart technology will be intertwined with all aspects of our lives. Enabling this technological revolution will require steady supplies of specialty metals including tin, tungsten, indium and the rare earth elements. The rare earth elements, indium and tungsten have respectively been ranked first, second and third of the most critical commodities (Skirrow et al., 2013), and according to a study by MIT, tin comes out as the metal to be most impacted by new technology.

Supplying Sn, W and other critical metals into the future is contingent on new ore deposit discoveries, which in turn relies on improved understanding of how and where these elements are concentrated to ore grades in the Earth's upper crust. With this in mind, the Economic Geology Research Centre (EGRU) at James Cook University presents "Sn-W-Critical Metals & Associated Magmatic Systems", a 4-day conference held in late June 2019 on the shores of Lake Tinaroo on the Atherton Tablelands of north Queensland. The conference brings together leading researchers from across the globe - from academia, government, and industry - to present and discuss advances and breakthroughs in understanding the setting, genesis and characteristics of Sn-W-critical-metal mineralisation, and related magmatic systems.

Carl Spandler

Associate Professor, EGRU Director

James Cook University



The presentations cover broad aspects of ore geology, including the evolution and fertility of magmatic rocks, the chemistry and hydrothermal solubility of ore minerals, ore genesis processes, advanced exploration techniques, and case studies of ore deposits from across the globe. We are especially proud to include a session in honour of former EGRU Director and author of the *Geology of Tin Deposits*, Dr Roger Taylor, in recognition of his contribution to the understanding of Sn magmatic systems in Australia, and globally.

The conference venue lies within a world-renowned Sn-W mining district. Complementing the oral program will be field trips to the historic Herberton Sn mining district and the Mount Carbine vein-style W deposit. These visits have been made possible thanks to the support of Speciality Metals International Ltd. and the Herberton Mining Museum.

On behalf of the organising committee, I welcome you to tropical north Queensland. We hope the scientific sessions, field trips and social atmosphere of the conference will not only provide the environment for building new collaborations and connections, but will also provide new knowledge and inspiration for researchers and explorers working on these critical commodities.

Reference: Skirrow, R.G., Huston, D.L., Mernagh, T.P., Thorne, J.P., Dulfer, H., & Senior, A.B. 2013. Critical commodities for a high-tech world: Australia's potential to supply global demand. Geoscience Australia, Canberra

The conference committee wishes to thank the following for their generous support of the conference and the associated field trips.

## Mount Carbine Tungsten Mine Field Trip



## Herberton Mining Museum Trip



Herberton Branch



# Contents

<b>The chemical variability of cassiterite microstructures</b>	1
Jason M. Bennett, Anthony I. S. Kemp, Steffen Hagemann, Marco Fiorentini, Malcolm P. Roberts	
<b>The character, setting and genesis of magmas associated with Sn-W critical metal mineralisation in eastern Australia</b>	5
Phillip L. Blevin	
<b>The magmatic evolution and rare metal potential of the Peak Range Volcanics, central Qld</b>	8
Ross Chandler, Carl Spandler	
<b>New Sn &amp; W ore exploration toolkit: chemistry of zircon, cassiterite and volcanic rocks</b>	11
Yanbo Cheng, Carl Spandler, Zhaoshan Chang	
<b>Element partitioning in the formation of a microgranite sill with associated Mo (+/- W) deposits in the Herberton District, north-east Queensland, Australia</b>	14
Gavin W. Clarke	
<b>Effects of exsolving fluids on the mineralogy and geochemistry of the Cattle Camp Granite, Herberton Tinfield, north-east Queensland, Australia: a cautionary tale</b>	19
Gavin W. Clarke	
<b>Magmatic-hydrothermal features in Paleozoic Sn-W- base metal-mineralized and barren granites of Tasmania</b>	23
David R. Cooke, Wei Hong, Lejun Zhang, Colin Jones, Evan Orovan	
<b>The trace element geochemistry of cassiterite in Tasmanian tin deposits</b>	27
Joshua Denholm, Aleksandr Stepanov, Ralph Bottrill	
<b>The Cantung Tungsten Mine, Northwest Territories, Canada: an overview of the mine geology and summary of ongoing research projects</b>	29
H. Falck, H. E. Jamieson, B. Kazamel, E. Salmabadi, K. Hickey, J. Hanley, E. Adlakha, A. Roy-Garand, C. Lentz, V. Elongo, H. Legros, P. Lecumberri-Sanchez, K.L. Shelton	
<b>The Mactung Tungsten Deposit, Northwest Territories, Canada: an overview of the geology and summary of ongoing research projects</b>	33
H. Falck, E. Martel, B. Fischer, A.L. Gebru, D.R. Lentz, E. Adlakha, J. Hanley, A. Roy-Garand, V. Elongo, H. Legros, P. Lecumberri-Sanchez, G. Kirkham	
<b>Status and exploration deployment recommendations of tin resources in China</b>	38
Fanying Gong, Guogang Xie, Yongsheng Li, Hairui Sun, Tingjie Yan, Zezhong Du	
<b>Evidence of a crustal source, independent of primary melt generation, for pluton-related W-Sn mineralization in the Dongpo orefield, Hunan Province, South China</b>	41
Chunli Guo, Robert A. Henderson	

# Contents

<b>Unidirectional solidification textures from the Sn-mineralised Heemskirk Granite, western Tasmania: characteristics, mineral chemistry and O-isotopes</b>	42
Wei Hong, David R. Cooke, Lejun Zhang, Nathan Fox, Jay Thompson	
<b>A regional appraisal of Queensland's critical elements resources</b>	44
Laurie Hutton	
<b>Geological characteristic and ore genesis of typical rare metal deposits in China</b>	48
Shao-Yong Jiang, Tao Liu, Hui-Min Su, Kui-Dong Zhao, Wei Chen	
<b>The magmatic hydrothermal transition at Bluestone Bay, Tasmania</b>	51
Colin L. Jones, Evan A. Orovan, David R. Cooke, Michael Roach	
<b>Towards an integrated model for magmatic and hydrothermal tin systems: examples from Africa</b>	54
Judith A. Kinnaird, Paul A.M. Nex	
<b>CO<sub>2</sub> escaping leads to wolframite precipitation</b>	57
Xiangchong Liu, Dehui Zhang	
<b>Temperature control on tin mineralisation in Gejiu East Tin Field, China and its implications for mineral exploration</b>	60
Jack Ma	
<b>Geology and metallogeny of tungsten and tin deposits in China</b>	64
Jingwen Mao, Hegen Ouyang, Shiwei Song, Shunda Yuan, Zhenhua Zhou, Wei Zheng, Huan Li, Peng Liu, Yanbo Cheng, Maohong Chen	
<b>Tin isotope fractionation in ores and rocks: genetic and exploration implications</b>	65
Ryan Mathur, Wayne Powell	
<b>Tungsten transport in ore-forming fluids: insights from <i>ab initio</i> molecular dynamics simulations</b>	68
Yuan Mei, Weihua Liu, Xin-Song Wang, A.E. Williams-Jones	
<b>North Queensland tectonics &amp; the tin-gold connection</b>	70
John E. Nethery	
<b>Composition, source, and petrogenesis of the Mole Granite, New England Batholith, NSW</b>	74
Marc Norman	
<b>Tin-indium-silver-base metal polymetallic epithermal bonanza lodes from the Dover Castle district, Herberton tin-fields, NE Queensland</b>	77
Nicholas H. S. Oliver, Matthew Haindl, Shane Mardon, Paul Dirks, Yanbo Cheng, Craig Nettlebeck, Carl Spandler	

# Contents

<b>The Watershed tungsten deposit, NE Queensland, Australia: An example of a Permian metamorphic tungsten upgrade after a Carboniferous magmatic-hydrothermal mineralisation event</b>	82
Jaime Poblete, Paul Dirks, Jan-Marten Huizenga, Zhaoshan Chang	
<b>Magmatic and hydrothermal evolution of the Yichun Ta-Sn-Li deposit, south China</b>	85
Peter J. Pollard	
<b>Influence of protolith chemistry on the regional distribution of Phanerozoic magmatic tin deposits</b>	86
Rolf L. Romer, Uwe Kroner	
<b>Exogenic control on the distribution of endogenic Sn-W-Ta, Au, and U mineralization in the Appalachians and the Variscides</b>	89
Rolf L. Romer, Uwe Kroner	
<b>Geology and ore genesis of the Yangibana LREE district, Western Australia</b>	92
Paul Slezak, Carl Spandler, Andy Border, Kieren Whittock	
<b>Geology and tectonic setting of the Toongi rare metal deposit, central NSW</b>	96
Carl Spandler, Caitlin Morris	
<b>The Tellerhäuser tin-zinc-indium deposit – new geological insights unlocking value</b>	100
Antony Truelove	
<b>Magmatic and hydrothermal evolution of the tin-mineralisation at the Groenfontein Tin Mine in the Lebowa Granite Suite, South Africa</b>	104
L.C. Vonopartis, P.A. Nex, J.A. Kinnaird, L.J. Robb	
<b>Intensive Mesozoic Li-Be-Nb-Ta mineralization in the Kelumute-Jideke pegmatite field, Chinese Altai</b>	109
Chun-Long Wang, Shao-Yong Jiang, Ke-Zhang Qin	
<b>Geological features of the Jiaoxi tungsten deposit in the western Bangong-Nujiang metallogenic belt, Tibet, China</b>	113
Yong Wang, Juxing Tang, Liqiang Wang, Jan Marten Huizenga	
<b>Redox controls on granite related hydrothermal ore deposits</b>	116
Jo Ward, John Mavrogenes, Nick Tailby	
<b>Structural controls and geochronology constraints on the metallogenesis of the Lame Zn-Cu-Sn polymetallic skarn deposit, Guangxi Province, China</b>	118
Changhao Xiao	



# The chemical variability of cassiterite microstructures

Jason M. Bennett<sup>1,2</sup>, Anthony I. S. Kemp<sup>1</sup>, Steffen Hagemann<sup>1</sup>, Marco Fiorentini<sup>1,2</sup>, Malcolm P. Roberts<sup>3</sup>

<sup>1</sup>Centre for Exploration Targeting, School of Earth Sciences, UWA

<sup>2</sup>Australian Research Council Centre of Excellence for Core to Crust Fluid Systems (CCFS), Department of Earth and Planetary Sciences, Macquarie University, Sydney, Australia

<sup>3</sup>Centre for Microscopy, Characterisation and Analysis, UWA

## Abstract

Cassiterite is known to show complex microstructures under cathodoluminescent (CL) illumination. Here we present a summary of the results of a panchromatic CL, hyperspectral CL and quantitative X-ray element map study of these microstructures in cassiterite. We also present observations from Electron Probe Microanalysis (EPMA) and LA-ICP-MS trace element datasets that allow for further detailed analysis of these microstructures.

We show that sector zoning imparts a significant control on W and Fe uptake and distribution within cassiterite crystals, and that panchromatic CL imaging alone does not fully reveal the internal structure of cassiterite grains that have high Fe, Ta, Nb or W. We also show that the currently accepted coupled substitution mechanisms for W, Nb and Ta into the cassiterite lattice cannot account for the high contents observed in some samples, and that different sectors within the same crystal show different preferred substitutional stoichiometries. Furthermore, we discuss unusual Nb/Ta and Zr/Hf ratios, which imply the existence of fractionation processes during hydrothermal-metasomatic Sn mineralisation that can drive the Nb/Ta ratio to large values in excess of chondritic values (Nb/Ta >> 100).

## Introduction

The association of cassiterite (SnO<sub>2</sub>) with mineral systems enriched in 'critical' metals (such as W, Nb, Ta, Li and In; Chakhmouradian et al. 2015) for 21<sup>st</sup> century technology makes this mineral a prime target for research into its development as a multi-process recorder of mineralising systems. The keystone of the cassiterite 'multi-tool' is the application of the U-Pb isotopic system for geochronometry, allowing a direct constraint on the age of Sn-bearing mineralised systems.

Since the initial attempts at cassiterite U-Pb geochronology (Gulson and Jones, 1992) via Isotope-Dilution Thermal Ionisation Mass Spectrometry (ID-TIMS), the development of in-situ analytical approaches such as Secondary Ion Mass Spectrometry (SIMS) and Laser Ablation Inductively Coupled Plasma Mass Spectrometry (LA-ICP-MS) has led to a flurry of recent cassiterite geochronological studies (Liu et al., 2007; Yuan et al., 2011; Zhang et al., 2013, 2015, 2017; Li et al., 2016; Carr et al., 2017; Neymark et al., 2018; Cheng et al., 2019).

The power of in-situ analytical methods over bulk mineral techniques is their ability to target distinct growth histories within single grains. These separate growth stages are usually identified via cathodoluminescent (CL) imaging. However, cassiterite is well known to show complex CL microstructures and the chemical nature of these structures, and models for how they physically arise, are poorly constrained (Hall and Ribbe, 1971; Farmer 1991; Wille et al., 2018).

## The chemical basis of CL microstructures in cassiterite

The chemical basis for the CL response in cassiterite has been generally tied to a yellow 520-565 nm Ti activated emission and a blue 420-465 nm W activated emission (Hall and Ribbe, 1971; Farmer, 1991). While intrinsic luminescence may play a role in the CL response of natural cassiterite crystals and cannot be discounted, the strong correlation between chemistry and CL signature observed (Hall and Ribbe, 1971; Farmer et al., 1991) suggests that the microstructures observed via CL imaging techniques are dominantly due to the distribution and incorporation of minor components of Ti, Fe, Nb, Ta and W into the cassiterite lattice.

In our study, we compared panchromatic CL images (Figure 1) and hyperspectral CL maps with quantitative X-ray element maps (Figure 2) and found that the CL response in cassiterite is due to a complex interplay of Ti, Fe, Nb, Ta and W. Titanium does indeed activate a CL emission in cassiterite, but only up to a threshold of 0.4 at.% before concentration quenching occurs. The presence of Fe, Nb, Ta or W also quench the CL response. The blue W activated emission of Hall and Ribbe (1971) appears to only exist at sufficiently low W contents (<0.1 at.%), which also occur with moderate Ti contents (~0.2 at.%), implying that the presence of W itself does not result in CL activation but instead modifies the Ti emission.

Three distinct styles of CL microstructures are generally noted; variably coarse to fine scale oscillatory zoning, CL-dark sector zonation, and CL-bright features that cross-cut the oscillatory and sector zoning (Hall and Ribbe, 1971; Farmer, 1991; Carr et al., 2017; Wille et al., 2018). We found that the oscillatory zonation is mostly due to fine-scale oscillations in Fe and Ti, with minor contributions from W, Nb and Ta.

We also report two distinct CL-dark sectors; zones enriched in Fe (Figure 1a, and with low contents of

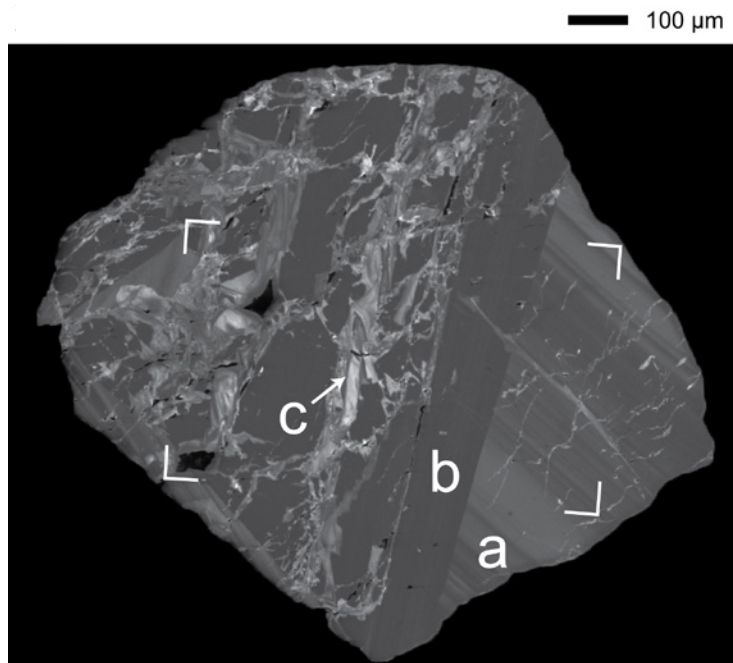


Figure 1: Panchromatic CL image of a cassiterite crystal from Saltwater Creek, Tasmania, showing three main types of CL microstructures. a) Oscillatory zonation. b) CL-dark sector zonation. c) CL-bright cross-cutting features. White corners refer to region in X-ray element map in Figure 2.

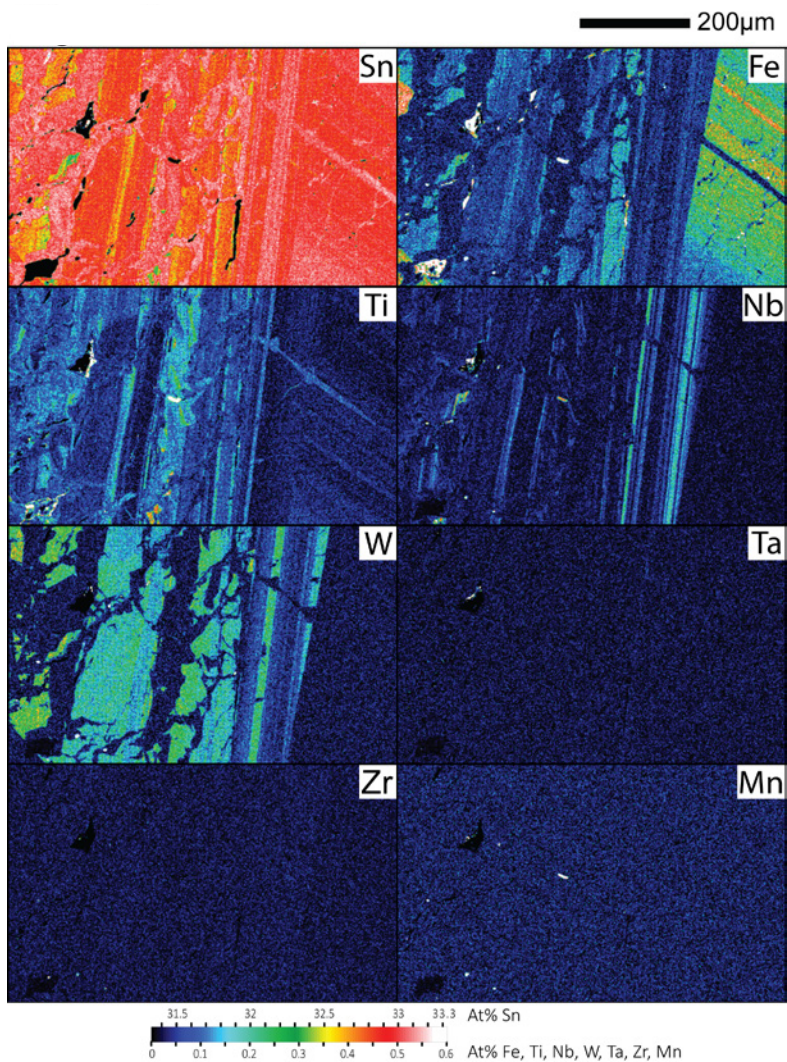


Figure 2: X-ray element maps for a cassiterite crystal from Saltwater Creek, Tasmania. Refer to Figure 1 for location within the crystal. The Fe and W maps highlight the strong sector zoning effect.

W, Figure 2) and zones enriched in W (Figure 1b, and with low contents of Fe, Figure 2). These two CL-dark sector zones are in many cases indistinguishable in panchromatic SEM-CL imaging, but hyperspectral CL may be able to distinguish these zones via subtle differences in their emission spectra (i.e., their colour).

The CL-bright cross-cutting features (Figure 1c) are rather uniform in their composition, despite the variable chemistry of their host cassiterite crystals. Titanium contents are usually around 0.2 at.%, with Fe, Nb, Ta and W contents below 0.1 at.%. These microstructures appear to represent late-stage annealing/fracture healing processes, with chemical re-equilibration. In some samples, small inclusions of iron oxides are present which may represent a local sink for the Fe, Nb, Ta and W cations ejected from the re-equilibrated lattice.

### The coupled stoichiometry of Fe, W, Nb and Ta substitutions

The Fe-enriched sector zones may be explained by a coupled  $\text{Fe}^{3+}+\text{OH}^-$  substitution mechanism previously described by Möller et al. (1988), along a limited solid solution series with the poorly described 'varlamoffite' species with the formula  $\text{Sn}_{1-x}\text{Fe}_x\text{O}_{2-x}(\text{OH})_x$  (Sharko, 1971; Jambor et al., 1995). The W-enriched sectors however remain unexplained by existing models for coupled W-Fe substitution mechanisms (Möller et al., 1988). The W-rich sectors of some cassiterite crystals require a component of either coupled  $\text{W}^{6+}+\text{W}^{4+}+\text{Fe}^{2+}$  or  $2\text{W}^{5+}+\text{Fe}^{2+}$  to maintain charge, or a component of direct  $\text{W}^{4+}$  substitution (Figure 3). A similar behaviour is exhibited in some Nb-rich samples, with stoichiometries only explainable by some component of  $\text{Nb}^{4+}$  alongside the well reported  $2\text{Nb}^{5+}+\text{Fe}^{2+}$  substitution mechanism (Möller et al., 1988). In addition, the sector zones of a cassiterite crystal from Blue Tier, Tasmania, show two different stoichiometries depending on the growth face present during incorporation (Figure 4).

### Nb/Ta and Zr/Hf ratios as a record of mineral system processes

The bulk rock Zr/Hf and Nb/Ta ratio of Sn-mineralised granites are well recognised to exhibit low values highly fractionated from typical crustal rocks (Ballouard et al., 2016). While the exact processes that cause this fractionation are debated (Stepanov et al., 2016), cassiterite might be expected to have Zr/Hf and Nb/Ta ratios similar to the bulk rock values of the host granite, and in many greisen-hosted cassiterite crystals this is indeed the case. However, distinct regions within some crystals exhibit ratios that appear to return to near chondritic values for Nb/Ta (~30), and some samples show ratios well beyond the chondritic ratio (Figure 5). A similar trend is seen in the Zr/Hf ratio, though no analyses exceed the chondritic ratio.

Cassiterite crystals from pegmatitic systems show an overall trend towards further highly fractionated low

values, but some analyses within each crystal define a trend in Nb/Ta ratios towards higher values. These higher Nb/Ta analyses correlate well with the CL-bright cross-cutting features.

### Conclusions

The complex microstructures usually observed in cassiterite under CL illumination provide a detailed record of various processes operating in the mineralising system during cassiterite precipitation and growth. Further detailed research into the chemical and isotopic properties of these microstructures will allow for detailed mineralisation models for any primary cassiterite bearing mineral assemblage. This will in turn further refine our understanding of Sn mineral systems, and processes that lead to enrichment in metals 'critical' for 21<sup>st</sup> century technology.

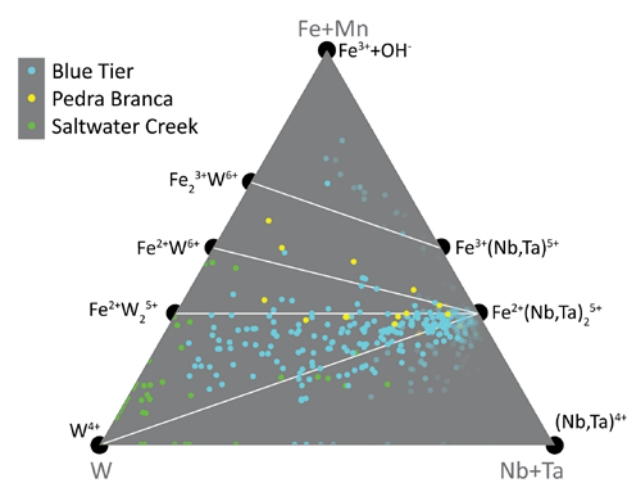


Figure 3: W-(Fe,Mn)-(Nb,Ta) coupled substitution ternary plot for three W-rich cassiterite crystals from Blue Tier and Saltwater Creek, Tasmania, and Pedra Branca, Brazil. The large number of analyses in the lower half of the figure imply the existence of  $\text{W}^{4+}$  substitution into the cassiterite lattice.

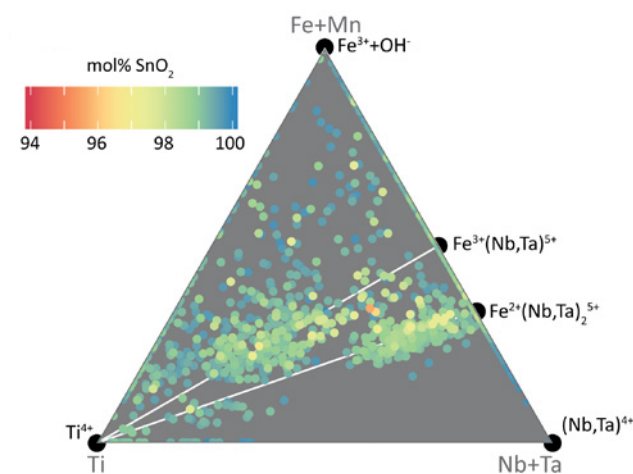


Figure 4: Ti-(Fe,Mn)-(Nb,Ta) coupled substitution ternary plot for a cassiterite crystal from Blue Tier, Tasmania. Points are coloured according to the total  $\text{SnO}_2$  content of the crystal (i.e. purity). The two populations are analyses from distinct sector zones within the crystal, which suggests different Fe-(Nb,Ta) substitution mechanisms are preferred depending on the orientation of the growth face.

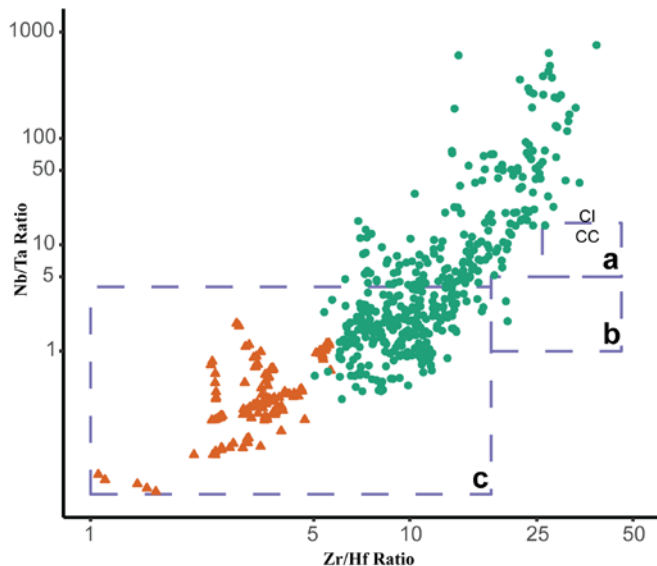


Figure 5: Zr/Hf vs Nb/Ta ratios in cassiterite crystals from pegmatite (orange triangle) and greisen (green circle) mineralised systems. The chondritic ratio (CI) and the ratio for typical continental crust (CC) are annotated. The dashed boxes refer to the typical range of bulk rock values for unmineralised peraluminous granites (a), Sn-W-(U) related mineralised granites (b), and rare metal Ta-Cs-Li-Nb-Be-Sn-W granites (c), as reported from Ballouard et al., 2016. Note the greisen samples define a trend towards Nb/Ta ratios in excess of 100, and exist entirely above the granitic fractionation fields.

## References

- Ballouard C, Poujol M, Boulvais P, et al (2016) Nb-Ta fractionation in peraluminous granites: A marker of the magmatic-hydrothermal transition. *Geology* 44:231–234. doi: 10.1130/G37475.1
- Carr PA, Norman MD, Bennett VC (2017) Assessment of crystallographic orientation effects on secondary ion mass spectrometry (SIMS) analysis of cassiterite. *Chem Geol* 467:122–133. doi: 10.1016/j.chemgeo.2017.08.003
- Chakhmouradian AR, Smith MP, Kynicky J (2015) From “strategic” tungsten to “green” neodymium: A century of critical metals at a glance. *Ore Geol Rev* 64:455–458. doi: 10.1016/j.oregeorev.2014.06.008
- Cheng Y, Spandler C, Kemp A, et al (2019) Controls on cassiterite (SnO<sub>2</sub>) crystallization: Evidence from cathodoluminescence, trace-element chemistry, and geochronology at the Gejiu Tin District. *Am Mineral* 104:118–129. doi: 10.2138/am-2019-6466
- Farmer CB (1991) Cathodoluminescence and Growth of Cassiterite in the Composite Lodes at South Crofty Mine, Cornwall, England. *Mineral Mag* 55:447–458. doi: 10.1180/minmag.1991.055.380.14
- Gulson BL, Jones MT (1992) Cassiterite: Potential for direct dating of mineral deposits and a precise age for the Bushveld

- Complex granites. *Geology* 20:355. doi:10.1130/0091-7613(1992)020<0355:CPFDDO>2.3.CO;2
- Hall MR, Ribbe PH (1971) An Electron Microprobe Study of Luminescence Centers in Cassiterite. *Am Mineral* 56:31–45
- Jambor JL, Pertsev NN, Roberts AC (1995) New Mineral Names - Varlamoffite. *Am Mineral* 80:845–850
- Li C, Zhang R, Ding X, et al (2016) Dating cassiterite using laser ablation ICP-MS. *Ore Geol Rev* 72:313–322. doi: 10.1016/j.oregeorev.2015.07.016
- Liu Y, Li Z, Li H, et al (2007) U-Pb geochronology of cassiterite and zircon from the Dulong Sn-Zn deposit: Evidence for Cretaceous large-scale granitic magmatism and mineralization events in southeastern Yunnan province, China. *Acta Petrol Sin* 23:967–976
- Möller P, Dulski P, Szacki W, et al (1988) Substitution of tin in cassiterite by tantalum, niobium, tungsten, iron and manganese. *Geochim Cosmochim Acta* 52:1497–1503. doi: 10.1016/0016-7037(88)90220-7
- Neymark LA, Holm-Denoma CS, Moscati RJ (2018) In situ LA-ICPMS U-Pb dating of cassiterite without a known-age matrix-matched reference material: Examples from worldwide tin deposits spanning the Proterozoic to the Tertiary. *Chem Geol* 483:410–425. doi: 10.1016/j.chemgeo.2018.03.008
- Sharko ED (1971) Nature and properties of varlamoffite (oxidation products of stannite). *Int Geol Rev* 13:603–614. doi: 10.1080/00206817109475474
- Stepanov AS, Meffre S, Mavrogenes J, Steadman J (2016) Nb-Ta fractionation in peraluminous granites: A marker of the magmatic-hydrothermal transition: COMMENT. *Geology* 44:e394–e394. doi: 10.1130/G38086C.1
- Wille G, Lerouge C, Schmidt U (2018) A multimodal microcharacterisation of trace-element zonation and crystallographic orientation in natural cassiterite by combining cathodoluminescence, EBSD, EPMA and contribution of confocal Raman-in-SEM imaging. *J Microsc* 270:309–317. doi: 10.1111/jmi.12684
- Yuan S, Peng J, Hao S, et al (2011) In situ LA-MC-ICP-MS and ID-TIMS U-Pb geochronology of cassiterite in the giant Furong tin deposit, Hunan Province, South China: New constraints on the timing of tin-polymetallic mineralization. *Ore Geol Rev* 43:235–242. doi: 10.1016/j.oregeorev.2011.08.002
- Zhang R-Q, Lu J-J, Wang R-C, et al (2015) Constraints of in situ zircon and cassiterite U-Pb, molybdenite Re-Os and muscovite <sup>40</sup>Ar-<sup>39</sup>Ar ages on multiple generations of granitic magmatism and related W-Sn mineralization in the Wangxianling area, Nanling Range, South China. *Ore Geol Rev* 65:1021–1042. doi: 10.1016/j.oregeorev.2014.09.021
- Zhang R, Lehmann B, Seltmann R, et al (2017) Cassiterite U-Pb geochronology constrains magmatic-hydrothermal evolution in complex evolved granite systems: The classic Erzgebirge tin province (Saxony and Bohemia). *Geology* 45:1095–1098. doi: 10.1130/G39634.1
- Zhang R, Lu J, Wang R, et al (2013) Contrasting W and Sn mineralization events and related granitoids in Wangxianling-Hehuaping area, Nanling Range, South China. In: *Mineral Deposit Research for a High-Tech World. 12th SGA Biennial Meeting*. pp 1343–1346

# The character, setting and genesis of magmas associated with Sn-W critical metal mineralisation in eastern Australia

Phillip L Blevin

*Geological Survey of New South Wales*

## Introduction

Mineral system models for granite-related Sn deposits (e.g. Blevin, 1998) typically emphasise reduced, peraluminous S-type granites derived from dominantly metasedimentary crustal protoliths as the main progenitors for Sn-W mineralisation. These granite magmas are inferred to have evolved towards the thermal minimum in the haplogranite system principally through extended Rayleigh-style fractional crystallisation processes. This acts to drive up concentrations of ore-forming elements such as Sn, W, Nb and Ta that behave incompatibly in such magmas. Conversely, Cu and Mo are sequestered into crystallising phases either through substitution for Fe and Ti, or sequestered into sulfides whose early precipitation is encouraged by the reduced oxidation states of the bulk magma (Blevin & Chappell, 1992 and references therein).

In contrast to this model, in mainland eastern Australia, in particular the late Permian to early Triassic of the southern New England Orogen (SNEO) of New South Wales and the Carboniferous of far northern Queensland (FNQ), a significant class of Sn (-W, Bi, Mo) deposits are associated with oxidised granite suites that are demonstrably of I-type (metaluminous) ancestry (Blevin et al., 1996). The Renison Bell deposit in Tasmania, Australia's largest Sn deposit and largest known Sn resource, is also associated with an I-type granite (Blevin & Chappell, 1995; Hong et al., 2017). Current known Sn resources at deposits such as Renison Bell, coupled with historical production from eastern mainland Australia, makes eastern Australia unusual in terms of Sn metallogeny in having most of its Sn production sourced from I-type magmas, rather than the typical S-type dominated magmatic relationships of Sn systems globally.

## Characteristics of I-type related Sn systems

I-type Sn systems occur in regions characterised by high-K, relatively felsic granite magmatism and do not represent isolated 'special cases' of magma genesis in their respective provinces. Although strongly reduced amphibole-bearing I-type granites are known to exist, I-type Sn regions typically contain I-type suites that are only weakly reduced to moderately oxidised. Some, as in the SNEO and FNQ, can be strongly oxidised and magnetite-bearing. Halogen abundances in I-type granites are dominated by F over B. Fluorite is common in alteration assemblages and topaz occurs in higher temperature alteration zones and as a magmatic phase in

highly fractionated differentiates. Although beryl (as an indicator of elevated melt concentrations of Be) is often present in the most differentiated phases, Li is typically only modestly elevated.

Regions hosting I-type Sn granites are characterised by the occurrence of polymetallic Sn, Sn-W, W-Mo-(Bi), Mo and granite (intrusion) related Au deposits. Many individual systems and camp- to regional-scale mineral fields are typically polymetally zoned from W in the higher temperature centres through Sn and outwards to more distal and lower temperature Ag, Pb-Zn and As dominated base metal mineralisation styles.

Primary Sn mineralisation typically comprises lode vein, sheeted veins and stockworks in the apical portions of granite cupolas and their overlying rocks. Disseminated greisens may also be present. Breccia-hosted systems are less commonly developed, consistent with the significantly lower B contents of I-type, relative to S-type Sn systems (Pollard et al., 1987). However, the bulk of cassiterite recovered from I-type Sn systems in the SNEO and FNQ has been from alluvial and placer deposits shed from the extensive low-grade vein systems. Many of these were, and remain, too low grade (<0.1% Sn) to be of economic significance as hard rock resources. In the SNEO, these can represent extensive systems (many kilometres in strike length) that have not been explored to the stage of attaining JORC-style resource status. Pegmatites and associated Ta, Nb, Li mineralisation are either absent, or if present, are only very minor. In the SNEO the Mole Granite is associated with late pegmatite systems preserved within a roof pendant that are characterised by the presence of beryl (as an indicator of elevated melt concentrations of Be) and F (as extensive topazisation). Only weak enrichment of Li is present.

## Comparison with S-type related Sn systems

Oxidation-fractionation characteristics of Sn-related I-type granites fall into an intermediate field between strongly reduced S-type and the strongly oxidised I-type magmas that are associated with Cu, Cu-Au and Mo. In that regard they resemble granites elsewhere in eastern Australia that are associated with W skarns and intrusion-related Au. Other characteristics of highly fractionated metaluminous I-type over peraluminous S-type granites is markedly lower P and higher Th and Y-HREE with increasing fractionation in the I-type suites. Tin does not increase in concentration to levels present in highly fractionated S-type magmas, presumably due to partitioning of Sn into Fe-Ti phases

being enhanced by the elevated oxidation states in I-type melts. An exception is the large Mole Granite system in SNEO. Mole Granite zircons have oxygen isotope values of  $\delta^{18}\text{O}_{\text{zirc}} = 8.1 \pm 0.3\text{‰}$ , indicating significant supracrustal involvement above that of most of the other Sn-mineralised I-type granites in SNEO ( $\delta^{18}\text{O}_{\text{zirc}} \approx 7\text{‰}$ ). The Mole Granite is also strongly reduced, like other granites with similar  $\delta^{18}\text{O}_{\text{zirc}}$  values, indicative of metasedimentary contamination or melting of mixed sources, and can be seen as a transitional case between oxidised I-type and reduced S-type magmas.

S-type granites are also typically enriched in B (sourced from the metasedimentary protolith component) which also acts to drive the efficiency and extent of fractional crystallisation processes through boron's ability to enhance the water solubility of silicic melts (Manning and Pichavant, 1985). Abundant tourmaline as a late magmatic and hydrothermal phase in these magmas is an almost ubiquitous feature of these systems. Examples are well represented in eastern Australia (Wagga Tin Belt in NSW including the Ardlethan deposit; the Cooktown region in FNQ including the Collingwood deposit; and in eastern Tasmania including Lottah and Mount Paris).

### Formation of I-type Sn systems

There are a range of scenarios that help understand the polymetallic nature of high-level greisen and vein-hosted I-type systems, and perhaps their size relative to many S-type deposits:

1. Reduced efficiency of Sn concentration mechanisms in moderately reduced, or moderately oxidised magmas.
2. Concentration of a range of ore-forming elements (W, Mo, As, Bi, Au) in addition to Sn into residual melt phases due to lack of opportunity for removal into Fe-Ti oxides and biotite due to the low abundance of these minerals in 'minimum melts'. Ore-forming element ratios in associated mineral systems are dependent on subtle chemical and oxidation variability between magma batches and the timing of volatile exsolution.
3. Absence of significant B contents in I-type magmas. Water and volatiles such as F and Cl have a smaller effect of depolymerising silicate melts that is so effective in allowing fractional crystallisation processes to extend to lower temperatures.
4. Sequestration of Sn and other metals into Fe-Ti oxides and biotite allows these minerals to act as a protore for later hydrothermal circulation to scavenge these elements and precipitate them into late-forming low-grade fracture and vein systems (e.g. Wang et al., 2013).

In the Tingha region of the SNEO, joint-hosted vein systems are not symmetrically arranged radially around the cupola of the highly fractionated and oxidised Gilgai Granite. In addition, Re-Os dating of molybdenite occurrences within the granite are coeval with granite crystallisation, both of which predate cassiterite ages

in the radially arranged fracture and vein systems that are superimposed on the northern half of the exposed granite.

These results suggest the post-emplacement and post-crystallisation operation of hydrothermal cells within and around the I-type Gilgai Granite, with Sn, W, Mo Bi and other metals being scavenged from biotite and Fe-Ti oxide phases. This process represents secondary scavenging and remobilising of ore-forming elements, rather than a strictly magmatic-hydrothermal process involving partitioning of melt-hosted incompatible elements directly into an exsolving magmatic aqueous volatile phase during crystallisation. Heat drivers for this process could include the elevated regional heat flow in the SNEO caused by the high rate of granite emplacement and attendant volcanism at the time of granite emplacement, as well as radiogenic heat production within the granite, due to its elevated K, Th and U contents.

### Tin deposits and the volcano-plutonic connection

Although I- and S-type granite-related Sn systems in mainland eastern Australia contrast geochemically, recent advances in mapping and more precise geochronology in NSW has shown that both systems have close spatial and temporal relationships with contemporaneous volcanism. The large S-type-related Ardlethan Sn deposit within the Wagga Tin Belt of the Lachlan Orogen, is essentially indistinguishable in age from the regionally extensive Gurrugong Volcanic Group, into which part of the granite and associated hydrothermal system intrude. Similar intimate temporal relationships also exist between the Wandsworth Volcanic Group and the I-type granite-related Sn systems of the SNEO.

Although in both cases there is a broad petrographic and chemical similarity between the contemporaneous volcanics and granites (S-type in the Lachlan Orogen, and I-type in the SNEO), precise geochemical matching between the granites and volcanics is not evident. Better stratigraphic preservation in the SNEO indicates that the Wandsworth Volcanic Group developed as a volcanic pile over 2,000 m thick in places within a period of 2.5 My at ~253 Ma. Water undersaturated felsic magmas intruded up to the base of the volcanic pile and, in some instances, into the pile itself forming stockwork, sheeted vein- and breccia-hosted mineralisation within the volcanic package. This requires a significant thickness of volcanics to have been deposited and retained in place during granite emplacement and mineralisation, which extended to ~245 Ma in the SNEO. A similar scenario is also postulated for the Wagga Tin Belt systems of the Lachlan Orogen, although preservation of the volcanic sequence is much poorer. Similar relationships are also apparent in the Carboniferous I-type Sn systems of FNQ (Chang et al., 2017; Cheng et al., 2018). However, these relationships generally do not appear to apply to the Sn

skarn and carbonate replacement systems, which form at greater depths.

#### References

- Blevin, P. L., 1998. Palaeozoic Sn±W deposits. *AGSO Journal of Geology and Geophysics*, 17(4):75-79.
- Blevin, P. L., and Chappell, B. W., 1992. The role of magma sources, oxidation states and fractionation in determining the granite metallogeny of eastern Australia. *Transactions of the Royal Society of Edinburgh, Earth Sciences*, 83:305-316.
- Blevin, P. L., and Chappell, B. W., 1995. Chemistry, origin and evolution of mineralised granites in the Lachlan Fold Belt, Australia; the metallogeny of I- and S-type granites. *Economic Geology*, 90:1604-1619.
- Blevin, P. L., Chappell, B. W., and Allen, C. M., 1996. Intrusive metallogenic provinces in eastern Australia based on granite source and composition. *Transactions of the Royal Society of Edinburgh: Earth Sciences*, 87:281-290.
- Chang, Z., Clarke, G., Cheng, Y., Poblete, J., and Liu, K., 2017. Sn-W-Mo mineralization in north-east Queensland. In: Phillips, G. N. (ed). *Australian Ore Deposits*, The Australasian Institute of Mining and Metallurgy, Melbourne, pp. 681-688.
- Cheng, Y., Chang, Z., Poblete, J., Liu, K., Spandler, C., Clarke, G., and Dirks, P., 2018. Tin and tungsten deposits in northeast Queensland, Australia: past, present, and prospectivity. 15th Quadrennial IAGOD International Association on the Genesis of Ore Deposits Symposium, Salta, pp. 75-76.
- Hong, W., Cooke, D. R., Huston, D. L., Maas, R., Meffre, S., Thompson, J., Zhang, L., and Fox, N., 2017. Geochronological, geochemical and Pb isotopic compositions of Tasmanian granites (southeast Australia): Controls on petrogenesis, geodynamic evolution and tin mineralisation. *Gondwana Research*, 46:124-140.
- Manning, D. A. C., and Pichavant, M., 1985. Volatiles and their bearing on the behaviour of metals in granitic systems. In: Taylor, R. P and Strong, D. F. (eds). *Recent advances in the geology of granite-related mineral deposits*, Canadian Institute of Mining and Metallurgy Special Volume 39, pp. 13-24.
- Pollard, P. J., Pichavent, M., and Charoy, B., 1987. Contrasting evolution of fluorine-rich and boron-rich tin systems. *Mineralium Deposita*, 22:315-21.
- Wang, R. C., Xie, L., Chen, J., Yu, A., Wang, L., Lu, J., and Zhu, J., 2013. Tin-carrier minerals in metaluminous granites of the western Nanling Range (southern China): Constraints on processes of tin mineralization in oxidized granites. *Journal of Asian Earth Sciences*, 74:361-372.

# The magmatic evolution and rare metal potential of the Peak Range Volcanics, central Qld

Ross Chandler<sup>1</sup>, Carl Spandler<sup>2</sup>

<sup>1</sup>Geoscience, Australian National University, Canberra ACT, Australia

<sup>2</sup>Geoscience, James Cook University, Townsville Qld, Australia

The Oligocene Peak Range Volcanics (PRV) crop out as a series of prominent domes, peaks and pinnacles to the east of Clermont in central Queensland (Wellman and McDougall, 1974). The volcanic rocks have intruded through, and erupted onto, sedimentary rocks of the Bowen Basin above what is likely to be a deep suture zone between the Thompson and New England Orogen. The PRV belong to the Cosgrove hotspot track (Fig 1), which represents the world's longest continental volcanic chain (Davies et al., 2015).

The PRV can be divided into a northern group of peraluminous rhyolites and a southern group of metaluminous trachytes and peralkaline rhyolites. The focus of this study is on the rocks of the southern group, which can be further divided by their dominant mafic mineral speciation into (in order of increasing peralkalinity): (i) augite trachytes, (ii) hornblende trachytes, (iii) hornblende rhyolites, (iv) Na-amphibole rhyolites and (v) aegirine rhyolites. The three aegirine rhyolite bodies (Christmas, Clarrys and Pitts Domes) consist of a glomeroporphyritic arrangement of

microcline-rimmed albite-quartz-sanidine-aegirine (Fig. 2) in a fine-grained, allotriomorphic sanidine-quartz-aegirine groundmass. Existing interstitially to the groundmass minerals is a late stage magmatic apaitic assemblage of dalyite ( $K_2ZrSi_6O_{15}$ ), a eudialyte-like mineral and aegirine (Fig. 2C, D). Secondary minerals include kaolin clays, Fe-rich chlorite, hematite, secondary quartz, Ca-bastnäsite, Zr-gel, allanite (Ce), monazite and columbite, which occur in overprinting, replacement, interstitial and vug-filling textures. The aegirine rhyolite bodies display peralkaline index values of  $>1.3$  (Fig. 3) and extreme enrichment in trace elements, such as Zr contents up to 5700 ppm, Nb up to 900 ppm, and Hf up to 130 ppm (Fig. 3). REE are enriched by between 200 and 1000 times chondritic values, with LREE enrichment, and distinct negative Eu anomalies.

Major and trace element geochemistry are used to show that the separate PRV rock types of each represent a distinct step in a fractionation sequence from least evolved augite trachytes to most evolved aegirine rhyolites (Fig. 3). This range of rock types can be modelled by alkali-

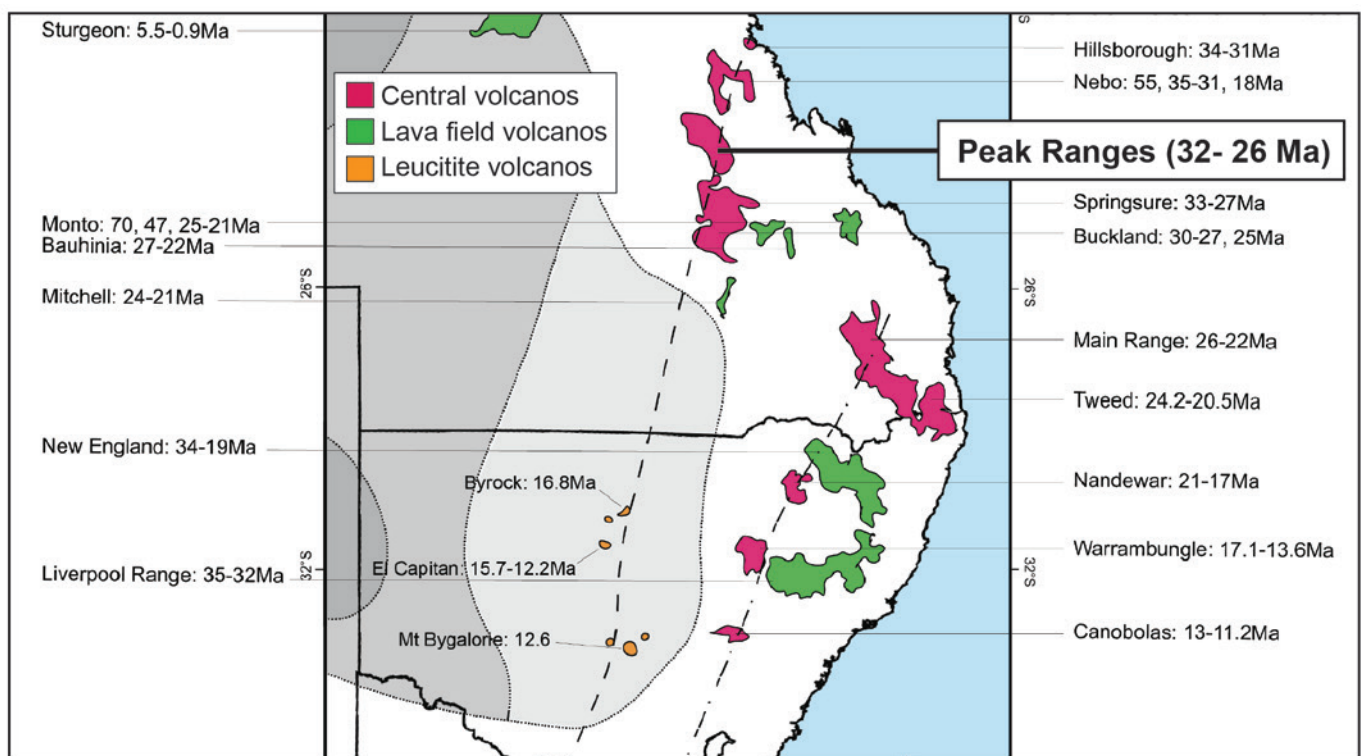


Figure 1. Cenozoic intraplate volcanic provinces of Eastern Australia (adapted from Chandler, 2018).

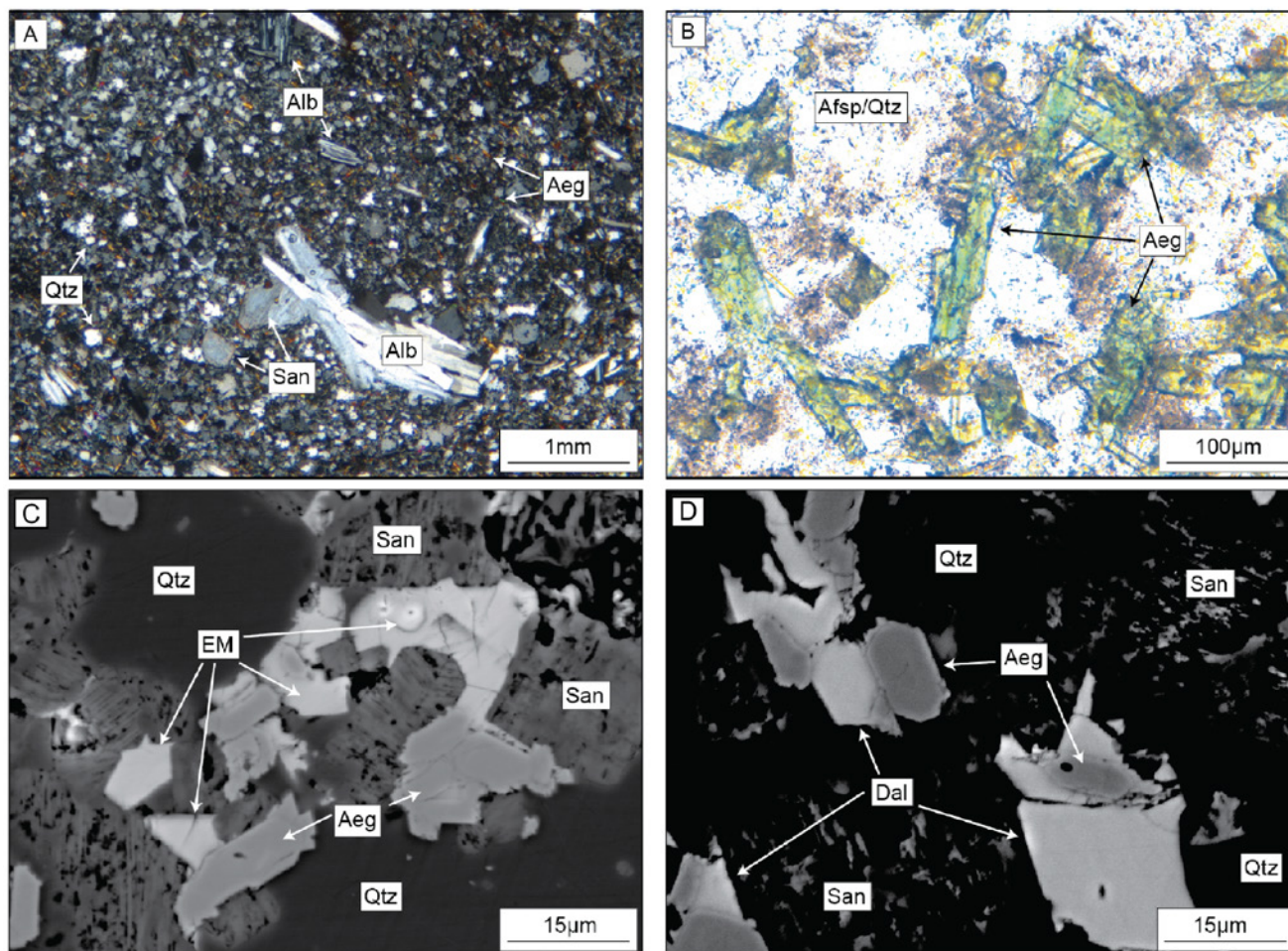


Figure 2. (A) Cross polarized and (B) plane polarised light and (C,D) backscatter electron images of aegirine rhyolite samples. Mineral abbreviation; Qtz = quartz, Alb = albite, Aeg = aegirine, San = sanidine, Afsp = alkali-feldspar, EM = eudialyte mineral, Dal = dalyite.

feldspar-dominated fractional crystallisation of an alkali basalt melt at a shallow crustal position. Neodymium isotope compositions of a range of rock types returned initial  $\epsilon_{Nd}$  within a tight range from +3 to +4, which is consistent with a mantle source for these volcanics, as has also been found for other rare metal enriched peralkaline volcanics of eastern Australia (Spandler and Morris, 2016). Thus, the extreme trace element enrichment and high peralkalinity of the aegirine rhyolites is the product of the extended fractionation of a melt formed by low-degree partial melting of an enriched mantle source. Minor trace elements redistribution occurred upon fluid exsolution at a late magmatic stage, and post-magmatic alteration features noted in some bodies are suggested to be from subjacent devolatilising bodies of magma.

The extreme enrichment of rare metals, the large tonnages (>500 Mt), the outcropping nature and the geographical location of the aegirine rhyolite bodies in the southern PRV all indicate their potential to be significant economic

resources of rare metals (Zr, Nb, Hf, Ta and REE). The economic potential may well be boosted in the future with further research work, particularly examining the role of local upgrading of metal contents by the action of hydrothermal fluids.

#### References

- Chandler, R. (2018). The magmatic evolution and rare metal potential of the Peak Range Volcanics, central QLD. Unpublished honours thesis.
- Davies, D. R., Rawlinson, N., Iaffaldano, G. and Campbell, I. H. (2015). Lithospheric controls on magma composition along Earth's longest continental hotspot track. *Nature*, 525, 511-511.
- Spandler, C. and Morris, C. (2016). Geology and genesis of the Toongi rare metal (Zr, Hf, Nb, Ta, Y and REE) deposit, NSW, Australia, and implications for rare metal mineralization in peralkaline igneous rocks. *Contributions to Mineralogy and Petrology* 171, 104.
- Wellman, P. and McDougall, I. (1974). Cainozoic igneous activity in eastern Australia. *Tectonophysics*, 23, 49-65.

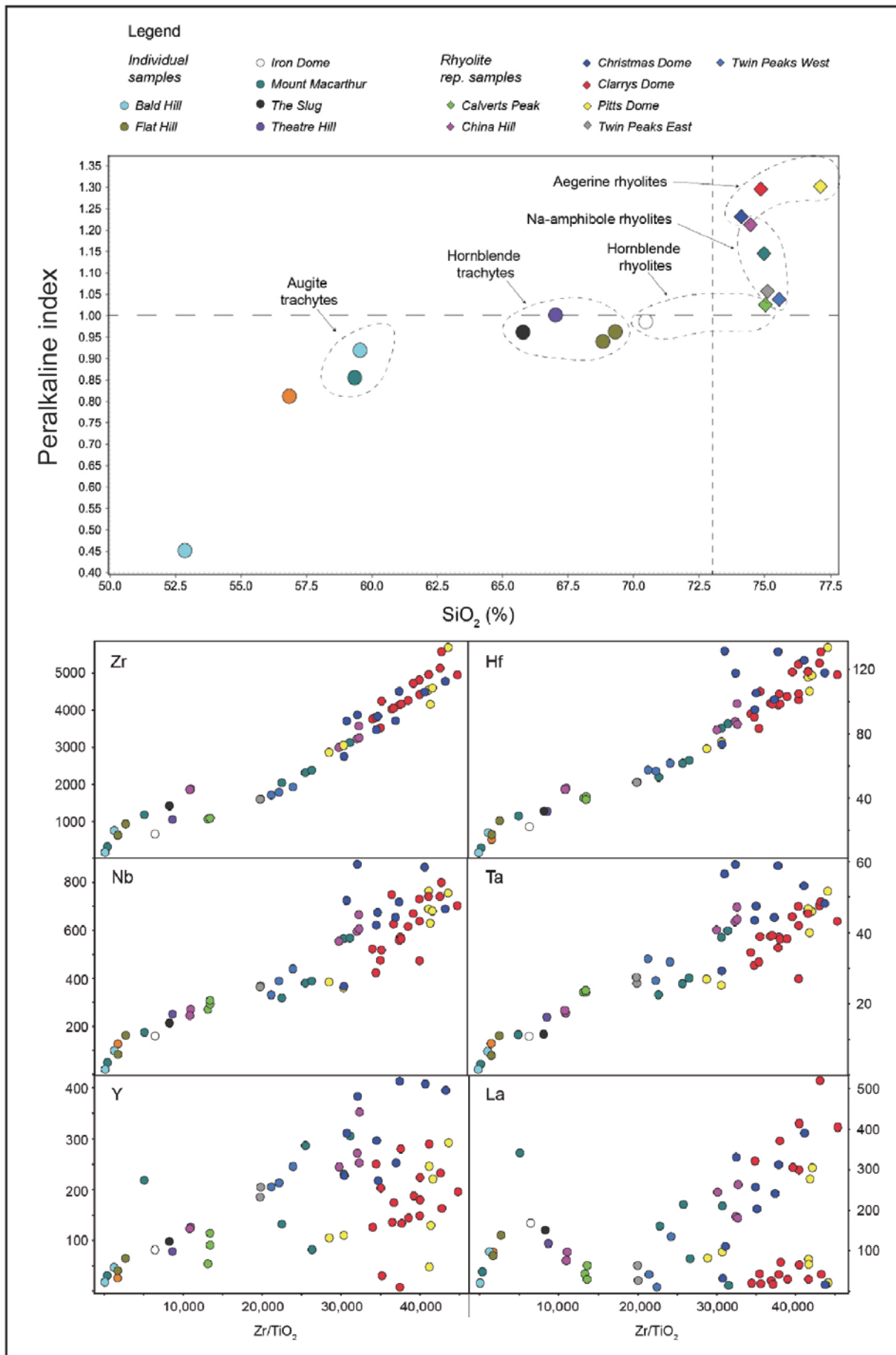


Figure 3. Bulk rock geochemical data for samples of the Peaks Range Volcanics. Both SiO<sub>2</sub> and Zr/TiO<sub>2</sub> are proxies for progressive fractionation. Note the increase in peralkalinity with increasing SiO<sub>2</sub> content, and increase in rare metal content with increasing Zr/TiO<sub>2</sub> content.

# New Sn & W ore exploration toolkit: chemistry of zircon, cassiterite and volcanic rocks

Yanbo Cheng<sup>1</sup>, Carl Spandler<sup>1</sup>, Zhaoshan Chang<sup>1,2</sup>

<sup>1</sup>Economic Geology Research Centre (EGRU), James Cook University, Townsville, Queensland, Australia

<sup>2</sup>Department of Geology and Geological Engineering, Colorado School of Mines, Golden, Colorado, USA

Magmatic source, redox state, and the degree of magma fractionation are petrogenetic factors that control the development of metal-fertile magmas leading to magmatic-hydrothermal mineral deposits. Over the past decade there has been increased interest in using accessory minerals to evaluate the prospectivity of magma-related hydrothermal mineralization, largely porphyry Cu-Au (-Mo) deposits. One of the examples is using zircon rare earth elements as oxy-barometers. Similar to porphyry Cu±Au systems, Sn±W mineralization is also primarily associated with magmatic rocks, but these mineralization systems have not been the subject of significant study in recent years. Almost all previous studies on Sn and W genesis and exploration have focused on the ore associated granitic rocks, whereas there has been little attention paid to explore the potential of other rocks and minerals. To address this deficiency, we examine the in-situ trace element composition of zircon and cassiterite, and bulk rock geochemical and zircon Hf isotopic features of volcanic-intrusive rocks from several world's best known Sn-W-Mo districts. Thereby, their potentials as new Sn and W exploration tools have been revealed.

This study investigates the redox characteristics of the granites related to W and Sn mineralization, and

further discusses the magmatic controls leading to Sn, W, porphyry Cu-Au, porphyry Mo and granite-related W-Mo deposits. To distinguish these deposits we analysed and compiled the trace element characteristics of zircons from porphyry Cu-Au deposits (1015 zircon analyses), Sn-dominant deposits (196 zircons), porphyry Mo deposits (158 zircons), W-dominant deposits (75 zircons) and W-Mo deposits (61 zircons). Strict criteria have been applied to avoid contamination by small mineral inclusions. Our new results suggest that zircon chemistry is effective in highlighting a decreasing trend in redox state from porphyry Cu-Au±Mo, via porphyry Mo, Mo-W, W-dominant, to Sn-dominant systems. The CeN/CeN\* and EuN/EuN\* ratios of zircons are useful magma fertility discriminators for the above hydrothermal mineral deposits. When combined with Mo/W tonnage ratios, the CeN/CeN\* ratio of zircon is also a good indicator of the oxygen fugacity of W-Mo deposits, which can be further employed to determine the style of Mo-W mineralization (Figure 1). This is consistent with the observation that the positive correlation of oxidation state of granite and the Mo/W ratio for the W-Mo deposits in Lachlan Fold Belt, Australia (Blevin and Chappell, 1992).

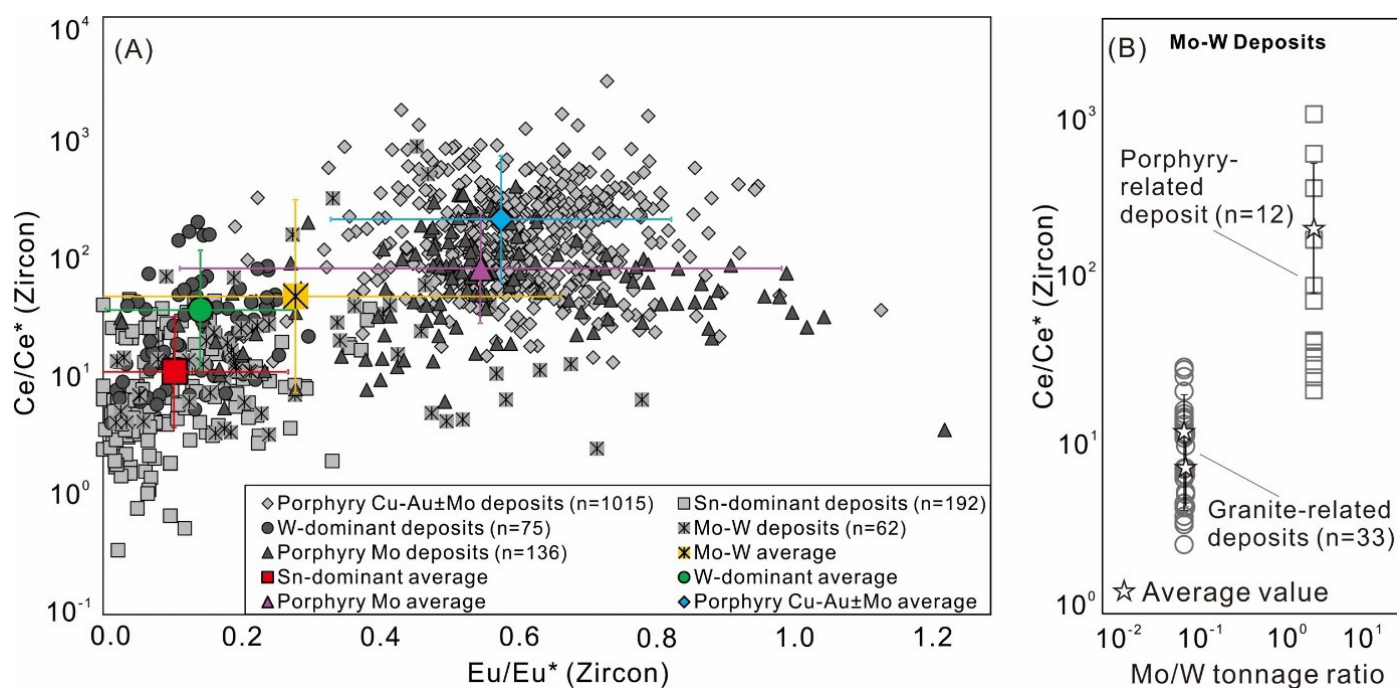


Figure 1. (A) Ce anomaly vs Eu anomaly of zircons from intrusions associated with Sn-dominant, W-dominant, W-Mo, porphyry Mo and porphyry Cu-Au±Mo deposits. (B) Mo/W tonnage ratio versus Ce anomaly of zircon from intrusions associated with porphyry type Mo-W deposits and granite-related Mo-W deposits (Cheng et al., in prep.).

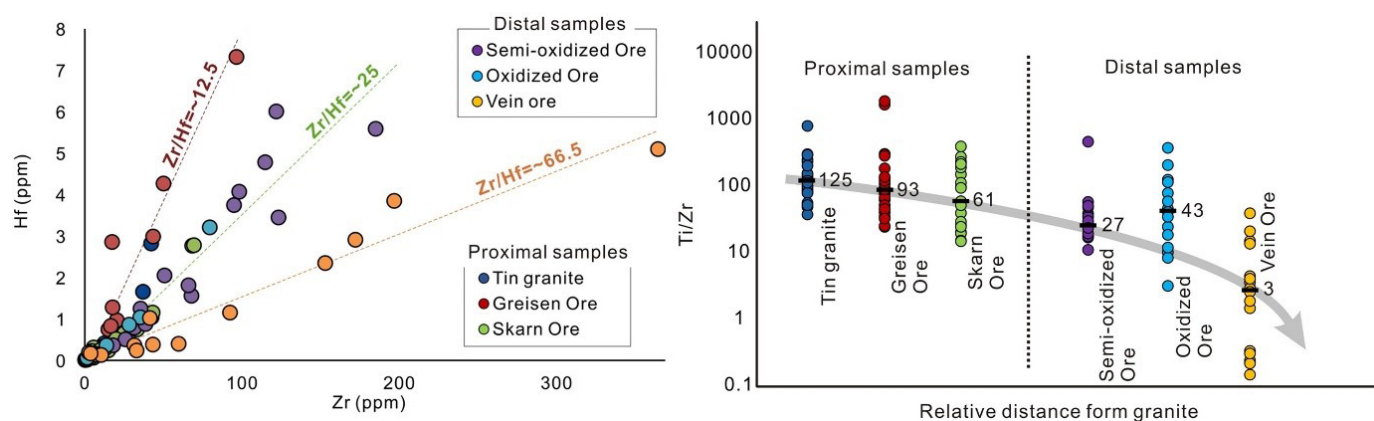


Figure 2. Zr vs. Hf, and Ti/Zr against sample location for the cassiterite samples from world-class Gejiu tin district, Yunnan province, China (Cheng et al., 2019).

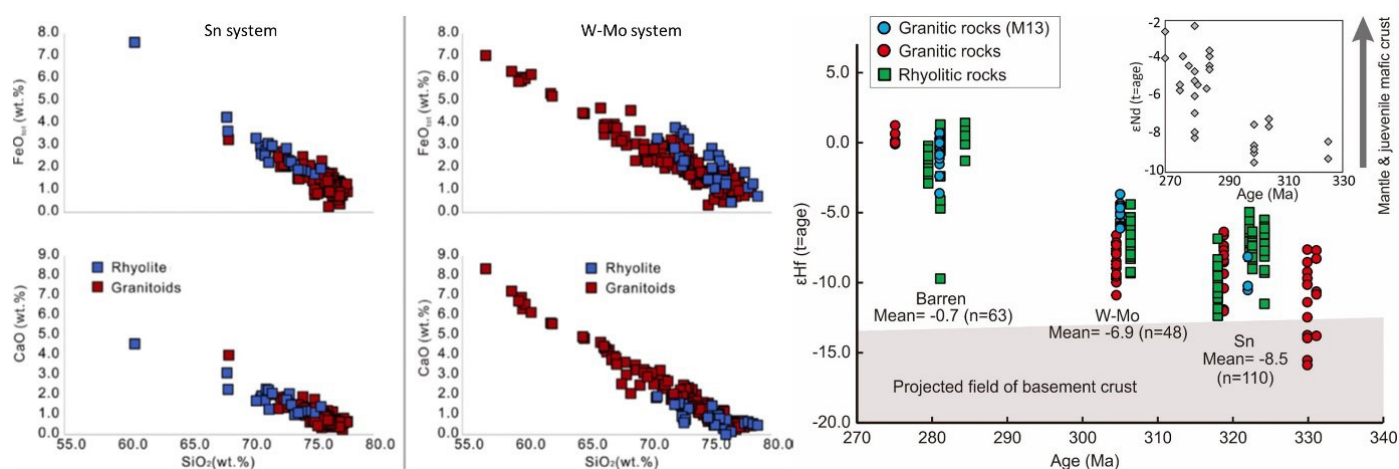


Figure 3 Binary plots of whole rock geochemical composition and zircon Hf isotope composition of granite and rhyolite in the Herberton Sn-W-Mo mineral field, Queensland, Australia (Cheng et al., 2018; WR geochemistry data of granites is courtesy of David Champion; M13 is from Murgulov et al., 2013).

Cassiterite is the most important tin mineral in nature. Therefore, the chemistry of cassiterite may return insightful understandings on cassiterite crystallization under hydrothermal conditions, which will be helpful for developing tin ore exploration. A set of cassiterite samples from six different mineralization environments from the world class Gejiu tin district, SW China, were examined. Cassiterite Zr/Hf ratios tend to increase, and Ti/Zr ratios tend to decrease, with distance away from the causative granite intrusion (Figure 2). Zr/Hf ratios of the six samples vary from greisen-hosted cassiterite to vein-hosted cassiterite, which is attributed to different F and B activities in the different environments. Cassiterite Ti/Zr ratios vary by over an order of magnitude in all of the samples, which may reflect a progressive depletion of Ti relative to Zr from the fluid as it migrated and evolved away from the intrusion. This consistent with results of some studies that show higher solubility of Zr in fluids compared to Ti (e.g., Kessel et al., 2005). In these cases, Zr/Hf and Ti/Zr ratios of cassiterite have potential to be used as a broad tool for vectoring toward a tin mineralized intrusive system.

To discern differences between “fertile” and “non-fertile” igneous rocks associated with Sn-W-Mo mineralisation and reveal the genetic links between coeval intrusive and extrusive rocks, we integrate whole rock geochemistry, geochronology and Hf isotope signatures of igneous zircons from contemporaneous plutonic and volcanic rocks from the world-class Herberton Mineral Field of Queensland, Australia, where Sn and W ( $\pm$ Mo) deposits are abundant (e.g., Chang et al., 2017). The intrusive rocks and associated intra-plutonic W-Mo mineralisation formed from relatively oxidised magmas after moderate degrees of crystal fractionation. The geochemical and isotopic features of the coeval volcanic succession are best reconciled utilising the widely-accepted volcanic-plutonic connection model (Bachmann and Bergantz, 2008), whereby the volcanic rocks represent fractionated derivatives of the intrusive rocks. Intrusions associated Sn mineralisation formed from relatively low  $fO_2$  magmas that fractionated extensively to produce highly evolved granites that host Sn mineralisation. Coeval volcanic rocks of this suite are compositionally less evolved than the intrusive rocks, thereby requiring a different model

to link these plutonic-volcanic sequences. In this case, we propose that the most fractionated magmas were not lost to volcanism, but instead were effectively retained at the plutonic level, which allowed further localized build-up of volatiles and lithophile metals in the plutonic environment. This disconnection to the volcanism and degassing may be a crucial step for forming granite-hosted Sn mineralization. Therefore, magmatic provinces that contain Sn-rich fractionated rhyolites may be less prospective for granite-hosted Sn mineralisation, whereas the less evolved rhyolite with reduced redox state and poor fluxing component content may be more prospective for Sn exploration.

### Acknowledgements

We would like to thank Australian Research Council, Geological Survey of Queensland, National Science Foundation of China, China Geological Survey, Yunnan Tin Group, Carbine Tungsten Limited, Consolidated Tin Mines Limited, and Wolfram Camp Mining Pty Ltd for providing financial and in-kind supports for this research. We also benefited from discussions with many colleagues during field trips, conferences / seminars, paper reviews, personal communications, etc.

### References

Bachmann O., Bergantz G.W. (2008). The magma reservoirs that feed supereruptions. *Element* 4: 14–21.

Blevin, P.L., Chappell, B.W. (1992). The role of magma sources, oxidation states and fractionation in determining the granite metallogeny of eastern Australia. *Earth and Environmental Science Transactions of the Royal Society of Edinburgh* 83, 305-316.

Chang, Z., Clarke, G., Cheng, Y., Poblete, J., Liu, K. (2017). Sn-W-Mo mineralisation in north-east Queensland. In: Phillips, N. (ed.), *Australian Ore Deposits*, AusIMM Monograph 32, 681-688.

Cheng, Y., Spandler, C., Chang, Z., Clarke, G. (2018) Volcanic-plutonic connections and metal fertility of highly evolved magma systems: a case study from the Herberton Sn-W-Mo Mineral Field, Queensland, Australia. *Earth and Planetary Science Letters*, 486, 84-93.

Cheng, Y.B., Spandler, C., Kemp, A., Rusk, B., Mao, J.W., Hu, Y., Blake, K. (2019). Correlated cathodoluminescence features, trace element chemistry and geochronology of cassiterite (SnO<sub>2</sub>) from the world-class Gejiu tin district, SW China. *American Mineralogist* 104, 118–129.

Cheng, Y.B., Chang, Z.S., Spandler, C. (in prep). Zircon trace element as a magma fertility discriminator. *Economic Geology*.  
Kessel, R., Ulmer, P., Pettke, T., Schmidt, M.W., Thompson, A.B. (2005). The water-basalt system at 4 to 6 GPa: Phase relations and second critical endpoint in a K-free eclogite at 700 to 1400 °C. *Earth and Planetary Science Letter*, 237, 873–892.

Murgulov, V., Griffin, W.L., O'Reilly, S.Y. (2013). Carboniferous and Permian granites of the northern Tasman orogenic belt, Queensland, Australia: insights into petrogenesis and crustal evolution from an in situ zircon study. *International Journal of Earth Sciences* 102, 647–669.

# Element partitioning in the formation of a microgranite sill with associated Mo (+/- W) deposits in the Herberton District, north-east Queensland, Australia

Gavin Wallace Clarke

*Geosciences, James Cook University, Townsville, Queensland, Australia*

## Abstract

Within the Herberton district of north-east Queensland the Cattle Camp Granite pluton contains a texturally zoned sill that grades upwards from porphyritic microgranite, through aplite, to (pegmatitic) miarolitic granophyre wherein Mo +/- W mineralised quartz pods/pipes/veins occur intermittently. This textural zoning signifies the upward accumulation of an aqueous fluid phase in the residual melt that would have promoted crystallisation from the base upwards. Geochemical trends for the most part suggest crystal-melt fractionation was the principal process controlling elemental distribution. However, trend reversals evident in progression from the usual apical miarolitic granophyre to that which lies immediately adjacent a mineralised quartz pipe imply other processes were also involved. The presence of fluorine-bearing minerals, coupled with the distribution of fluorine and elements that preferentially complex with it (e.g. HREE), indicate fluorine enrichment in the emergent aqueous fluid phase exerted a strong influence on the chemical compositions of granite forms crystallised, and of the components concentrated in the associated mineralised quartz pipes/veins.

## Geological setting

The Herberton – Mt Garnet Tinfield of north-east Queensland has been an important mining area since 1880 when lode tin was found at Herberton. Within the Herberton district, the close spatial association of most forms of mineralisation with granite bodies and their host rocks has been well documented (e.g. Blake, 1972; Clarke, 1990), with deposits principally occurring in and around five major granitic units. Of these, the Cattle Camp Granite is the largest and best exposed pluton in the district.

In the upper levels of the Cattle Camp Granite are a number of microgranite dykes and sills. One of the most prominent is a shallow-dipping sill that is close to 7km long, and up to 80m thick in places. This sill is texturally zoned (Fig. 1) with porphyritic microgranite at the base grading upwards into an aplitic saccharoidal zone, which in turn grades into miarolitic granophyre wherein small bodies of pegmatite, and pipes / veins infilled with quartz with apatite, albite, molybdenite, pyrite and occasional wolframite, occur intermittently. Within the aplitic to weakly granophyric portions, comb layers with large quartz and alkali-feldspar crystals are also evident. The

formation of comb layers and granophyric intergrowths signifies crystallisation in the presence of an aqueous fluid phase (Moore & Lockwood, 1973; Swanson, 1977; Fenn, 1977, 1986). The prevalence of miarolitic cavities (often infilled with volatile- enriched micas, chlorite and fluorite) in the uppermost zone implies this aqueous fluid phase accumulated most prominently beneath the sill roof (Bowden & Kinnaird, 1984). This is to be expected as dissolved magmatic fluids such as water will tend to redistribute in a magma body so that their chemical potentials are everywhere equalised, thereby promoting enrichment of fluids towards the lower-T and lower-P roof zone (Kennedy, 1955). Such enrichment depresses the liquidus for this zone (Fenn, 1977; Swanson, 1977), thereby promoting crystallisation of the sill from the base upwards (Kennedy 1955; Sparkes et al, 1984).

## Whole-rock geochemistry

Utilising atomic absorption spectroscopy, Gibbs (1987) analysed samples collected from a stream-incised section through the microgranite sill, while the author of this extended abstract used X-ray fluorescence spectrometry to analyse blast samples gathered intermittently along the length of the sill (Clarke, 1990). In both cases progression from basal porphyritic microgranite through to apical pegmatite-bearing miarolitic granophyre involves little anomalous variation in Si, Al Fe and K contents, but definitively entails:

- declines in amounts of Ca, Mg, Ti, P and affiliated compatible trace-elements Nb, V, Sr & Ba (e.g. Fig. 2);
- increases in the levels of Na, and relatively incompatible lithophile trace-elements such as Rb (e.g. Fig. 2), Cs, Ta & Sc.

Instrumental neutron activation analyses provided by Dr. Richard Taylor also revealed that this progression is accompanied by the following (see Fig. 3):

- a deepening negative Eu anomaly;
- slight lowering of values for the lightest REE;
- significant enrichment in HREE.

Enrichments in Y, Zr and U are also evident.

However, further progression to include miarolitic granophyre lying immediately adjacent to a molybdenite-bearing quartz pipe entails the dramatic reversal of trends, i.e.:

- (a) significant loss of 'incompatible' elements accumulated in the residual melt (+ aqueous fluid), e.g. Rb, Cs, Ta, Sc, Zr, Y (e.g. Fig. 2) and HREE (Fig. 3);
- (b) relative enhancement of components utilised in minerals crystallised, e.g. Si, Mg, K and affiliated trace-elements Nb, Ba & Sr (e.g. Fig. 2), plus the lightest REE (Fig. 3), and;
- (c) continued low levels of Ca, P, Ti and V ~ comparable to miarolitic granophyre elsewhere in the roof-zone of the sill (e.g. Fig. 2).

Conversely, instrumental neutron activation analysis of rock collected from the adjoining topazitic quartz pipe indicates it contains levels of HREE (Fig. 3) and associated Y, Zr and Th even higher than for miarolitic granophyre that abuts pegmatite!

More recent x-ray fluorescence spectrometry analyses not only broadly confirm these trends, but also reveal that:

- (a) whole-rock chlorine contents are quite low (below 0.03 wt.%) throughout, and
- (b) whole-rock fluorine contents increase with progression from the porphyritic microgranite (0.07 wt.%) to the apical miarolitic granophyre (0.25 wt.%), then drop in the granophyre adjacent to the quartz pipe BUT are markedly elevated in the pipe itself (0.16 – 2.60 wt.%, see Fig. 4).

Finally, with one exception, the oxygen and hydrogen isotopic values for all rock-types examined, from host granite through the various microgranite types to the pipe quartz, are remarkably similar ( $\delta^{18}\text{O}$  0/00: +8 to +10;  $\delta\text{D}$  0/00: -99 to -106). The exception is the miarolitic granophyre associated with pegmatite, which exhibited incipient features of weathering resulting in displaced values ( $\delta^{18}\text{O}$  0/00: +5.1;  $\delta\text{D}$  0/00: -129).

### Discussion

Geochemical trends registered for the progression from basal porphyritic microgranite through to apical pegmatite-bearing miarolitic granophyre are relatively common for granite systems, and are generally considered (e.g. Pollard, 1988) to be the result of protracted crystal-melt fractionation involving the deposition of feldspars, ferro-magnesian minerals and small amounts of accessory minerals such as allanite and monazite.

However, trend reversals evident for an advance from the most common apical miarolitic granophyre to that which lies immediately adjacent a mineralised quartz pipe imply processes other than just simple crystal fractionation were at work when these rocks were formed. Moreover, the proximity of the latter to the mineralised pipe raises the possibility that those elements anomalously depleted in that miarolitic granophyre partitioned into the emergent aqueous fluid which then transferred into the void and eventually deposited the mineralised quartz-rich pipe.

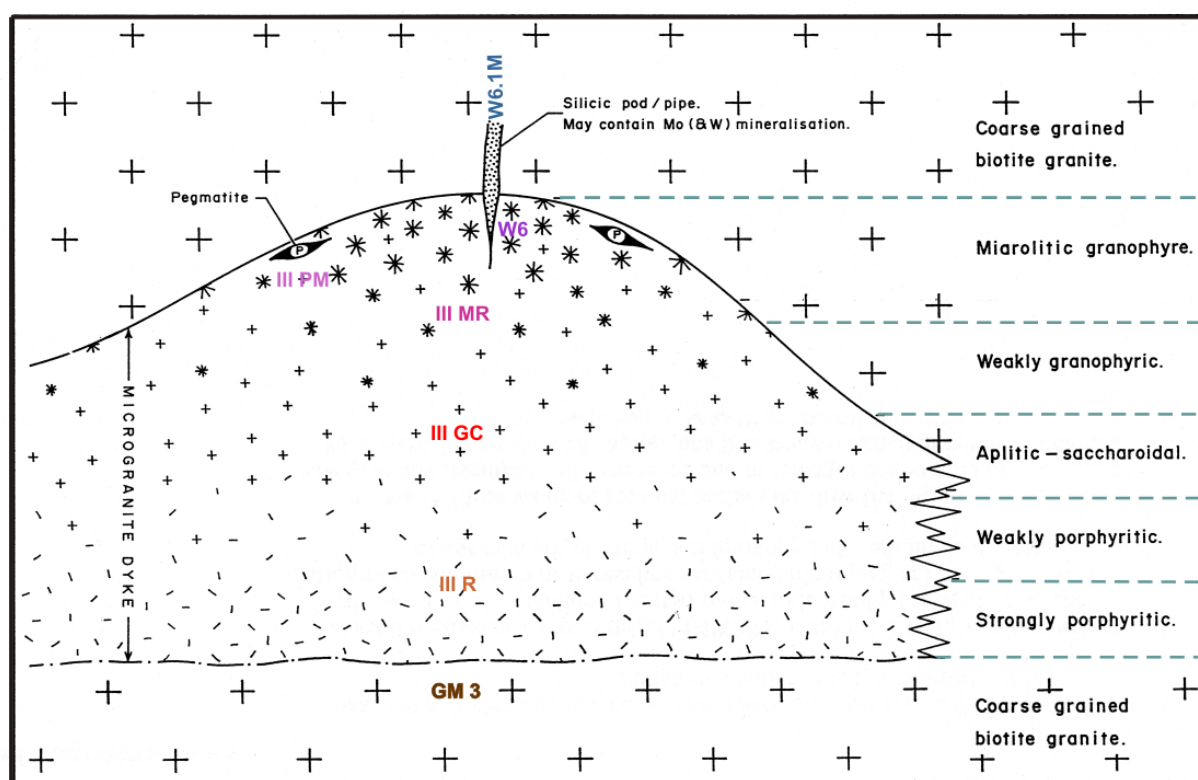


Figure 1. Schematic cross-section through the prominent microgranite sill located in upper levels of the Cattle Camp Granite pluton.

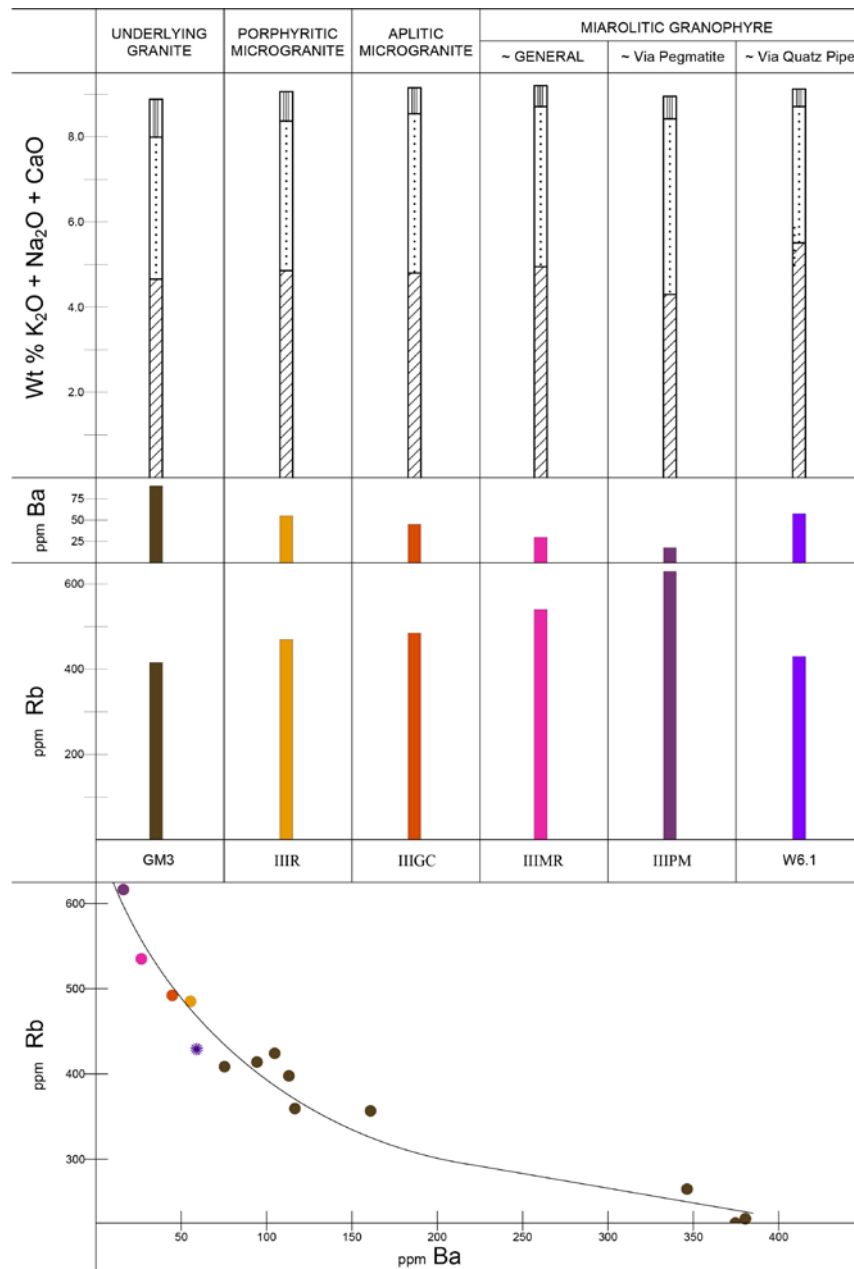


Figure 2. Whole-rock alkali-metal and alkaline-earth trends for samples collected from the Cattle Camp Granite microgranite sill area.

Results of ion exchange experiments on the behaviour of alkali-metal and alkaline-earth trace-elements in the system feldspar – hydrothermal solution indicate Sr and Ba tend strongly to enter feldspars rather than into solution, whereas Rb and Cs usually distribute in favour of the solution (Iiyama, 1972). Moreover, factors determining the distribution of Rb in granitoids include the geochemical association of this element (and presumably Cs also) with any fluorine which may accumulate in the residual magma during the final stages of crystallisation (Aleksandrov & Garanin, 1980; Cerny et al, 1985). Differentiation of REE can also occur under supercritical conditions, with HREE being preferentially mobilised and retained in fluoride complexes by a fluorine-rich vapour phase (Mineyev, 1963; Mineyev

et al, 1966). A build-up of fluorine in the residual melt should also be accompanied by a concentration of elements that complex with fluorine, such as Y, U, Zr & Hf (Taylor & Fryer, 1983; Dietrich, 1968) and Si.

It is therefore pertinent to report that the distribution of fluorine-bearing minerals such as yttrio-fluorite (observed infilling miarolitic cavities; Gibbs, 1987) and topaz (most prevalent in siliceous pods and pipes), plus the whole-rock geochemical trends for fluorine, strongly suggests that in addition to water, fluorine was a major component of the aqueous fluid that emerged during the formation of the microgranite sill. Hence the concentration of a fluorine-rich fluid towards the apical parts of the sill, and eventual breakdown of fluorine complexes during crystallisation can easily account for

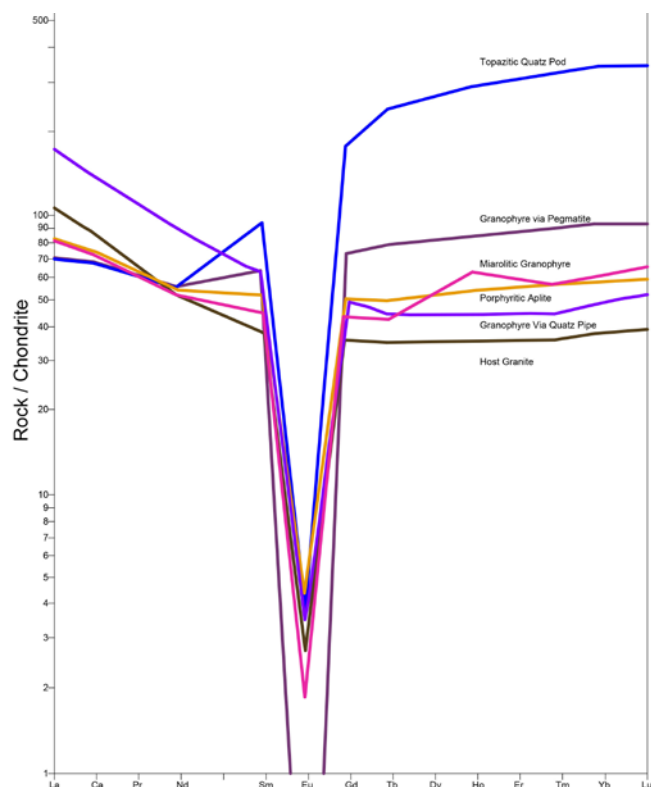


Figure 3. Chondrite-normalised REE patterns for samples collected from the Cattle Camp Granite microgranite sill area.

the porphyry-to-miarolitic granophyre geochemical trends exhibited for the bulk of the sill, plus the loss of fluoro-complexing elements from miarolitic granophyre immediately adjacent to quartz pipes and veins but enhancement of such in those siliceous structures.

Since these quartz lodes can also contain molybdenite (+/- wolframite) mineralisation, it is of further significance to note that the most stable oxyhalide complexes of Mo and W (in their penta- & hexa-positive states) are fluoro-complexes such as  $[\text{MoO}_2\text{F}_4]^{-2}$  and  $[\text{WO}_2\text{F}_4]^{-2}$  (Bailer & Busch, 1956).

### Acknowledgements

Funding for the initial blast sampling and general PhD work came from associates, particularly Dr Roger Taylor (when Assoc. Professor of Economic Geology) at the School of Earth Sciences, JCU, Townsville, Australia. Initial X-ray fluorescence spectrometry analyses were carried out by Frank Dunphy at Queens University at Kingston, Ontario, with funding for the task coming from the Rotary Organisation via a Rotary Foundation Scholarship. Subsequent additional analyses (esp. Cl & F) were done at the JCU Advanced Analytical Centre, at cost to the author. Instrumental neutron activation analyses were done by, and at cost, to Dr. Richard Taylor at the University of Montreal, Canada. Oxygen and hydrogen isotope analyses were kindly provided by Dr John Bowman at the University of Utah, Salt Lake City, USA.

### References

- Aleksandrov IV, Garanin AV (1980) Factors governing rare & ore element distributions in granitoids: *Geochemistry International* 17/6: 61-65
- Bailer JC, Busch DR (1956) *The chemistry of co-ordination compounds*: Reinhold, New York
- Blake DH (1972) *Regional and economic geology of the Herberton Tinfield, North Queensland*: BMR Australia Bulletin 124
- Bowden P, Kinnaird JA (1984) The petrology and geochemistry of alkaline granites from Nigeria: *Physics of the Earth & Planet Interiors* 35: 199-211
- Cerny P, Meintzer RE, Anderson GM (1985) Extreme fractionation of rare-element granitic pegmatites ~ selected examples of data and mechanisms: *Canadian mineralogist* 23: 381-421
- Clarke GW (1990) *The role of fluids in the evolution of granites and associated Mo, W and Sn deposits, Herberton District, North Queensland*: Unpublished PhD thesis, James Cook University, 693p
- Dietrich VR (1968) Behaviour of zirconium in certain artificial magmas under diverse P-T conditions: *Lithos* 1: 20-29
- Fenn PM (1977) The nucleation and growth of alkali-feldspars from hydrous melts: *The Canadian Mineralogist* 15: 135-161
- Fenn PM (1986) On the origin of graphic quartz: *American Mineralogy* 71: 325-330
- Gibbs DR (1987) *The origins of granophyric intergrowths, pegmatite and aplitic textures in a texturally zoned granite dyke*: Unpublished Honours thesis, James Cook University
- Iiyama JT (1972) *Behaviour of trace elements in feldspars under hydrothermal conditions*: IN MacKenzie WS, Zussman J 'The Feldspar': Proceedings of a NATO Advanced Study Institute, Manchester University Press
- Kennedy GC (1955) Some aspects of the role of water in rock melts: *Geological Society of America Special Paper* 62: 489-504
- Mineyev DA (1963) Geochemical differentiation of the rare earths: *Geochimiya* 12 1082-1100
- Mineyev DA, Dikov YP, Sobolev BP, Borutskaya VL (1966) Differentiation of rare-earth elements under supercritical conditions: *Geochemistry International* 3:357-359
- Moore JG, Lockwood JP (1973) Origin of comb-layering and orbicular structures, Sierra Nevada Batholith, California: *Geological Society of America Bulletin* 84: 1-20
- Pollard PJ (1988) Petrogenesis of tin-bearing granites of the Emuford district, Herberton Tinfield, Australia: *Australian Journal of Earth Science* 35: 39-57
- Sparkes RSJ, Huppert HE, Turner JS (1984) The fluid dynamics of evolving magma chambers: *Philosophical Transactions of the Royal Society of London* A310: 511-534
- Swanson SE (1977) Relation of nucleation and crystal-growth rates to the development of granitic textures: *American Mineralogy* 62: 966-978
- Taylor RP, Fryer BJ (1983) Rare-earth element geochemistry as an aid to interpreting hydrothermal ore deposits: IN Evans (Ed) 'Metallurgical Associations with Acid Magmas: 357-365.

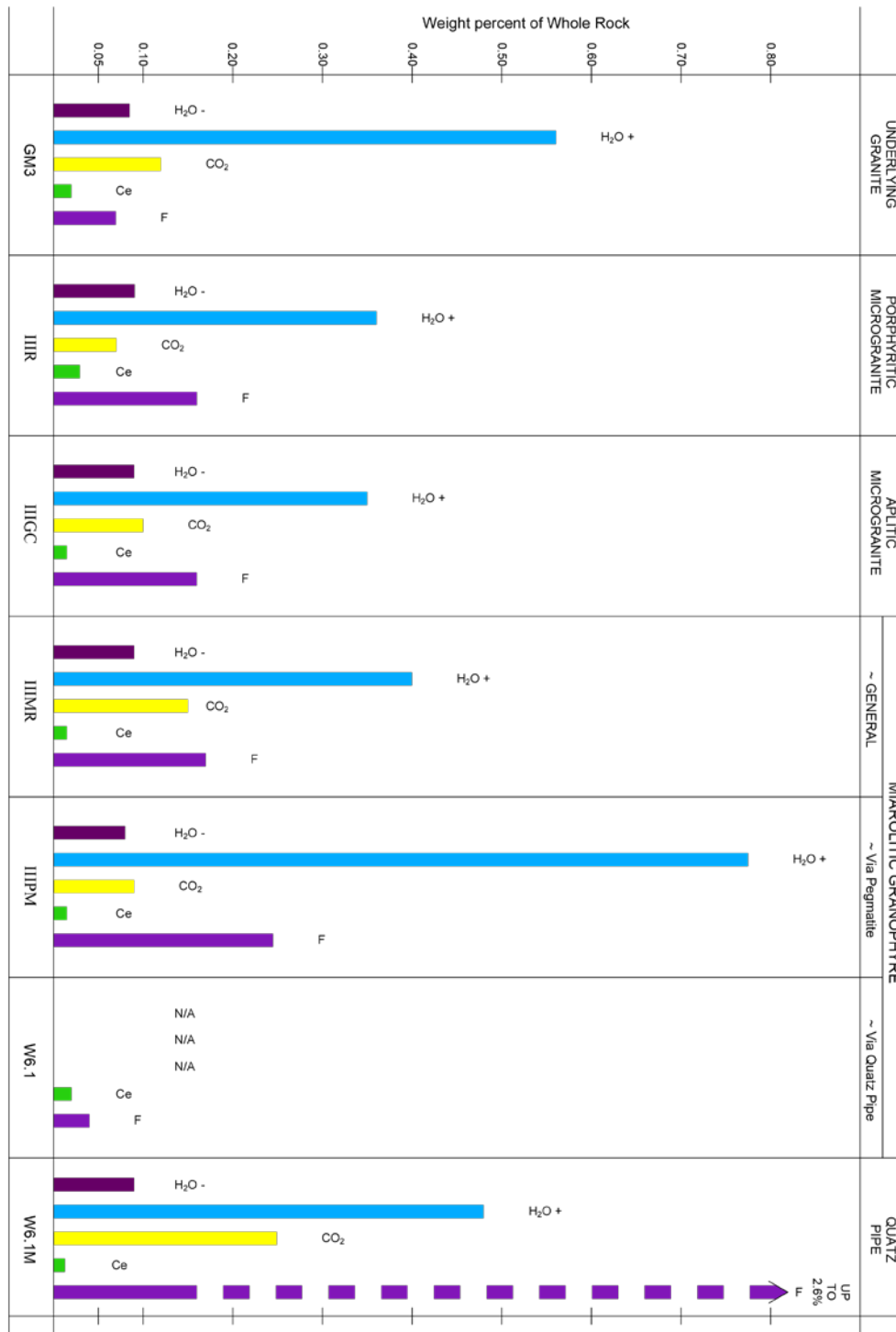


Figure 4. Whole-rock volatile component trends for samples collected from the Cattle Camp Granite microgranite sill area.

# Effects of exsolving fluids on the mineralogy and geochemistry of the Cattle Camp Granite, Herberton Tinfield, north-east Queensland, Australia: a cautionary tale

Gavin Wallace Clarke

*Geosciences, James Cook University, Townsville, Queensland, Australia*

## Geological setting

The Herberton – Mt Garnet Tinfield of north-east Queensland consists essentially of a belt of metasediments (Mid-Silurian / Lower Carboniferous) intruded by a series of granitoids associated with widespread felsic volcanism (Upper Carboniferous – Lower Permian). Closely associated with the granitoids, both spatially and temporally, are significant deposits of tin, tungsten and metal-sulphide ore (Blake, 1972). One of the most important areas of mineralisation in this Tinfield is that centred around the township of Herberton.

Extensive mapping (~ 200km<sup>2</sup>) has shown that the Herberton district is predominantly composed of eight major plutonic units, and that the present distribution of these units is the product of (a) the original location, size and shape of each consecutive intrusion, and (b) subsequent dislocation due to major tectonic readjustments (Clarke, 1990). Of the eight plutonic units, it is the Cattle Camp Granite that exhibits the greatest intact areal extent (~40km<sup>2</sup>), and in manifesting as a stream-incised rugged range provides up to 400m of intermittent vertical exposure.

## Sampling strategies and analytical results

To ascertain the presence of any mineralogical changes inherent in the exposed vertical profile of this granite pluton, five sample traverse lines scaling the range were incrementally sampled via sledge-hammer to obtain fresh rock slab and thin-section block samples. Drill-and-blast sampling was also done along the central traverse line to obtain pristine bulk samples for geochemical analyses. Other drill-and-blast samples were also collected from lowest and highest localities on flanking traverse lines to verify any base-to-top differences detected.

It is apparent from slab modal analyses that while the rocks at the base of the range are of monzogranite, those from levels over 900m RL are predominantly of syenogranite. The transition between is rather abrupt with the drop in plagioclase (>27% to <20%) and rise in quartz (<35% to >38%) contents occurring within an interval of 50m elevation. The rise in the abundance of alkali-feldspar (<34% to >39%) is more gradual, taking place in an interval of 100 vertical metres, so that one sample (i.e. CC2) actually represents an intermediate stage in the transition in the alkali-feldspar levels ~ the shortfall in (plagioclase) feldspar content being balanced by extra amounts of quartz being present.

These changes in quartz, plagioclase and alkali-feldspar contents are mirrored by comparative changes in weight percentages of SiO<sub>2</sub>, CaO and K<sub>2</sub>O. Thus the trends for these components, along with those for associated trace elements (esp. Sr, Ba, Rb etc) signify that in terms of crystal-melt fractionation, this is a 'reverse-zoned' pluton (Fridrich & Mahood, 1984; Bourne & Danis, 1987).

One characteristic feature of the larger granite units around Herberton is that their overall grain size gradually diminishes from being predominantly coarse-grained in their core regions, through seriate to porphyritic medium- to fine-grained near their intrusive margins. Such a textural transition is apparent with progression up the steep northern slopes of the Herberton Range, but continues further on the more gradual southern backslopes of the range. Hence in its post-tectonic rest position, the Cattle Camp Granite pluton had a roof which sloped down towards the Wild River catchment area, wherein lies a likely listric extensional fault (see Fig. 1(a)).

To distinguish further changes with progression into this uppermost part of the pluton, four of the rock slab + thin-section blocks sampling traverses were extended over these backslopes, and some drill-and-blast samples were also collected for geochemical analyses. A measure of relative 'grain coarseness' for samples from each site was obtained through modifying the rock-slab modal analysis technique by setting the grid mesh spacings to 3mm, and recording whether the mineral grain observed at each grid intersect was either a new mineral grain or the same grain seen at the previous grid point. The relative 'grain coarseness' value was derived by expressing the 'same grain' counts as a percentage of the total number of points counted (Fig1(b)). The use of this form of 'grain size index' also meant that results for samples from a lateral traverse progressing out to a side contact of the granite can be included in comparative compositional diagrams.

When plotted in relation to sample 'grain coarseness' determinations, compositional values for purely magmatic mineral components, such as ppm Sr in K-feldspars, MgO/(MgO+FeO) ratios for igneous biotites, and maximum plagioclase anorthite contents, define relatively consistent pluton core-to-margin trends (Fig.1(c)). However, although modal analyses of sidewall samples show them to also be of syenogranite, those for samples from the uppermost region reveal an apparent

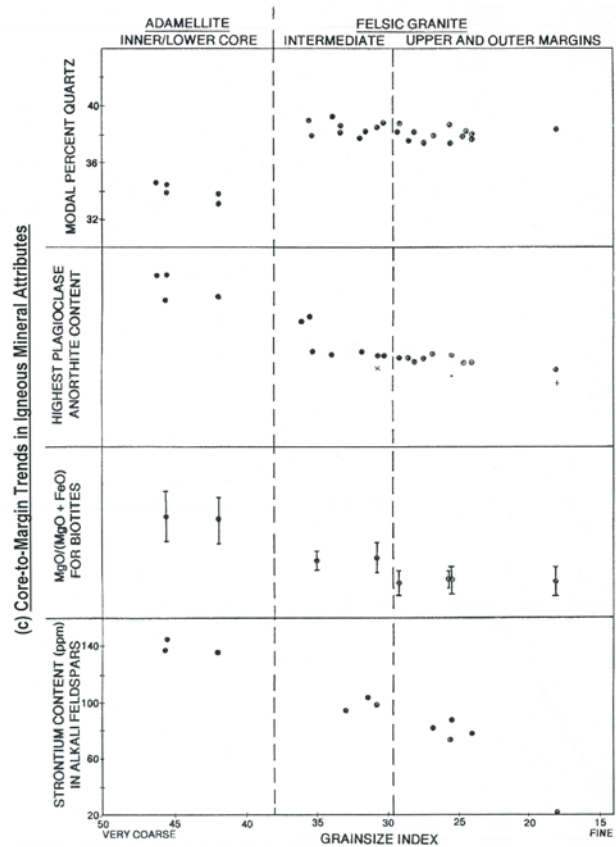
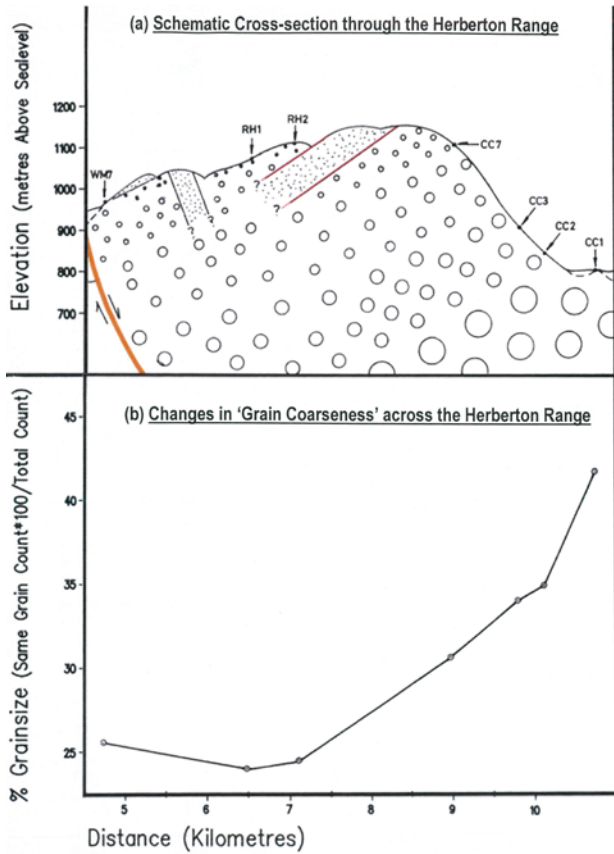


Figure 1. Schematic cross-section through Herberton Range (wherein changes in circle sizes denote changes in relative grain size), plus derived values for 'Grain Coarseness', and trends for magmatic mineral components plotted against site 'Grain Coarseness' values.

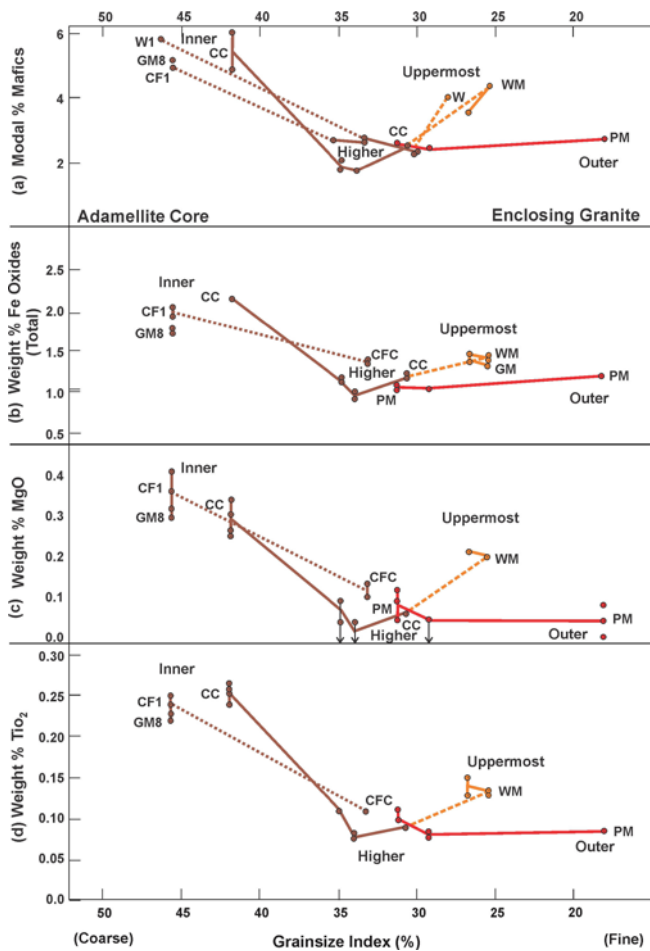


Figure 2. Intra-plutonic trends in proportions of mafic minerals, and associated major-element cation constituents Fe-Oxide (Total), MgO, and TiO<sub>2</sub>.

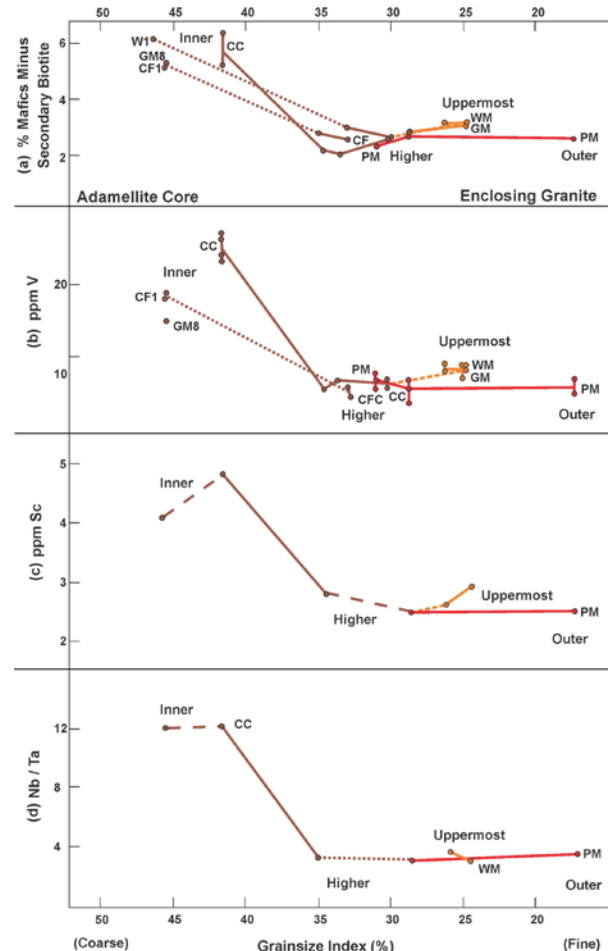


Figure 3. Intra-plutonic trends in proportions of initial igneous mafic minerals, and associated trace-element constituents V, Sc, Nb and Ta.

trend reversal to monzogranite (i.e. lower alkali-feldspar and higher plagioclase + mafic mineral contents than the underlying syenogranite).

Microscopic analysis of thin-sections revealed there to be, in samples from the uppermost zone, a significant amount of distinctly different 'post-magmatic' biotites which have either grown off igneous biotites to partially replace adjacent K-feldspar or intergrown with secondary trails of albite. This upsurge in secondary biotite development is obviously accompanied by whole-rock increases in the levels of associated major constituent elements such as Fe, Mg & Ti (Fig. 2), but has had far less influence on the levels of trace elements usually affiliated with these major elements (Fig. 3). Point-counting of thin-section mineralogies can be used to gain an insight into what percentage of the mafic minerals are post-magmatic in derivation, and when this proportion is deducted from the modal total, the relative amounts of initial igneous mafic minerals can be ascertained and plotted (Fig. 3(a); Clarke, 1990). Similarities between this plot and those for V and Sc (Fig.3(b) & (c)) show that these trace elements are principally affiliated with primary (igneous) but not secondary (replacement) mafic minerals. Similarly, proportions of Nb and Ta seem also to be predominantly igneous in derivation, with Nb/Ta values for the syenogranite and the uppermost zone being virtually the same (Fig.3(d)).

Of even greater significance is the prevalence in the uppermost zone of post-magmatic plagioclase – principally albite and myrmekite – evident along microfractures and alkali-feldspar grain boundaries, and emanating off igneous plagioclases in lobate forms to replace adjacent K-feldspar. This upsurge in secondary plagioclase development is responsible for requisite rises in Na<sub>2</sub>O and CaO (in myrmekite) contents (Fig.4(a) & (b)) but minimal uptake in Sr (Fig. 5(b)). Moreover, when the proportions of post-magmatic plagioclase (as determined by thin-section point-counts) are deducted, and the remaining portions of mostly magmatic plagioclase are ascertained and plotted, the resultant outline is quite similar to that for Sr contents (Fig. 5(a) & (b)). Surprisingly, increased replacement of F-feldspar by secondary plagioclases has resulted in an increase, rather than a decrease in Ba levels, thereby producing an anomaly in the associated Ba/Sr values which are otherwise relatively uniform throughout the rest of this granite pluton (Fig.5(c)).

The growth of myrmekite (and secondary biotite) from alkali-feldspar can be expected, from stoichiometric considerations, to entail the addition of Al in the rocks so altered, but for the uppermost zone of this pluton these alterations did not entail significant changes in supposed affiliated Ga contents. Hence plots of Al<sub>2</sub>O<sub>3</sub>/(Ga x 1000) for this zone rise anomalously off the underlying core-to-marginal magmatic fractionation trend (Fig.4(c)).

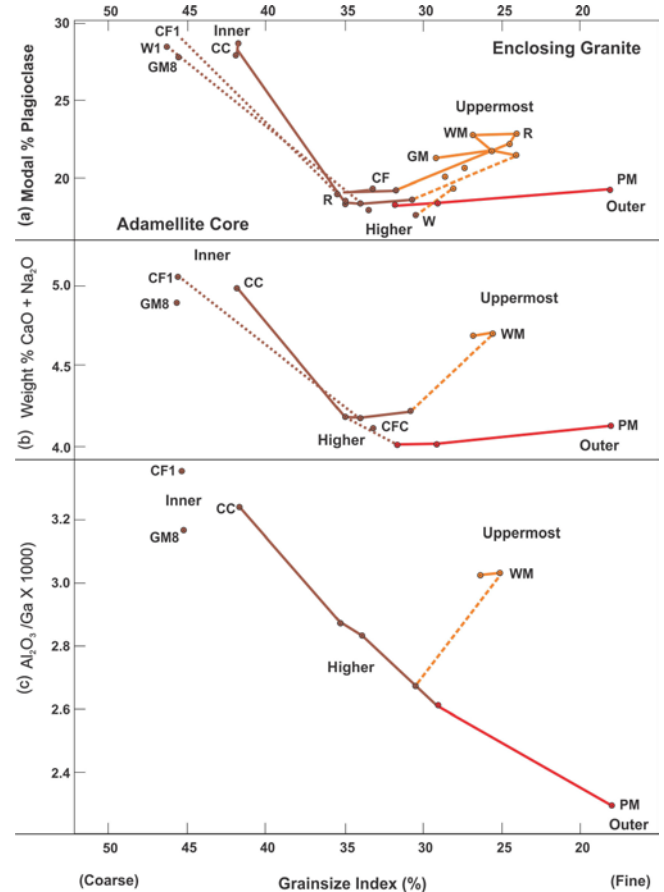


Figure 4. Intra-plutonic trends in proportions of plagioclase feldspars, and associated cation constituents such as CaO + Na<sub>2</sub>O, Al<sub>2</sub>O<sub>3</sub> and Ga.

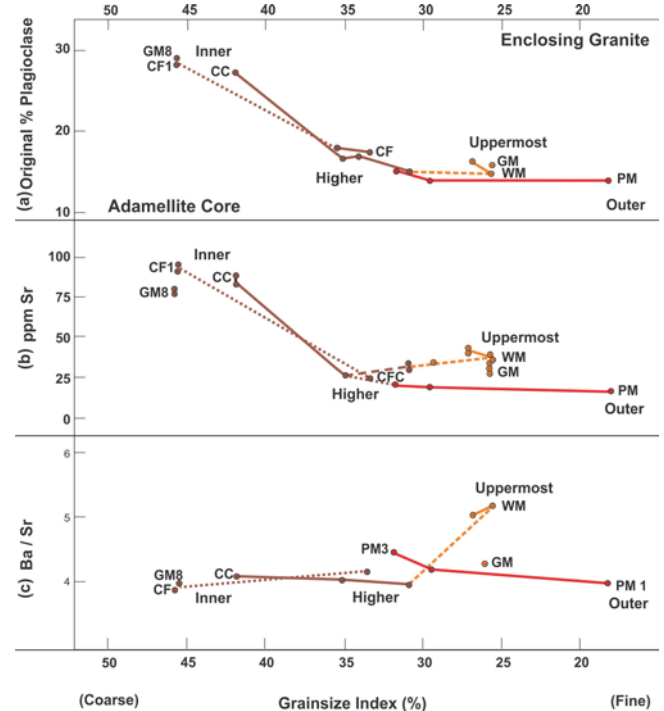


Figure 5. Intra-plutonic trends in proportions of initial igneous plagioclase, trace-element Sr and associated Ba/Sr ratio.

Significant decreases in K-feldspar proportions due to replacement by post-magmatic plagioclase towards the top of the Cattle Camp granite naturally entail decreases in K contents, and since several ppm Th can be contained in alkali-feldspars (Smith, 1974), a drop in Th contents as well. However, the levels of Rb, which has similar ionic radius, electronegativity and ionization potentials to potassium, actually remain quite high in the uppermost zone, despite the prevalence of alkali-feldspar replacement. Likewise with ppm U, although this element mostly occurs in quite resilient accessory phases such as allanite and xenotime.

## Discussion

From the trends noted above, it should be quite apparent that the use of ratios such as Th/U, and K/Rb, as well as Ba/Rb, Sr/Ba, Fe/V, Fe/Sc, Ti/Nb, Ti/Ta, and Al/(Ga x 1000) for discerning purely igneous developments within the uppermost zone of the Cattle Camp Granite could be quite misleading, whereas the use of Sr/Rb and Nb/Ta can still be quite insightful. Conversely, comparative deviations in ratios entailing Sr or Rb versus K or Ba, Ti versus Nb or Ta, Fe versus V or Sc, and Al versus Ga can in this case highlight regions of anomalous post-magmatic replacement activity, and intimate what alteration-related changes have occurred. It can also indicate which analytical results to avoid when assessing inherent magmatic trends and likely causative processes.

Elsewhere in the region, however, pervasive alterational features noted above can actually be well developed throughout a granite body, and such granites are typically the ones most closely associated with significant tin mineralisation (e.g. Clarke, 1990). Considerable care should therefore be taken to always temper geochemical findings and interpretations with detailed assessments of the mineralogical components and processes involved in formation.

## References

- Blake, D.H., 1972: "Regional and Economic Geology of the Herberton Tinfield, North Queensland", B.M.R. Aust., Bull. 124
- Bourne, J. & Danis, D. 1987: A proposed model for the formation of reversely zoned plutons based on a study of the Lacorne Complex, Superior Province, Quebec", *Can. J. Earth Sci.*, 24, pp 2506 – 2520.
- Clarke, G.W., 1990: "The role of fluids in the evaluation of granites, and associated Mo, W and Sn deposits, Herberton District, North Queensland", Unpubl. PhD Thesis, Earth Sciences, James Cook Univ.
- Fridrich, C.J., & Mahood, G.A., 1984: "Compositional layers in a zoned magma chamber of the Grizzly Peak Tuff", *Geology*, 15, 299 – 303.
- Smith, J.V., 1974: "Feldspar Minerals", Vol. 2: "Chemistry and textural properties", Springer-Verlog, New York.

# Magmatic-hydrothermal features in Paleozoic Sn-W- base metal-mineralized and barren granites of Tasmania

David R. Cooke<sup>1,2</sup>, Wei Hong<sup>2</sup>, Lejun Zhang<sup>1,2</sup>, Colin Jones<sup>1,2</sup>, Evan Orovan<sup>1,2</sup>

<sup>1</sup>*Transforming the Mining Value Chain, an ARC Industrial Transformation Research Hub, University of Tasmania, Private Bag 79, Hobart Tasmania 7001, Australia*

<sup>2</sup>*Centre for Ore Deposit and Earth Sciences (CODES), University of Tasmania, Private Bag 79, Hobart, Tasmania 7001, Australia*

Granitoid magmatism affected the eastern and western Tasmanian terranes extensively from around 400 to 350 Ma (Hong et al., 2017a). Large granite batholiths of Eastern Tasmania were emplaced in a N-trending belt parallel to the eastern, active continental margin of Australia (Fig. 1a). These granitoids have pre- syn and post-collisional timings relative to the Tabberraberan Orogeny. The post-collisional eastern Tasmanian granitoids produced Sn, base metal and intrusion-related gold deposits that are hosted in the granitoids and surrounding Siluro-Devonian turbidites of the Mathinna Group. The eastern Tasmanian batholiths were uplifted and eroded significantly, resulting in extensive exposures of granitoids across NE Tasmania.

Eastern and Western Tasmania amalgamated during the Tabberaberran Orogeny at or before 390 Ma. Post-collisional granitoid magmatism followed in western Tasmania between 375 and 350 Ma and was localized on poorly understood NNE-trending cross-orogen lineaments, hundreds of kilometers behind the Early Devonian magmatic arc defined by the older N-trending batholiths of eastern Tasmania. The western Tasmanian granitoids define at least four W-trending batholiths, which are less deeply exhumed than their eastern Tasmanian counterparts. The shallower levels of erosion mean that there are extensive areas where the western Tasmanian granites underlie local country rocks, with significant polymetallic mineralization hosted in the roof zones overlying the sub-surface granitoids (e.g., Zeehan and Dundas mineral fields; Seymour et al., 2007; Fig. 1c)

The geology of Western Tasmania is complicated, with bedrocks ranging from Paleoproterozoic schists through Neoproterozoic shallow marine passive margin sediments (including dolomites) and mafic volcanics, Cambrian ultramafics associated with minor Ni-Cr-Cu-PGE mineralization, bimodal back-arc volcanics and related volcanoclastic rocks that host Cambrian VHMS deposits, Ordovician hematitic quartz-rich conglomerate and overlying limestones that host Ordovician Irish-type mineralization, and Siluro-Devonian shallow marine shales and sandstones. This diversity of rock types and multiple mineralizing events in Western Tasmania has led to a diverse array of mineralization styles in western Tasmania, including granite-hosted Sn-W veins and greisens, carbonate and ultramafic-hosted Sn-W-Fe calcic and magnesian skarns, Zn-Pb-Ag-(Cu) carbonate replacement deposits and polymetallic veins, and highly

unusual Ni skarns that formed where Paleozoic Sn granites intruded Ni-bearing Cambrian ultramafic rocks. Many of the Paleozoic granitoids in Tasmania show textural features consistent with volatile exsolution, including quartz, K-Feldspar, tourmaline and/or magnetite-bearing unidirectional solidification textures (USTs), miarolitic cavities, pegmatoidal pods, diffuse alteration patches and late-stage veins. Tourmaline orbicules are a common (and locally abundant) but contentious feature of some of the granitoids. These magmatic-hydrothermal textures can be found in both mineralized and barren granitoids in Tasmania, but there are distinctions in the mineral chemistry of tourmaline that helps to discriminate the textures associated with mineralization from those unrelated to ore.

The Heemskirk Granite batholith in western Tasmania is possibly the most productive of Tasmania's granites in terms of producing Sn-base metal and Ni mineralization (Table 1). The batholith crops out extensively on the western coastline as the Heemskirk granite (Klominsky, 1972; Hajitaheri, 1985; Fig. 2a and b). The roof of the granite plunges eastwards beneath the Zeehan and Dundas mineral fields, where the Proterozoic and Paleozoic wallrocks host extensive polymetallic veins, skarns and carbonate replacement deposits. The batholith resurfaces as a minor exposure of the Pine Hill granite immediately south of Tasmania's largest Sn mine (Renison Bell), and then extends in the subsurface further to the east, cropping out again at Granite Tor on the Central highlands (Fig. 1c). Between Pine Hill and Granite Tor, the batholith intruded the Cambrian VHMS belt, causing Devonian metasomatism at the southern end of the Cambrian polymetallic Rosebery VHMS deposit.

At Trial Harbour, an exceptional exposure of the Heemskirk granite shows the contact zone between the upper I-type sill of the Heemskirk granite (red phase) and the lower, S-type white granite sill (Hong et al., 2017b; Figs. 2b and c). A spectacular array of magmatic-hydrothermal features formed in the roof of the white granite, providing evidence for extensive fluid exsolution that is consistent with the widespread mineralization associated with the batholith. At Trial Harbour, these textural features change from deep-seated diffuse tourmaline-quartz alteration patches in the lower parts of the exposure, upwards through tourmaline-quartz-filled miarolitic cavities to a roof zone characterized

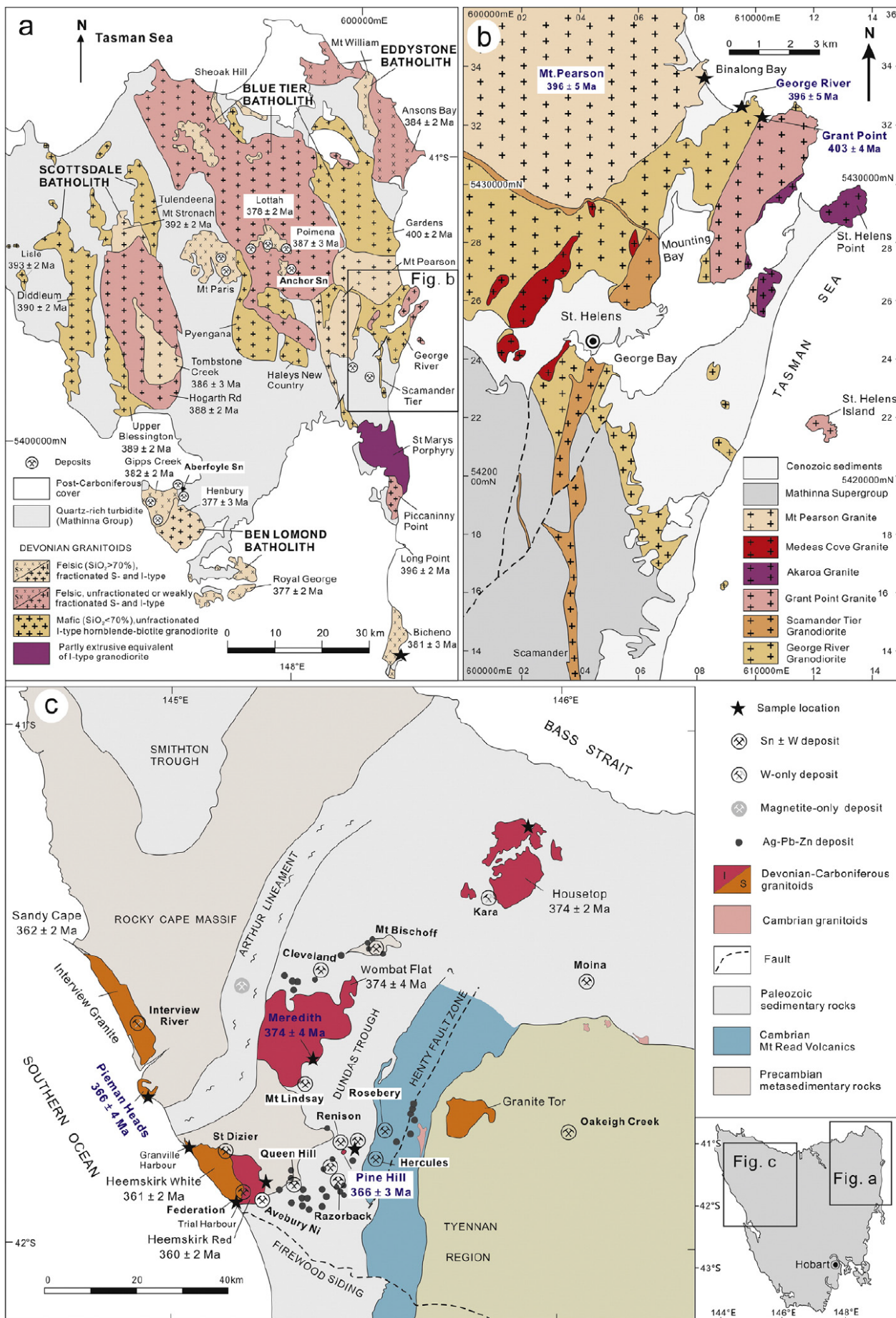


Figure 1. (a) Generalized geological map showing rock outcrop and major Sn deposits in northeastern Tasmania (after Black et al., 2005; Seymour et al., 2007). (b) Simplified geological map showing granitic rocks in the St. Helens area, eastern Tasmania (after McClenaghan, 2006b). (c) Simplified geological map of northwest Tasmania and major granite-associated Sn-W deposits (after Solomon and Groves, 2000). Zircon U-Pb ages of granites are compiled from Black et al. (2005), Kositcin and Everard (2013), and Hong et al. (2017a) (bold blue). Figure reproduced from Hong et al. (2017a).

by abundant quartz-rich USTs (Fig. 2c). The most spectacular and enigmatic component of the outcrop are the extensively developed spherical tourmaline-quartz orbicules that range up to 15 cm in diameter. The orbicules at Trial Harbour are preferentially developed in an aplitic orbicular sill that sits immediately below the UST layers that characterize the roof of the white granite. The orbicular sill was fed by a narrow (20 cm wide) orbicular dyke (Fig. 2c). The orbicules show evidence for both a magmatic and hydrothermal origin. They crop out extensively around the contact zone between the red and white granite, extending more than 10 km north of Trial Harbour and also occurring around the margins of the ~30 x 10 km Heemskirk granite exposure

(Fig. 2a). Orbicules also occur in barren granitoids in western and eastern Tasmania (e.g., Pieman Heads and Bicheno granites), but their abundance in Trial Harbour and their intimate spatial and temporal relationships to USTs, miarolitic cavities and tourmaline patches are the best indicator of magmatic fertility for mineralization in these granitoids.

### Acknowledgements

We thank Ron Berry, David Huston, David Champion, Mostafa Fayek, Roland Maas, Sebastien Meffre, Jay Thompson and Nathan Fox for their input into this research.

Table 1. Sn, W, Fe, and Ni deposits of the Heemskirk Granite, western Tasmania (from Hong et al. 2017b).

Mineral field	Deposit	Commodity	Tonnage (Mt)	Grade	Reference
South Heemskirk	Tenth Legion	Sn-Fe	0.9	0.4–0.5% Sn	Purvis (1989)
			6	60% Fe	Purvis (1989)
	Colemans	Sn	0.5	0.2% Sn	Purvis (1989)
	Sweeneys	Sn	0.5	0.6% Sn	Purvis (1989)
	Federation	Sn	>1.5	0.5–0.6% Sn	Purvis (1989)
	Avebury	Ni	29.3	0.9% Ni	Keays and Jowitt (2013)
North Heemskirk	St. Dizier	Sn-W-Fe	~2.6	0.5% Sn, 0.05% WO <sub>3</sub>	Seymour et al. (2007)
Zeehan	Severn	Sn	4.17	0.98% Sn	Callaghan (2013)
	Montana	Sn	0.51	1.91% Sn	Callaghan (2013)
	Queen Hill	Sn	3.6	1.2% Sn	Seymour et al. (2007)
	Oonah	Sn	1	0.7–1% Sn	Purvis (1989)

### References

- Black, L.P., McClenaghan, M.P., Korsch, R.J., Everard, J.L., and Foudoulis, C., 2005, Significance of Devonian–Carboniferous igneous activity in Tasmania as derived from U–Pb SHRIMP dating of zircon: *Australian Journal of Earth Sciences* 52, 807–829.
- Callaghan, T., 2013. Heemskirk tin project–Tasmania: Tasmanian Geoscience Forum, Cradle Mountain, Tasmania.
- Hajitaheri, J., 1985, The origin of mineralisation in South Heemskirk granite, Western Tasmania, Australia: Ph.D. thesis, University of Tasmania, Hobart, 322 p.
- Hong, W., Cooke, D.R., Huston, D.L., Maas, R., Meffre, S., Thompson, J., Zhang, L., and Fox, N., 2017a, Geochronological, geochemical and Pb isotopic compositions of Tasmanian granites (southeast Australia): Controls on petrogenesis, geodynamic evolution and tin mineralisation: *Gondwana Research*, v. 46, p. 124–140.
- Hong, W., Cooke, D.R., Zhang, L., Fox, N., and Thompson, J., 2017b, Tourmaline-rich features in the Heemskirk and Pieman Heads granites from western Tasmania, Australia: Characteristics, origins, and implications for tin mineralization: *American Mineralogist*, v. 102, p. 876–899.
- Keays, R.R., and Jowitt, S.M., 2013, The Avebury Ni deposit, Tasmania: A case study of an unconventional nickel deposit. *Ore Geology Reviews*, 52, 4–17.
- Klominsky, J., 1972. The Heemskirk Granite Massif, Western Tasmania: Ph.D. Thesis, University of Tasmania, Hobart (unpublished).
- Kositcin, N., and Everard, J.L., 2013. New SHRIMP U–Pb zircon ages from Tasmania: mineral resources Tasmania: *Tasmanian Geological Survey Record* 2013 (02), 1–47.
- McClenaghan, M.P., 2006, Digital Geological Atlas 1:25 000 scale series, sheet 6041 Beaumaris, sheet 6042 St Helens, and Sheet 6043 Binalong, Mineral Resources Tasmania.
- Purvis, J.G., 1989, Tasmanian tin prospects part 1: West Tasmania Tin Province: *Tasmanian Geological Survey Bulletin*, 51–64.
- Seymour, D.B., Green, G.R., and Calver, C.R., 2007, The geological and mineral deposits of Tasmania: a summary: *Tasmanian Geological Survey Bulletin* 72, p. 1–29.
- Solomon, M., and Groves, D.I., 2000, The geology and origin of Australia's mineral deposits: Centre for Ore Deposit Research, University of Tasmania, and Centre for Global Metallogeny, University of Western Australia, 521 p.

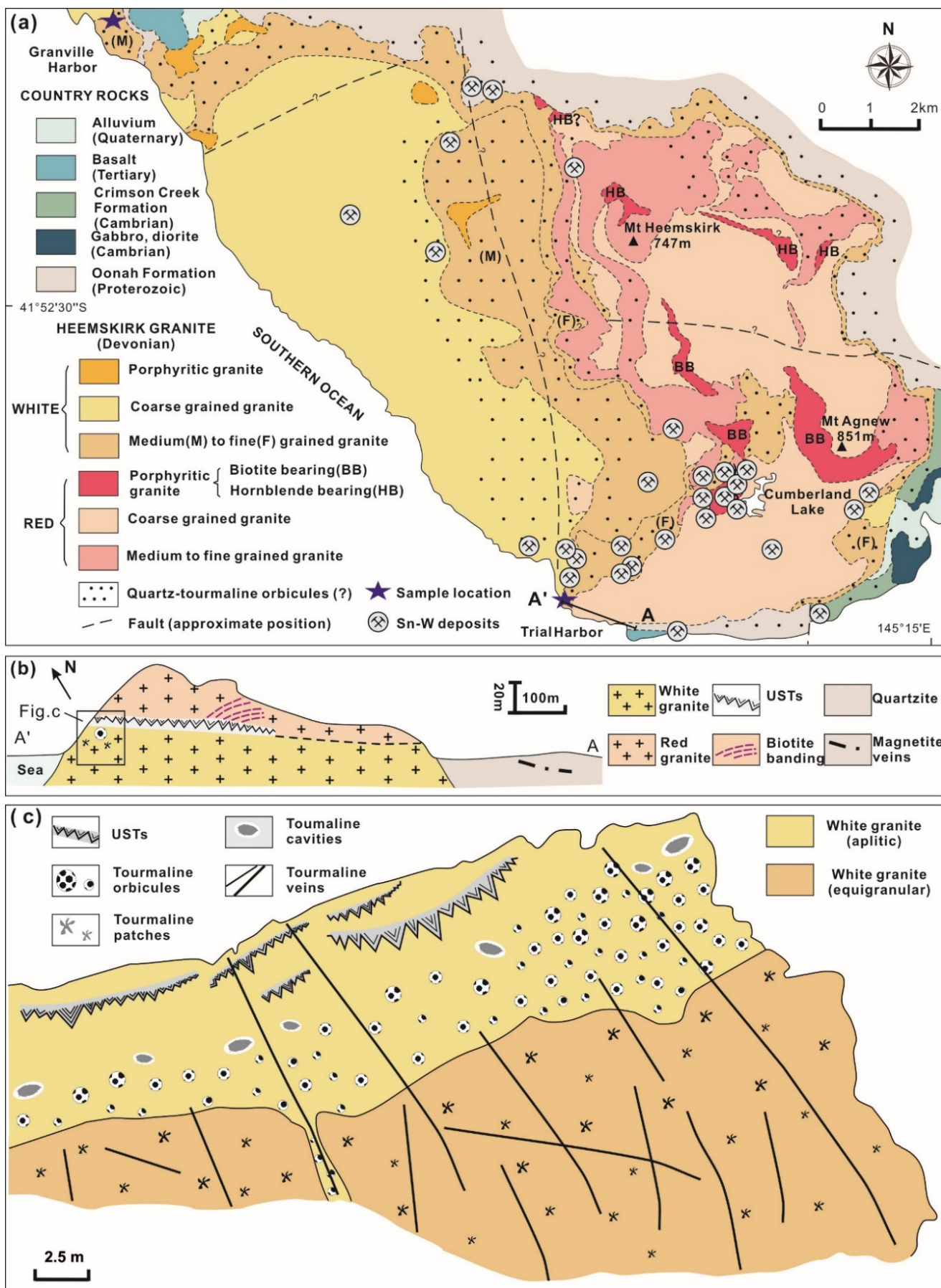


Figure 2. (a) Geological map showing principal feature of the Heemskirk Batholith and associated Sn-W deposits (modified from Klominsky 1972; Hajitaheri 1985). (b) Simplified cross-section A-A' describing the geological outcrop at Trial Harbor, southern edge of the Heemskirk Batholith, where tourmaline-rich features, USTs, and biotite banding occur around the contact between the white and the red granites. (c) Sketched cross-section showing relative spatial distributions of tourmaline patches, orbicules, cavities, and veins that are hosted in the white granite. Reproduced from Hong et al. (2017b).

# The trace element geochemistry of cassiterite in Tasmanian tin deposits

Joshua Denholm<sup>1</sup>, Aleksandr Stepanov<sup>2</sup>, Ralph Bottrill<sup>3</sup>

<sup>1</sup>CODES, University of Tasmania, Hobart, Australia

<sup>2</sup>China University of Geosciences, Wuhan, China

<sup>3</sup>Mineral Resources Tasmania, Australia

Cassiterite (SnO<sub>2</sub>) occurs in a number of styles of tin mineralisation in Tasmania, including in greisen deposits, quartz-cassiterite±mica-wolframite-sulphide vein and stockwork deposits, proximal skarn deposits, carbonate replacement/distal skarn deposits, and associated alluvial deposits. Cassiterite can contain a variety of trace elements including Fe, Ti, W, Nb, Ta, Zr, Hf, V, Cr, U, and Sc, and the relationship between such trace elements and the style of tin mineralisation has been a topic of research for at least 60 years (Dudykina, 1959). However, the trace element chemistry of Tasmanian cassiterite has only been considered in a small number of studies (e.g. Yim, 1994) and cassiterite geochemistry was analysed in bulk cassiterite concentrates or with less sensitive methods such as electron microprobe analysis (EMPA).

In this study, cassiterite was analysed by laser ablation with inductively coupled plasma mass spectrometry (LA-ICP-MS), to define the trace element characteristics of cassiterite from each of the main deposit styles in Tasmania. Quartz ± mica – sulphide greisen hosted cassiterite from Anchor, Royal George and Rex Hill (with additional greisen from Aberfoyle), quartz-cassiterite±mica-wolframite-sulphide vein hosted cassiterite from Aberfoyle and Storeys Creek, stockwork hosted cassiterite from Great Pyramid, cassiterite from carbonate replacement/distal skarn deposits including Renison Bell and Cleveland, and cassiterite from proximal skarns including Mount Lindsay, Big Wilson and Granville, were analysed.

The LA-ICP-MS analyses of cassiterite show that the concentrations of many trace elements can be extremely variable even within a single sample. However, cassiterite from different styles of mineralisation still forms clear compositional clusters. Samples of greisen hosted cassiterite from deposits including Anchor, Aberfoyle, Royal George and Rex Hill contains the highest concentrations of Nb, Ta, Zr and Hf. The cassiterite chemistry from these deposits likely reflect two main styles of greisenisation: greisen at Anchor and Aberfoyle formed by auto-metasomatism of highly fractionated granites, where Nb, Ta, Zr and Hf were already concentrated, or in contrast at Royal George and Rex Hill, older granites were greisenised and Nb-Ta availability depends on the alteration of mica (Stepanov et al., 2014). High Zr and Hf may also indicate the high temperature of crystallisation.

Cassiterite hosted in quartz – cassiterite - wolframite veins from Aberfoyle and Storeys Creek contains high Zr and Hf, but low Fe (<1000 ppm) and Sc. Low Fe concentrations in this type of cassiterite may reflect a low Fe content in hydrothermal fluids, as these veins contain low abundances of Fe bearing minerals other than wolframite. Cassiterite from Great Pyramid quartz-cassiterite stockwork deposit is characterised by the lowest content of Zr and Ti, which likely indicates low temperature conditions of formation. This is also indicated by fluid inclusion data (Ruxton and Plummer, 1988) and the absence of metamorphism in the host sediments.

Cassiterite from proximal skarn deposits is variable, which is likely a reflection of the complex nature of these deposits. However, cassiterite from proximal skarns contains very high Fe, W and Ti. Cassiterite from carbonate replacement/distal skarn deposits is characteristically low in Nb and Ta but very high in Fe – a potential reflection of the lower mobility of Nb and Ta in hydrothermal fluids but a very high Fe availability, as evidenced by the massive pyrrhotite and pyrite commonly seen in these deposits.

The data collected in this study is consistent with Cheng et al. (2019). Iron, Ti and W are the most abundant trace elements in non-pegmatitic cassiterite (pegmatite hosted cassiterite can contain very high concentrations of Nb and Ta; Tindle and Breaks, 1998), however can exist in highly variable concentrations. Elements such as Nb, Ta, Zr, Hf, Sc, U, V and Cr vary more based on the deposit type. Cassiterite from greisen deposits contained the highest Ta and Hf in both datasets, however the data in this study shows that Tasmanian greisen hosted cassiterite contains the highest Nb and Zr concentrations. Elemental correlations are also consistent, where there are positive correlations between Nb and Ta, Zr and Hf, V and Sc, and W and U in this study.

Another similarity between the two studies is the presence of high and low W-U clusters, which were also observed in this study. These are most pronounced in the greisen cassiterite data, as clusters of >1000 ppm W and 0-100 ppm U, and <1000 ppm W and <10 ppm U. Cheng et al. (2019) suggested this was likely due to dissolution-recrystallization of cassiterite, and the stripping of these elements during this process. Zones of differing

W-U content showed different cathodoluminescence characteristics, which crosscut the primary oscillatory zoning. This should be tested for cassiterite from Tasmanian deposits by a combination of CL and detailed LA-ICP-MS work.

Overall, cassiterite from different styles of mineralisation in Tasmania can be differentiated by trace element chemistry. Trace element compositions of cassiterite could be a useful tool for the exploration of tin deposits, and the identification of the sources of alluvial tin placers.

#### References

Cheng, Y., Spandler, C., Kemp, A., Mao, J., Rusk, B., Hu, Y., Blake, K., 2019. Controls on cassiterite (SnO<sub>2</sub>) crystallization: Evidence from cathodoluminescence, trace-element chemistry, and geochronology at the Gejiu Tin District. *American Mineralogist*. 104, 1.

Dudykina, A.S., 1959. Paragenetic associations of element

admixtures in cassiterite of different genetic types of tin ore deposits. *Proceedings of the Institute of Geology of Ore Deposits, Petrography, Mineralogy and Geochemistry, Academy of Sciences*. 28, 111–121.

Ruxton, P.A., Plummer, G., 1988. Geology, metal zonation and fluid inclusion history of the Scamander Mineral Field, Northeast Tasmania - with particular reference to the Great Pyramid Tin Deposit. *Journal of the Geological Society*. 145, 137–138.

Stepanov, A., A. Mavrogenes, J., Meffre, S., Davidson, P., 2014. The key role of mica during igneous concentration of tantalum. *Contributions to Mineralogy and Petrology*. 167, 6.

Tindle, A.G., Breaks, F.W., 1998. Oxide minerals of the Separation Rapids rare-element granitic pegmatite group, northwestern Ontario. *Canadian Mineralogist*. 36, 609–635.

Yim, W.W.S., 1994. Particle size and trace element distribution characteristics of cassiterite as an aid to provenance study of stanniferous placers in northeastern Tasmania, Australia. *Journal of Southeast Asian Earth Sciences*. 10, 131–142.

# The Cantung Tungsten Mine, Northwest Territories, Canada: an overview of the mine geology and summary of ongoing research projects

H. Falck<sup>1</sup>, H. E. Jamieson<sup>2</sup>, B. Kazamel<sup>2</sup>, E. Salmabadi<sup>3</sup>, K. Hickey<sup>3</sup>, J. Hanley<sup>4</sup>, E. Adlakha<sup>4</sup>, A. Roy-Garand<sup>4</sup>,  
C. Lentz<sup>5</sup>, V. Elongo<sup>6</sup>, H. Legros<sup>6</sup>, P. Lecumberri-Sanchez<sup>6</sup> and K.L. Shelton<sup>7</sup>

<sup>1</sup>*NWT Geological Survey, Yellowknife, NT, Canada*

<sup>2</sup>*Geological Sciences and Geological Engineering, Queen's University, Kingston, ON*

<sup>3</sup>*Department of Earth, Ocean and Atmospheric Sciences, University of British Columbia Vancouver, BC*

<sup>4</sup>*Department of Geology, Saint Mary's University, Halifax, NS.*

<sup>5</sup>*Department of Earth Sciences, University of New Brunswick, Fredericton, NB*

<sup>6</sup>*Department of Earth and Atmospheric Sciences, University of Alberta, Edmonton, AB*

<sup>7</sup>*Department of Geological Sciences, University of Missouri, Columbia, MO USA*

The tungsten endowment of the Cantung W-Cu-Au skarn has been one of the most significant sources of the critical metal for the past 50 years. Since the opening of the Cantung mine in 1962, an estimated total of 6.97 Million tonnes (Mt) of ore has been extracted at an average grade of approximately 1.4% WO<sub>3</sub>. The most recent resource calculations (Delaney and Bakker, 2014) reported 3.483 Mt grading 0.97% WO<sub>3</sub> of Indicated Resources including 1.649 Mt grading 0.81% WO<sub>3</sub> of Probable Mineral Reserve and an additional 1.24 Mt of Inferred Mineral Resource grading 0.8% WO<sub>3</sub>. Despite its high grade, the mine has experienced numerous shutdowns during periods of low tungsten prices and profitability was limited, in part, due to high operating costs and problems with metallurgical recovery. The tungsten content of the tailings is considerable, with the potential for 4.9 to 6.0 Mt grading 0.28-0.32% WO<sub>3</sub>.

The mine is situated in the Canadian Cordillera, associated with Mid-Cretaceous felsic plutonic suites that were emplaced near the transition between shallower water carbonates of the Mackenzie Platform and siliciclastic rocks of the Selwyn Basin. Cretaceous magmatism (ca. 124–90 Ma; Mortensen et al., 2000; Hart et al., 2004) throughout Laurentian and peri-Laurentian rocks in the northern Cordillera is the product of subduction of the Farallon Plate and accretion of the Alexander terrane along the ancestral west coast of North America (Nelson and Colpron, 2007). Compression and associated uplift occurred through the Late Aptian to Early Albian stages of the Cretaceous (Hadlari et al., 2009). During this time, Proterozoic rift-related metasedimentary rocks and Cambrian to Devonian passive margin rocks were deformed into a thin-skinned fold and thrust belt, with dextral strain accommodated along transpressional structures active since the Early Cretaceous and continuing into the Cenozoic (Gabrielse et al., 2006). Most of the metasedimentary rocks in the northern portion of the Canadian Cordillera are of sub-greenschist facies metamorphic grade (e.g., Gordey and Anderson, 1993).

The Cantung stratigraphy has been deformed into a

regional NW-SE-trending syncline which defines the Flat River Valley (Figure 1) (Armstrong et al., 1983). Locally, the ore-hosting stratigraphy has been folded into a near-recumbent macroscopic fold (the Mine Fold) with a shallow, south-dipping axial plane (Figure 2). The local stratigraphy consists of the Lower Argillite, Swiss Cheese Limestone, Ore Limestone, Upper Argillite and Dolomite units. The Lower Argillite Member belongs to the Proterozoic Vampire Formation and comprises metamorphosed mudstone and fine-grained sandstone. The overlying units are members of the Lower Cambrian Sekwi Formation. The Swiss Cheese Limestone consists of interbedded dolomitic siltstone and fine-grained impure limestone. The overlying Ore Limestone is a relatively pure carbonate layer up to 50 m in thickness with minor dolomitic and argillitic laminations. The Upper Argillite is a heterogeneous layer of interbedded pyritic shale, carbonate, and turbiditic quartzite. Overlying the Upper Argillite is a 500 m thick sequence of dolomite interbedded with sandstone, siltstone, limestone and shale. The uppermost exposed unit in the area is the Cambrian Rabbitkettle Formation, which unconformably overlies the Sekwi Formation and comprises thinly bedded, silty to graphitic limestone and black shales (cf Rasmussen et al., 2011).

## Interactions between regional deformation and pluton emplacement

The underground orebody is developed along the lower, overturned limb of a large near-recumbent antiform, which exerts a first-order control on the distribution and grade of mineralization. This fold has a strongly curved hinge line and is largely oblique to the regional NW-SE structural trend suggesting a complex deformation history. The attitude and geometry of the Mine Fold does not correlate with regional-scale fold structures observed outside the mine.

The regional set of upright NW-SE-trending F<sub>1</sub> folds and corresponding axial planar S<sub>1</sub> foliation are a product of a major crustal shortening event, D<sub>1</sub>, which affected

Cantung and the surrounding regions. Geological mapping in the region has not identified any correlative structures to the Mine Fold antiform. The Mine Fold geometry is hypothesised to be the result of sub-vertical shortening and northward flow of Vampire and Sekwi Formation rocks during emplacement of the Tungsten Suite. In the Cantung area, the Tungsten suite is expressed by the Mine Stock and Circular Stock monzogranitic plutons that intruded the stratigraphic sequence and are responsible for the contact metamorphism. Aplitic and kersantitic lamprophyre dykes are also found near the mineralization (Mathieson and Clark, 1984). Thermal weakening localized shortening within the contact metamorphic aureole. The local presence of limestone units immediately above the Mine Stock also favoured ductile flow. Shortening resulted in the development of the  $S_2$  crenulation cleavage. It is possible that shortening may have been initiated by emplacement of the larger parent magma body prior to final emplacement of the Mine Stock (Rasmussen et al., 2011). The only other localities where inclined folds are observed, marking deviations from the upright regional fold train, are localities that consist predominately of carbonate units and a large intrusive body emplaced in close proximity.

### Apatite mineral chemistry

Skarn-hosted apatite REE geochemistry exhibit four different patterns; however, the two most noteworthy are: i) negatively sloped (average LaN/YbN range 3.9 to 10) REE patterns with negative Eu anomalies (average EuN/Eu\* ranging 0.3 to 0.4; whereby  $Eu^* = \sqrt{[SmN \cdot GdN]}$ ), and ii) concave up (i.e. relatively low MREE) patterns with positive Eu anomalies (EuN/Eu\* ranging 1.5 to 8.8).

Both patterns were observed in zoned apatite, and the second pattern is unique considering experimental work by Ayers and Watson (1993) show that MREE are most compatible with hydrothermal apatite and  $Eu^{2+}$  is the least compatible REE. This data may be explained by the fractionation of MREE into apatite, or mixing of two different fluids. Fractionation of MREE from a type-i fluid by apatite crystallization could form a positive Eu anomaly; however,  $Eu^{2+}$  rich cores of zoned apatite are inconsistent with this model. Additionally, local phases show low REY and did not fractionate MREE from the fluid. Alternatively, MREE may have been fractionated from the source magma and produced a MREE depleted fluid. Such a magma would likely have been amphibole-saturated.

Primary melt inclusions occur within magmatic apatite in the Mine Stock Intrusion, offering an opportunity to characterize the primary tungsten (+Cu, Bi, Au) content of magmas spatially and genetically associated with the Cantung skarn. Melt inclusions show a range in composition from felsic to mafic affinities, with more mafic inclusions associated with Si- and LREE-depleted xenocrystic apatite cores (Adlakha et al., 2018). Mafic magmas in the system are also evidenced by the presence of lamprophyre dykes near sites of mineralization. The data suggest a possible link between mixing of mafic and felsic magmas with skarn mineralization.

The relationship between melt inclusions and apatite composition is being investigated. This work will determine the chemical composition (major and trace elements, including ore metals) of melt inclusions using LA-ICPMS to evaluate the tungsten “fertility”. The technique will be employed on the Mine Stock pluton

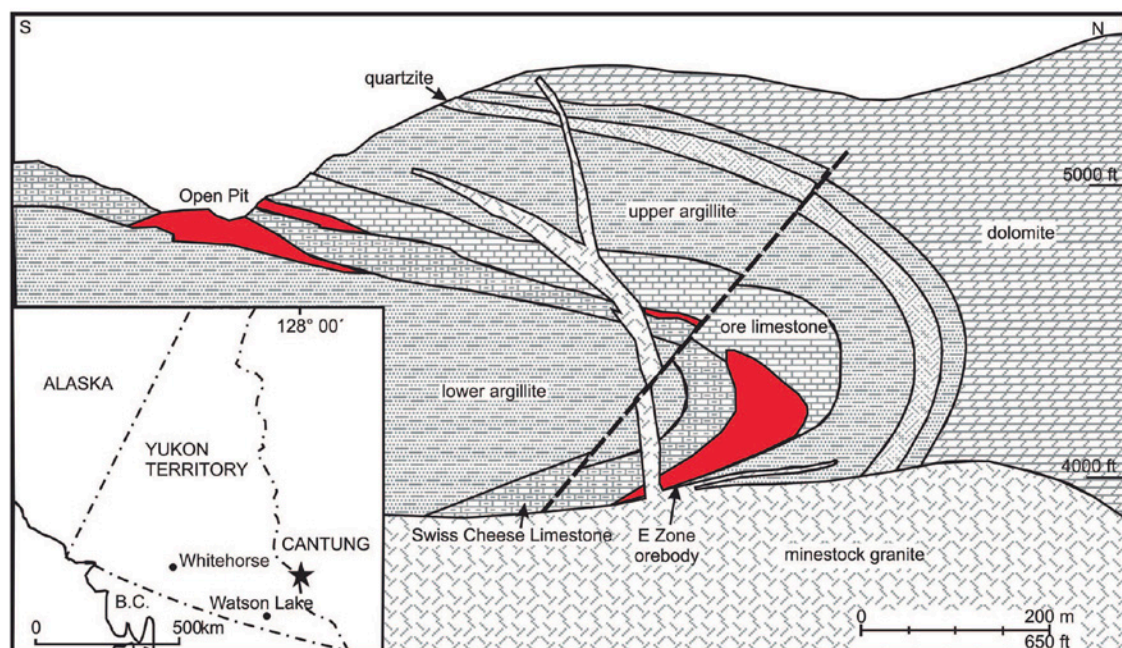


Figure 1. Cross section of the Cantung W-Cu-Au skarn and surrounding areas looking West. (From Adlakha et al. 2018) The skarns and associated W-mineralization are hosted in Sekwi Formation carbonates in the lower limb of a near-recumbent antiform (the “Mine Fold”). The lower limb of the Mine Fold is truncated by the Mine Stock, a 98.2 Ma monzogranite intrusion that is part of the Tungsten plutonic suite. Formation of the skarn post-dates formation of the Mine Fold, and emplacement of the Mine Stock.

and determine the parental magmatic affinity of the magmas at depth (e.g., VAG, syn-collisional), including the potential role of mafic magmas in the evolution of tungsten skarns.

The results of apatite studies have been applied to interpreting regional stream sediment surveys. Heavy mineral separates from stream sediments collected from the Flat River Valley to the north and south of the mine site have been characterized using automated mineralogy methods (SEM-MLA). Scheelite is identified locally within a few hundred meters of the mine site, whereas regionally, a range of apatite compositions with at least 6 distinct REE patterns have been identified. A comparison between these and the apatite generations observed at Cantung in the skarn mineralization and associated intrusions is in progress.

### Origin of mineralizing fluids

To determine the role of mantle components in the magma associated with mineralization, the isotopic signature of the tungsten-bearing mineral, scheelite, as well as the isotopic signatures of local lithologies are being investigated. As scheelite is a Ca tungstate, it can incorporate significant amounts of Sr in its Ca site. The Sr isotopic signature for scheelite crystals hosted in argillites located below the skarn orebodies is expected to be representative of the least modified magmatic fluid. Thus, it can be compared to those of other lithologies including the granitic plutons and the lamprophyre dykes. The results will provide information on the nature of the magmatic system and the mechanisms involved in Cantung mineralization.

### Gold-Bismuth mineralization

Early exploration efforts tested for gold at Cantung, but low gold grades combined with low prices resulted in a cessation of fire assaying. However, a correlation between elevated concentrations of gold within the copper concentrate and elevated bismuth concentrations was noticed by the mill metallurgists and researchers examining scheelite-bearing quartz veins (Yuvan et al., 2007).

Samples from the E-Zone and Open Pit, including samples from recently developed underground headings (Amber Zone, West Extension) were used to investigate the nature of the gold. Gold was present as electrum with approximately 30 wt.% silver. The associated mineral assemblage included predominantly native bismuth with bismuth tellurides (with variable amounts of selenium with the bismuth and tellurium), very minor amounts of bismuthinite, as well as hessite. The textures exhibited by gold, bismuth and the bismuth tellurides suggest they began saturation during the growth of the silicate minerals and persisted until the silicates had been completely formed. Their textures also suggest they saturated from the fluid as low temperature polymetallic melts out of which each mineral exsolved. Bismuth melts formed in the presence of aqueous hydrothermal fluids have the capacity to sequester gold from hydrothermal fluids, without gold concentrations in these fluids having to reach saturation (Douglas et al., 2000). Furthermore, experimental modelling has shown a liquid bismuth melt in equilibrium with a hydrothermal fluid with a lower  $fO_2$  for a fixed pH and temperature can incorporate more Au than the same fluid with a higher  $fO_2$  (Tooth et

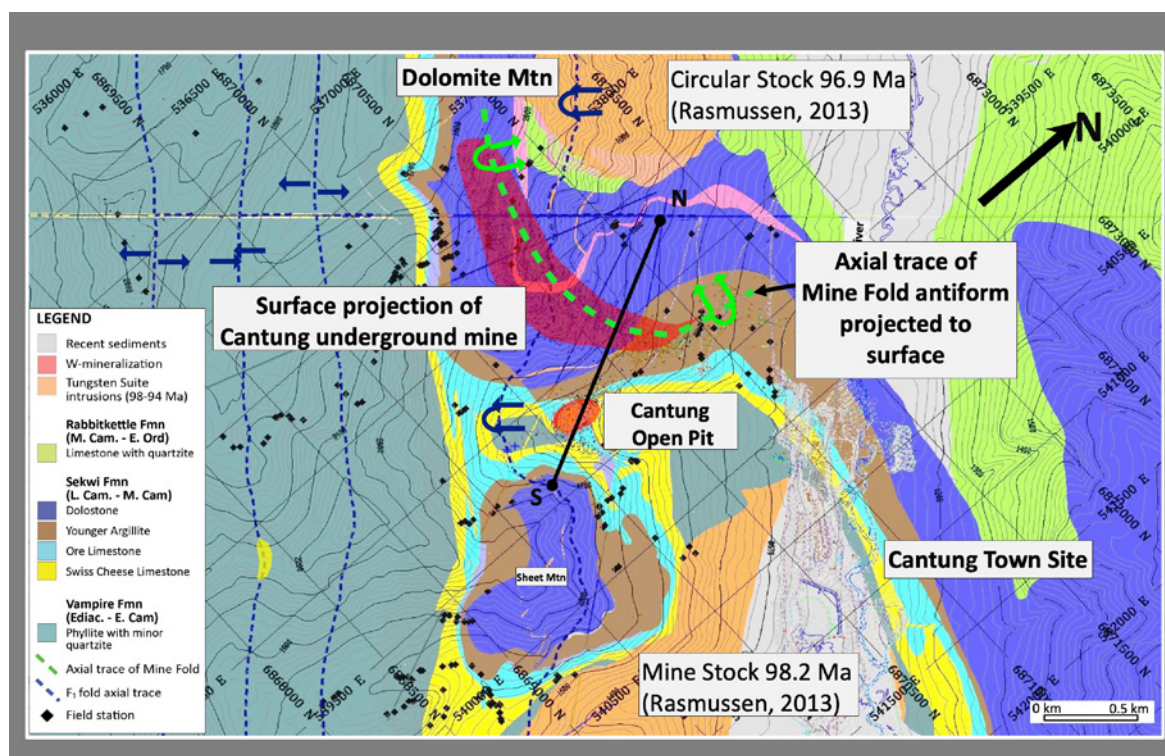


Figure 2. Surface geology at the Cantung Mine (From Salmabadi et al. 2019; modified from Blusson, 1968). The location of the cross section is marked by the N-S line. The projections of ore zones to the surface are shown in red shading.

al., 2008). The same concentration of gold dissolved in a bismuth melt can occur from a fluid with two orders of magnitude less gold concentration than that of the fluid previously mentioned if it has a very low  $fS_2$  (below pyrrhotite stability). This means that a bismuth melt saturating from a fluid with low  $fO_2$  and  $fS_2$  values, at a fixed temperature and pH, can incorporate the highest Au-concentration at a fixed chloride concentration.

### Tailings characterization and tungsten mobility in the environment

An additional research objective is to create a comprehensive plan for reprocessing all tailings, recovering previously lost tungsten, as well as producing a sulphide concentrate from which copper and gold might be extracted. To characterize the tailings, fifty samples with varying tungsten content from 0.11 to 0.65% W were collected from four tailings ponds, and one sample from the Flat River tailings. The automated mineralogy results demonstrated significant variation in the relative amounts of silicates, pyrrhotite, carbonates and oxides in the tailings, which may influence reprocessing design and environmental behavior. There is up to 30% pyrrhotite in the tailings, but little pyrite. In contrast, the Flat River tailings exhibit extensive oxidation with less than 2% sulphide remaining, and 60% iron oxides. The scheelite grain size appears to be bimodal, based on the samples analysed to date. More than 50% of the scheelite is partially liberated. Bottle Roll tests demonstrated potential issues for most samples as the concentration of calcium was elevated (400 to 600 ppm) such that it is likely to interfere with a fatty-acid type of surfactant used in froth flotation.

For the tungsten mobility project, porewater samples were collected using suction lysimeters and by centrifuging tailings samples. The variable pH and Eh conditions, and striking differences in mineralogy mean that Cantung is an ideal place to study W mobility.

### References

- Adlakha, E., Hanley, J. Falck H., and Boucher, B. 2018. The origin of mineralizing hydrothermal fluids recorded in apatite chemistry at the Cantung W-Cu skarn deposit, NWT, Canada. *European Journal of Mineralogy*, v. 30, n.6, p. 1095-1113.
- Armstrong, D.W., Harris, F.R., Kerrigan, J.E., Kiehn, O.A., Johnson, R.E., 1983. *Technological Assessment Report of Canada Tungsten Mining Corporation Ltd., Tungsten, NWT*. Amax Engineering and Management Services Company, Canada.
- Ayers, J. C., Watson, E. B. 1993. Apatite/fluid partitioning of rare-earth elements and strontium: Experimental results at 1.0 GPa and 1000 C and application to models of fluid-rock interaction. *Chemical Geology*, v. 110, n.1-3, p. 299-314.
- Delany, B. and Bakker F.J., 2014 *Technical Report on the Cantung Mine Northwest Territories Canada*, North American Tungsten Corporation, Sept. 19, 2014. 148 p.
- Douglas, N., Mavrogenes, J., Hack, A., England, R., 2000, The liquid bismuth collector model: An alternative gold deposition mechanism, in Skilbeck, C.G., and Hubble, T.C.T., eds., *Understanding planet Earth; searching for a sustainable future; on the starting blocks of the third millennium: Australian Geological Convention, 15th, Sydney, Abstracts: Sydney, Geological Society of Australia, 135 p.*
- Gabrielse, H., Murphy, D.C., Mortensen, J.K., 2006. Cretaceous and Cenozoic dextral orogen-parallel displacements, magmatism, and paleogeography, north-central Canadian Cordillera. In: Haggart, J.W., Enkin, R.J., Monger, J.W.H. (Eds.), *Paleogeography of the North American Cordillera: Evidence For and Against Large-Scale Displacements: Geological Association of Canada Special Paper 46*, p. 255–276.
- Gordey, S.P., Anderson, R.G., 1993. Evolution of the Northern Cordilleran Miogeocline, Nahanni Map Area (1051), Yukon and Northwest Territories. *Geological Survey of Canada Memoir 428*.
- Hadlari, T., Thomson, D., Schröder-Adams, C.J., Lemieux, Y., MacLean, B., Gabites, J., 2009. Evolution of a Northern Cordilleran foreland basin inferred from Cretaceous stratigraphy. Seismic Sections, and Detrital Zircons, Mackenzie Mountains, NWT. *Frontiers + Innovation, CSPG CSEG CWLS Convention*, p. 128–130.
- Hart, C.J.R., Goldfarb, R.J., Lewis, L.L., Mair, J.L., 2004. The northern cordilleran mid- Cretaceous plutonic province: ilmenite/magnetite-series granitoids and intrusion-related mineralization. *Resour. Geol.* v. 54, p. 253–280.
- Mathieson, G. A., Clark, A. H., 1984. The Cantung E Zone scheelite skarn orebody, Tungsten, Northwest Territories; a revised genetic model. *Economic Geology*, v. 79, n. 5, p. 883-901.
- Mortensen, J.K., Hart, C.J.R., Murphy, D.C., Heffernan, S., 2000. Temporal evolution of Early and mid-Cretaceous magmatism in the Tintina Gold Belt. In: Jambor, J. (Ed.), *The Tintina Gold Belt: Concepts, Exploration and Discoveries*. British Columbia and Yukon Chamber of Mines Special Volume, 2, p. 49–57.
- Nelson, J., Colpron, M., 2007. Tectonics and metallogeny of the British Columbia, Yukon and Alaska Cordillera, 1.8 Ga to present. In: Goodfellow, W.D. (Ed.), *Mineral Resources of Canada: A Synthesis of Major Deposit-types, District Metallogeny, the Evolution of Geological Provinces, and Exploration Methods: Geological Association of Canada Special Publication*, v. 5, p. 755–792.
- Rasmussen, K.L., Lentz, D.R., Falck, H., Pattison, D.R.M., 2011. Felsic magmatic phases and the role of late-stage aplitic dykes in the formation of the world-class Cantung Tungsten skarn deposit, Northwest Territories, Canada: *Ore Geology Reviews*, v. 41, p. 75-111.
- Rasmussen, K.L., Mortensen, J.K. 2013 Magmatic petrogenesis and the evolution of (F:Cl:OH) fluid composition in barren and tungsten skarn-associated plutons using apatite and biotite compositions: case studies from the northern Canadian Cordillera. *Ore Geol. Rev.*, v. 50, p. 118–142.
- Tooth, B., Brugger, J., Ciobanu, C., Liu, W., 2008. Modeling of gold scavenging by bismuth melts coexisting with hydrothermal fluids. *Geology*, v. 36, no. 10, p. 815–818.
- Yuvan, J., Shelton, K., Falck, H., 2007. Geochemical investigations of the high-grade quartz-scheelite veins of the Cantung Mine, Northwest Territories. In: Wright, D.F., Lemkow, D., Harris, J.R. (Eds.), *Mineral and Energy Resource Assessment of the Greater Nahanni Ecosystem under Consideration for the Expansion of the Nahanni National Park Reserve, Northwest Territories: Geological Survey of Canada Open File 5344*, p. 177–190.

# The Mactung Tungsten Deposit, Northwest Territories, Canada: an overview of the geology and summary of ongoing research projects

H. Falck<sup>1</sup>, E. Martel<sup>1</sup>, B. Fischer<sup>1</sup>, A.L. Gebru<sup>2</sup>, D.R. Lentz<sup>2</sup>, E. Adlakha<sup>3</sup>, J. Hanley<sup>3</sup>, A. Roy-Garand<sup>3</sup>,  
V. Elongo<sup>4</sup>, H. Legros<sup>4</sup>, P. Lecumberri-Sanchez<sup>4</sup>, and G. Kirkham<sup>5</sup>

<sup>1</sup>NWT Geological Survey, Yellowknife, NT, Canada

<sup>2</sup>Department of Earth Sciences, University of New Brunswick, Fredericton, NB

<sup>3</sup>Department of Geology, Saint Mary's University, Halifax, NS.

<sup>4</sup>Department of Earth and Atmospheric Sciences, University of Alberta, Edmonton, AB

<sup>5</sup>Kirkham Geosystems, Vancouver, BC

The Mactung W-Cu-Au skarn deposit, discovered in 1962 on the border between the Northwest Territories and Yukon, Canada, contains a significant drill-defined resource of tungsten oxide (an Indicated Mineral Resource of 33.0 Million tonnes (Mt) grading 0.88% WO<sub>3</sub>, including a Probable Mineral Reserve of 8.5 Mt grading 1.18% WO<sub>3</sub>, and additional Inferred Resources of 11.9 Mt grading 0.78% WO<sub>3</sub>; Narisco, 2009). A review of the prefeasibility study duplicated the global resource but also showed the sensitivity of resource estimates to the selection of cut-off grade, providing a model estimate of 17 Mt total mineral resources with within an optimized pit shell, which demonstrate reasonable prospects of eventual economic extraction (note that this is not a "Mineral Resource" for National Instrument 43-101 purposes) grading 0.969% WO<sub>3</sub> and 0.078% Cu at a cutoff grade of 0.5% versus 10 Mt grading 1.21% WO<sub>3</sub> and 0.117% Cu at a higher cut-off of 0.8% (Kirkham, 2018). Both gold and bismuth are anomalous in at least some parts of the orebody (Gebru, 2017), but too few samples have been assayed for these metals to be included in a resource estimation.

The Mactung deposit is located within the foreland fold-and-thrust belt of the Cordilleran orogen, within a succession that includes late Neoproterozoic to early Devonian, terrigenous and carbonate strata deposited on the eastern slope of the Selwyn Basin, and Middle to Late Devonian, terrigenous clastic strata of a successor basin. The deposit is associated with Mid-Cretaceous felsic plutonic suites that were emplaced (ca. 124–90 Ma; Mortensen et al., 2000; Hart et al. 2004) throughout Laurentian and peri-Laurentian rocks of the northern Cordillera, a result of subduction of the Farallon Plate and accretion of the Alexander terrane along the ancestral west coast of North America (Nelson and Colpron, 2007). Compression and associated uplift occurred from the Late Aptian through Early Albian stages of the Cretaceous (Hadlari et al., 2009). During this time, the supracrustal rocks were deformed into a thin-skinned fold and thrust belt, with dextral strain accommodated along transpressional structures from the Early Cretaceous into the Cenozoic (Gabrielse et al., 2006).

Regional metamorphism associated with deformation produced biotite in mudrocks and converted carbonate rocks to marbles, generating micaceous foliation in the former and cleavage in the latter.

Two intrusions at Mactung, the Cirque Lake stock north of the orebody and the Rockslide Mountain stock south of it (Figure 1), comprise various phases of biotite granitoid rock dated at 97.1 to 97.6 Ma ( $\pm 0.2$  to 0.4 Ma; Gebru, 2017), except for a phase of the Cirque Lake stock dated at 92.1  $\pm 0.2$  Ma (Selby et al., 2003). The intrusions caused thermal metamorphism and metasomatic alteration in the country rocks. The thermal metamorphism converted terrigenous mudstones to hornfels, calcareous mudstones to calc-silicate rocks, and marbles to re-crystallized marbles. The metasomatic alteration did not affect the intrusions themselves, but in the country rocks, led to the development of various types of scheelite-bearing and scheelite-poor skarns in the limestone, marble, and calc-silicate hornfels, and bleaching and invasion of quartz  $\pm$  calc-silicate veins in the terrigenous hornfels.

At Mactung, two contact metasomatic skarn zones developed in originally carbonate rocks (Figure 2A). The Lower ore zone developed in the Early Cambrian Sekwi Formation, and the Upper ore zone in the Cambro-Ordovician Rabbitkettle Formation. The Sekwi Formation host was a limestone debrite of varying thickness that probably originated by slope failure of semi-lithified nodular lime muds. The Rabbitkettle Formation host consists of three stacked layers collectively forming the Upper ore zone. The lowermost layer coincides with the basal member of the formation (member D), which is a phosphatic, quartz-sandy limestone conglomerate to calcareous sandstone interstratified with thin-bedded silty limestone, and the skarnoid, calc-silicate equivalents of those rocks. Member D probably originated through prolonged bottom current winnowing, repeated sediment gravity flows possibly caused by seismic events, and episodic fluvial input on a carbonate shelf where phosphogenesis was a significant contributor to sediment formation (Fischer et al., 2018). The middle and upper layers of the Upper ore zone are in member

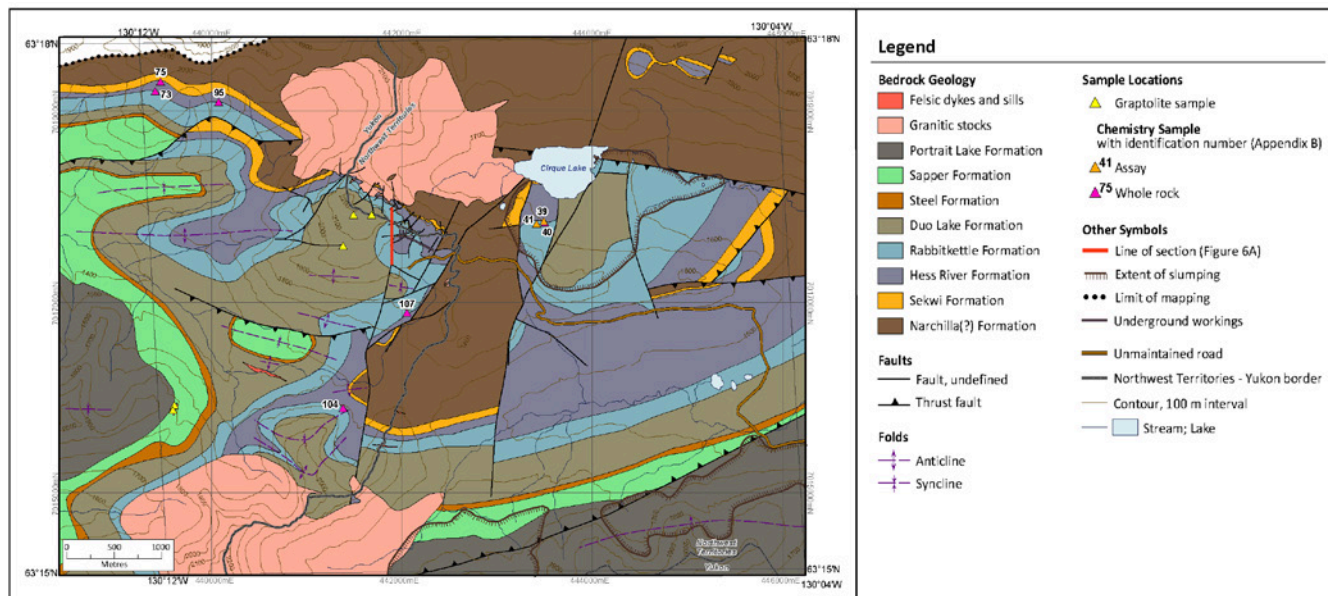


Figure 1. Simplified bedrock geology of the Mactung area. Known mineralization is within the Sekwi and Rabbitkettle formations south of the Cirque Lake stock. The adit entrance is at the eastern end of the underground workings. Contour lines are 100 m apart. (From NTGS Open File report 2018-02).

EF of the Rabbitkettle Formation. Member EF consists of interbedded limestone and mudstone and the hornfelsed and skarnoid equivalents of those rocks. The middle and upper layers of the Upper ore zone coincide with thick intervals of calc-silicate rock; protoliths were mainly limestone and minor mudstone. These thick intervals are separated by layers of unmineralized rock; protoliths were mainly mudstone. In the Lower ore zone, the intensity of metasomatic alteration increases across a series of intergradational zones, from bleached limestone on the eastern periphery of the deposit, through scheelite-poor marble skarn to scheelite-bearing pyroxene skarn and finally to scheelite-rich pyrrhotite skarn in the core of the Lower ore zone (Atkinson and Baker, 1986; Harris 1980). Tungsten is hosted mainly in scheelite, copper in chalcopyrite, and gold mainly in native bismuth. Skarn mineralization was co-eval with crystallization of the oldest phases of the two stocks  $97.2 \pm 0.2$  Ma by Re-Os of molybdenite in quartz veins (Gebru, 2017), and  $97.1 \pm 4.1$  Ma by U-Pb of titanite in skarn (Selby et al., 2003). Both the Lower and Upper ore zones dip gently to the south, concordant with bedding. Folds on the property are mostly open, although two tight folds are recognized (one on Fold Mountain and an underground one affecting the Sekwi Formation). Plunges are shallow to the west or west-northwest in the west part of the map area, shallow to the east in the east part of the map area, and perhaps shallow to the northeast on Fold Mountain. A north-verging thrust fault passes north of the deposit, truncated by the Cirque Lake stock. A few north-trending steep faults cross the map area, one of them displacing part of the Rockslide Mountain stock but apparently truncated by the Cirque Lake stock (Abbott, 2013), which if true implies that the fault pre-dates one pluton and post-

dates the other. A number of northeast- and northwest-trending faults on the north face of Mount Allan show metre-scale displacements.

### Petrogeochemical and geochronological examination of granitic phases

The two granitoid intrusions associated with the Mactung deposits are comprised of a number of phases, including a leucogranite and a K-feldspar and plagioclase porphyritic biotite granite, with a related plagiogranite and associated undivided granite dykes that are fractionation and alteration products (Gebru, 2017; Selby et al., 2003). Major- and trace-elements have been used to discriminate between the distinct phases of biotite granite and the leucogranite. The biotite granite has an arc-like affinity, possibly derived from the recycling of I-type crust. The leucogranite is transitional with a highly fractionated S- and crustal A-type affinity; due to its low Na/K, Zr, REE, and higher Rb, a source involving anatexis of a supracrustal sequence in a syn-collisional setting is hypothesized. Tracer isotopes in the Sm-Nd and Rb-Sr systems further indicate a very old continental crust as the likely magma source for the granitoids. Source rocks have crustal residence age of 1.9-2.3 Ga. The  $\delta^{18}\text{O}$  values of Mactung granitoids indicate strong metasedimentary contamination from the source region or during magma ascent. Depth of magma generation was likely deeper than 20 km (Gebru, 2017).

U-Pb age data of zircon grains were obtained by ID-TIMS analytical techniques for five samples from three rock types of Mactung granitoids: an aplitic dyke south of the Mactung skarn tungsten deposit yields igneous crystallization age of  $97.1 \pm 0.2$  Ma; porphyritic biotite granite from the main phase of the Mactung pluton

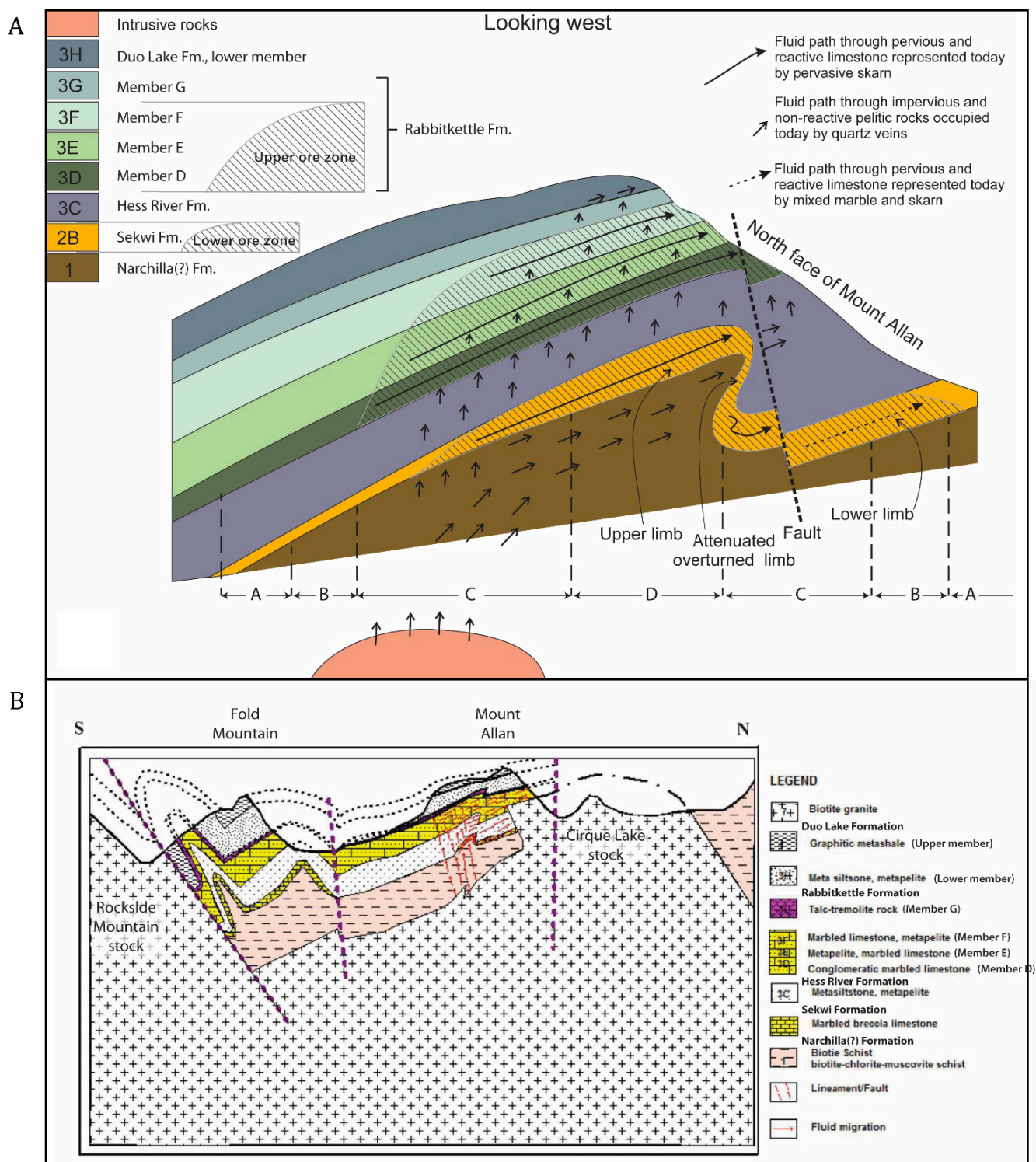


Figure 2. Cross sections of the Mactung deposit:

A) Mineralization models for Mactung (from Fischer et al. 2018 NTGS Open File report 2018-02), showing hypothetical migration patterns of metasomatic fluids on a schematic cross-section looking west. Mineralizing fluids arise from an undiscovered pluton presumed to lie buried south of the deposit. Note the Z-fold in the Sekwi Formation. The alteration zones A to D within ore-bearing units (the Sekwi Formation and members D, E and F of the Rabbitkettle Formation) are as follows: A = Marbles variably bleached and cross-cut by garnet and garnet-pyroxene skarn, B = Garnet-pyroxene skarn (local remnant bleached marble), C = Pyroxene skarn, no remnant marble, D = Pyrrhotite-pyroxene skarn, no remnant marble.

B) Regional N-S cross Section showing the setting for the Mactung Deposit and the relationship of the Cirque Lake and Rockslide stocks (From A.L. Gebru, 2017 Ph.D. Thesis UNB.) Mineralizing fluids arise from the Cirque Lake stock, which joins the Rockslide Mountain stock underneath the Mactung deposit. Cross-section extends from north of the Cirque Lake stock to the north face of Rockslide Mountain in the south, at the same easting as the section in A). Fm = Formation.

gives a crystallization age of  $97.6 \pm 0.2$  and  $97 \pm 0.1$  Ma. Leucocratic granite dyke, a marginal phase in the southeast of the pluton, gives an age of  $97 \pm 0.3$  Ma. Ar-Ar dating of micas yielded ages largely falling between  $95.6 \pm 0.3$  to  $91.1 \pm 0.7$  Ma. The Ar-Ar dates demonstrate the reheating of the crust near Mactung and a possible emplacement of late-stage granite phases up until 91 Ma. The less evolved biotite granite is directly associated with the W-(Cu-Bi-Au) mineralization, based on field relationships, metallogenic aspects of the intrusion, alteration-mineralization effects, and previously published Re-Os dating of molybdenite and new multifaceted geochronological data (Selby et al., 2003; Gebru, 2017).

The source pluton is agreed to lie beneath the orebody. One suggestion is that the source is a buried pluton that has not yet been discovered (Atkinson and Baker, 1986); a more recent suggestion is that the Cirque Lake pluton extends south under the ore zones (Gebru, 2017) (Figure 2B). The fluorine and chlorine composition of biotite appears to be important prognostic criteria in identifying fertile granites for tungsten mineralization.

### Apatite mineral chemistry

Three generations of skarn-hosted fluorapatite associated with the Mactung deposit were characterized in order to understand the chemical evolution and signatures of mineralizing fluids.

Early type-i apatite is texturally associated with detrital phosphate nodules in skarned limestone and is likely the earliest generation of apatite based on textural analysis. The apatite contains variable  $\Sigma$ REY, negative sloping chondrite normalized REY patterns, and weak negative Eu anomalies. These patterns are similar to those of the phosphate nodules, suggesting that these apatites are recrystallization products, possibly during contact metamorphism prior to the onset of hydrothermal fluids.

Type-ii apatite occur with hedenbergite, titanite, anorthite, and late scheelite. The type-ii apatite are paragenetically early in the mineral assemblage and show no zoning using cathodoluminescence. Individual grains in a single sample may show contrasting compositions, reflecting a continuum between two end-member REY patterns, similar to type-i and type-iv patterns observed for apatite at Cantung (Adlakha et al., 2018). High  $\Sigma$ REY patterns are relatively flat with negative Eu anomalies; whereas, low  $\Sigma$ REY patterns show MREE depletion and positive Eu anomalies. The REY variation may reflect fractionation of MREE by apatite or other phases, or two fluids of contrasting compositions. Fractionation of MREE by apatite is unlikely as the apatite are not zoned and scheelite or other phases did not fractionate MREE based on textural and trace element data. Therefore, REY patterns likely reflect two fluids of contrasting composition. Considering the similarities in mineral chemistry between Mactung and Cantung apatite, fluids for the two deposits were likely similar. Additionally,

host rock and co-crystallizing phases had little influence on fluid and apatite chemistry, considering the skarns which host the apatite from the two deposits are drastically different (pyroxene skarn at Mactung and biotite-amphibole skarn at Cantung).

Late type-iii apatite is associated with cross-cutting quartz-scheelite veins. Apatite contains high  $\Sigma$ REY, exhibits bowl-shaped REY patterns corresponding to low MREE, and no Eu anomaly. Vein-hosted scheelite REY patterns indicate that they did not fractionate MREE. Type-iii apatite composition, therefore, likely records MREE depleted mineralizing fluids. The source and composition of fluid recorded by such apatite is still poorly understood and research is currently being conducted in order to constrain the origin of the fluid.

The relationship between melt inclusions and apatite composition is also being investigated. This work will determine the chemical composition (major and trace elements, including ore metals) of melt inclusions using LA-ICPMS to evaluate the tungsten "fertility". The technique will be employed on the Cirque Lake and the Rockslide Mountain stocks and determine the parental magmatic affinity of the magmas at depth (e.g., VAG, syn-collisional), including the potential role of mafic magmas in the evolution of tungsten skarns.

Mactung and the other tungsten deposits found in the Selwyn basin share common features and are spatially associated with felsic plutons of the same plutonic suite. Studies of Cantung among these deposits, have demonstrated a potential interconnection to mafic magma, based on the results of the study of apatite chemistry and melt inclusions (Adlakha et al., 2018) and the presence of co-eval lamprophyre dykes near the orebodies. In this context, we suspect that Mactung can originate from the same processes as Cantung. In order to determine whether Mactung is purely related to the granitic plutons, a comparative isotopic study is being done. As scheelite is a Ca tungstate, it can incorporate significant amounts of Sr in its Ca site. The Sr isotopic signature of scheelite hosted in clastic units located below the skarn orebodies, representative of the least modified primary magmatic fluid, is being compared to those of other local lithologies. The results will highlight the processes responsible for the Mactung mineralization.

### References

- Abbott, J.G., 2013. Bedrock geology of the Macmillan Pass area, Yukon and adjacent Northwest Territories (NTS 105O/1, 2 and parts of 105O/7, 8 and 105P/4, 5). Yukon Geological Survey, Geoscience Map 2013-1, 1 map at 1:50 000 scale and legend sheet.
- Adlakha, E., Hanley, J. Falck H., and Boucher, B. 2018. The origin of mineralizing hydrothermal fluids recorded in apatite chemistry at the Cantung W-Cu skarn deposit, NWT, Canada. *European Journal of Mineralogy*, v. 30, n.6, p. 1095-1113.
- Atkinson, D. and Baker, D.J., 1986. Recent developments in the geologic understanding of Mactung. In Morin, J.A. (editor), *Mineral Deposits of Northern Cordillera*; Canadian Institute

of Mining and Metallurgy, Special Volume 37, p. 234-244.

Fischer, B.J., Martel, E., and Falck, H., 2018. Geology of the Mactung tungsten skarn and area– Review and 2016 field observations; Northwest Territories Geological Survey, NWT Open File 2018-02, 84 pages and appendices.

Kirkham, G., 2018. Appendix A: Mactung deposit resource report. In: Fischer, B.J., Martel, E., and Falck, H., Geology of the Mactung tungsten skarn and area – Review and 2016 field observations; Northwest Territories Geological Survey, NWT Open File 2018-02, 84 pages and appendices.

Gabrielse, H., Murphy, D.C., Mortensen, J.K., 2006. Cretaceous and Cenozoic dextral orogen-parallel displacements, magmatism, and paleogeography, north-central Canadian Cordillera. In: Haggart, J.W., Enkin, R.J., Monger, J.W.H. (Eds.), Paleogeography of the North American Cordillera: Evidence For and Against Large-Scale Displacements: Geological Association of Canada Special Paper 46, p. 255–276.

Geburu, A., 2017. Petrogenesis of granitoids in the vicinity of the Mactung tungsten skarn deposit, Northeast Yukon-Northwest Territories: Characterization of skarn mineralization and causative plutons through geological, petrochemical, mineralogical, and geochronological analysis; Unpublished Ph.D. thesis, University of New Brunswick, 752 p.

Hadlari, T., Thomson, D., Schröder-Adams, C.J., Lemieux, Y., MacLean, B., Gabites, J., 2009. Evolution of a Northern Cordilleran foreland basin inferred from cretaceous stratigraphy. Seismic Sections, and Detrital Zircons, Mackenzie Mountains, NWT. *Frontiers + Innovation, CSPG CSEG CWLS Convention*, p. 128–130.

Harris, F.R., 1980. Geology of the Macmillan tungsten deposit,

AMAX of Canada Limited, April, 1980; Northwest Territories Geological Survey, Mactung collection, Report number MT 1980-28, 15 p.

Hart, C.J.R., Goldfarb, R.J., Lewis, L.L., Mair, J.L., 2004. The northern Cordilleran mid- Cretaceous plutonic province: ilmenite/magnetite-series granitoids and intrusion-related mineralization. *Resource Geol.* v. 54, p. 253–280.

Mortensen, J.K., Hart, C.J.R., Murphy, D.C., Heffernan, S., 2000. Temporal evolution of Early and mid-Cretaceous magmatism in the Tintina Gold Belt. In: Jambor, J. (Ed.), *The Tintina Gold Belt: Concepts, Exploration and Discoveries*. British Columbia and Yukon Chamber of Mines Special Volume, 2, p. 49–57.

Narisco, N., 2009. Technical report on the Mactung property. Prepared by Wardrop for North American Tungsten Corporation Ltd., April 3, 2009; Northwest Territories Geological Survey, Mactung collection, Report number MT 2009-04, 333 p.

Nelson, J., Colpron, M., 2007. Tectonics and metallogeny of the British Columbia, Yukon and Alaska Cordillera, 1.8 Ga to present. In: Goodfellow, W.D. (Ed.), *Mineral Resources of Canada: A Synthesis of Major Deposit-types, District Metallogeny, the Evolution of Geological Provinces, and Exploration Methods: Geological Association of Canada Special Publication*, v. 5, p. 755–792.

Selby, D., Creaser, R.A., Heaman, L.M., and Hart, C.J.R., 2003. Re-Os and U-Pb geochronology of the Clear Creek, Dublin Gulch, and Mactung deposits, Tombstone Gold Belt, Yukon, Canada: absolute timing relationships between plutonism and mineralization. *Canadian Journal of Earth Sciences*, Volume 40, p. 1839-1852.

# Status and exploration deployment recommendations of tin resources in China

Fanying Gong, Guogang Xie, Yongsheng Li, Hairui Sun, Tingjie Yan, Zezhong Du

*Development and Research Center, China Geological Survey*

*(Mineral Exploration Technical Guidance Center, Ministry of Natural Resources), Beijing 100083*

Tin is a nonferrous metal raw material that is extremely important in daily life. The yearly tin production across the globe totals 0.28 Mt. China, Indonesia and Burma are the top three countries in tin production, accounting for 35.88%, 19.74%, and 11.84%, respectively (Liu, 2018). Compared to other countries, China is endowed with more abundant tin resources/reserves and is the top ranked in the world regarding both measured reserves and recoverable reserves. The world-famous Gejiu and Dachang ultra-large-sized tin-polymetallic oil fields are located in China. However, with greater tin production and consumption than tin reserve growth, China has gradually turned from a tin net exporter into a net tin importer. Currently, China's economy is transforming from a high-speed growth stage into a high-quality development stage; this transformation brings higher requirements for efficient supply of mineral resources. Although some positive prospecting results have been obtained in the depth and periphery of old mines and new mines in China, the supply situation of tin resources remains a severe issue. This paper summarizes the exploration status of tin resources in China and provides recommendations regarding the exploration of future tin resources.

## Resource characteristics

China has relatively abundant tin resources and massive amounts of large-sized tin deposits. Tin resources are mainly distributed in 19 provinces (regions), mainly Yunnan, Hu'nan, Guangxi, Inner Mongolia, Guangdong, and Jiangxi. The measured tin reserve of the aforementioned six provinces (regions) accounts for over 90% of China's total tin reserve. In recent years, with continuous breakthroughs being made in tin mineral deposits in the southern slope of the Great Khingan Mountains, Inner Mongolia, such as the Weilasituo Sn-polymetallic (80000t) deposit and the Baiyinchagan Sn deposit (0.24 Mt), the percentage of Sn deposits in northern China has been increasing.

As of the end of 2013 China had 893 Sn producers, among which, 32 are medium-large sized and above deposits. The genetic types of tin ore in China mainly include primary Sn ores (80%) and alluvial tin ores (16%). Primary tin ores can be subdivided into five types: granite-related bedded-stratiform tin ore, granite-related vein-like tin ore, skarn-greisen tin ore, skarn tin ore, and continental volcanic tin ore. The former three tin ore types are the most predominant. These ores were

principally formed in the Mesoproterozoic~Neogene time, mainly in the Middle Jurassic-Cretaceous. Tin resources are low-grade, with 80% of the measured tin reserves having tin grades of 0.1%, and are primarily large-medium sized deposits. Tin resources in China are shallowly buried (mostly located above the depth of 100 m) and at depths in the range of 300–500 m. Tin ore is associated with many components. The associated minerals/elements mainly include Cu, Pb, Zn, W, Sb, Mo, Bi, Ag, Nb, Ta, Be, Ga, Ge, Cd, Fe, S, and fluorite.

## Exploration status

As of the end of 2017 China had 4.5 Mt of measured tin reserves (the amount of tin metal). In 2017, an additional 8,6000 t of measured tin reserves were explored in China. Among the over 300 Sn occurrences that have been explored in China, 109 are potentially to be developed as mines (accounting for 32.54%). As of the end of 2017, China had issued 87 tin exploration licenses; independently issued mineral species exploration licenses are relatively few and dominated by W, Cu, Mo, and other associated minerals. However, the exploration and mining policies on critical minerals, such as W, objectively limit the comprehensive utilization of tin by mining enterprises.

The investment in China's mineral exploration and development has been continuously decreasing for six years, with an accumulative decline of 40%. Since the Prospecting Breakthrough Strategic Action was implemented in 2011, China has invested 1.067 billion yuan (in CNY) in tin exploration, including 739 million CNY from private capital, accounting for 69.22% of the total investment. The investment mainly focused on seven integrated tin exploration areas (Chaling in Hu'nan, Lianhuashan in Guangdong, the Houpoao area in Guangdong, the periphery of the Dulong Mine in Maguan County, Yunnan, Tengchong-Lianghe in Yunnan, Yanbei in Huichang, Tongkengzhang in Xunwu, Jiangxi, and Heyuan in Ningdu-Luoling in Shichenghai, Jiangxi), a batch of resource reserves and new producers were added, with particularly great prospecting progress made in Nanling, central-eastern Inner Mongolia, Dulong in Maguan, Yunnan and Xiushui in Jiangxi. Great prospecting breakthroughs have been made in Weilasituo in the southern slope of the Greater Khingan Mountains, Inner Mongolia, with an estimated additional >100 Mt of tin resources. It is expected that the great breakthrough will form the third tin resource production base,

following Nanling and Gejiu in Yunnan, China. Positive tin prospecting results have been made in the Zhaxi integrated exploration area, southern Inner Mongolia; the Cuonadong Be–W–Sn deposit was recently discovered, with an estimated 0.1 Mt of tin resources, indicating a positive prospecting prospect. These results show that China has great tin prospecting potential. However, the international mining situation is stagnant, the amount of exploration investment has dropped sharply, and new metallogenic theory application and achievement transformation are lagging. Furthermore, the absence of effective deep prospecting methods and techniques and comprehensive ore dressing and smelting techniques are still constraining tin exploration.

### Resource potential

According to the evaluation results of China's mineral resource potential, China has 4.5 Mt of measured tin reserves; it is predicted that 18.61 Mt of Sn resources is located above the depth of 2000 m. The top ten provinces in tin resources are listed in decreasing order as follows: Hu'nan, Yunnan, Guangxi, Inner Mongolia, Guangdong, Xinjiang, Jiangxi, Fujian, Zhejiang, and Heilongjiang. In China, 1179 Class-I tin predicted mineral areas were delineated, including 1127 granite types (accounting for over 95% of China's ores), 30 continental volcanic types, and 22 alluvial tin types. Moreover, 109 Class-III tin predicted areas were delineated, nine of which have over 0.4 Mt, 44 of which have 0.05–0.4 Mt Sn, and 56 of which have < 0.05 Mt Sn.

In recent years, in addition to the prospecting progress made in the depth and periphery of known mines, discoveries of the Baiganhu tin-polymetallic ore field in Xinjiang, the Greater Khingan Mountains area in Inner Mongolia, Dulong in Maguan, Yunnan, etc. highlight the great tin prospecting potential of China.

### Recommendations on exploration deployment

Currently, in China, definite requirements have been proposed for strengthening environmental protection. From the perspective of national development strategy, the resource and environmental constraints tend to be urgent, the situation of mineral resource supply is severe, and the tasks to be performed are daunting. The geological prospecting industry in China is slowing down and also facing new opportunities and huge challenges.

On the basis of the evaluation results of China's mineral resources potential, the authors systematically summarized the potential evaluation results, combined the tin exploration progress and mineral geological survey results since the implementation of the Prospecting Breakthrough Strategic Action, analyzed selected exploration areas for China's tin resources and proposed nine tin exploration deployment areas for future work, i.e., the southern slope of the Greater Khingan Mountains (Weilasituo, Baiyinnuoer, Huanggangliang, etc.), Xinghualing–Qianlishan in Hunan, Dachang–

Jiufeng in Guangxi, Dulong in Maguan, Yunnan, the Tengchong–Lushui area in Yunnan, Yanbei in Huichang, Jiangxi, the Lianhuashan fault belt in Guangdong, the Zuluhong area in Xinjiang, and the Xiaobiakeng river mouth in Heilongjiang. The aforementioned areas are mostly located in national-level integrated exploration or important ore cluster areas and have been developed to various extents. The authors proposed the following recommendations:

1) Focusing on our own country, central financial support should be strengthened. With integrated tin exploration areas and significant ore cluster areas as basic units, the following tasks should be performed:

- a) optimize resource cluster areas,
- b) deploy mineral exploration programs,
- c) strengthen deep prospecting prediction, anomaly verification and deep verification,
- d) decrease commercial mineral exploration risk, and
- e) promote prospecting breakthroughs.

2) The mine administration system should be improved and private investment should be encouraged. Moreover, the following tasks should be performed:

- a) further explore the effective form and flexible mechanism of financial investment to promote commercial exploration,
- b) encourage social capital investment,
- c) optimize exploration areas within the aforementioned nine exploration areas,
- d) focus on skarn, greisen, tectonic altered rock, and altered granite type deposits,
- e) perform special deep exploration of tin resources,
- f) increase the degree of work on low-level resources, and
- g) measure a batch of resource reserves.

In addition, the following tasks should be performed: improve the mineral resource loyalty system, play an economic regulation role in encouraging exploration, effectively restrain “delineation but no exploration,” and guide enterprises to perform reserve increasing exploration.

3) The beneficiation and smelting techniques should be enhanced, and comprehensive prospecting should be strengthened, e.g., W associated with Sn, wollastonite associated with Sn, and fluorite-associated with Sn.

This paper was funded by Deep Resource Predication Evaluation and Reserve Increasing Exploration Results Integration Subject (No. 2018YFC0603704), Demonstration Project of Prospecting Predication and Technical Application in Integrated Exploration Areas (No. 121201004000150017).

### References

Zhang JB, Ding JH, Nan GL, 2015. The characteristics and potential of tin resources in China[J], *Geology in China*, 42 (2):839-852.

Liu S, Liu XJ, Peng SY, 2018. Exploration progress and demand-supply situation analysis of tin mineral resources in China [J]. *Western Resources*, 5:78-80.

Xia QL, Wang XQ, Xiao W, et. al. 2014. Potential evaluation and selection of prospecting strategic areas of tin resources in China[J]. 33(suppl):833-834.

Development and Research Center, China Geological

Survey (Mineral Exploration Guidance Center, Ministry of Natural Resources), 2011-2017 progress report on integrated exploration areas, internal data.

Development and Research Center, China Geological Survey, Geological Exploration Results Bulletin.

Reserves Department of Former Ministry of Land and Resources, 2017 Mineral Reserve Bulletin.

# Evidence of a crustal source, independent of primary melt generation, for pluton-related W-Sn mineralization in the Dongpo orefield, Hunan Province, South China

Chunli Guo<sup>1</sup>, Robert A. Henderson<sup>2</sup>

<sup>1</sup>Key Laboratory of Metallogeny and Mineral Assessment of Ministry of Natural Resources, Institute of Mineral Resources, Chinese Academy of Geological Sciences, Beijing 100037, China

<sup>2</sup>Economic Geology Research Centre, College of Science and Engineering, James Cook University, Townsville, Qld 4811, Australia

The Dongpo orefield is located within the Nanling Range, South China. This mountain belt is host to W-Sn deposits of global significance, as well as a diversity of other ore systems of large size. Crust of the mountain belt represents the southern margin the Jiangnan Orogen formed by Neoproterozoic collision of the Yangtze and Cathaysian blocks. It subsequently experienced Jurassic reactivation by extension associated with granitoid plutonism, for which the Qin-Hang deep fault belt was a focus, to which the ore systems relate. The Dongpo orefield relates genetically to the Qianlishan pluton although its deposits typically occur within its host rock envelope. The pluton was emplaced as two sequential phases, the second of which is characterized by the occurrence of rare lithium-bearing zinnwaldite mica diagnostic of rare metal granites associated with W-Sn mineralization. Within the Dongpo orefield W-Sn mineralisation of greisen-skarn type is generally proximal to the pluton, with vein-type Pb-Zn-Ag mineralization of more distal occurrence. The orefield is also spatially associated with, but otherwise unrelated to, a regionally developed granitic dyke swarm expressive of Jurassic extension and its link to magma generation.

Geochemical profiling and U-Pb zircon geochronology show that dyke swarm and the Qianlisan pluton are consanguineous and coeval, sharing a very close genetic relationship in addition to their intimate spatial association. Zircon  $\delta^{18}\text{O}$  values for samples from both pluton and dykes are generally in the range of 8.5 to 9.5, consistent with a crustal magma sources. Zircon  $\epsilon\text{Hf}(t)$  values obtained from the pluton range widely (-11.1 to -5.1) and show a continuous frequency distribution. In contrast,  $\epsilon\text{Hf}(t)$  values obtained from the dike swarm,

although similar in range to those from the pluton, show a clear bimodal frequency distribution (-11.9 to -8.0 and -7.3 to -4.1), interpreted to reflect anatectic melt generation from one of two lithologically distinct lower crustal metasedimentary domains. Small melt batch and rapid transport through the crust, as characteristic of dike generation, has preserved the source signatures. Such discrete sources are not apparent in  $\epsilon\text{Hf}(t)$  values from the pluton which were generated from somewhat more diverse, although similar, anatectic melt sources, with melt amalgamated and mixed in one or more magma chambers as typical of intrusions of this size.

Both the dykes and pluton share common sources, but only the pluton, in particularly its second phase, is associated with W-Sn mineralization. Therefore, its metal endowment must have been acquired within the crust above, and separate from, the anatectic melt source. We ascribe this addition by crustal assimilation to a large scale, complex conduit architecture with slow passage of the mineralizing granite phase through the crust. This circumstance facilitated a large volume thermal envelope and the capacity to scavenge metal bearing hydrothermal fluids for incorporation into the magma. With emplacement of phase 2 of the pluton, and its progressive crystallization, the scavenging process of hydrothermal fluid to the magma was reversed. Progressive concentration of an aqueous phase ensued, with its focused movement along just a few conduits adjacent to (skarn), or within (greisen), the pluton facilitating its transport with pressure/temperature/solute concentration relationships, and reaction with adjacent rocks, controlling the loci of mineralization.

# Unidirectional solidification textures from the Sn-mineralised Heemskirk Granite, western Tasmania: characteristics, mineral chemistry and O-isotopes

Wei Hong<sup>1</sup>, David R. Cooke<sup>1,2</sup>, Lejun Zhang<sup>1,2</sup>, Nathan Fox<sup>1</sup>, Jay Thompson<sup>1</sup>

<sup>1</sup>Centre for Ore Deposits and Earth Sciences (CODES), University of Tasmania, Private Bag 79, Hobart, TAS 7001, Australia,

<sup>2</sup>Transforming the Mining Value Chain, an ARC Industrial Transformation Research Hub, University of Tasmania, Private Bag 79, Hobart 7001, Australia

Tasmania is the most productive tin mineralisation province in Australia. Several world-class Sn-W deposits are associated with Devonian-Carboniferous, moderately to highly fractionated granitoids in western Tasmania, including the Renison Bell Sn, Mt Bischoff Sn, Cleveland Sn, Kara W-Fe, and King Island W deposits (Seymour et al., 2007; Hong et al., 2017a). The Heemskirk Granite from western Tasmania is genetically and spatially associated with abundant Sn-W skarn and greisen deposits (>0.14 Mt Sn), Ag-Pb-Zn veins (> 750 ton Ag), and an unusual hydrothermal Ni deposit (29.3 Mt @ 0.9% Ni; Seymour et al., 2007; Hong et al. 2017a). Distinctive magmatic-hydrothermal, tourmaline-rich features have been developed in the apical carapaces of the Sn-mineralised Heemskirk Granite. They can be categorized into tourmaline-quartz patches, tourmaline-filled orbicules, cavities, and veins (Hong et al., 2017b), as well as abundant quartz-rich unidirectional solidification textures (USTs). The UST layers defined morphologically as mineral crystals grown in one direction from a solid groundmass (Shannon et al., 1982). They consist mainly of hexagonal, coarse-grained quartz (>95%) with minor K-feldspar, plagioclase, biotite, muscovite, tourmaline, magnetite, and trace amounts of accessory minerals. Multiple UST-quartz layers are typically intercalated with aplitic layers, and locally extend for hundreds of meters. The UST layers commonly occur in granitic sills overlying the tourmaline patches and orbicules, and are cut by the tourmaline-quartz-muscovite veins subvertically extending from the lowermost to the uppermost areas of exposed intrusion.

Scanning electron microscope-cathodoluminescence (SEM-CL), laser ablation-inductively coupled plasma-mass spectrometry (LA-ICP-MS), and secondary ion mass spectrometry (SIMS) have been used to reveal cryptic internal textures, trace element and oxygen isotope compositions of quartz and/or magnetite within the USTs and aplite phase of the Heemskirk Granite. The aplitic quartz is characterised by homogeneous and CL-bright intensity, with minor CL-dark patches. The UST quartz grains have distinct CL textures: their upper bases are homogeneous and CL-bright with minor thin CL-dark fractures, and their trigonal apexes have CL-oscillatory growth zones. The UST-quartz grains have lower Ti, Li, and Sn contents than the aplitic quartz. Higher Al, Li, Na,

K, Mn, Fe, Ge, Rb, and Cs concentrations are detected in the UST quartz. Ti-in-quartz geothermometric study shows that the UST and aplitic quartz formed at temperatures of  $545\pm 40^\circ\text{C}$  and  $580\pm 20^\circ\text{C}$ , under pressures of ca. 1.3 kbar. In the UST-quartz, the CL-bright bases have higher concentrations in trivalent (e.g.,  $\text{Al}^{3+}$ ,  $\text{Fe}^{3+}$ ) and tetravalent cations ( $\text{Ti}^{4+}$ ) than the oscillatory CL-zoned lower apices. Elevated Al, K, and Rb concentrations in UST quartz from the base to the apex are explained to be products of contamination of micro- and nano-scale fluid inclusions. CL-dark patches and fractures in CL-bright UST quartz are revealed to display lower O-isotope compositions. The ranges of Al/Ti and Ge/Ti ratios in aplitic quartz of the Heemskirk Granite overlap those from the S-type granites of SE Bohemia (Czech) and SW England (Breiter et al., 2013; Drivenes et al., 2016), implying that the Heemskirk Granite has undergone high degrees of crystal fractionation that is compatible with whole rock compositions (Hong et al., 2017a). The UST-quartz crystals have Al/Ti values of 5.8 to 32, and Ge/Ti values of 0.02 to 0.16, one order of magnitude higher than the aplitic quartz phenocrysts, indicating the UST quartz crystallised from a more evolved fluid. Magnetite crystals in USTs overgrown by chlorite are detected by LA-ICP-MS analysis to contain low Cr, V, Ni, Co, Cr, Sc, and high Ti, Al, Mn, Sn, Ga contents. These compositional features differ greatly from magnetite from other igneous rocks and mineral deposits. The magnetite grains within the USTs and intergrown aplite are interpreted to have a hydrothermal in origin, precipitating at high temperatures. The  $\delta^{18}\text{O}_{\text{V-SMOW}}$  values of fluids in equilibrium with aplitic quartz (average +5.4‰) are lower than the whole-rock  $\delta^{18}\text{O}_{\text{V-SMOW}}$  of the host granite, likely suggesting that small volumes of light O-isotope fluids (e.g., meteoric and/or formation waters) were mixed with the melts from which aplitic quartz crystallised. The  $\delta^{18}\text{O}_{\text{V-SMOW}}$  compositions of fluids in equilibrium with the UST quartz change from +5.7 to +10.2‰ (average +7.8‰,  $n = 12$ ), consistent with a magmatic-hydrothermal fluid largely derived from the granitic melt. The quartz-rich and magnetite-bearing UST layers in the Heemskirk Granite are proposed to have precipitated from a magmatic-hydrothermal aqueous fluid exsolved from the granitic melt during emplacement into the shallow crust (6-10

km). Multiple comb-quartz layers and aplite interlayers cut by K-feldspar muscovite seals provide unambiguous physical evidence for fluctuating pressure conditions during granitic melt crystallisation, when the exsolved fluids accumulated and escaped episodically during this process. Periodic pressure buildup and release continued until the vapor pressure could no longer break the carapace, which terminated the unidirectional solidification growth of quartz and other minerals. These processes lead to the remaining volatiles trapped as miarolitic cavities, pegmatite pods, discontinuous vein dikes, and tourmaline-quartz nodules in the roof zones of the Heemskirk Granite.

Quartz-rich USTs are easily mistaken for quartz veins, pegmatite, and stockscheider pods because of their megacrystic grain sizes. Our study can therefore help understanding of USTs and associated features that develop in the apical regions of granitic intrusions worldwide. UST-quartz layers are geological indicators of granitoid that experienced high degree of fluid exsolution during the late stage of magmatic crystallisation. They are also reported to occur in the granites associated with many porphyry Cu-Au-Mo and W deposits (e.g., Lowenstern and Sinclair, 1996; Harris et al., 2004; Cannell et al., 2005; Lickfold et al., 2007). Recognition of UST layers can provide significant indications for in search of mineralised intrusions.

#### References

Breiter, K., Ackerman, L., Svojtka, M., Müller, A., 2013. Behavior of trace elements in quartz from plutons of different geochemical signature: A case study from the Bohemian Massif, Czech Republic. *Lithos* 175-176, 54-67.

Cannell, J., Cooke, D.R., Walshe, J.L., Stein, H., 2005. Geology, mineralization, alteration and structural evolution of the El

Teniente porphyry Cu-Mo deposit. *Economic Geology* 100, 979-1003.

Drivenes, K., Larsen, R.B., Müller, A., Sørensen, B.E., 2016. Crystallization and uplift path of late Variscan granites evidenced by quartz chemistry and fluid inclusions: Example from the Land's End granite, SW England. *Lithos* 252, 57-75.

Harris, A.C., Kamenetsky, V.S., White, N.C., Steele, D.A., 2004. Volatile phase separation in silicic magmas at Bajo de la Alumbrera porphyry Cu-Au deposit, NW Argentina. *Resource Geology* 54, 341-356.

Hong, W., Cooke, D.R., Huston, D.L., Maas, R., Meffre, S., Thompson, J., Zhang, L., Fox, N. 2017a. Geochronological, geochemical and Pb isotopic compositions of Tasmanian granites (southeast Australia): Controls on petrogenesis, geodynamic evolution and tin mineralisation. *Gondwana Research* 46, 124-140.

Hong, W., Cooke, D.R., Zhang, L., Fox, N., Thompson, J., 2017b. Tourmaline-rich features in the Heemskirk and Pieman Heads granites from western Tasmania, Australia: Characteristics, origins, and implications for tin mineralization. *American Mineralogist* 102, 876-899.

Lickfold, V., Cooke, D.R., Crawford, A.J., Fanning, C.M., 2007. Shoshonitic magmatism and the formation of the Northparkes porphyry Cu-Au deposits, New South Wales. *Australian Journal of Earth Sciences*, 54, 417-444.

Lowenstern, J.B., Sinclair, W.D., 1996. Exsolved magmatic fluid and its role in the formation of comb-layered quartz at the Cretaceous Logtung W-Mo deposit, Yukon Territory, Canada: *Transactions of the Royal Society of Edinburgh. Earth Sciences* 87, 291-303.

Seymour, D.B., Green, G.R., Calver, C.R., 2007. The geological and mineral deposits of Tasmania: a summary. *Tasmanian Geological Survey Bulletin* 72, p. 1-29.

Shannon, J.R., Walker, B.M., Carten, R.B., Geraghty, E.P., 1982. Unidirectional solidification textures and their significance in determining relative ages of intrusions at the Henderson Mine, Colorado. *Geology* 10, 293-297.

# A regional appraisal of Queensland's critical elements resources

Laurie Hutton

*Geological Survey of Queensland, Department of Natural Resources, Mines and Energy, Brisbane, Qld, Australia*

## Introduction

New technologies being developed around the world require a different suite of elements from the traditional more commonly mined ores (Figure 1). Sourcing these new elements poses both challenges and opportunities for the mining industry and governments around the world. Queensland has resources of several of these elements and is well placed to support global demand.

Several emerging commodities are regarded as critical based on perceived supply issues, while some existing elements (such as tin) are also showing a resurgence due to increased demand from hi-tech industries. New technologies which use these critical elements include screens and devices, electric/hybrid vehicles, catalytic converters, electric motors, wind turbine generators, alloys for use in military and civilian planes and also space craft.

## What is a critical element?

Critical elements are defined as those which are required for modern technologies or for developing industries, and for which there may be supply issues either now or in the future. Examples of possible supply issues are:

- Majority of supply from a politically unstable region (e.g. cobalt), or
- Shortages of supply to meet expected demand (e.g. lithium).

Queensland has known resources of the elements discussed in this paper, however very few are at the resource definition stage, and more needs to be done to understand their distribution and abundance. The Geological Survey of Queensland is currently collecting data on critical elements in the Northwest Minerals Province (Figure 1). The purpose of collecting the data is to better understand Queensland's endowment in these elements which will play an important role in future technologies.

This paper will discuss the distribution of critical elements in North Queensland, focussing mainly on those required for battery technologies and Rare Earth Elements. Many of the critical elements are found in the Mount Isa province (Figure 1), and are different to the suite of elements in northeast Queensland. A brief discussion of the geological elements of these two areas will give insight into the distribution.

## Battery Elements

The anticipated increasing demand in electric vehicles

over petrol and diesel vehicles is driven by pollution reduction in cities, reduction of greenhouse gas emissions, and a perception of finite fuel supplies. A prime demand in electric vehicles is battery storage – preferably low weight batteries.

Lithium-ion batteries are currently going through a new phase, transitioning from small batteries in portable electronic devices to larger batteries in electric vehicles (EVs) and stationary storage cells for renewable energy. This shift has seen rapid growth in demand, up from one per cent of the battery market in mid-1990s to 49 per cent currently. Although cellular phones and other portable devices contain just a few grams of minerals, batteries for the EV and clean energy sectors contain kilograms. Production is quickly becoming increasingly sophisticated, cheaper and more efficient, with 2020 predicted as the tipping point for the market.

The key elements required by battery manufacturers are copper, lithium, cobalt, nickel, manganese and graphite, as well as vanadium (needed for large storage grids). Currently most manufacturers source these elements from China and the Democratic Republic of the Congo (DRC), but recent sharp price increases for some of these metals, and forecasts that current projects will not be able to meet demand in the near future indicate a clear opportunity for Queensland to capitalise on this emerging market.

## Lithium

The mineral lepidolite has been known in Queensland for some time but its distribution has been uncertain. Recently lepidolite has been the focus of exploration in the Georgetown region in north Queensland. Significant quantities have been found at Buchanans Creek and the adjacent Grants Gully south of Georgetown. The lithium is contained in pegmatites which are late stage differentiates of a granite. Exploration of this deposit is continuing and drilling to define a resource is expected later this year.

Minor lepidolite and zinnwaldite (another Li-bearing mica) has been reported from the Lord Nolan and Swipers Gully tin deposits associated with pegmatites in the Stanthorpe area. Lithium has also been reported from the Bitumen and Cobree prospects in a re-sedimented Tertiary sandstone in the Broken River area in northeast Queensland. Recently, lepidolite has been identified at Gingeralla, west of Mount Garnet and southwest of Cairns, also in pegmatite.

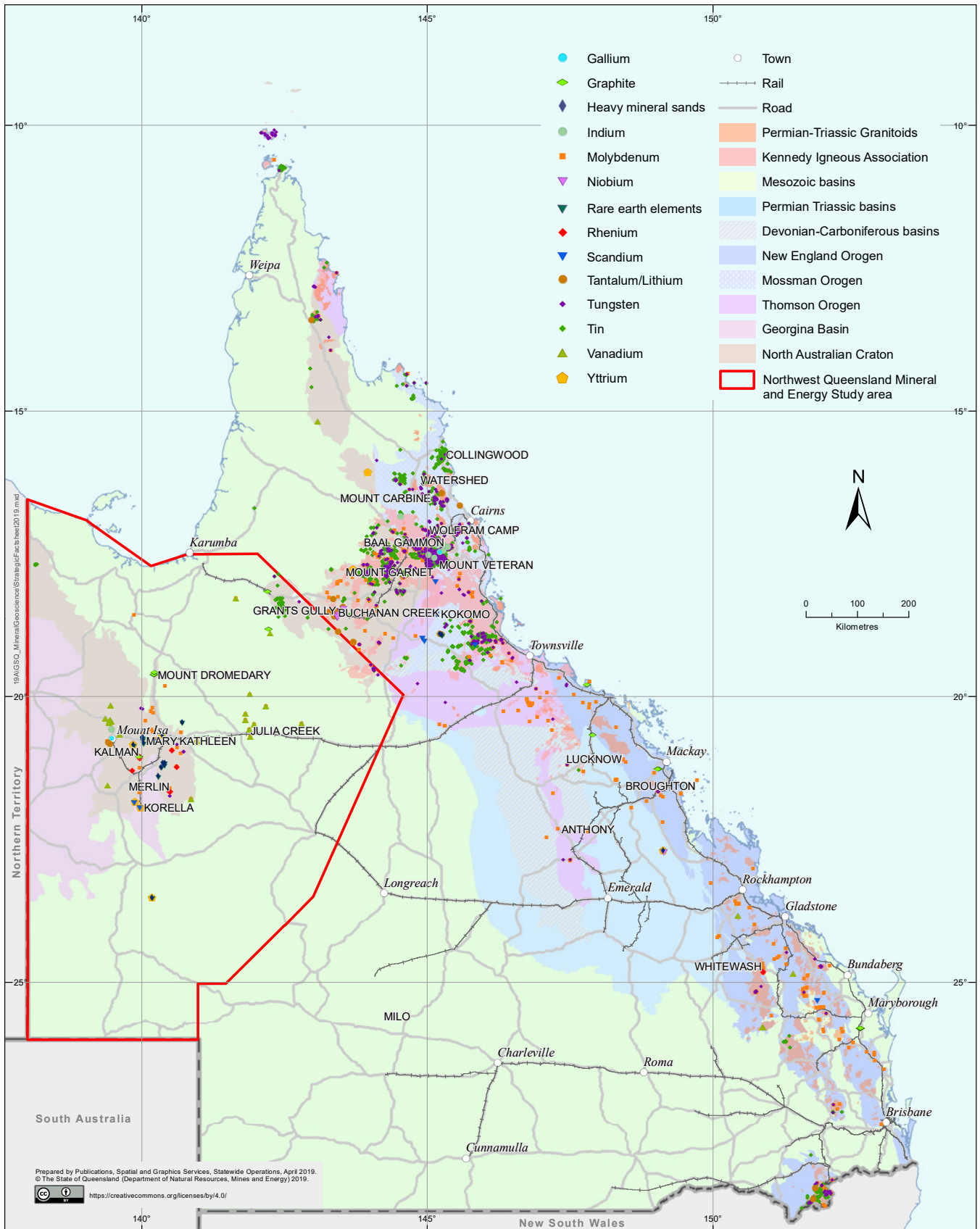


Figure 1. Map of Queensland showing the distribution of critical elements and Rare Earth Element occurrences, and the location of the Northwest Queensland mineral and energy study area (red polygon).

### Cobalt

Many of Queensland's known cobalt resources are contained in lateritic deposits formed by weathering of nickeliferous serpentinites and other ultramafic rocks in the Greenvale, Marlborough (Gladstone Pacific

Nickel) and Kilkivan (Pembroke) areas. Significant deposits include Greenvale, Bell Creek, Minnamoolka, Lucknow, Lucky Break and Marlborough.

In southeast Queensland, D'Aguiar Gold Ltd is investigating lateritic Ni-Co deposits hosted by the

Mount Mia Serpentinite (Wandilla Province) at Mount Cobalt and Black Snake. Resources have not yet been calculated for these deposits.

Cobalt is also associated with copper in brecciated sediment-hosted base metal deposits in northwest Queensland, including Mount Isa, Mammoth and Mount Cobalt. The Mount Isa orebodies contain approximately 0.14% cobalt in both the copper and silver-lead-zinc ores. Refining recovers <1000 t of cobalt per annum, but ~10,000 tpa of cobalt is associated with pyrite and arsenic and is discarded in tailings. Various processes have been investigated for economic recovery of the metal, but none have proved viable. Cobalt production from Mount Isa was reported up until June 2005.

Cobalt also occurs in other zinc and copper-gold ores of the Mount Isa Province, for example Walford Creek. Cobalt has not been recovered at Mount Gordon and remains in the tailings.

### **Graphite**

Historically, graphite was produced from two deposits in Queensland - at Mount Bopple (Bauple) near Maryborough and at Jacks Creek near Collinsville.

More recently, graphite has been found at the Mount Dromedary flake graphite deposit located 125 km north of Cloncurry. The deposit is hosted in schist and slate and outcrops over a 3km strike length. Flake sizes are in the range of 27% jumbo, 18% coarse, 6% medium, 23% fine and 26% very fine. The flake size and grade increases with depth. The deposit could supply export quality graphite for battery manufacture.

Further east, at a location 70km south of Croydon, significant graphite mineralisation occurs at the Esmeralda Project near Prospect Station where graphite is associated with the Esmeralda Granite. The granite-hosted graphite may be formed from assimilation of highly carbonaceous metasedimentary rocks, or may be formed from hydrothermal sources. The latter deposit types are typically of very high purity graphite in either flake or crystalline form, forming the basis for high grade, high value resources.

### **Rare Earth Elements (REE)**

Light Rare Earth Elements are known from many parts of Queensland but are concentrated in northwest Queensland. The largest deposit occurs in the tailings at the Mary Kathleen uranium (U) mine east of Mount Isa. The deposit is hydrothermal, related to ~1540 Ma granites, and had a grade of 3% total REE. Main elements are Lanthanum, Cerium and Neodymium

Heavy Rare Earth Elements are identified at several exploration locations in Queensland but are concentrated in northwest Queensland (such as the Milo Prospect). None are at the resource identification stage.

Yttrium is known in Queensland from the Korella prospect associated with phosphate mineralisation in the

Georgina Basin south of Mount Isa.

Scandium is known at two of the Sconi deposits (Lucknow, Kokomo) in north Queensland; two of only a few defined scandium resources in the world.

### **Vanadium**

Vanadium is increasingly being regarded as a critical element. Apart from its chief use in the production of high quality steel, it is also used in batteries – chiefly in grid storage devices.

Several vanadium deposits are known from the Julia Creek area, where they occur associated with oxidised oil shale and mixed layer clays within the Toolebuc Formation. Six separate deposits have identified inferred resources of Vanadium amounting to several thousand million tonnes of ore at grades up to 0.43%.

Vanadium is also known at Eulogie and Hawkwood in central Queensland, associated with magnetite in gabbroic intrusions, and associated with uranium mineralisation associated with albite-calcite-dolomite-chlorite-quartz-hematite-magnetite-rich albitites at Vahalla north of Mount Isa. Vanadium is likely associated with magnetite.

### **Geological controls to critical elements in the Mount Isa Inlier**

Relatively high Rare Earth Element and Cobalt element abundances commonly occur associated with Iron Oxide Copper Gold (IOCG) mineralisation in the eastern part of the Mount Isa Inlier. The association of Copper, Cobalt, with minor Nickel is considered to be derived from an alkaline mafic to ultramafic assemblage (Collerson, 2018). This interpretation is as yet untested by peer review and is at odds with the established model of skarn development related to the intrusion of granitoids in the Mary Kathleen area. Rare ultramafic rocks are present but are clearly not a major lithology in the region. The alkaline mafic to ultramafic rocks are considered related to mantle plumes, postulated to be a driver for the A- and I type felsic magmatism associated with the IOCG mineralisation. (Betts and others, 2007; Geological Survey of Queensland, 2011).

As well as copper-cobalt-REE abundances associated with the IOCG deposits in the Eastern Fold Belt, cobalt is associated with basin hosted mineralisation at Mount Isa and Walford Creek. The cobalt at Mount Isa is closely associated with pyrite and arsenopyrite making it difficult to process. Source rocks of the copper mineralisation at Mount Isa are uncertain but have been linked to tholeiitic basalt in the Eastern Creek Volcanics. These basalts occur in a large continental rift setting which is regarded as forming in a back arc – clearly not related to the plume magmatism which is postulated for the copper-cobalt-REE mineralisation in the Eastern succession.

Copper and cobalt at Walford Creek are closely associated with lead and zinc mineralisation, in a basinal

setting. Source rocks are uncertain but basic rocks of the Peters Creek Volcanics or perhaps the Siegal Volcanics are possible sources.

A feature of the Mount Isa Inlier sequence is the frequent and widespread mafic igneous intrusions and volcanics. It is this large volume of mafic rocks, admittedly derived in different geological settings, that has contributed to the copper-cobalt-REE endowment of the province.

### **Geological controls to critical elements in northeast Queensland.**

Late Palaeozoic tectonic settings in northeast Queensland are continental margin volcanic arc and back arc settings – similar to the continental back arc at Mount Isa. However the igneous rocks in northeast Queensland are dominated by oxidised and reduced I-type and S-type granites; quite different to the plume related A and I type granites in Mount Isa. Also in northeast Queensland, mafic rocks are less common. These associations lead to a different suite of deposits, dominated by tin, tungsten, gold, with minor molybdenite and wolframite. Critical elements such as indium and gallium are also present; a stark contrast to the association in Mount Isa. Clearly the geological processes which lead to the concentration of critical elements are different in the two regions.

As well as the tin-tungsten mineralisation, two other settings in northeast Queensland contain critical elements. Ultramafic serpentinite crops out in a north-south belt and is capped by deep weathering profiles. These rocks host the nickel-cobalt-scandium deposits which form the Sconi deposits. The nickel and cobalt here occur as oxides within the weathering profile requiring

different processing to the cobalt sulphides at Mount Isa. However the deposits are large and look likely to be mined in the future.

Lithium bearing pegmatites have been identified within the Georgetown Inlier in northeast Queensland. The known distribution of the pegmatites within the Georgetown Inlier relate them to a large aeromagnetic anomaly interpreted as a granite pluton (I-type?). The rocks are classified as 'LCT pegmatites' according to the USGS classification (Bradley & McCauley, 2013), which typically contain lithium, cesium, tin, rubidium, and tantalum. Beryl is commonly associated with LCT pegmatites (Bradley & McCauley, 2013). The beryl-bearing pegmatites associated with the Sybella Granite southwest of Mount Isa will be geochemically assessed for LCT pegmatite geochemistry and possible links to lithium-bearing mineralogy.

### **References**

- Betts, P.G., Giles, D, Schaeffer, B.F., & Mark, G., 2007: '1600-1500Ma hotspot track in eastern Australia: implications for Mesoproterozoic continental reconstructions. *Terra Nova*, vol19 pp 496-501.
- Bradley, D, and McCauley, A, 2013, A preliminary deposit model for lithium-cesium-tantalum (LCT) pegmatites (ver. 1.1, December 2016): U.S. Geological Survey Open-File Report 2013–1008, 7 p., <https://doi.org/10.3133/ofr20131008>
- Collerson, K.D., 2018; Cobalt and HREE mineral systems in the Mount Isa Block. Report for the Queensland Department of Natural Resources Mines and Energy, <https://bit.ly/2IPTbB0>
- Geological Survey of Queensland, 2011: North-west Queensland Mineral and Energy Province Report. Queensland Department of Employment, Economic Development and Innovation, Brisbane.

# Geological characteristic and ore genesis of typical rare metal deposits in China

Shao-Yong Jiang, Tao Liu, Hui-Min Su, Kui-Dong Zhao, Wei Chen

State Key Laboratory of Geological Processes and Mineral Resources, Collaborative Innovation Center for Exploration of Strategic Mineral Resources, School of Earth Resources, China University of Geosciences, Wuhan 430074, China

Rare metals deposits are important critical mineral resources, which are driving some of the biggest advancement in the cutting-edge technology fields such as new materials, new energy, information technology, aeronautics and astronautics, and high-tech industries. As demand for these metals explodes rapidly, it is urgent to carry out in-depth studies on the formation and enrichment mechanisms, distribution regularity and mineral exploration of the rare metal deposits and the green usage of these metals. In this paper, we will summarize the main geological characteristics and ore genesis of typical rare metal deposits in China, and introduce several of the most important rare metal deposits in China.

## Geological characteristics of rare metal deposits in China

In this paper, the rare metal elements refer to lithium (Li), beryllium (Be), rubidium (Rb), cesium (Cs), zirconium (Zr), hafnium (Hf), niobium (Nb) and tantalum (Ta). Since tungsten (W) and tin (Sn) are dominant mineral resources in China, most researchers in China do not attribute these two elements to rare metal elements group (Wang et al., 2013, 2016), but many scholars in the world believe that both W and Sn belong to this category. The elements Li, Be, Rb and Cs are also called alkaline earth elements, and the elements Zr, Hf, Nb and Ta are called high field strength elements. The high field strength elements form smaller cations with a valence of +4 or +5, and  $Zr^{4+}$  and  $Hf^{4+}$ ,  $Nb^{5+}$  and  $Ta^{5+}$  have nearly the same ionic radius and very similar chemistry.

Rare metal deposits are widely distributed across the whole of China, but different metals show different distribution patterns, and are mostly concentrated in several metallogenic belts, such as the Nanling W-Sn-rare metal province, the Mufushan pegmatite Ta-Nb ore belt in Hunan-Hubei-Jiangxi boundary area, the northeastern Jiangxi Ta-Nb-Li ore belt, the western Sichuan pegmatite Li ore belt, the middle-south section of Daxing'anling Sn-rare metal province, the Bailongshan pegmatite Li-Rb ore belt of Xinjiang, the Altai Keketuohai pegmatite Li-Be-Nb-Ta ore belt, as well as several isolated large deposits such as the Baerzhe Zr-REE-Nb deposit in Inner Mongolia, the Nanping pegmatite Ta-Nb deposit in Fujian.

These deposits show different ore grade and reserves, but generally low grade ores. Various metal associations occur in the Chinese rare metal deposits, including Nb-

Ta only, Nb-REE, Zr (-Hf), Li only, Be only, Rb only, Li-Be-Rb-Cs, Nb-Ta-Zr-Hf, and W-Sn-Na-Ta. The major ore types include the Granite-type, Pegmatite-type, Alkaline granite-type, Carbonatite-type, Volcanic rock-type and Hydrothermal type. Most of them are magmatic rock associated and in many cases the ore forming processes are related to highly fractionated granitic rocks. Commonly the ore metals are concentrated in the latest magmatic stage and transition to early hydrothermal stages.

Granite-type rare metal deposits include the highly fractionated granite and the alkaline granite. The former mainly occurs in Himalayan, Kunlun Mountain, Xingmeng Mountain and South China, and typical examples include the Yichun 414 giant Ta-Nb-Li deposit in Jiangxi Province. The typical examples of the latter include the giant Baerzhe Zr-REE-Nb deposit in Inner Mongolia. In recent years, China has discovered a new rare metal metallogenic belt associated with highly differentiated granites in southern Tibet, showing great rare metal resource potential (Wu et al., 2017). China's tungsten deposits are mainly related to the granitic-hydrothermal mineralization with seven super large deposits (Mao et al., 2013). Many granite-related tungsten-tin deposits in South China are co-associated with the rare metal mineralization such as Ta, Nb, Li, Rb, Be and Cs (e.g., Mao et al., 2013; Guo et al., 2018).

China's most famous pegmatite-type rare metal deposits are the Keketuohai No.3 pegmatite dyke in Chinese Altai (Wang et al., 1981) and the Nanping pegmatite dyke in Fujian (Chen, 2014). In recent years, China has made major breakthroughs in pegmatite-type rare metal prospecting, and successfully discovered the Jiajika-Keertying super-large pegmatite Li ore belt in Sichuan Province, the super-large Renli pegmatite Ta-Nb deposits in Hunan Province, and the pegmatite Li-Rb ore belt in Bailongshan area of Xinjiang.

Many super-large REE-Nb deposits are associated with alkaline rock-carbonatite complexes. This type of rare metal deposits is concentrated in a few localities in China (Wang et al., 2015). Baiyun Obo is the world's largest REE-Nb-Fe deposit with 35 million tons of REO. The Mianning-Dechang carbonatites in western Sichuan produce the second largest REE-Nb deposit in China, followed by the Zhushan carbonatites in the South Qinling Orogeny that produce the third largest carbonatite-type REE-Nb deposit in China.

Other types of rare metal deposits, such as the volcanic rock-type and hydrothermal type are not as important as the above-mentioned types in China, and will not be discussed in detail here.

### Controlling factors for rare metal deposit formation

The geochemical properties and the behavior of the rare metals under various geological processes and physicochemical conditions determine the characteristics of their mineralization. At present, research on the geochemical properties and behavior of the rare metal elements is still required, and many issues regarding rare metal mineralization mechanism remain controversial. For example, studies on the properties of high field strength elements Nb and Ta show that they have the same valence state, similar ionic radius, and almost identical chemical properties, which are called twin pairs. The Nb/Ta ratio of most mantle-derived rocks is close to the Bulk Earth value, suggesting that partial melting of the mantle can only cause very limited fractionation, but in the continental crust, the ratio varies greatly and exhibits a characteristic Nb loss (Rudnick et al., 2000). In theory, pairs of twin elements like Nb and Ta should be consistent with the mantle in the continental crust. Where did the lost Nb go? The low Nb/Ta ratio has become the paradox of the continental crust and is currently a frontier of academic research (Tang et al., 2000).

An important prerequisite for mineralization is the source supply of the ore metals. In general, the abundance of the rare metals in the Earth is very low, and their contents in the mantle and the crust are very different. The rare metal mineralization is closely related to major geological events and the cycling of the elements in the Earth crust and mantle. Numerous studies have shown that the Nb and rare earth elements are enriched in alkaline rock-carbonatite complexes that originate from the mantle, while highly differentiated granites in the crust and the LCT (Li-Cs-Ta) type pegmatite are enriched in ore metals like Li, Be, Rb, Cs, Nb and Ta, and the crust-mantle mixed-source alkaline granite and NYF (Nb-Y-F) type pegmatite have high abundances of Nb, Ta, Zr, Hf and Y. The mobilization, transportation, enrichment and mineralization of these elements are controlled by geological processes within the crust, the mantle and/or interaction between the mantle and crust.

Alkaline granite and the NYF type pegmatite often contain abundant rare metals such as Nb, Ta, Zr, Hf, and REE. The possible formation of alkaline granite includes the differentiation of basaltic magma, partial melting of deep crustal materials, or the mixing of crust-derived magma and mantle-derived mafic magma (Dostal et al., 2015; Siegel et al., 2018). The genetic mechanism of the NYF type pegmatite includes low degree partial melting of the lower crustal material (such as granulite, granite, quartz diorite), the extreme fractionation of mantle-

sourced magma (such as basaltic, tonalitic magma), the magma generated in the lower crust and upper mantle transition zone, and the anataxis of depleted granulite source zone (McCauley et al., 2014; London, 2018; Siegel et al., 2018).

It is still highly controversial how these different crust-mantle processes control rare metal mineralization, and it demands further detailed study. At present, China's largest alkaline granite type rare metal deposit is the Baerzhe Zr-REE-Nb deposit. Whether similar deposits exist in this area or other areas with similar geological conditions is worthy of further exploration.

Highly differentiated or highly evolved granites refer to granites that have undergone a high degree of crystallization differentiation, which are often closely related to the rare metal mineralization not only in China but also across the world. However, there exist various viewpoints regarding the petrogenesis of highly differentiated granitic magma, such as magma crystallization differentiation, the specific mechanism of separation of minerals and magma (i.e., gravity sorting, flow differentiation, convection, etc.), and the crystal accumulation (Wu et al., 2017). Because granitic magma tends to have high viscosity and may be present as crystal mush, it will make the magma crystallization differentiation difficult, and the increase of the content of F, B and Li in the magma can reduce the magma viscosity. These magmatic processes still need to be further investigated.

In general, in the process of rare metal mobilization, transportation and enrichment during magmatism and crust-mantle interaction, the following factors place major constraints on the formation of large rare metal ore deposits. First, the abundance of rare metal in magma source regions; second, whether these elements can be efficiently mobilized from the source rock into the magma, and third is the rare metal behavior during the magma differentiation crystallization and fluid exsolution processes.

The ore-forming mechanism of the rare metal deposits is closely related to various geological processes, such as supercontinent formation, plate subduction, magma source region characteristics, magma crystallization differentiation, as well as epigenetic process at the Earth's surface. The specific physical and chemical conditions of the ore-forming system are also important for deposition of the rare metal minerals, such as the volatile contents, temperature, pressure, oxygen fugacity, pH, elemental partition coefficient, fluid dissolution, fluid metasomatism and element solubility.

Recent studies have shown that granite and/or pegmatite in metamorphic core complexes are closely related to the genesis of rare metal mineralization. Typical examples are the rare metal pegmatite deposits in the Lewisian metamorphic core complex in Scotland, the rare metal pegmatites in the Bohemian metamorphic core complex

in the Czech Republic, and the granitic pegmatite in the Congo Manono-Kitotolo metamorphic complex, which host the world's largest Sn-Nb-Ta-Li deposits. Most of the rare metal deposits with economic significance in China are also related to the granite and/or pegmatite accompanying the development of metamorphic dome structure or core complex that formed by regional extension, such as the Wugongshan metamorphic core complex (Yashan Ta-Nb-Li deposit) and the Yajiang-Malcon gneiss dome complex (Jiajika-Keertying Li deposits)(Xu et al., 2018).

### Typical examples of rare metal deposits in China

The Yichuan Ta-Nb-Li deposit in Jiangxi Province is one of the biggest highly fractionated granite type rare metal deposits in China. In this deposit, four granite phases occur from bottom to top including the two-mica granite, muscovite granite, albite granite and lepidolite-albite granite. In all these granites, plagioclase is albitic with  $An < 5$  and the rocks can also be classified as alkali-feldspar granite type. Ore minerals include columbite, tantalite, lepidolite, and Nb-Ta-rich cassiterite and they all are of magmatic origin. LA-ICP-MS U-Pb dating of zircon yields an age of ~155 Ma for the granite. Zircon  $\epsilon_{Hf}(t)$  show a variation range from -11 to -9, indicating a dominant crustal source for the magma.

The most representative example of the alkaline granite type in China is the giant Baerzhe Zr-REE-Nb deposit in Inner Mongolia of northeastern China. In this deposit, the ore-related granites include albite granite, arfvedsonite-aegirine granite and pegmatite-aplite dyke, and the ore minerals consist of zircon, yttrioceberysite, synchysite, pyrochlore, ferrocolumbite, monazite and fergusonite. LA-ICP-MS dating of zircon yields an age of ~123 Ma for the arfvedsonite-aegirine granite. The lanthanide tetrad effect of both whole rock and zircon indicates a strong melt-fluid interaction for petrogenesis and ore genesis.

The Yushishan rare metal deposit is a recently found large Nb-Ta-Zr-Hf-REE deposit in Gansu Province of northwestern China. This deposit occurs in metamorphosed and deformed felsic volcanic rocks, called leptynite by local geologists. The main ore types include disseminated, banded and vein type ores. The ore minerals include columbite, tantalite, aeschynite, polycrase, bastnäsite, monazite, zircon and thorite. Monzonite occurs in the north part of the mining area and aegirine syenite occurs as dyke and vein within the ore-bearing metamorphic strata. LA-ICP-MS dating of zircon and apatite from the monzonite and aegirine syenite rocks show an age of ~500 Ma indicating their emplacement age. However, the titanite in both rocks show two stage formation ages of ~500 Ma and ~460 Ma, and their trace element signatures indicate either magmatic or metamorphic origin. Hence we suggest

the formation of this deposit is likely related to the syn-tectonic alkaline granite magmatism and related hydrothermal events.

**Acknowledgements:** This study is financially supported by the National Key R&D Program of China (no. 2017YFC0602405).

### References

- Chen GJ, 2014. On Nb-Ta-Sn element geochemistry of the Nanping rare metal granitic pegmatite ore field. *Fujian Geology*, 4, 262-270.
- Dostal J, Shellnutt JG, 2015. Origin of peralkaline granites of the Jurassic Bokan Mountain complex (southeastern Alaska) hosting rare metal mineralization. *International Geology Review*, 58, 1-13.
- Guo NX, Zhao Z, Gao JF, Chen W, Wang DH, Chen YC, 2018. Magmatic evolution and W-Sn-U-Nb-Ta mineralization of the Mesozoic Jiulongnao granitic complex, Nanling Range, South China. *Ore Geology Reviews*, 94, 414-434.
- London D, 2018. Ore-forming processes within granitic pegmatites. *Ore Geology Reviews*, 101, 349-383.
- Mao JW, Cheng YB, Chen MH, Pirajno F, 2013. Major types and time-space distribution of Mesozoic ore deposits in South China and their geodynamic settings. *Mineralium Deposita* 48, 267-294.
- McCauley A, Bradley DC, 2014. The global age distribution of granitic pegmatites. *Canadian Mineralogists*, 52, 183-190.
- Rudnick RL, Barth M, Horn I, McDonough WF, 2000. Rutile-bearing refractory eclogites: missing link between continents and depleted mantle. *Science*, 287, 278-281.
- Siegel K, Vasyukova OV, Williams-Jones AE, 2018. Magmatic evolution and controls on rare metal-enrichment of the Strange Lake A-type peralkaline granitic pluton, Québec-Labrador. *Lithos*, 308-309, 34-52.
- Tang M, Lee C-TA, Chen K, Erdman M, Costin G, Jiang H, 2019. Nb-Ta systematics in arc magma differentiation and the role of eclogites in continent formation. *Nature Communications*, 10, 1-8.
- Wang XJ, Zou TR, Xu JG, 1981. Study of pegmatite minerals of the Altai Region. Science Press, Beijing.
- Wang DH, Wang RJ, Li JK, Zhao Z, Yu Y, 2013. The progress in the strategic research and survey of rare earth, rare metal and rare-scattered elements mineral resource. *China Geology*, 40, 361-370.
- Wang DH, Wang RJ, Sun Y, Li JK, Zhao Z, Zhao T, Qu WJ, Fu XF. 2016. A review of achievements in the Three-type Rare Mineral Resources (Rare metals, Rare elements and Rare scattered metals) survey in China. *Acta Geoscientica Sinica*, 37, 569-580.
- Wang RJ, Wang DH, Li JK, Sun Y, Li DX. 2015. Rare metals, rare earth elements and rare dispersed elements mineral resources and their development and utilization. Geological Publishing House, Beijing.
- Wu FY, Liu X, Ji WQ, Wang J, Yang L, 2017. Identification and research of highly fractionated granites. *Science in China: Earth Sciences*, 47, 745-765.
- Xu ZQ, Wang RC, Zhao ZB, Fu XF, 2018. On the structural backgrounds of the large-scale "Hard-rock type" lithium ore belts in China. *Acta Geologica Sinica*, 92, 1091-1106.

# The magmatic hydrothermal transition at Bluestone Bay, Tasmania

Colin L. Jones<sup>1,2</sup>, Evan A. Orovan<sup>1,2</sup>, David R. Cooke<sup>1,2</sup>, Michael Roach<sup>1</sup>

<sup>1</sup>Centre for Ore Deposit and Earth Sciences (CODES), University of Tasmania, Hobart, Tasmania, Australia

<sup>2</sup>Transforming the Mining Value Chain (TMVC), ARC Industrial Transformation Research Hub, University of Tasmania, Hobart, Tasmania, Australia

## Introduction

The Lachlan Orogen (500 to 440 Ma) gave rise to extensive sedimentary deposits that extended south to include the Mathinna Supergroup. In Tasmania, these turbidites were intruded by the eastern Tasmanian granites as a result of the Devonian Tabberabberan Orogen (Black et al., 2005). The earlier emplaced eastern Tasmanian granites include I-type hornblende-biotite granodiorites that commonly contain abundant mafic enclaves: younger more fractionated granites include felsic S-type granites (McClenaghan, 2006; Black et al., 2010).

Bluestone Bay features Devonian granites hosting a concentration of magmatic hydrothermal transition textures of rare exposure and extent. The aim of this paper is to describe the magmatic and magmatic-hydrothermal transition textures at the apex of a surficial felsic pluton. Bluestone Bay appears barren from a metallogenic perspective, but this may not have always been the case.

## Methods

The location of Bluestone Bay is shown in Figure 1. Rocks were cut and polished at the Department of Earth Sciences, University of Tasmania, so as to display their textures preferably in cross-sectional or longitudinal views. Polished 30 micron thick thin sections of selected features were made for petrographic examination at the Department of Earth Sciences Lapidary, University of Tasmania. Electron microscope studies were performed on carbon-coated slides using a Hitachi SU-70 FESEM. A working distance of 4.8 mm was used and typically a 15 kV accelerating voltage was employed, and the Oxford AZtec EDS/EBSD system and software were used with HKI, ICSD. The American Mineralogist phase databases were used to identify elements and minerals. Uranium Pb isotope geochronology using LA-ICP-MS was completed on zircon after cathodoluminescence imaging, or monazite and xenotime after back-scattered electron studies.

## Orthomagmatic intrusions

The oldest rock at Bluestone Bay is an unfractionated hornblende-biotite-bearing granodiorite that was dated at  $402.3 \pm 3.2$  Ma (zircon, MSWD = 1.0). The granodiorite had been intruded by a plagioclase-phyric granodiorite aged  $403.7 \pm 6.0$  Ma (zircon, MSWD = 1.5). These rocks, in turn, have been intruded by compositionally highly-

fractionated alkali-feldspar granites of two distinct types: a coarse-grained (zircon,  $384.0 \pm 2.5$  Ma, MSWD = 1.08) granite that was crosscut by a fine-grained alkali feldspar granite (monazite,  $382.7 \pm 1.7$  Ma, MSWD = 1.4). The fine-grained granite was fluid- and F-rich and exclusively hosted the magmatic hydrothermal transition textures (Jones, 2018).

## Magmatic hydrothermal transition textures

The magmatic hydrothermal transition textures had a particular relationship to each other that was most apparent in the central area of the eastern headlands of Bluestone Bay (EHBB), where the textures converged in a striking meso- and macro-scale manner (Figs. 1 and 2). The EHBB presents as a progressively deroofed structure. Uppermost is an eroded roof of granodiorite, tens of square metres in area, below this are the surficial outermost layers of unidirectional solidification textures (USTs) covering several hundred square metres. The northern end the UST has been eroded, exposing the textures comprising the uppermost portion of the apex of a pluton (Fig. 3). These textures include channels of interconnected miarolitic cavities and pegmatites that are of multi-metre dimensions (Fig. 3). The miarolitic pegmatites are surrounded by, and crisscross, aplite. In a central area the pegmatites coalesce and lead to a defect in the UST layer where the UST is absent and the pegmatite occupies the space. These escape structures may have allowed egress of volatile-rich fluids that crosscut surrounding rocks and formed pegmatites external to the pluton. Partial defects in the USTs occur where a top layer(s) of UST remains intact over the pegmatite, perhaps indicating points of re-modelling of the inner layer of the UST by the pegmatite. The textures record the presence of an exsolved vapor at meso- and macro-scale. These textures also host dense networks of quartz, actinolite and sulfide veins containing fluorite, amid pervasive, intense K-feldspar alteration and miarolitic cavities that contain chalcopyrite, pyrite and magnetite (Figs. 2 and 3). Aplites are typically a transitional texture from the fine-grained granite to pegmatites and miarolitic cavities at the northern part of the EHBB, and it is commonly the texture of dikes crosscutting the granodiorite. At the eastern headland, the aplites contain quartz with a vermicular texture. Carbonates, rare earth minerals (monazite, synchesite and xenotime), iron oxides and fluorite are part of the mineral assemblage.

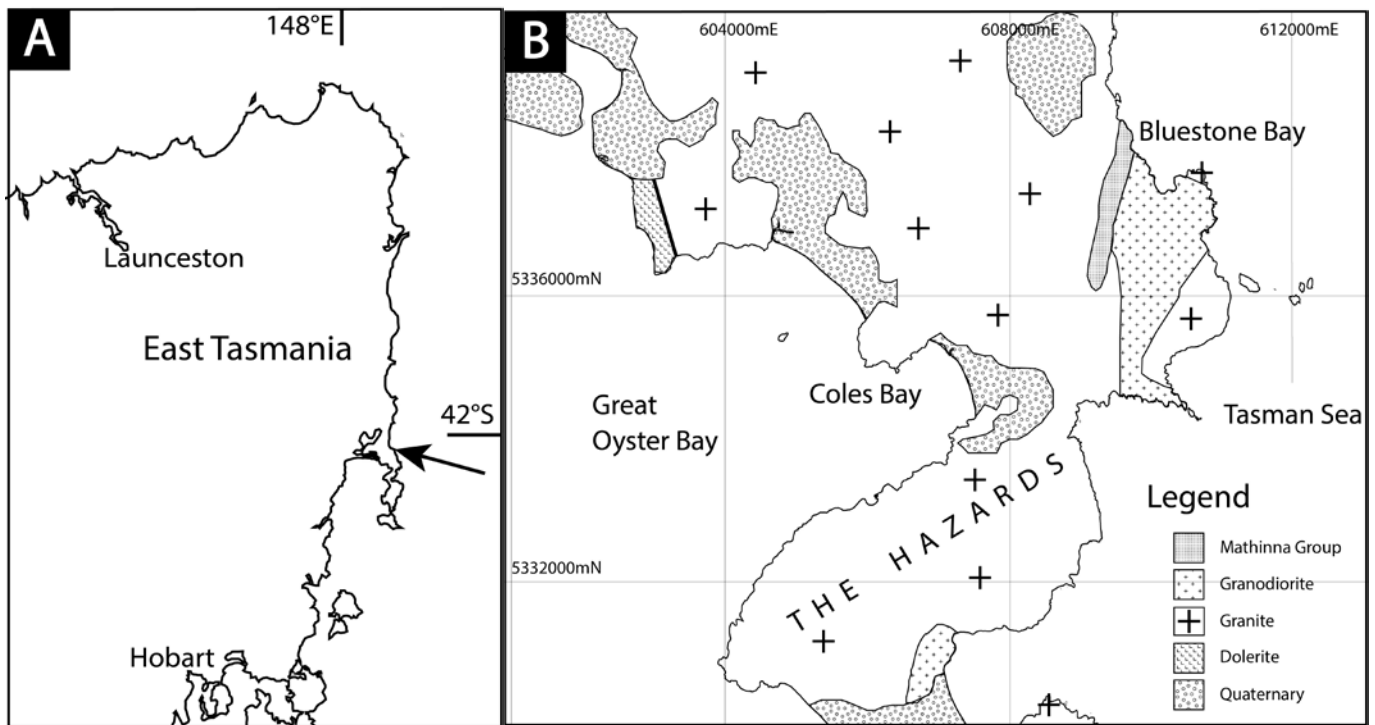


Figure 1. A. Location map showing the position of Bluestone Bay (arrow) at the northern end of the Freycinet Peninsula in Tasmania. B. Geological map of the northern Freycinet Peninsula. Derived from Everard (2001).

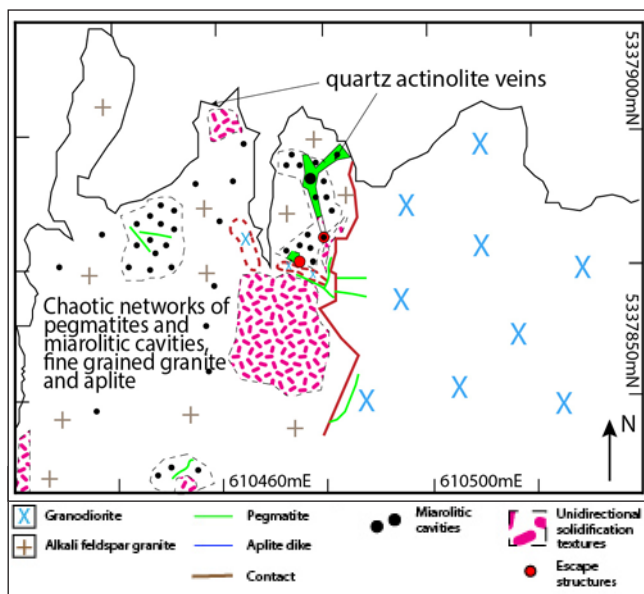


Figure 2. Mapping of Bluestone Bay. The magmatic-hydrothermal transition textures are concentrated at the eastern headland of the bay, but textures crosscutting the granodiorite are widespread.

Miarolitic cavities that are confined to the fine-grained granite outside the EHBB are commonly fist-sized and lined with quartz and K-feldspar with no other contents or connections. At the EHBB, miarolitic cavities are typically connected by honeycomb arrays of anhedral to subhedral quartz, the cavities are associated with, and form part of, the core zone of pegmatites. The cavities contain silicates, including quartz, albite, K-feldspar, biotite, chlorite, zircon, uranium and thorium silicates; the sulfides pyrite, chalcopyrite, and galena; the

carbonates bismuthite, Mn-bearing siderite and calcite (locally as pseudomorphs after anhydrite); and fluorite, magnetite, hematite, and rutile. Lining the cavities are crystals of quartz and alkali feldspars in varying proportions and these crystals project into the voids with euhedral faces. A stable mineral assemblage of hematite, calcite, siderite and the rare-earth carbonate synchesite, fluorite and small galena crystals (up to 100 microns in length) was found around the miarolitic cavities. Zoned xenotime with monazite inclusions is abundant around some cavities. Zircon, monazite, coffinite and thorite are accessory phases.

The USTs are exposed for over a metre in depth. The upper surface is a rough undulating platform of coarse K-feldspar and quartz megacrysts (Fig. 3). Exposed sections normal to the surface show K-feldspar and quartz laths projecting downwards and outwards in plumose, feather-like arrays. There are long, acicular, altered biotite grains projecting downward and aligned between the K-feldspar megacrysts. The megacrysts are simply twinned K-feldspar with prominent quartz exsolution textures running in subparallel arrays with adjacent granophyric texture. These textures extend for variable (up to 35 cm typically) depths before an abrupt transition to a thin (often millimetre thick) aplitic texture. The aplite gives way to further plumose K-feldspar as the sequence is repeated.

Six dates were obtained for aplite at the EHBB: The most precise was  $388.0 \pm 2.1$  Ma (xenotime, MSWD = 1.5), all were within 1 sigma of each other. The pluton is older than the fine-grained granite outside the EHBB ( $382.7 \pm 1.7$  Ma, as above).

## Conclusions

The EHBB presents the deroofed apex of a superficial alkali feldspar I-type granitic pluton intruding a granodiorite. The magmatic hydrothermal transition textures reflect the physicochemical exsolution of a magmatic fluid and its passage to, and exit from, the cupola of the pluton.

## References

Black, L.P., Everard, J.L., McClenaghan, M.P., Korsch, R.J., Calver, C.R., Fioretti, A.M., Brown, A.V., and Foudoulis, C., 2010, Controls on Devonian–Carboniferous magmatism in Tasmania, based on inherited zircon age patterns, Sr, Nd and Pb isotopes, and major and trace element geochemistry: *Australian Journal of Earth Sciences*, v. 57, p. 933–968.

Black, L.P., McClenaghan, M.P., Korsch, R.J., Everard, J.L., and Foudoulis, C., 2005, Significance of Devonian–Carboniferous igneous activity in Tasmania as derived from U–Pb SHRIMP dating of zircon: *Australian Journal of Earth Sciences*, v. 52, p. 807–829.

Everard, J.L., 2001, Intrusive relationships of granite and dolerite at Lagunta Creek, Freycinet Peninsula: *Papers and Proceedings of the Royal Society of Tasmania*, v. 135, p. 63–74.

Jones, C.L., 2018, Magmatic and magmatic hydrothermal transition textures at Bluestone Bay: Unpublished B.Sc Honours thesis, Hobart, Australia, University of Tasmania, p. 159.

McClenaghan, M.P., 2006, The geochemistry of Tasmanian Devonian–Carboniferous granites and implications for the composition of their source rocks: *Tasmanian Geological Survey Record 2006/06*, p. 1–31.

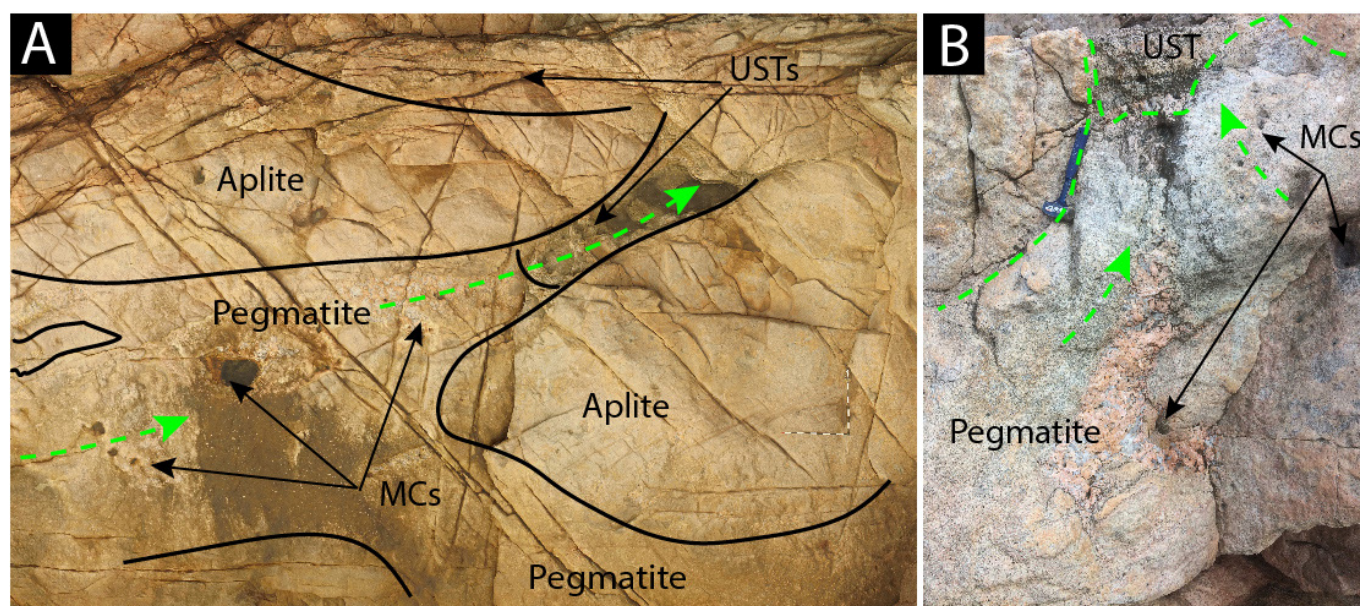


Figure 3. The inter-relationship between some magmatic-hydrothermal textures at the eastern headland of Bluestone Bay.

A. Orthomosaic image of part of the eastern headland of Bluestone Bay. The lines indicate the approximate limit of pegmatites in the fine-grained granite. The rule, right side, is 1 m x 1 m. Unidirectional solidification textures are deficient above the eroded cavity to the right, which is fringed by a pegmatite and the lower arrow points towards the pegmatite and escape structure shown in B. The dashed green lines indicate sense of flow.

B. A near vertical section showing an area where a pegmatite is capped by a small volume of UST surrounded by a domain of interconnected miarolitic cavities in aplite. The textural relationships illustrate the potential dynamic structure of a periodically vented vapor filled cavity at the top of a pluton; an escape structure. Abbreviations: MC = miarolitic cavity.

# Towards an integrated model for magmatic and hydrothermal tin systems: examples from Africa

Judith A. Kinnaird, Paul A.M. Nex

*School of Geosciences, University of the Witwatersrand, Johannesburg, South Africa*

## Introduction

Although tin was used in bronze implements in Europe as early as 3,500 B.C. the pure metal was not used until about 600 B.C. In Africa, the earliest use seems to have been dated to the 9th century AD in Nigeria, where exquisite bronze artefacts from three sites in the Igbo-Ukwu area, Anambra State have been recovered (Wikipedia, 2019). Bronzes dated between the thirteenth and nineteenth centuries have been excavated in northern South Africa, Botswana and Zimbabwe (Miller, 2002; Chirikure et al., 2007; Denbow and Miller, 2007). Significant African tin production began at the start of the 20th century with maximum output in the late 1970's. Since then production in Africa has declined to less than 2% of world output. The increase in price of the commodity together with a resurgence of interest in tin for its use in an indium-tin alloy for touch screens, has led to a re-evaluation of some formerly abandoned mining areas, and the development of new prospects in Africa.

## History of tin production in Africa

In the early part of the 20th century, tin output in Nigeria was second only to that of Russia in terms of world production. Cassiterite had been mined on a commercial scale since 1904 and before the discovery of oil, tin was the major source for foreign exchange in the country. During the Second World War, cassiterite, together with Nb and Ta ores, was mined to supply the needs for the war efforts and tin production boomed during the 1950s, reaching 12,000 t/yr, but the subsequent depletion of subsurface deposits, coupled with a downturn of the tin price, led to a reduction of production from ~3,800 t/yr in 1979, to less than 3,200 t/yr in 1981, and then to 203 t/yr in 1995. Since then there has been a cyclic trend in production as Nigeria fell behind DRC and Rwanda in African tin output. However, in 2017, there was an upsurge in production to 5960 tons (USGS, 2019) of tin from concentrate as increased numbers of artisanal miners worked placer ore for a source of income as the naira depreciated against the dollar. Extensive alluvial cassiterite resources still remain underneath the Ngell basalts of Plateau State.

The DRC has also had a long history of tin production although since 2008 output has declined considerably, due to political instability and religious clashes which, since the mid-1990's, left control of the commodity to armed groups (Kinnaird et al, 2016). Nevertheless, in 2007-2008 the cassiterite export from DRC was estimated at 18,000-25,000 tons (Garrett and Mitchell, 2009) and,

after the government ban on all mineral exports in 2010 was lifted in 2012, the country is now the leading African tin producer, with an estimated output of ~9000 t in 2018 (USGS, 2019).

In Rwanda, primary mineralisation and alluvial/eluvial deposits have been mined since the early 1930's. In the 1970's, state-controlled companies took over and only since 2007 have mining licences have been granted to private national/international companies, although most of the mines operate at the artisanal scale. The average annual tin export between 2009 and 2013 was 4,955 tons, although in 2013 was only ~2000 t but as output from Nigeria had dwindled it was the second largest cassiterite producer on the continent and now lies behind DRC and Nigeria with an estimated 2900 tons in 2018 (USGS, 2019)

Cassiterite production from new discoveries could boost the rankings of African tin production with the Achmmach quartz-tourmaline vein-hosted tin prospect in northern Morocco (Kasbah Resources, 2014, 2018) and the high-grade Bisie chloritised schist-hosted wood tin prospect in DRC (Witley & Leighton, 2015).

Reported smelter production of tin metal ceased in Nigeria and Rwanda in 2005 and 2006, respectively and no formal tin smelter is operational in Africa since this date. In 2012, African tin mine production decreased by about 26% compared with that of 2011 and by 2014 the total tonnage was ~127,500. Output decreased at artisanal and small-scale mining operations in DRC and in 2018 the DRC accounted for <50% of African tin mine production, Rwanda, 15%; Nigeria, 32%; and Egypt, <3%. No refined tin has been produced since 2012.

## The occurrence of tin deposits in Africa

Although across Africa, tin-bearing deposits range in age from Archaean to Mesozoic, with localised Pleistocene alluvial deposits, there were major eras of tin mineralisation related to continental amalgamation in the early and late Neoproterozoic and to the fragmentation of Gondwana in the Mesozoic (Fig. 1).

Cassiterite occurrences across the continent can be grouped into five eras of mineralisation:

- (1) Small-scale deposits in Archaean granite-greenstone terranes of the Man Shield in Sierra Leone, the Congo Craton, the Zimbabwe Craton and the Kaapvaal Craton;
- (2) Palaeoproterozoic pegmatites in the Birimian Province (2100 to 2000) of West Africa, the Ubendian

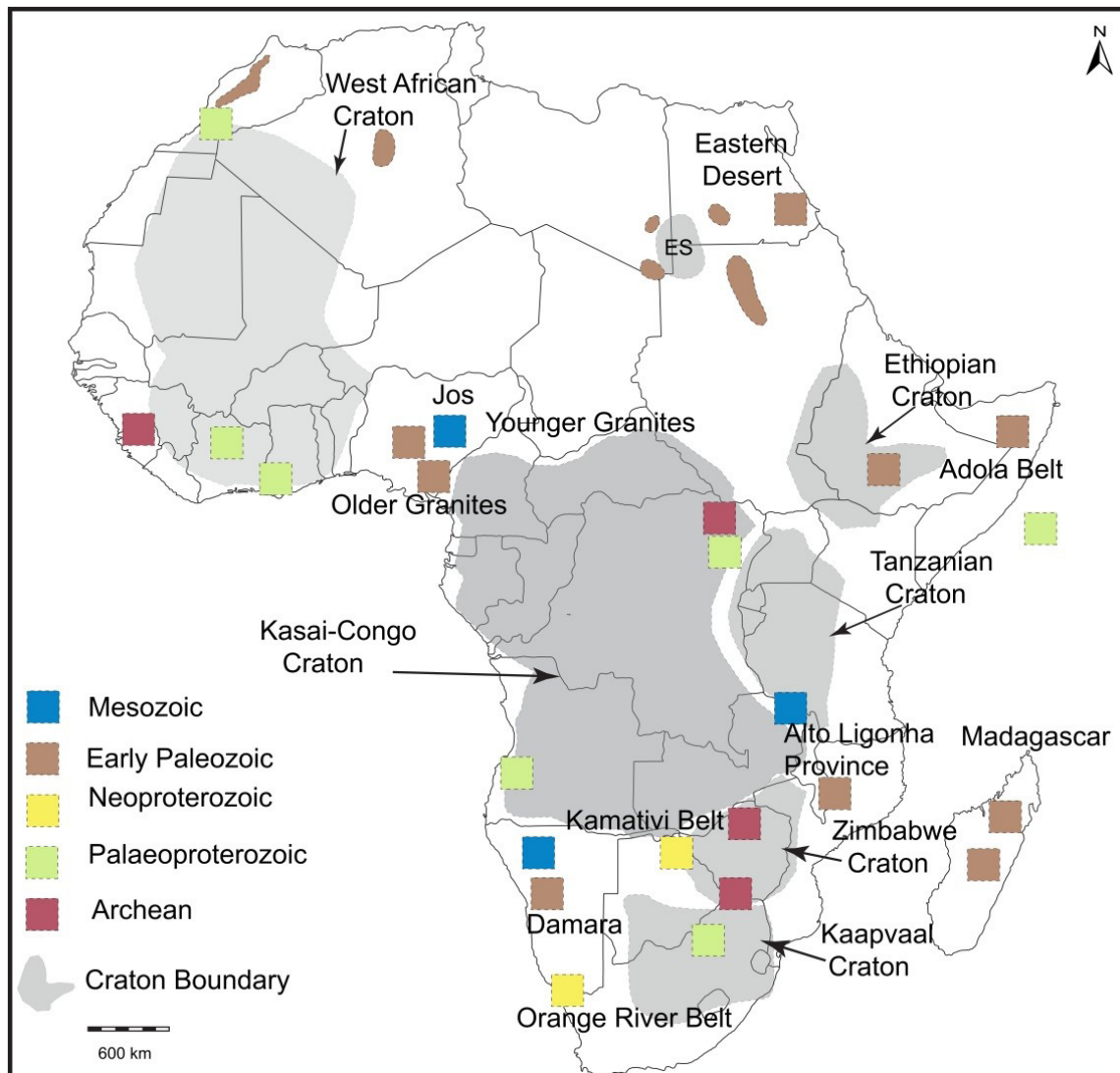


Fig. 1 Map of Africa showing the age and distribution of significant Sn-(Nb-Ta) pegmatite and Sn-(Nb-Ta) granite provinces (modified after Melcher et al., 2015).

Belt in Central Africa and in granites of the Bushveld Complex in South Africa;

- (3) early Neoproterozoic in the Kibaran Belt of Central Africa, the Kamativi Belt in Zimbabwe, and in the Orange River-Namaqua Province of Namibia/South Africa;
- (4) late Neoproterozoic to early Palaeozoic belts of ca. 600 to 500 Ma age, that resulted from the amalgamation of Gondwana. Rare metal mineralisation associated with granites and pegmatites is common in many countries on the African Nubian Shield, including Ethiopia, Somalia, Sudan, Saudi Arabia and Egypt; on the West African shield in Nigeria; in the Kibara belt of Rwanda and DRC; in the Mozambique Belt of eastern Africa and the Damara Belt in Namibia;
- (5) the Mesozoic alkaline ring complexes of the Jos Plateau in Nigeria.

In addition, Pleistocene to Recent alluvial deposits derived from granites and pegmatites of varying ages occur particularly in Nigeria, DRC and Rwanda.

Tin provinces where the tin mineralisation occurs within rocks of very different ages occur in Nigeria, South Africa and Namibia. For example, in Nigeria, cassiterite occurs in Panafrican pegmatites, Mesozoic ring complexes and in Pleistocene alluvial deposits.

### Geology of tin deposits

Tin-bearing magmas are generally of monzo- to syenogranite composition. Primary cassiterite-hosting deposits require a combination of factors: i) the generation of magma ii) ascent of the magma through structurally-controlled passageways iii) crystallisation of the magma with or without fluid separation iv) generation of a hydrothermal fluid phase v) escape of a hydrothermal fluid. The style of tin deposits can be grouped into different categories based on whether, and when, a fluid phase separated from the magma:-

1. Zoned and unzoned pegmatites can be generated as small melt fractions without a parental granite at depth. Magmatic cassiterite may have crystallised at the pegmatitic stage and/or from later hydrothermal

alteration of the pegmatite, including the formation of greisen as in the Neoproterozoic Uis pegmatites of Namibia.

2. Disseminated mineralisation in granite cupolas where fluid was retained as in the Lease Granite of the Palaeoproterozoic Bushveld Complex in South Africa.
3. Irregular greisenised or tourmalinised zones of a granite cupola where hydrothermal fluids separated from the magma prior to the ductile-brittle transition as in the Jurassic Rishi Granite of Nigeria.
4. Pipes, stockworks, sheeted veins and greisens within a granite cupola after the ductile-brittle transition as in the Bobbejaankop and Lease Granites of the Palaeoproterozoic Bushveld Complex in South Africa.
5. Exogranitic greisens and sheeted veins within the country rock with associated alteration of the country rock and localised occurrence of skarns as in the Mutue Fides-Stavoren tinfield of South Africa
6. Later endo-, or exogranitic quartz-rich cassiterite-wolframite bearing veins representing the last stage in fluid evolution as at Rooiberg in the Palaeoproterozoic Bushveld Complex in South Africa.
7. Metamorphic re-distribution of cassiterite into zones of altered host rock as in the Bisie Tin prospect in the DRC.
8. Alluvial and eluvial deposits derived from any of the above cassiterite-bearing deposits as on the Ngell Plateau of Nigeria.

Using examples from Namibia, Nigeria and South Africa, it is possible to show that the various styles of tin-bearing deposits can be viewed in a unified model depending on where the magma crystallised, whether a fluid phase evolved, and if so, whether this occurred prior to the ductile-brittle phase transition and whether the fluids breached the carapace and resulted in mineralisation in the country rocks.

## References

- Chirikure, S., Hall, S., Miller, D., 2007. One hundred years on: what do we know about tin and bronze production in Southern Africa? In: La Niece, S., Hook, D., Craddock, P. (Eds.), *Metals and Mines Studies in Archaeometallurgy*. British Museum Press, London, pp. 112-119.
- Denbow, J. and Miller, D.E., 2007. Metal working at Bosutswe, Botswana. *Journal of African Archaeology* 5, 280-313.
- Garrett, N. and Mitchell, H., 2009. Trading conflict for development. Utilising the Trade in Minerals from Eastern Democratic Republic of the Congo for Development: Resource Consulting Services 50 pp. <http://www.lse.ac.uk/internationalDevelopment/research/CrisisStates/download/others/Trading%20Conflict%20for%20Development2.pdf>.
- Kasbah Resources, 2014. Presentation from website <http://www.kasbahresources.com/>.
- Kasbah Resources 2018: Kasbah delivers positive Achmmach tin project definitive feasibility study. [http://www.kasbahresources.com/site/PDF/1730\\_0/2018AchmmachTin Project Definitive FeasibilityStudy](http://www.kasbahresources.com/site/PDF/1730_0/2018AchmmachTin%20Project%20Definitive%20FeasibilityStudy)
- Kinnaird, J.A., Milani, L., & Nex, P.A.M. 2016. Tin in Africa. Special Issue of Episodes, Mineral Fields of Africa for IGC 2016. 39 (2) 361-380
- Melcher, F., Graupner, T., Gäbler, H.-E., Sitnikova, M., Henjes-Kunst, F., Oberthür, T., Gerdes, A. and Dewaele, S., 2015, Tantalum-(niobium-tin) mineralisation in African pegmatites and rare metal granites: Constraints from Ta-Nb oxide mineralogy, geochemistry and U-Pb geochronology: *Ore Geology Reviews*, 64, 667-719.
- Miller, D.E., 2002. Smelter and smith: metal fabrication technology in the Southern African early and late iron age. *Journal of Archaeological Science*. 29, 1083-1131.
- U.S.Geological Survey, 2019. Mineral Commodity Summaries, February 2019
- Wikipedia, 2019. Igbo-Ukwu. <https://en.wikipedia.org/wiki/Igbo-Ukwu>
- Witley, J.C. and Leighton, R.G., 2015. NI 43-101 Technical Report - Mineral Resource Estimate, Bisie Tin Project, North Kivu Province, Democratic Republic of Congo. MSA Group, pp 178.

# CO<sub>2</sub> escaping leads to wolframite precipitation

Xiangchong Liu<sup>1</sup>, Dehui Zhang<sup>2</sup>

<sup>1</sup>Institute of Geomechanics, Chinese Academy of Geological Sciences

<sup>2</sup>School of Earth Sciences and Resources, China University of Geosciences, Beijing

Wolframite is the main ore mineral in the vein-type tungsten deposits of southern China (Mao et al., 2013a). It is highly disputed how wolframite in these deposits is precipitated from hydrothermal fluids (e.g. Ni et al., 2015; Wei et al., 2012; Xiong et al., 2017). Mixing of magmatic fluids and meteoric fluids is proposed to be the dominant mechanism for precipitating the wolframite in the Xihuashan tungsten deposit (Wei et al., 2012). However, many other hydrogen and oxygen isotopic measurements suggest that the mineralizing fluids were not mixed with meteoric fluids at the main mineralization stage (e.g. Gong et al., 2015; Liu et al., 2011; Wang et al., 2007; Zhu et al., 2015). Ni et al. (2015) argued that simple cooling caused precipitation of wolframite, but the efficiency of heat transfer from hydrothermal fluids to wallrock is severely limited by the low thermal conductivity of rocks (cf. Heinrich et al., 2005). The third mechanism is CO<sub>2</sub> escaping and pH increase after a decrease in fluid pressure (e.g. Xiong et al., 2017). CO<sub>2</sub>-bearing fluid inclusions have been found from quartz, topaz, and wolframite (e.g. Chen et al., 2018; Li et al., 2018; Xiong et al., 2017; Zhou et al., 2017), but it remains poorly understood whether and how CO<sub>2</sub> loss accompanying a decrease in fluid pressure causes a significant decrease in tungsten solubility.

A thermodynamic model in the system of Fe-W-Cl-Na-C-O-H was established to examine how CO<sub>2</sub> escaping alters chemical equilibrium and tungsten solubility. Twenty-two species were considered in the model: H<sup>+</sup>, OH<sup>-</sup>, HCl<sup>0</sup>, Cl<sup>-</sup>, Na<sup>+</sup>, NaCl<sup>0</sup>, NaOH<sup>0</sup>, H<sub>2</sub>WO<sub>4</sub><sup>0</sup>, HWO<sub>4</sub><sup>-</sup>, WO<sub>4</sub><sup>2-</sup>, NaWO<sub>4</sub><sup>-</sup>, NaHWO<sub>4</sub><sup>0</sup>, Fe<sup>2+</sup>, FeCl<sup>+</sup>, FeCl<sub>2</sub><sup>0</sup>, FeOH<sup>+</sup>, FeO<sup>0</sup>, HFeO<sup>2-</sup>, FeWO<sub>4</sub>(s), CO<sub>2(aq)</sub>, HCO<sub>3</sub><sup>-</sup> and CO<sub>3</sub><sup>2-</sup>. These species involves with 16 reactions in solutions (Table 1), the equilibrium constants of which were calculated from the empirical formula proposed by Wood and Samson (2000) and the thermodynamic data in SUPCRT (Johnson et al., 1992).

The other four equations were obtained from the charge and mass balance shown in Table 2. The activity coefficients of electrically charged species in solutions were calculated by an extended Debye-Hückel equation (B-dot equation) proposed by Helgeson (1969). The empirical equation fitted by Drummond (1981) was used to reproduce the activity coefficients of CO<sub>2</sub>, while the activity coefficients of the other neutral species were assumed to unity. The following parameters were used in the thermodynamic model: 300-400°C, 10 wt% NaCl, and 4-8 km, which are typical conditions for precipitating wolframite in the vein-type tungsten deposits of southern China. Assuming a hydrostatic gradient of 10 MPa/km and a lithostatic gradient of 25 MPa/km, the species concentrations at lithostatic pressure levels and hydrostatic pressure levels were compared to show the influences of CO<sub>2</sub> on chemical equilibrium. The equilibrium constants of the 16 reactions were calculated

Table 1. The 16 reactions in the thermodynamic model.

Number	Chemical reactions
1	$H^+ + WO_4^{2-} = HWO_4^-$
2	$H^+ + HWO_4^- = H_2WO_4^0$
3	$H^+ + Cl^- = HCl^0$
4	$H_2O = H^+ + OH^-$
5	$FeWO_4(s) = Fe^{2+} + WO_4^{2-}$
6	$Fe^{2+} + Cl^- = FeCl^+$
7	$Fe^{2+} + 2Cl^- = FeCl_2^0$
8	$Fe^{2+} + H_2O = FeOH^+ + H^+$
9	$Fe^{2+} + H_2O = FeO^0 + 2H^+$
10	$Fe^{2+} + 2H_2O = HFeO_2^- + 3H^+$
11	$Na^+ + Cl^- = NaCl^0$
12	$Na^+ + H_2O = NaOH^0 + H^+$
13	$Na^+ + WO_4^{2-} = NaWO_4^-$
14	$Na^+ + HWO_4^- = NaHWO_4^0$
15	$CO_2(aq) + H_2O = HCO_3^- + H^+$
16	$HCO_3^- = CO_3^{2-} + H^+$

Table 2 Mass and charge balance constraints used in the thermodynamic model

Number	Balance	Equation
17	Charge balance	$[H^+] + [Na^+] + [FeCl^+] + 2[Fe^{2+}] + [FeOH^+] = [HWO_4^-] + 2[WO_4^{2-}] + [Cl^-] + [OH^-] + [HFeO_2^-] + [HCO_3^-] + 2[CO_3^{2-}]$
18	Cl mass balance	$\Sigma Cl = [Cl^-] + [HCl^0] + [NaCl^0] + [FeCl^+] + 2[FeCl_2^0]$
19	$\Sigma Fe = \Sigma W$	$[H_2WO_4^0] + [HWO_4^-] + [WO_4^{2-}] = [FeCl^+] + [FeCl_2^0] + [Fe^{2+}] + [FeOH^+] + [FeO^0] + [HFeO_2^-]$
20	Fixed CO <sub>2</sub>	CO <sub>2</sub> solubility reproduced from the model in Mao et al. (2013b)

using the R package CHNOSZ developed by Dick (2017). At 300°C, pH has a range of 3.08-3.91 and tungsten solubility ranges from 8.19 to 18.05 ppm (Fig.1). At 400°C, pH increases to 3.58-5.42 and tungsten solubility increases to 59.97-155.41 ppm. The dominant tungsten species at 300-400°C is  $HWO_4^-$ . pH is negatively correlated to fluid pressure, while tungsten solubility is positively correlated to fluid pressure. After fluid

pressure decreases from the lithostatic level to the hydrostatic level, pH increases by 0.42-0.52 log unit at 300°C and by 0.88-1.16 log unit at 400°C. Consequently, tungsten solubility decreases by 27.3-43.7 % at 300°C and by 36.0-46.6 % at 400°C. The decreased degree of tungsten solubility increases with depth. Therefore,  $CO_2$  escaping accompanying a drop of fluid pressure is one of the mechanisms precipitating wolframite efficiently.

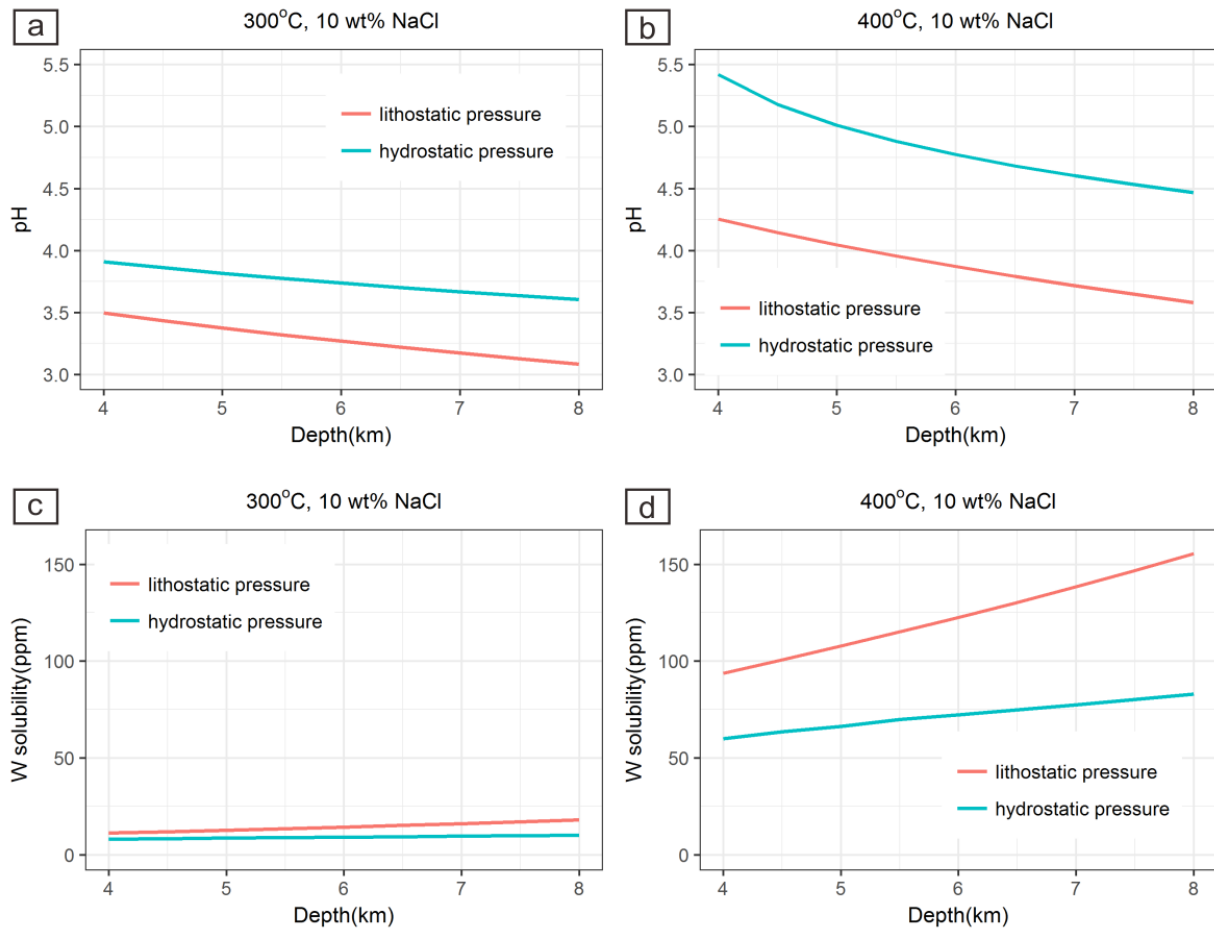


Figure 1. The isothermal change of pH (Fig. 1a and 1b) and tungsten solubility (Fig. 1c and 1d) from the lithostatic to the hydrostatic levels at a depth of 4-8 km.

## References

Chen, L.-L., Ni, Pei, Li, Wen-Sheng, Ding, J.-Y., Pan, J.-Y., Wang, G.-G., Yang, Y.-L., 2018. The link between fluid evolution and vertical zonation at the Maoping tungsten deposit, Southern Jiangxi, China: Fluid inclusion and stable isotope evidence. *Journal of Geochemical Exploration*, 192: 18-32.

Dick, J., 2017. CHNOSZ: Thermodynamic Calculations for Geobiochemistry, <https://CRAN.R-project.org/package=CHNOSZ>.

Drummond, S.E., 1981. Boiling and mixing of hydrothermal fluids : chemical effects on mineral precipitation. Ph.D. thesis, Pennsylvania State University.

Gong, X. et al., 2015. A study of ore-forming fluids in the Shimensi tungsten deposit, Dahutang tungsten polymetallic ore field, Jiangxi Province, China. *Acta Geologica Sinica-English Edition*, 89(3): 822-835.

Heinrich, C.A., Halter, W., Landtwing, M.R., Pettke, T., 2005. The formation of economic porphyry copper (-gold) deposits: constraints from microanalysis of fluid and melt inclusions. *Geological Society, London, Special Publications*, 248(1): 247-263.

Helgeson, H.C., 1969. Thermodynamics of hydrothermal systems at elevated temperatures and pressures. *American Journal of Science*, 267(7): 729-804.

Johnson, J.W., Oelkers, E.H., Helgeson, H.C., 1992. SUPCRT92: A software package for calculating the standard molal thermodynamic properties of minerals, gases, aqueous species, and reactions from 1 to 5000 bar and 0 to 1000°C. *Computers & Geosciences*, 18(7): 899-947.

Li, W.-S., Ni, Pei, Pan, Jun-Yi, Wang, G.-G., Chen, L.-L., Yang, Y.-L., Ding, J.-Y., 2018. Fluid inclusion characteristics as an indicator for tungsten mineralization in the Mesozoic

Yaogangxian tungsten deposit, central Nanling district, South China. *Journal of Geochemical Exploration*, 192: 1-17.

Liu, J., Mao, J., Ye, H., Zhang, W., 2011. Geology, geochemistry and age of the Hukeng tungsten deposit, Southern China. *Ore Geology Reviews*, 43(1): 50-61.

Mao, J., Yanbo, C., Maohong, C., Pirajno, F., 2013a. Major types and time-space distribution of Mesozoic ore deposits in South China and their geodynamic settings. *Mineralium Deposita*, 48(3): 267-294.

Mao, S., Zhang, D., Li, Y., Liu, N., 2013b. An improved model for calculating CO<sub>2</sub> solubility in aqueous NaCl solutions and the application to CO<sub>2</sub>-H<sub>2</sub>O-NaCl fluid inclusions. *Chemical Geology*, 347: 43-58.

Ni, P., Wang, X.D., Wang, G.G., Huang, J.B., Pan, J.Y., Wang, T.G., 2015. An infrared microthermometric study of fluid inclusions in coexisting quartz and wolframite from Late Mesozoic tungsten deposits in the Gannan metallogenic belt, South China. *Ore Geology Reviews*, 65, Part 4(0): 1062-1077.

Wang, Q. et al., 2007. Characteristics and significance of the fluid inclusions from Yaogangxian tungsten deposit in south of Hunan. *Acta Petrologica Sinica*, 23(9): 2263-2273 (in Chinese with English abstract).

Wei, W.F. et al., 2012. Infrared microthermometric and stable isotopic study of fluid inclusions in wolframite at the Xihuashan tungsten deposit, Jiangxi province, China. *Mineralium Deposita*, 47(6): 589-605.

Wood, S.A., Samson, I.M., 2000. The hydrothermal geochemistry of Tungsten in Granitoid environments: I. relative solubilities of ferberite and scheelite as a function of T, P, pH, and mNaCl. *Economic Geology*, 95: 143-182.

Xiong, Y.Q., Shao, Y.J., Zhou, H.D., Wu, Q.H., Liu, J.P., Wei, H.T., Zhao, R.C., Cao, J.Y., 2017. Ore-forming mechanism of quartz-vein-type W-Sn deposits of the Xitian district in SE China: Implications from the trace element analysis of wolframite and investigation of fluid inclusions. *Ore Geology Reviews*, 83: 152-173.

Zhou, L. et al., 2017. A preliminary study of fluid inclusions of topaz crystal from Mapping tungsten deposit, southern Jiangxi Province. *Mineral Deposits*, 36(4): 921-934 (In Chinese with English Abstract).

Zhu, X.Y. et al., 2015. The differences of the ore-forming fluid between the vein-type and skarn type tungsten deposits. *Acta Petrologica Sinica*, 31(4): 941-953 (in Chinese with English abstract).

# Temperature control on tin mineralisation in Gejiu East Tin Field, China and its implications for mineral exploration

Jack Ma

*Yunnan Tin Australia*

The Gejiu Tin Field is located in Yunnan (China) covering some 1,700 km<sup>2</sup> and is currently the largest tin producer in the world. Gejiu is situated towards the western margin of the South China Block, which is separated from Sanjiang Fold System of Tethys Domain by the Red River Fault Zone.

Gejiu Tin Field is divided by the Gejiu Fault into the east and west fields, with Gejiu East Tin Field being the major source of tin production. Gejiu East comprises a sequence of Triassic carbonates with a thickness exceeding 3,000 m. The dominant structure feature in the Gejiu East is the Wuzishan Anticlinorium, within which a series of east-west faults have developed and divide the Gejiu East Tin Field into five major mine areas (Fig. 1).

Late Yanshanian granites intruded the core of the anticlinorium with complex contact shapes. Granite contacts are commonly 200-2,000 meters below present surface with zircon U-Pb age dating returning 81-83Ma (Cheng, 2009). Tin mineralisation is closely related to medium-fine grained biotite granite. Accumulated tin metal discovered so far in Gejiu East is more than 3 million tonnes, making it one of the largest tin fields in the world.

## Fluid inclusions

A total of 267 fluid inclusion temperature measurements were collated for this study from Gejiu East Tin Field, Yunnan, China. The dataset was collected over a time span of 31 years and a total of 14 different minerals were used (Zhuang, 1984; Wang, 1990; Wang, 1992; Wei, 1993; Tan, 2003; Qin, 2006; Yang, 2010; Liao, 2010; Zhang, 2012; Yang, 2012; Lv, 2015). Temperature that were measured include homogenisation and decrepitation.

Sample collection sites cover the entire Gejiu East Tin Field and are generally evenly distributed. Temperature measurements are interpreted in conjunction with their associated mineralisation type and mineralogy. According to the mineralised zones from which samples were collected, sample origins can be grouped into manto oxide tin ore and contact zone skarn sulphide tin-copper ore.

The temperature measurements data from Gejiu East Tin Field (Fig. 2 & Table 1) suggest that during granite cooling stage, ore forming minerals precipitated in the temperature ranging from 480°C to 200°C. It seems that the 480°C-350°C range is characterised by a rapid temperature drop, while the 350°C-200°C range is more gradual. Ore forming mineral precipitation, especially

for tin, peaked at 350°C, at which minerals crystallised at a high rate as a result of wide fluid circulation at a high fluid pressure.

Manto mineralisation occurred at temperatures ranging between 420-270°C, while precipitation peaked at 350°C and 280°C, indicating two major fluid pulses. Skarn mineralisation temperature ranges between 460°C and 290°C, with precipitation concentrated in two sub-ranges: 430-390°C of mainly skarn minerals, and 370-290°C of sulphide precipitation. The skarn ore forming temperatures are generally higher than those of manto, reflecting their respective distances to the granite heat source.

## Mineralisation stages in Gejiu East Tin Field

Based on sample mineralogy and spatial distribution relative to granite intrusion, ore forming temperatures were analysed and a three-stage tin mineralisation process has been proposed: (1) early stage skarn stringer; (2) skarn manto; and (3) contact sulphide (Fig. 3).

Early stage skarn stringer mineralisation was formed between 430-390°C and peaked at 430°C, suggesting significant amount of dry skarn minerals forming at 430°C. During this stage, limited tin-bearing fluid moved out of the granite and upwards. Cassiterite began to precipitate between 420°C and 390°C, resulting in stringer mineralisation. This stage effectively set up the heat field around granite, which provided space for late stage mineralisation. If the current geothermal gradient of about 40°C/km in Gejiu area and ancient geothermal gradient as 30-40°C/km are taken into account, the space for mineralisation would be a zone of 1000-1300 m outwards from the granite contact.

Skarn manto was formed during a relatively stable temperature field in Gejiu area, with significant fluid pressure. When the temperature at the contact zone decreased to 420°C, significant amounts of wet skarn minerals precipitated near the contact, leaving a high-temperature fluid. As fluid moved away from contact zone, it cooled down gradually. As estimated by the proposed geothermal gradient, when the fluid was about 570 m away from the contact zone and its temperature dropped to about 400°C, the fluid began to react with carbonates resulting in precipitation of cassiterite, either in the form of replacement or vein. Continuous slow cooling caused significant cassiterite precipitating between 350°C and 280°C, resulting in the manto sulphide orebody. Sulphide has since then been oxidised to form the manto oxide ore.

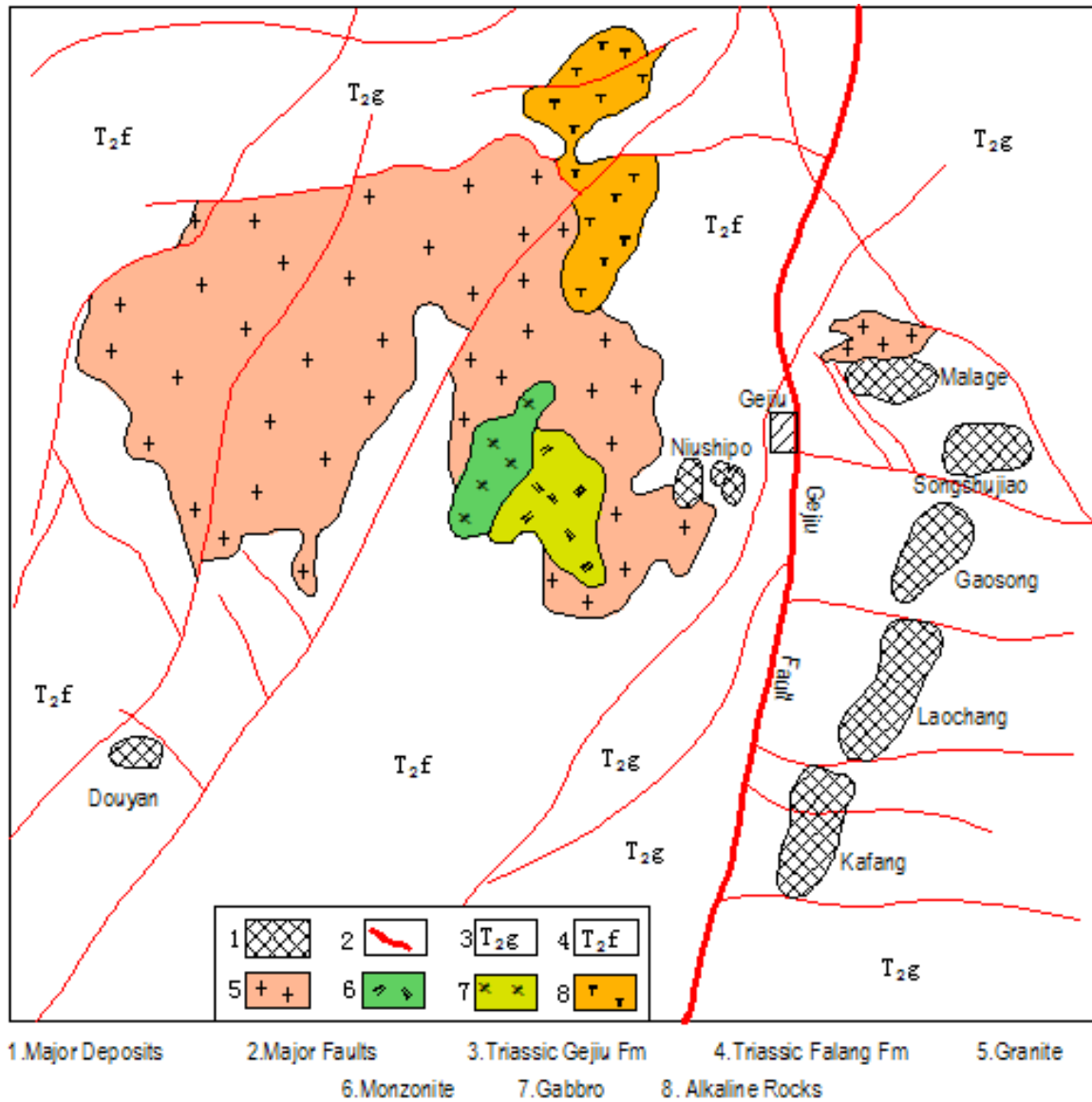


Figure 1. Simplified geology of the Gejiu Tin Field (after Geological Survey Team 308).

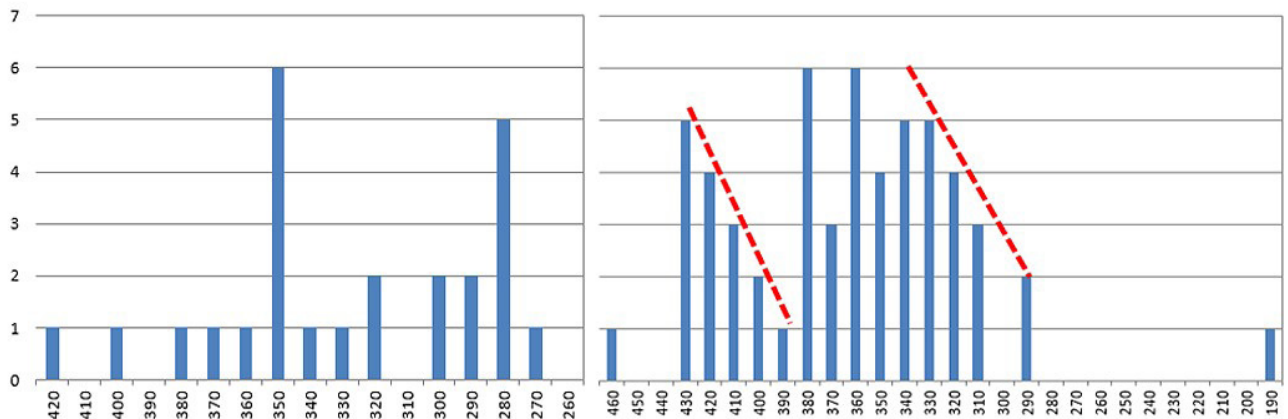


Figure 2. Temperature frequency distribution of manto oxide ore (left) and contact zone skarn sulphide ore (right).

Table 1: Temperature ranges of various minerals.

Host mineral	Inclusion temperature(C°)									Range
	550	500	450	400	350	300	250	200	150	
Quartz	—————									550-160
Cassiterite	—————									480-240
Essonite	—————									450-430
Fluorite	—————									430-200
Diopside	—————									430-380
Tourmaline	—————									420-270
Davidsonite	—————									410-320
Arsenopyrite	—————									400-330
Pyrrhotine	—————									380-220
Molybdenite	—————									300-290
Galena	—————									290-280

Contact sulphide stage began when most fluid as well as heat moved away from contact zone, leading rapid drop in temperature and pressure. Addition of meteoric water into the system would also facilitate the temperature drop. The drop in pressure stopped the fluid moving far away from contact zone. Cooling and contraction of the granite and early stage skarn resulted in cracks and voids in the zone. At around 380°C, tin and copper would precipitate as replacement or fissure fill ore in host rock and greisen ore inside granite. Mineralisation during this stage occurred mostly within 150 m of the contact. The end of this stage signifies the conclusion of Gejiu tin mineralising process.

In summary, the Gejiu East Tin Field has undergone three mineralising stages and the process has confined within 1300 m of the contact. Precipitation of cassiterite and other minerals is controlled by the heat gradient around granite. Late stage mineralisation may also alter product of previous stage, resulting in a complex mineral assemblage in Gejiu East Tin Field.

**Implications for mineral exploration**

The second stage skarn manto mineralisation discussed above suggested this type of mineralisation would have been formed within a space of approximate 400 m thick starting from 570 m outside granite contact. A favourable

zone for cassiterite crystallization around granite contact zone may exist. In Gejiu East Tin Field, this zone is typically represented by oxide manto tin mineralisation which has been a significant ore source in the area.

A recent review of mineralisation system in Gejiu's Gaosong Tin Mine area (Kang et al., 2016) supports the existence of such a favourable zone. Furthermore, localisation of some orebodies in Gaosong area do not follow "fault plus carbonate strata" rule, with some orebodies being distant from fault structures. This may suggest that heat gradient around granite intrusion may have played a more prominent role than previously recognised. Although fault structures and fracture zones within strata will facilitate fluid movement and mineral precipitation and remain as significant mineralisation hosts, porosity of host rock may have allowed fluid passage. Therefore, exploration effort may need to extend from traditional "fault plus carbonate strata" area to the entire 400 m favourite zone around the granite contact.

**Acknowledgements**

Dr. Joe Xie is thanked for his assistance during the finalisation of this paper. This paper is intended to present some thoughts based on observations from Gejiu East Tin Field, which certainly requires further refinement and discussion.

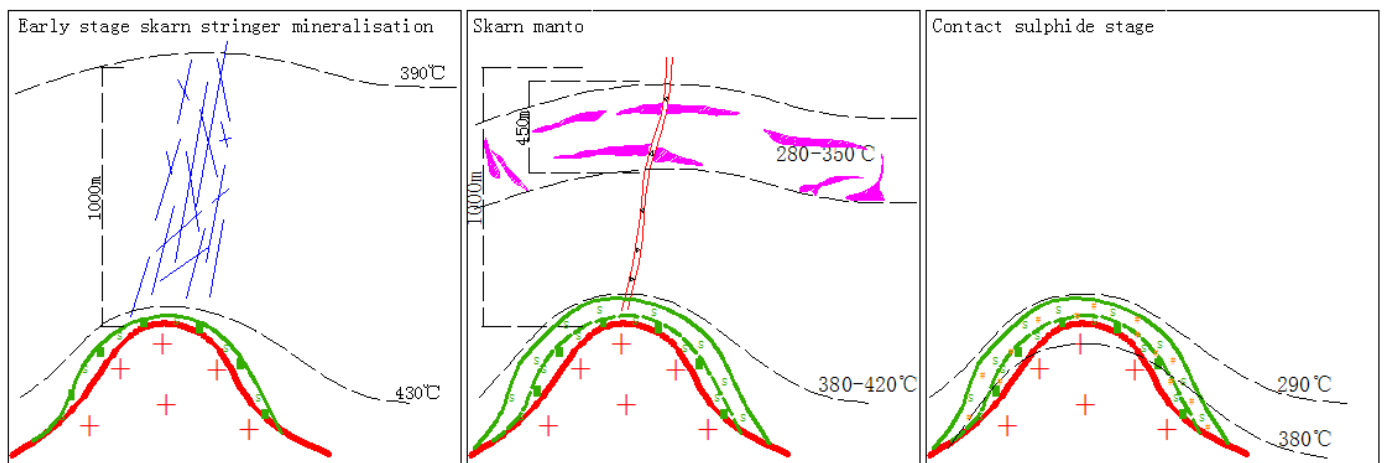


Figure 3. Schematic diagrams of mineralisation stages in Gejiu East Tin Field

## References

- Cheng Y. (2009). Zircon dating of granites related to Yunnan Gejiu tin deposits and its implications. *Mineral Deposits* 28, 297-312 (in Chinese).
- Kang D., He, K., Li, J., Liu C., Ni C. (2016). Ore body special distribution of Damalu area, Gaosong, Gejiu Tin Field. *Modern Mining* 566, 154-157 (in Chinese).
- Liao S., Chen S., Deng X. (2010). Fluid inclusion characters and their implications of Xiao copper-tin polymetallic deposit, Gejiu. The twelfth National Mathematical Geology and Geo-Information Forum.
- Lv M. (2015). Mineralogical genesis and its fluid inclusion study of cassiterite from Gejiu Tin Mine. Thesis for master Degree, Kunming University of Science and Technology, pp. 46-65.
- Qin D., Li Y., Fan G., Chen A., Tan S., Hong T., Li L., Lin X. (2006). Geochemistry of Gejiu tin mine and its mineralisation evolution. *China Engineering Science* 8, 30-38.
- Tan S., Qin D., Fan Z., Xue C., Chen A., Xia J. (2003). Geology and exploration potential of stringer tin deposit in Gejiu. *Mineral Resources and Geology* 17, 307-311.
- Wang X., Zhu J., Shen W. (1992). The origin of ore forming material in Gejiu Tin Mine. *Journal of Guilin Metallurgy & Geology College* 12, 164-170.
- Wang Y. (1990). Geochemical characters of fluid inclusions from stringer tin mineralisation of Laochang, Gejiu Tine Mine. *Yunnan Geology* 18, 36-46.
- Wei M. (1993). Geology-geochemistry study of Gejiu skarn tin mine in China. *Geochemistry*, 2:146-153.;
- Yang Y., Ye L., Bao T. (2012). Characters and their studies of fluid inclusion data from Gejiu Tin Mine. *Mineral Deposit* 31, 667-668.
- Yang Z., Mao J., Chen Y., Cheng Y., Chang Y. (2010). Geological and geochemical characters and genesis of Kafang Copper deposit, Gejiu, Yunnan. *Acta Petrologica Sinica* 26, 831-842.
- Zhang D., Xu J., Xu X., Li J., Mao S., Wang K., Li Y. (2011). Depth of rock and ore forming: major influence factors and pressure estimation method. *Geological Bulletin* 30, 112-123.
- Zhuang Y. (1984). *Geology of Gejiu Tin Mine*. Metallurgy Publishing, pp. 226-231.

# Geology and metallogeny of tungsten and tin deposits in China

Jingwen Mao<sup>1</sup>, Hegen Ouyang<sup>1</sup>, Shiwei Song<sup>1</sup>, Shunda Yuan<sup>1</sup>, Zhenhua Zhou<sup>1</sup>, Wei Zheng<sup>1</sup>, Huan Liu<sup>1</sup>,  
Peng Liu<sup>3</sup>, Yanbo Cheng<sup>2</sup>, Maohong Chen<sup>1</sup>

<sup>1</sup>*MLR Key Laboratory of Metallogeny and Mineral Assessment, Institute of Mineral Resources, Chinese Academy of Geological Sciences, Beijing, 100037, China*

<sup>2</sup>*Economic Geology Research Centre (EGRU), James Cook University, Townsville, 4811, Australia*

Tungsten and Sn deposits in China are widely distributed in the South China block (i.e., Yangtze Craton-Cathaysian block), Himalaya-Tibetan-Sanjiang, Kunlun-Qilian-Qinling-Dabie-Sulu orogens, and Central Asian Orogenic Belt. Among these, the South China block hosts the majority of the mineralization with about 73% (9.943 million tonnes WO<sub>3</sub>) and 85% (6.561 million tonnes Sn) of the country's total W and Sn resources, respectively. The W resource mainly occurs as skarn (63%), quartz-vein (17%), porphyry (17%) and greisen (3%) type deposits, whereas the Sn is present in skarn (81%), quartz veins that are typically tourmaline-bearing (6%), sulfide-rich veins or mantos (5%), greisen (5%), and porphyry (3%) type deposits.

The W and Sn mineralization formed during numerous events from Neoproterozoic to Paleocene with a peak in the Middle Jurassic to Early Cretaceous, and with an uneven spatial and temporal distribution pattern. The Neoproterozoic Sn (W) deposits (850-790 Ma) occur in the southern and western margins of the Yangtze Craton; the early Paleozoic W (Sn) deposits (450-410 Ma) are mainly distributed in the northern Qilian and the westernmost part of the eastern Kunlun orogens; the late Paleozoic Sn and W deposits (310-280 Ma) are mainly developed in the western part of the Central Asian Orogenic Belt; the Triassic W and Sn deposits (250-210 Ma) are widely scattered over the whole country; the Early Jurassic to Cretaceous W and Sn deposits (198-80 Ma) mainly occur in eastern China; and the late Early Cretaceous to Cenozoic Sn and W deposits (121-56 Ma) are developed in the Himalaya-Tibetan-Sanjiang orogen.

The petrological characteristics of W- and Sn-related granitoids in China vary with the associated ore elements and can be divided into Sn-dominant, W-dominant, W-Cu, and Mo-W (or W-Mo) groups. The granitoids associated with Sn- and W-dominant magmatic-hydrothermal systems are highly fractionated S- and I-type, high-K calc-alkaline and (or) shoshonitic intrusions that show metaluminous to peraluminous nature. They exhibit enrichments in F, B, Be, Rb, Nb, and Ta, depletions in Ti, Ca, Sr, Eu, Ba, and Zr, and strongly negative Eu anomalies. The granitoids associated with W-Cu and W-Mo deposits are of high-K calc-alkaline to shoshonitic nature, metaluminous, depleted in Nb and Ta, and display weakly negative Eu anomalies. Granitoids associated with Sn- and W-dominant deposits are reduced, whereas those linked to W-Cu and Mo-W deposits are relatively more oxidized. The magma sources of W-dominant granitoids are ancient crust, whereas those connected with Sn, Mo-W, and W-Cu deposits are from variable mixing of ancient and juvenile crustal components.

The spatial and temporal distribution pattern of W and Sn deposits in China is intimately related to the regional geodynamic evolution. The Neoproterozoic Sn deposits are associated with peraluminous, highly fractionated, and volatile enriched (boron and fluorine) S-type granites sourced from melting of ancient crust in a post-collisional setting related to the assembly of the Rodinia supercontinent. The early Paleozoic W deposits are genetically associated with highly fractionated S-type granites formed during post-collisional events and were derived from partial melting of a thickened continental crust in the context of Proto-Tethyan assembly. Granitoids associated with late Paleozoic Sn and W deposits were derived from the melting of ancient and juvenile crust with I-type affinity associated with the closure of the Paleo-Asian Ocean. Although the Triassic W and Sn deposits are related to the assembly of much of Asia within the Pangea supercontinent, their geological settings are variable. Those in the South China block and Himalaya-Tibetan-Sanjiang belt are associated with collision and magma derivation through partial melting of a thickened continental crust, whereas in the Kunlun-Qilian-Qinling-Dabie-Sulu orogen and Central Asian Orogenic Belt, a post-collisional extensional setting dominates. The Early Jurassic (198-176 Ma) W deposits, located in the northern part of northeast China, are associated with highly fractionated I-type granites derived from melting of juvenile crust and emplaced during the subduction of the Mongol-Okhotsk oceanic plate. The extensive group of Middle Jurassic to Cretaceous W and Sn deposits formed in two stages at 170-135 Ma and 135-80 Ma. The former stage is associated with highly fractionated S- and I-type granites that are products of partial melting of thickened crust with heat input possibly from a slab window associated with the Paleo-Pacific oceanic plate subduction beneath the Eurasian continent. The later stage is closely associated with NNE-trending strike-slip faults along the Eurasian continental margin and is coeval with the formation of rift basins, metamorphic core complexes, and porphyry-epithermal Cu-Au-Ag deposits. These processes, which were instrumental for the formation of a wide range of mineral deposits, can be ascribed to regional lithospheric thinning and delamination of the thickened lithosphere and thermal erosion in a post-subduction extensional setting. The 121-56 Ma Sn deposits in Himalaya-Tibetan-Sanjiang orogen are associated with S-type granite or I-type granodiorite emplacement in a back-arc extensional setting during Neo-Tethys plate subduction.

# Tin isotope fractionation in ores and rocks: genetic and exploration implications

Ryan Mathur<sup>1</sup>, Wayne Powell<sup>2</sup>

<sup>1</sup>Juniata College, Huntingdon Pa USA

<sup>2</sup>Wayne Powell- CUNY, Brooklyn, NY USA

## Abstract

This presentation will focus on how Sn isotope compositions of ores and rocks provide insight into ore genesis and exploration applications. Analytical techniques for the separation of Sn from these different chemical matrices can be found in Mathur et al. (2017). Systematic variations of Sn isotope values in ores occur in all types of Sn deposits where cassiterites are approximately 2‰ heavier than later formed stannite in 6 different deposits analyzed. We interpret that the systematic variation, regardless of Sn deposit, is related to oxidation of Sn from the tin chloride rich mineralization fluids. The lower values in the stannite represent the residual lighter Sn remaining (inferred from general mass balance considerations). To augment this observation, experimental data demonstrates that lower temperature (at 25°C) redox reactions produce larger isotope fractionation in comparison to Sn vapor formed at 150°C. A first order exploration tool could be the Sn isotope composition of the rocks related to mineralization. The relationship of the Sn isotope composition of the hydrothermal fluid that precipitated the ores and the associated felsic rocks is not clear given our current understanding of Sn isotope fractionation. However, we present data from surrounding intrusions from 5 of the Sn ore deposits and the Sn isotope compositions of igneous rocks have lower Sn isotope values ( $\delta^{124}\text{Sn} = -1.2$  to  $-1.8\text{‰}$ ) than published rock standards ( $\delta^{124}\text{Sn} = +0.1$  to  $+0.6\text{‰}$ ) not associated with mineralization. These general observations have both genetic and exploration importance.

## Introduction

Measurable isotopic fractionation of tin has been reported for ores (Haustein et al., 2010), igneous rocks (Badullovich et al., 2017; Creech et al., 2017), and archaeological bronze artifacts (Balliana et al., 2013; Mason et al., 2016; Yamazaki et al., 2014). The isotopic variation measured in these materials implies that high-temperature geological processes fractionate tin isotopes. Out of these papers, only Badullovich et al. (2017) presented evidence for an associated mechanism that induced the observed variation: partitioning of tin between magma and chromite during fractional crystallization of basalt in which all tin is in its oxidized state ( $\text{Sn}^{4+}$ ). However, with few exceptions, the environmental conditions in which tin ores develop contrast sharply with that of the Hawaiian lava lake setting studied by Badullovich et al. (2017): highly evolved felsic magmas, involvement of a saline hydrothermal fluid, evolving redox conditions, and distinct mineral assemblages in which cassiterite ( $\text{SnO}_2$ )

is predominant. Without an understanding of causative mechanisms of fractionation in typical hydrothermal tin ore systems, interpretation of these initial datasets by geologists and archaeologists is limited.

The solubility of tin in granitic magmas is redox dependent. Experimental studies have demonstrated that under reduced conditions, where tin exists predominantly in the  $\text{Sn}^{2+}$  state, cassiterite solubility is two orders of magnitude greater than under oxidized conditions where  $\text{Sn}^{4+}$  is the dominant stable species (Linnen et al., 1996; Linnen et al., 1995). Oxygen fugacity values for tin granites lie below the QFM buffer, allowing for high dissolved Sn contents (Heinrich, 1990). In the hydrothermal fluids that evolve from these granites initially, tin is predominantly in the form of  $\text{Sn}^{2+}$  chloride complexes ( $\text{SnCl}_2^0$ ,  $\text{SnCl}_3^{1-}$ ,  $\text{SnCl}_4^{2-}$ ,  $\text{Sn}(\text{OH})\text{Cl}$ ) (Sherman et al., 2000).

Cassiterite ( $\text{SnO}_2$ ) is the primary economic tin mineral, and its precipitation from reduced, magma-derived hydrothermal fluids requires electron transfer to produce  $\text{Sn}^{4+}$  (Heinrich, 1990). Possible triggers for oxidation include mixing with meteoric waters, pH change due to progressive hydrolysis (greisen development), or vapor separation (e.g., Heinrich, 1990). Regardless of the specific process, redox reactions are essential to the genesis of all primary cassiterite ores.

In well-studied multi-valent transition metal isotopic systems such as Cu and Fe, it has been established that redox reactions impart significant fractionation, with oxidation favoring the heavier isotope. Given that Sn undergoes a redox transformation in hydrothermal fluids during mineralization, it is likely that the electron transfer required for the formation of cassiterite or soluble  $\text{Sn}^{4+}$ -complexes such as  $\text{SnCl}_6^{2-}$  or  $\text{Sn}(\text{OH})_4$  will favor the heavier isotopes of tin.

## Results and Implications

Natural mass dependent fractionation is evident, as the slope of  $\delta^{124}\text{Sn}$  vs.  $\delta^{120}\text{Sn}$  is 2 with an  $r^2=0.98$  (Fig. 1) for the rocks and minerals. Cassiterite and stannite show statistically distinct populations regardless of deposit type, where cassiterite has a higher mean  $\delta^{124}\text{Sn}$  value ( $+0.64 \pm 0.48\text{‰}$  ( $1\sigma$ )) than stannite  $\delta^{124}\text{Sn}$  ( $-1.36 \pm 0.45\text{‰}$  ( $1\sigma$ )), whereas the rocks associated with mineralization have distinctly lower  $\delta^{124}\text{Sn}$  isotope values in comparison to the rock standards.

The mean values of cassiterite and stannite show similar variation across the three deposits studies, with a  $\delta^{124}\text{Sn}$  range of 1.7‰ for cassiterite and 1.4‰ for stannite. However, in each of the five deposits studied, Sn in

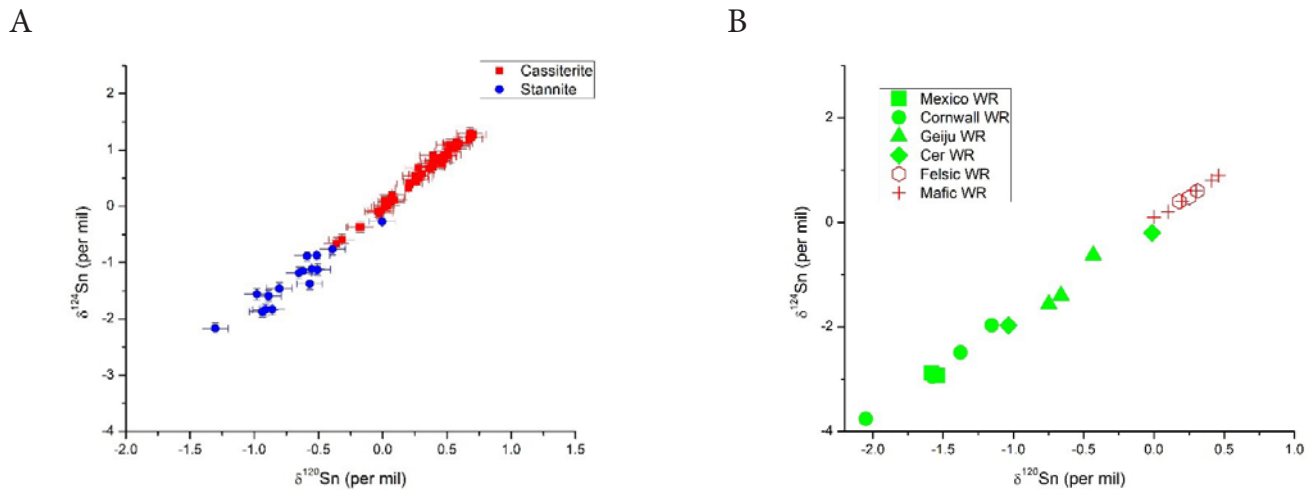


Figure 1. Plots of mass dependent Sn isotope fractionation for samples A) ores of cassiterite and stannite, and B) felsic igneous rock samples near Sn mineralization.

stannite has lower values than cassiterite. To quantify this relationship, a comparison of the mean values of the two phases within different deposits was calculated using the following expression:

$$\delta^{124}\text{Sn}_{\text{cassiterite} - \text{stannite}} = \text{mean } \delta^{124}\text{Sn}_{\text{cassiterite}} - \text{mean } \delta^{124}\text{Sn}_{\text{stannite}}$$

Tin mineralization from all three ore districts have similar values, 2.3 (Cornwall), 2.0 (Cinovec-Krupka) and 1.6 (Bolivia), with a total range of  $\delta^{124}\text{Sn}_{\text{cassiterite} - \text{stannite}}$  of 0.78‰, and an overall average of 2.0‰. Thus, each locality displays a similar and consistent shift in Sn isotopic composition between cassiterite and stannite regardless of mineralization style and depth of emplacement.

It is well established that tin is transported in hydrothermal fluids in the reduced state ( $\text{Sn}^{2+}$ ) in tin granites, and that formation of cassiterite and stannite requires an oxidative transition to  $\text{Sn}^{4+}$ . Furthermore, it has been demonstrated repeatedly that oxidation of multi-valent metals imparts significant isotopic fractionation favoring the heavy isotope (Dauphas et al., 2009; Dauphas et al., 2014; Domagal-Goldman and Kubicki, 2008; Sherman, 2013). For some metals, such as Cu, oxidation-induced fractionation is observed in the products of low-temperature, near-surface reactions (Mathur et al., 2010). In cases such as Fe, identifying the component of fractionation associated with redox reactions is confounded by overprints due to numerous coincident fractionation mechanisms, particularly partitioning between coexisting phases (Dauphas et al., 2014).

Based on Nuclear Resonant Inelastic X-Ray Scattering (NRIXS) and Mossbauer spectroscopy experiments, Polyakov et al. (2005) predicted that oxidation state would have a large effect on fractionation of Sn. Since neither low-temperature processes nor partitioning between co-precipitating minerals complicate the hydrothermal Sn isotopic system examined here, fractionation due to high temperature redox changes likely would be evident. In each of the five tin deposits studied there is a large Sn isotopic variation between early cassiterite and later stannite, between 1.6 and 2.4‰

in  $\delta^{124}\text{Sn}$ . Given the oxidation-dependent mechanism for cassiterite precipitation (Heinrich, 1990), and the results of the synchrotron experiments of Polyakov et al. (2005), this isotopic shift is most likely attributable to the oxidation of  $\text{Sn}^{2+}$  in the hydrothermal fluids. Oxidation-driven precipitation of cassiterite by oxidation left the hydrothermal solution enriched in tin of lighter isotopic composition. Subsequent oxidation of the residual  $\text{Sn}^{2+}$  resulted in the precipitation of stannite with negative  $\delta^{124}\text{Sn}$  values.

Although oxidation-related isotopic fractionation is evident in the three deposits regardless of temperature and depth of emplacement, there is a range of the  $\delta^{124}\text{Sn}_{\text{cassiterite} - \text{stannite}}$  values. This variation could be due to variations in the efficiency of cassiterite precipitation; lower yields of early cassiterite would result in lower values of  $\delta^{124}\text{Sn}_{\text{cassiterite} - \text{stannite}}$ . Alternatively, this range could be related to additional fractionation mechanisms. For instance, as illustrated in Figure 1, porphyries form in shallower environments in which Cl-bearing vapors act as an additional medium of metal transport (e.g., Landtwing et al., 2010). Partitioning of Sn between brine and vapor in a porphyry system likely induces fractionation, similar to that observed in the distillation experiments of Mathur et al. (2017). Fractionation due to partitioning of Sn between vapor and fluid could result in larger compositional variation of the tin minerals, or perhaps impart a shift in the isotopic composition of the fluids from which stannite precipitates.

The relationship between the rocks associated with mineralization and the ores is not easily established with the samples presented here. The igneous rocks presented here were sampled near the igneous source rocks and are thought to be related to the source rocks. Interestingly, all of the igneous rocks near mineralization centers have distinctly lower Sn isotope values in comparison to rocks with no mineralization. The exact cause for the signature is not well constrained at the moment as scant data exist for the causes of Sn isotope fractionation in igneous rocks. However, the data suggest there might be exploration potential for the Sn isotope composition of igneous rocks and proximity to mineralization.

## References

- Badullovich, N., Moynier, F., Creech, J., Teng, F. Z., and Sossi, P. A., 2017, Tin isotopic fractionation during igneous differentiation and Earth's mantle composition: *Geochemical Perspectives Letters*, v. 5, p. 24-28.
- Balliana, E., Aramendía, M., Resano, M., Barbante, C., and Vanhaecke, F., 2013, Copper and tin isotopic analysis of ancient bronzes for archaeological investigation: development and validation of a suitable analytical methodology: *Analytical and bioanalytical chemistry*, v. 405, no. 9, p. 2973-2986.
- Creech, J. B., Moynier, F., and Badullovich, N., 2017, Tin stable isotope analysis of geological materials by double-spike MC-ICPMS: *Chemical Geology*, v. 457, p. 61-67.
- Dauphas, N., Craddock, P. R., Asimow, P. D., Bennett, V. C., Nutman, A. P., and Ohnenstetter, D., 2009, Iron isotopes may reveal the redox conditions of mantle melting from Archean to Present: *Earth and Planetary Science Letters*, v. 288, no. 1, p. 255-267.
- Dauphas, N., Roskosz, M., Alp, E., Neuville, D., Hu, M., Sio, C., Tissot, F., Zhao, J., Tissandier, L., and Médard, E., 2014, Magma redox and structural controls on iron isotope variations in Earth's mantle and crust: *Earth and Planetary Science Letters*, v. 398, p. 127-140.
- Domagal-Goldman, S. D., and Kubicki, J. D., 2008, Density functional theory predictions of equilibrium isotope fractionation of iron due to redox changes and organic complexation: *Geochimica et Cosmochimica Acta*, v. 72, no. 21, p. 5201-5216.
- Haustein, M., Gillis, C., and Pernicka, E., 2010, Tin isotopy—a new method for solving old questions: *Archaeometry*, v. 52, no. 5, p. 816-832.
- Heinrich, C. A., 1990, The chemistry of hydrothermal tin(-tungsten) ore deposition: *Economic Geology*, v. 85, no. 3, p. 457-481.
- Linnen, R. L., Pichavant, M., and Holtz, F., 1996, The combined effects of  $fO_2$  and melt composition on  $SnO_2$  solubility and tin diffusivity in haplogranitic melts: *Geochimica et Cosmochimica Acta*, v. 60, no. 24, p. 4965-4976.
- Linnen, R. L., Pichavant, M., Holtz, F., and Burgess, S., 1995, The effect of  $fO_2$  on the solubility, diffusion, and speciation of tin in haplogranitic melt at 850°C and 2 kbar: *Geochimica et Cosmochimica Acta*, v. 59, no. 8, p. 1579-1588.
- Mason, A., Powell, W., Bankoff, H., Mathur, R., Bulatović, A., Filipović, V., and Ruiz, J., 2016, Tin isotope characterization of bronze artifacts of the central Balkans: *Journal of Archaeological Science*, v. 69, p. 110-117.
- Mathur, R., Powell, W., Mason, A., Godfrey, L., Yao, J., and Baker, M. E., 2017, Preparation and Measurement of Cassiterite for Sn Isotope Analysis: *Geostandards and Geoanalytical Research*, v. 41, no. 4, p. 701-707.
- Sherman, D. M., 2013, Equilibrium isotopic fractionation of copper during oxidation/reduction, aqueous complexation and ore-forming processes: Predictions from hybrid density functional theory: *Geochimica et Cosmochimica Acta*, v. 118, no. 0, p. 85-97.
- Sherman, D. M., Ragnarsdóttir, K. V., Oelkers, E. H., and Collins, C. R., 2000, Speciation of tin ( $Sn^{2+}$  and  $Sn^{4+}$ ) in aqueous Cl solutions from 25°C to 350°C: an in situ EXAFS study: *Chemical Geology*, v. 167, no. 1-2, p. 169-176.
- Yamazaki, E., Nakai, S., Sahoo, Y., Yokoyama, T., Mifune, H., Saito, T., Chen, J., Takagi, N., Hokanishi, N., and Yasuda, A., 2014, Feasibility studies of Sn isotope composition for provenancing ancient bronzes: *Journal of Archaeological Science*, v. 52, p. 458-467.

# Tungsten transport in ore-forming fluids: insights from *ab initio* molecular dynamics simulations

Yuan Mei<sup>1</sup>, Weihua Liu<sup>1</sup>, Xin-Song Wang<sup>2,3</sup>, A.E. Williams-Jones<sup>2</sup>

<sup>1</sup>CSIRO Mineral Resources, Clayton, Victoria, 3168, Australia

<sup>2</sup>Earth and Planetary Sciences, McGill University, 3450 University Street, Montreal H3A 0E8, Canada

<sup>3</sup>State Key Laboratory of Ore Deposits Geochemistry, Institute of Geochemistry, China Academy of Sciences, Guiyang 550005, China

Tungsten is a strategic metal mined mainly from hydrothermal tungstate minerals in which the tungsten is in both tetravalent (e.g., tungstenite,  $\text{WS}_{2(s)}$ ) and hexavalent (e.g., scheelite,  $\text{CaWO}_{4(s)}$ , and ferberite,  $\text{FeWO}_{4(s)}$ ) oxidation states (as reviewed by Brugger et al., 2016). To understand the transport of tungsten in ore-forming fluids and develop geochemical models for the formation of these deposits, we need reliable information on the speciation and thermodynamic properties of tungsten complexes in aqueous fluids over wide ranges of temperature, pressure and chemical composition. In the past four decades, there have been a limited number of experimental studies on W solubility and speciation in hydrothermal fluids (Bali et al., 2012; Redkin and Kostromin, 2010; Wesolowski et al., 1984; Wood, 1992; Wood and Samson, 2000; Wood and Vlassopoulos, 1989). These have shown that W is carried as a tetrahedral tungstate complex (predominantly as tungstate acid ( $\text{H}_2\text{WO}_{4(aq)}$ ) or cation-tungstate ion pair (e.g.  $\text{NaHWO}_{4(aq)}$ ) in hydrothermal fluids up to 600°C and 1 kbar, in highly saline and acidic solutions (i.e., up to 5 m NaCl or 5 m HCl). However, there has been no direct molecular-level study of the mechanism of tungsten complexation under hydrothermal conditions, and thus the role of  $\text{Na}^+$  and  $\text{Cl}^-$ , and ion pairing in aqueous tungsten species are poorly understood.

Our recent studies have demonstrated that *ab initio* molecular dynamic (MD) simulations are able to determine quantitative geometrical and thermodynamic properties for metal complexes in hydrothermal fluids for a wide range of T-P conditions (Mei et al., 2016; Mei et al., 2018; Mei et al., 2014; Mei et al., 2013). Therefore, in this study, we used *ab initio* MD simulations to calculate the speciation and geometries of tungsten W(VI) in NaCl bearing brines up to 600°C, 2 kbar, and investigate the mechanism of deprotonation of the tungstate acid ( $\text{H}_2\text{WO}_{4(aq)}$ ) and its association with  $\text{Na}^+$  and  $\text{Cl}^-$ . Our simulations show that W is mainly transported as tungstates ( $\text{H}_2\text{WO}_4$  and  $\text{HWO}_4^-$ ). The bond distances in  $\text{H}_2\text{WO}_4$  are 1.76 Å for W-O, and 1.86 Å for W-OH, whereas in  $\text{HWO}_4^-$ , the distances are slightly greater, 1.78 Å for W-O and 1.90 Å for W-OH. The geometrical properties are in excellent agreement (within 0.05 Å) with those estimated from previous experimental and theoretical studies (Barrio et al., 2007; Bostick et al., 2018; Mayhall et al., 2009; Zhang et al., 2018). We used the thermodynamic integration method to also determine the acidic constants

of tungstic acid, the stability constants of possible W(VI)-Cl complexes, and the formation constants of cation-tungstate ion pairs (e.g.,  $\text{NaHWO}_{4(aq)}$ ) at temperatures up to 600°C. The derived thermodynamic properties enable better understanding and quantitative modelling of tungsten mobility in hydrothermal systems (Lecumberri-Sanchez et al., 2017; Moura et al., 2014).

## References

- Bali, E., Keppler, H. and Audetat, A. (2012) The mobility of W and Mo in subduction zone fluids and the Mo-W-Th-U systematics of island arc magmas. *Earth and Planetary Science Letters* 351-352, 195-207.
- Barrio, L., Campos-Martín, J.M. and Fierro, J.L.G. (2007) Spectroscopic and DFT Study of Tungstic Acid Peroxocomplexes. *The Journal of Physical Chemistry A* 111, 2166-2171.
- Bostick, B.C., Sun, J., Landis, J.D. and Clausen, J.L. (2018) Tungsten Speciation and Solubility in Munitions-Impacted Soils. *Environmental Science & Technology* 52, 1045-1053.
- Brugger, J., Liu, W., Etschmann, B., Mei, Y., Sherman, D.M. and Testemale, D. (2016) A review of the coordination chemistry of hydrothermal systems, or do coordination changes make ore deposits? *Chemical Geology* 447, 219-253.
- Lecumberri-Sanchez, P., Vieira, R., Heinrich, C.A., Pinto, F. and Wälle, M. (2017) Fluid-rock interaction is decisive for the formation of tungsten deposits. *Geology* 45, 579-582.
- Mayhall, N.J., Rothgeb, D.W., Hossain, E., Jarrold, C.C. and Raghavachari, K. (2009) Water reactivity with tungsten oxides: H<sub>2</sub> production and kinetic traps. *The Journal of Chemical Physics* 131, 144302.
- Mei, Y., Etschmann, B., Liu, W., Sherman, D.M., Testemale, D. and Brugger, J. (2016) Speciation and thermodynamic properties of zinc in sulfur-rich hydrothermal fluids: Insights from *ab initio* molecular dynamics simulations and X-ray absorption spectroscopy. *Geochimica et Cosmochimica Acta* 179, 32-52.
- Mei, Y., Liu, W., Brugger, J., Sherman, D.M. and Gale, J.D. (2018) The dissociation mechanism and thermodynamic properties of HCl(aq) in hydrothermal fluids (to 700 °C, 60 kbar) by *ab initio* molecular dynamics simulations. *Geochimica et Cosmochimica Acta* 226, 84-106.
- Mei, Y., Liu, W., Sherman, D.M. and Brugger, J. (2014) Metal complexation and ion hydration in low density hydrothermal fluids: *Ab initio* molecular dynamics simulation of Cu(I) and Au(I) in chloride solutions (25–1000°C, 1–5000bar). *Geochimica et Cosmochimica Acta* 131, 196-212.
- Mei, Y., Sherman, D.M., Liu, W. and Brugger, J. (2013) *Ab initio* molecular dynamics simulation and free energy exploration of copper(I) complexation by chloride and bisulfide in hydrothermal fluids. *Geochimica et Cosmochimica Acta* 102, 45-64.

Moura, A., Dória, A., Neiva, A.M.R., Leal Gomes, C. and Creaser, R.A. (2014) Metallogenesis at the Carris W–Mo–Sn deposit (Gerês, Portugal): Constraints from fluid inclusions, mineral geochemistry, Re–Os and He–Ar isotopes. *Ore Geology Reviews* 56, 73-93.

Redkin, A.F. and Kostromin, N.P. (2010) On the problem of transport species of tungsten by hydrothermal solutions. *Geochemistry International* 48, 988-998.

Wesolowski, D., Drummond, S.E., Mesmer, R.E. and Ohmoto, H. (1984) Hydrolysis equilibria of tungsten(VI) in aqueous sodium chloride solutions to 300.degree.C. *Inorganic Chemistry* 23, 1120-1132.

Wood, S.A. (1992) Experimental determination of the solubility of  $WO_{3(s)}$  and the thermodynamic properties of  $H_2WO_{4(aq)}$  in the

range 300–600°C at 1 kbar: Calculation of scheelite solubility. *Geochimica et Cosmochimica Acta* 56, 1827-1836.

Wood, S.A. and Samson, I.M. (2000) The Hydrothermal Geochemistry of Tungsten in Granitoid Environments: I. Relative Solubilities of Ferberite and Scheelite as a Function of T, P, pH, and mNaCl. *Economic Geology* 95, 143-182.

Wood, S.A. and Vlassopoulos, D. (1989) Experimental determination of the hydrothermal solubility and speciation of tungsten at 500°C and 1 kbar<sup>1,2</sup>. *Geochimica et Cosmochimica Acta* 53, 303-312.

Zhang, N., Yi, H., Zeng, D., Zhao, Z., Wang, W. and Costanzo, F. (2018) Structure evolution of mononuclear tungsten and molybdenum species in the protonation process: Insight from FPMD and DFT calculations. *Chemical Physics* 502, 77-86.

# North Queensland tectonics & the tin-gold connection

John E. Nethery  
Nedex Pty Ltd

## Introduction

The tectonic and metallogenic model presented in this paper was influenced by the pioneering research of Dr Roger Taylor. The Herberton – Mount Garnet Tinfield, north Queensland, exhibits a series of subparallel WSW-trends and intersecting NW-trends in distribution of the individual tin centres. Additionally, the outer boundary of the tin-field and of “tin granites” was recognised as elongate in the same WSW-orientation that is oblique to the overall regional NW-trend of the Permo-Carboniferous Kennedy Igneous Association (Taylor and Steveson, 1972; Taylor, 1979). This zone was some 150 kilometres wide and extended 200 km from Tinaroo to the Einasleigh River, but is known to extend ENE a further 40 km from Tinaroo to the coast at White Rock. Sporadic occurrences extend WSW from the Einasleigh River for an additional 60 km to the Georgetown district and may extend a further 100 km to the Stanhills Tinfield south of Croydon, although uncertainty remains as to the age of the latter field.

A sub-parallel zone of Oweenee Granite dated 330 Ma with multiple tin occurrences, including Kangaroo Hills, is located 150 km to the south. An additional sub-parallel zone of Early Permian tin-bearing S-type granite is located about 100 km to the north (Figure 1). These three “tin-granite” trends coincide with axes of coeval oroclinal folds with implied crustal overthickening (see below).

## Regional tectonic model

The Palaeozoic Hodgkinson Basin and Broken River Basin are considered to be parts of the same basin based on similar stratigraphy, timing relationships and deformation history (Nethery, 2015). The basin was folded by a major Tabberabberan deformation circa 370 Ma to 325 Ma and is divided by a swath of Kennedy Igneous Association (KIA) intrusive and extrusive rocks. An imbricate thrust package inclusive of the entire Palaeozoic sequence including the Late Silurian to Early Devonian Chillagoe Formation bounds the edge of the Proterozoic craton. Previous modeling invoked overthrusting of the Proterozoic Georgetown Inlier towards the east, southeast and northeast (Shaw, Fawckner and Bultitude, 1987). More recently, field mapping and geophysical modeling of the Hodgkinson Basin invoked an east-over-west inversion closure (Vos et al., 2006). Neither model satisfactorily explains all of the observed structural parameters. Hunter - Bowen deformation is recognised in the eastern sector of the Hodgkinson – Broken River Basin (Davis et al., 2002), but lack of deformation in the latest Carboniferous to early Permian stratified volcanics precludes its influence in the west of the basin around

Chillagoe.

Mid-Carboniferous deformation linked to the Kanimblan Orogeny and Alice Springs Orogeny (Nethery, 2015) produced ENE to ESE-oriented oroclinal folds (megakinks), reverse faults and shallow thrusts throughout central Australia and the southern regions of the Tasmanides (Powell, 1984). Mid-Carboniferous ENE-oriented oroclinal folds and thrusting were invoked by Bell (1980) to explain the concept of a major convoluted linking structure involving the Palmerville, Burdekin, Clark River, and Millaroo faults, which he named the Big Bend Megafold. This interpretation rationalised major changes in orientation of the faults, foliation in Siluro-Devonian plutons of the Georgetown Block, and folding in Hodgkinson, Broken River, Burdekin and Drummond basins.

Revision of the Big Bend Megafold model was previously documented as extended abstracts (Nethery and Barr, 1996; Nethery, 2004). Evidence extends from Cape Melville in the north to at least the Drummond Basin in the south (Figure 2). Noteworthy are shallow dipping mylonitic thrusts at Cape Melville (1) and Mt Mulgrave (5), shallow east-verging back-thrusts overprinting steeply dipping Early Carboniferous inversion structures around Palmerville and Bellevue (4), asymmetric folding within and shallow thrusting at the base of the Carboniferous Boonmoo, Jamtin, Pratt (6) and Redcap (7) volcanic sequences, a high-grade metamorphic dome in the centre of the Georgetown Block (8), late Carboniferous east-west folding in the Bundock Basin and Montgomery Range Igneous Complex (11), north-verging thrusting on the Clark River Fault (12), east-west folding in the Burdekin Basin (14), shallow east-oriented thrusts in the Charters Towers Block (15, 16), northeast-oriented oroclinal folding in the St Anne's Salient of the northern Drummond Basin (20) and folding of the early phase of the Bulgonunna Group (17) (Nethery, 2015). The Alice Springs event waned, circa 310 Ma, and major dextral transensional arcuate fault systems developed, exemplified by the Neo-Palmerville (Nethery, 2015), Dargalong, Gamboola, Robertson River faults, connecting through the St Lawrence, Millaroo, and Mt Perry faults to the dextrally coupled Coffs Harbour - Texas Orocline.

In the Kennedy Igneous Province, four magmatic supersuites were defined by age and whole rock geochemical characterisation (Donchak and Bultitude, 1994). The Late Carboniferous supersuites are of I-type affinity, and span rhyolitic to andesitic compositions, whilst those of Early Permian age are of A-type affinity and - further to the northeast - are S-type, and are rhyolitic / granitic. The initial O'Brien's Creek Supersuite (326-

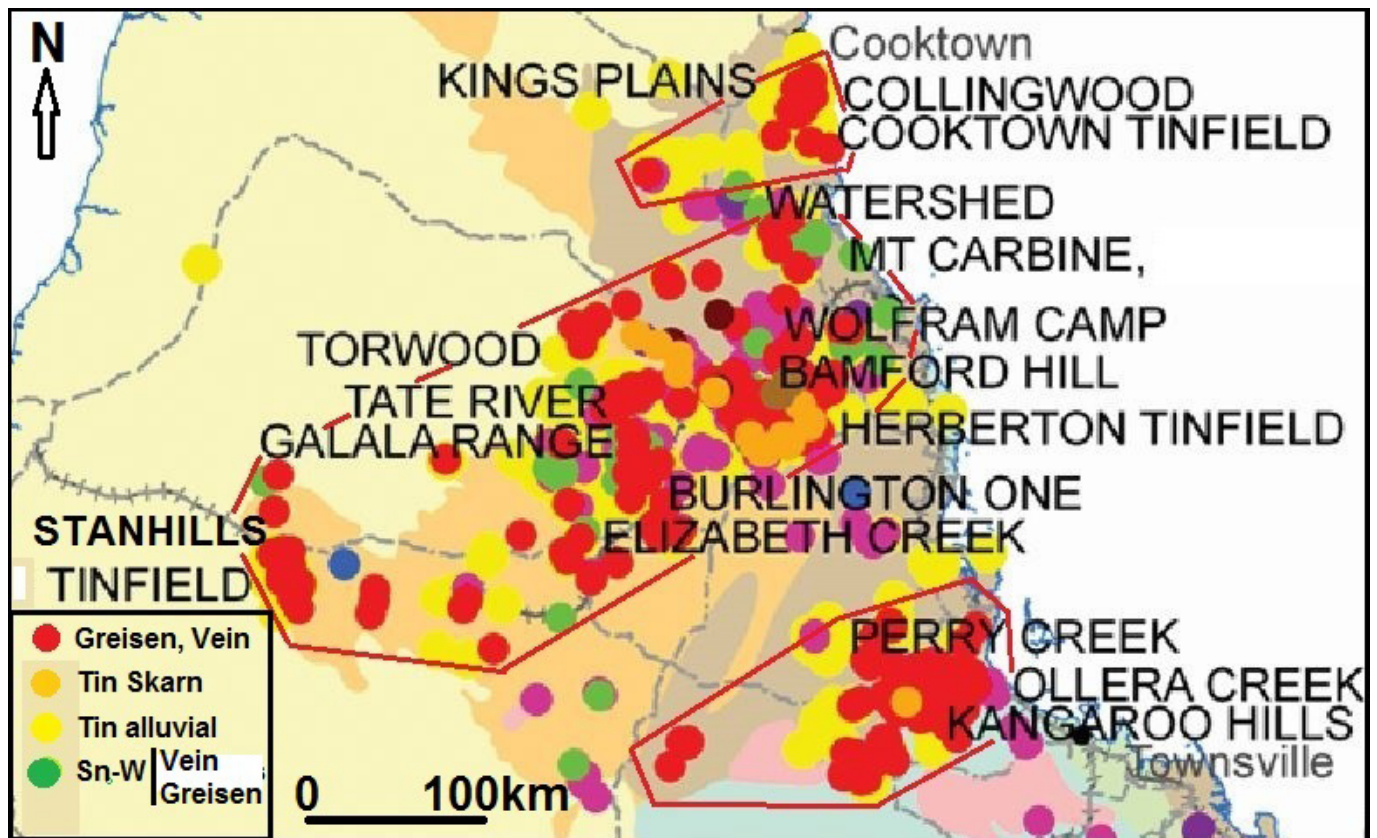


Figure 1. Distribution of tin-fields in NQ. (Section of Geology of Queensland 2013, Fig 10.21).

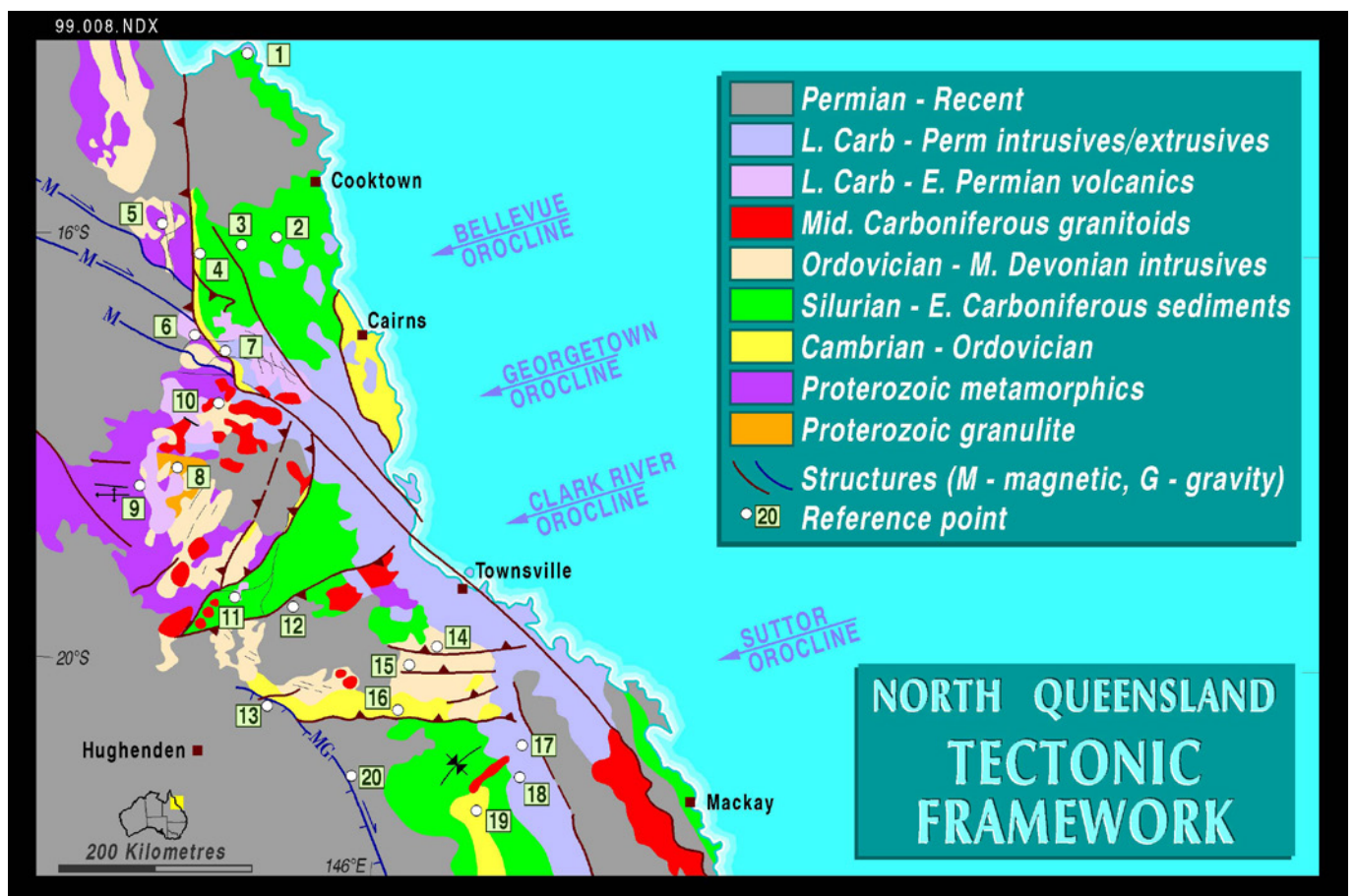


Figure 2. Simplified tectonic framework of North Queensland with numbered features relevant to Carboniferous Alice Springs Orogeny deformation, involving north to south compression.

303 Ma, mean 315 Ma) comprises fractionated reduced I-type plutons and extrusive rocks, with associated tin, tungsten, molybdenum and gold mineralisation (Georges and Nethery, 2009). The Ootann Supersuite (306-299 Ma, mean 300 Ma) comprises fractionated reduced to oxidised I-type plutons and associated tungsten, molybdenum, bismuth, copper, lead, zinc and minor gold mineralisation. The Almaden Supersuite (310-292 Ma, mean 300 Ma) comprises fractionated reduced to oxidised I-type plutons and associated tungsten, molybdenum, bismuth, copper, lead, zinc mineralisation. The final Lags Supersuite (290-280 Ma, mean 280 Ma) comprises A-type plutons / extrusives and minor base metal sulphides and sulphosalts, uranium, fluorine, and minor gold mineralisation.

The initial Carboniferous magmatic suite, and associated extrusives including the O'Brien's Creek Supersuite, are syn-kinematic, focused along the ENE- trending axes of the oroclines and are in part mildly deformed by the oroclinal folding event. This trend also applies to other mid Carboniferous granitic suites such as the Oweenee Granite, south of Greenvale, and the NE Drummond Basin granitoids, north of Mt Coolon. This is in contrast to the more voluminous Late Carboniferous – Early

Permian intrusives and extrusives of the Kennedy Igneous Association which have a southeast trend and are post-kinematic.

### The tin gold connection

An association of tin with Intrusion-Related Gold Systems was initially recognised in 1983 with the discovery of the Anastasia high-sulphidation deposit, in the Tate River – Lynd River district, where an early mesothermal alteration phase containing cassiterite and topaz is overprinted by a later assemblage including gold, alunite, dickite, chalcedony, enargite and other sulphosalts associated with autobrecciated rhyolite (Nethery, 1998). Rock chip samples of silicification were found to contain strongly anomalous gold values to 10 g/t, and tin in the range 100 to 2500 ppm.

Gold deposits including Red Dome, Mungana, Harpers, and Red Hill deposits in the Chillagoe Mineral Field, and the Triple Crown deposit near Mount Garnet related to the O'Brien's Creek Supersuite acid porphyries commonly contain +1000 ppm tin. Most of the gold in these deposits was introduced during retrograde hydrous alteration subsequent to the tin.

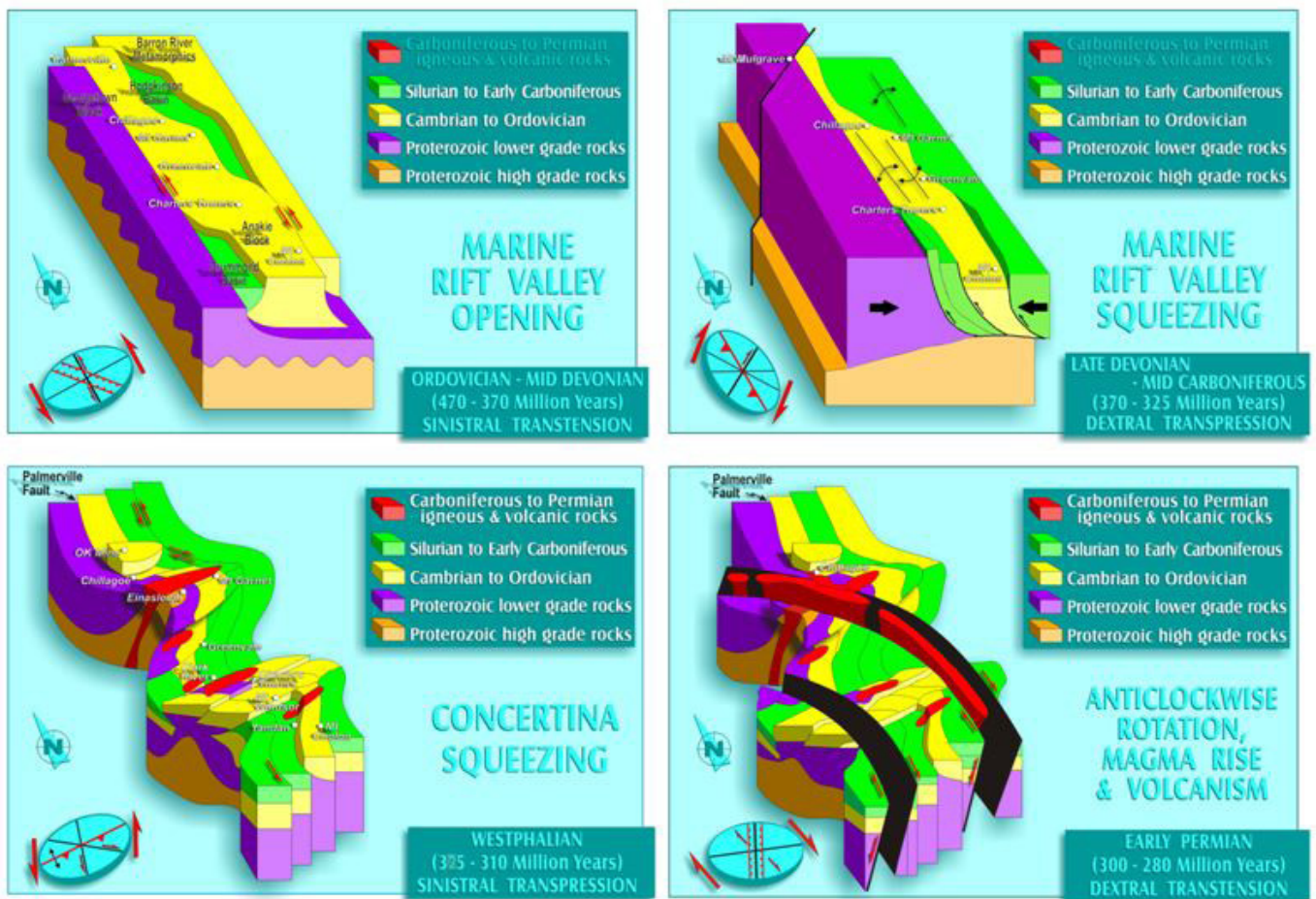


Figure 3: Schematic block models showing proposed tectonic stages through the Palaeozoic.

## References

- Bell, T.H., 1980. The deformation history of northeastern Queensland – A new framework. In Henderson, R A, & Stephenson, P J, (Eds). *The Geology and Geophysics of Northeastern Australia*. Geological Society of Australia, Queensland Division, Brisbane.
- Cheng, Y., Spandler, C., Chang, Z., and Clarke, G. 2018. Volcanic –plutonic connections and metal fertility of highly evolved magma systems: A case study from the Herberton Sn-W-Mo Mineral Field, Queensland, Australia. *Earth and Planetary Science Letters* 486 (2018) 84 – 93.
- Davis, B., Bell, C.C., Lindsay, M., and Henderson, R.A. 2002. A single late orogenic Permian episode of gold mineralization in the Hodgkinson province, north Queensland, Australia. *Economic Geology*, 97 (2). pp. 311-323.
- Donchak, P.J.T., and Bultitude, R.J., 1994. Geology of the Atherton 1:250000 sheet area. Queensland Geological Survey Record 1994/5.
- Georges, C., and Nethery, J.E., 1999. The Mid-Carboniferous tin – gold connection. In abstracts NE Queensland Mineral Exploration. AusIMM FNQ Branch Symposium November 1999.
- Nethery, J.E., 1998. Anastasia gold deposit. *Geology of Australian and Papua New Guinean Mineral deposits* Eds: D A Berkman and D H McKenzie) pp 723 – 728 (The Australasian Institute of Mining and Metallurgy: Melbourne).
- Nethery, J.E., 2004. The IRGS – Orocline connection. A provincial scale tectonic indicator applied to north Queensland. AIG Bulletin No 40. May 2004.
- Nethery, J.E., 2015. Chillagoe District mineralisation – A tectonic model. AIG Bulletin 62, pp 209 – 219(2015).
- Nethery, J.E., and Barr, M., 1996. Revised late Palaeozoic tectonics of north Queensland. Geological Society of Australia Abstracts No. 41, 13th AGC, Canberra, 1996, p 313.
- Nethery, J.E., and Barr, M.J., 1998. Red Dome and Mungana gold – silver – copper – lead – zinc deposits. In *Geology of Australian and Papua New Guinean Mineral deposits* (Eds: D A Berkman and D H McKenzie) pp 723 – 728 (The Australasian Institute of Mining and Metallurgy: Melbourne).
- Powell, C.McA., 1984. Terminal fold-belt deformation: Relationship of mid-Carboniferous megakinks in the Tasman fold belt to coeval thrusts in cratonic Australia. *Geology*, 12: 546 – 549.
- Shaw, R.D, Fawckner, J.F., and Bultitude, R.J., 1987. The Palmerville Fault system: a major imbricate thrust system in the northern Tasmanides, North Queensland, Australian Journal of Earth Sciences, 34: 69-98.
- Taylor R.G. and Steveson B.G., 1972. An analysis of metal distribution and zoning in the Herberton Tinfield, north Queensland, Australia. *Economic Geology*, 67, 1234 – 1240.
- Taylor R.G., 1979. Geology of tin deposits. *Developments in Economic Geology* 11. Elsevier 1979
- Vos, I.M.A., Bierlein, F.P., Barlow, M.A., & Betts, P.G., 2006. The Palmerville Fault, NE Queensland, Australia: A multi-disciplinary approach to understanding major fault systems. *Journal of Structural Geology*, 28, 2097 – 2108.

# Composition, source, and petrogenesis of the Mole Granite, New England Batholith, NSW

Marc Norman

*Research School of Earth Sciences, The Australian National University, 142 Mills Rd., Canberra ACT 2601 Australia*

The Mole pluton in the New England Batholith is a highly fractionated leucogranite that hosts a large number of Sn, W, Bi, As, and base metal deposits. Most of these are located near the roof the pluton, with a pronounced metallogenic zoning concentric to the large metapelite Torrington pendant and contacts with the volcanic and metasedimentary country rocks (Audétat et al., 2000). For example, Sn-dominant deposits tend to occur within the granite interior whereas W is concentrated predominantly around the contact with the roof pendant, and base metal deposits mainly within the country rocks. A notable feature of the Mole is the common occurrence of quartz-topaz silexites and griesens, and the abundance of tourmaline in many of the mineralized veins, indicating the fluorine- and boron-rich nature of the granite and associated fluids.

Here we present a reconnaissance study of the Mole granite that emphasizes whole rock major and trace element compositions, and the Hf-O isotopic and trace element compositions of magmatic zircons. The aim of this work is to better understand the petrogenesis of the Mole granite, including magmatic processes and conditions, the nature of its source, and possible relationships to mineralisation. Previous work on this project was presented by Laker et al. (2017), Laker (2017), Carr et al. (2017), and Norman (2017).

## Samples

Kleeman et al. (1997) identified three textural varieties that seem to correlate with location within the granite and may indicate with an inward progression of crystallisation. These varieties include: (1) megacrystic or porphyritic granite that occurs mainly toward the roof of the pluton, (2) a coarse-grained, seriate granite that comprises the main mass of the Mole, and (3) a microgranite that occurs predominantly as dikes and often associated with alteration or mineralisation. Examples of these textural varieties are shown in Fig. 1.

A key objective of this study was to investigate the age and geochemical relationships between the seriate and microgranite textural varieties as representing the main mass of the granite and potential associations with the mineralisation, respectively. For this, we selected three locations where both of these textural variants are well expressed (Wallaroo, Curnow, and Butler's Prospect) for detailed study of zircon ages, isotopes (Hf, O), and trace element compositions. Thin section images illustrating these coarse-fine pairs are shown in Fig. 2.

## Whole rock compositions

All samples studied here have highly evolved compositions ( $\text{SiO}_2$  75-78 wt%,  $\text{Al}_2\text{O}_3$  11-13 wt%,  $\text{Na}_2\text{O}+\text{K}_2\text{O}$  8-9 wt%,  $\text{K}_2\text{O} > \text{Na}_2\text{O}$ ). They are peraluminous (average ASI = 1.1) and plot near the 1-2 kbar  $P_{\text{H}_2\text{O}}$  minimum melt composition on a normative Q-Ab-Or diagram. Trace element compositions are consistent with a highly fractionated composition, e.g.,  $\text{Rb}/\text{Sr} = 31.5\text{-}197.8$  and  $\text{REE} = 100\text{-}200\times \text{PM}$  with deep negative Eu anomalies (Laker et al., 2017).

While the compositions of the seriate and microgranites are very similar, there are subtle differences. For example, the microgranites tend to have lower  $\text{TiO}_2$ ,  $\text{K}_2\text{O}/\text{Na}_2\text{O}$ ,  $\text{Fe}_2\text{O}_3^*+\text{MgO}$ , Sr, Ba, and Zr compared to the seriate granites, possibly indicating the influence of feldspar+biotite fractionation (Fig. 3). The deeper negative Eu anomalies ( $\text{Eu}/\text{Eu}^* < 1$ ) and higher  $\text{Rb}/\text{Sr}$  in the microgranites are also consistent with plagioclase fractionation. In addition, the microgranites tend to be enriched in mobile elements such as Cu, Mo, and U, possibly indicating an association with mineralising fluids (Plimer and Kleeman, 1985).

## Zircons

Zircons from the seriate and microgranites show dramatic differences in their morphology. For example, zircons from the seriate granites are abundant, have euhedral shapes with well-defined oscillatory zoning, few inclusions and lack inherited cores. In contrast, microgranites yielded fewer grains that have more inclusions, thick rims of low CL activity (dark) or were completely altered. Preliminary observations indicate that this alteration consists of a fine-grained assemblage and so the grains are not strictly 'metamict' due to radiation damage alone. Alternatively, the alteration might be due to reaction of the zircons with late-stage, F-rich fluids although additional work on this is needed.

U-Pb ages, O-isotopes, and Lu-Hf isotopes were all measured on the same grains by SHRIMP (U-Pb, O) and LA-MC-ICPMS (Lu-Hf). U-Pb dating by SHRIMP indicates no statistical differences in ages of the seriate and microgranites, with a weighted mean for all samples of  $247 \pm 2$  Ma. The Wallaroo microgranite yielded an age of  $241 \pm 8$  Ma and so might be slightly younger although only 4 grains could be measured resulting in a relatively large uncertainty. Previous U-Pb dating of cassiterite from various localities around the Mole granite also found an anomalously young age for the Wallaroo site



Figure 1. Hand specimen photos illustrating textural variants of the Mole granite. Upper left: metacrystic, lower left: upper right: microcrystic, lower right: fractures with quartz-cassiterite and alteration.

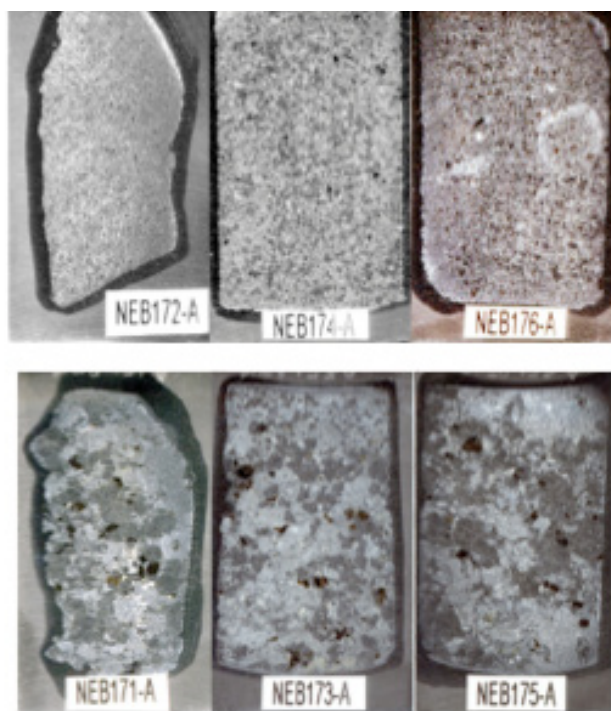


Figure 2. Thin sections of the microgranite (upper row) and seriate granite (lower row) samples studied for zircon ages and isotopic-trace element compositions.

(Prichard, 2013). The altered rims on zircons from the microgranites were strongly enriched in common Pb.

Zircon  $\delta^{18}\text{O}_{\text{VSMOW}}$  ranges from +7.8 to +8.3‰, again with no significant differences between the seriate and microgranites. The Hf isotopic compositions corrected to 247 Ma also show a narrow range ( $\epsilon\text{Hf} = +5.8$  to +6.2), similar to the I-Type granites of the Moonbi Supersuite (Jeon et al., 2014).

Trace element compositions were measured on a separate set of zircons by LA-Q-ICPMS. The time-resolved spectra were often complex, indicating considerable internal heterogeneity that complicated data reduction. Much of this heterogeneity appears to be associated with alteration that introduced variable amounts of  $\text{Ti} \pm \text{Al} \pm \text{P} \pm \text{Th} \pm \text{LREE}$ . Although no single parameter appears adequate to identify the altered grains, many of them have anomalously high Th/U, low Y/Ho, and elevated LREE. Fourteen grains were identified to be the best candidates to preserve primary compositions, all from samples of seriate granites. These had  $\text{U} = 112\text{-}535$ ,  $\text{Y} = 784\text{-}2460$ , and  $\text{Th}/\text{U} = 0.27\text{-}0.81$  with REE patterns typical of primary magmatic zircons from evolved granites. In contrast, zircons from the microgranites often had elevated REE patterns similar to those of the whole rock, consistent with alteration by fluids or melts. None of the zircons from microgranites studied were accepted as primary compositions.

For the zircons accepted as the best candidates for having primary magmatic trace element compositions, Ti concentrations ranged from 4.7-13.7 ppm, corresponding to temperatures of 750-660°C (assuming  $\alpha(\text{Ti}) = 0.8$ ). Uranium, Th, Hf, P, Nb, Ta in these grains show trends of increasing concentrations with decreasing Ti (Fig. 4). The magnitudes of the negative Eu anomalies ( $\text{Eu}/\text{Eu}^*$ ) increase with decreasing Ti, mimicking trends shown in the whole rock data, whereas the other REE show no clear trends with Ti. Assuming that U and Nb behaved as incompatible elements, the relative enrichments of these elements with decreasing Ti would correspond to ~80% crystallisation. Further work to evaluate redox conditions as indicated by Ce anomalies in the zircons is underway.

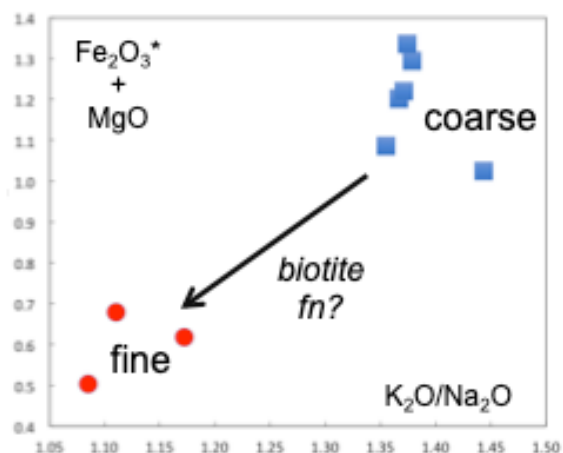


Figure 3. Whole rock  $\text{K}_2\text{O}/\text{Na}_2\text{O}$  vs.  $\text{Fe}_2\text{O}_3^* + \text{MgO}$ , where  $\text{Fe}_2\text{O}_3^*$  represents total iron.

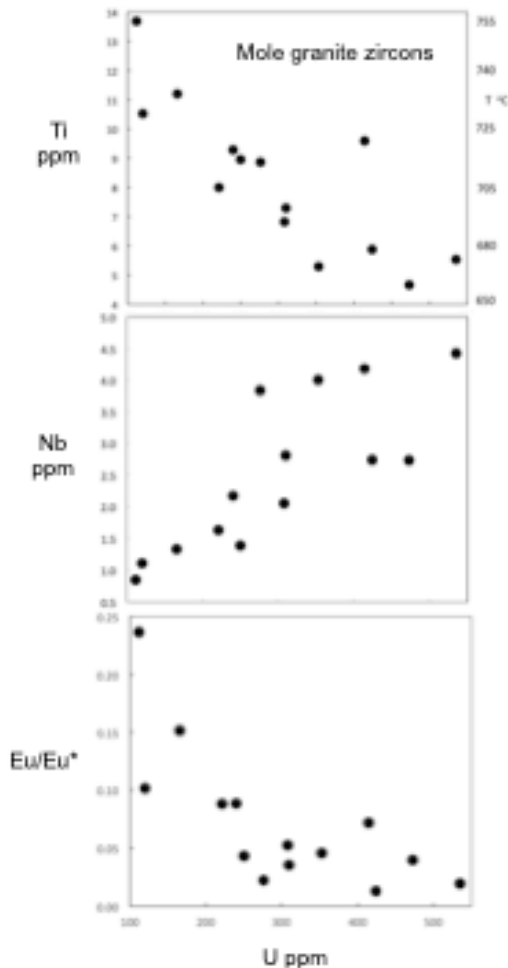


Figure 4. Trace element compositions of magmatic zircons.

### Petrogenesis of the Mole granite

Major element compositions and temperatures inferred from Ti contents of magmatic zircons indicate generation and crystallization of the main mass of minimum melt at ~2 kb, or a depth of ~7 km, apparently followed by migration to shallower depths (~2 km?), emplacement of the microgranites, and expulsion of mineralising fluids as indicated by fluid inclusions, geological relationships, alteration of zircons in the microgranite, and compositions of the mineralising fluids (Kleeman et al., 1997; Audétat et al., 2000). Trace element compositions of whole rocks and zircons indicate that the main mass of granitic melt underwent extensive fractional crystallisation (~80%), which could have enriched fluid-mobile elements such as F, B, Sn, W, and Bi in the melt prior to fracturing and generation of the hydrothermal systems.

The ages of magmatic zircon, molybdenite, and cassiterite associated with the Mole indicate that most of this activity occurred within a relatively brief interval of time at ~247 Ma, followed by reactivation in restricted zones at ~235-240 Ma. The Hf and O isotopic data are consistent with generation of the Mole granite from a moderately weathered and isotopically juvenile source similar to that of the Moonbi Supersuite.

### References

- Audetat A., Gunther D. & Heinrich C. A. (2000) Causes for large-scale metal zonation around mineralized plutons: fluid inclusion LA-ICP-MS evidence from the Mole Granite, Australia. *Econ. Geol.* 95, 1563-1581.
- Carr P., Bennett V., Norman M., Laker D., and Blevin P. (2017) Tourmaline chemistry from the polymetallic Mole Granite, NSW: Identifying the source and evolution of mineralising fluids. In: *Granites2017@benalla*, Australian Institute of Geoscientists Bulletin 65-2017, pp. 30-32. ISBN: 0-9750047-3-5, ISSN: 0812 60 89 (reviewed conference proceedings).
- Jeon H., Williams I. S. & Bennett V. C. (2014) Uncoupled O and Hf isotopic systems in zircon from the contrasting granite suites of the New England Orogen, eastern Australia: implications for studies of Phanerozoic magma genesis. *Geochim. Cosmochim. Acta* 146, 132-149.
- Kleeman J. D., Plimer I. R., Lu J., Forster H. J. & Davidson R. (1997). Timing and Mineralisation Events Associated with the Mole Granite, New South Wales. *Tectonics and Metallogensis of the New England Orogen*. Geological Society of Australia special Publication 19, 254-265.
- Laker D. (2017) Source material of the fractionated Mole Granite: whole rock and zircon analysis. Honours thesis, Research School of Earth Sciences, ANU. 91 pp.
- Laker D., Bennett V., Norman M. Carr P., and Blevin P. (2017) Source material and composition of the fractionated Mole Granite, NSW: an isotopic study of zircons. In: *Granites2017@benalla*, Australian Institute of Geoscientists Bulletin 65-2017, pp. 72-3. ISBN: 0-9750047-3-5, ISSN: 0812 60 89 (reviewed conference proceedings).
- Norman M. (2017) Use of molybdenite and cassiterite to constrain ages and fluid sources of granite-associated mineral systems. In: *Granites2017@benalla*, Australian Institute of Geoscientists Bulletin 65-2017, pp. 93-96. ISBN: 0-9750047-3-5, ISSN: 0812 60 89 (invited presentation, reviewed conference proceedings).
- Plimer I. R. & Kleeman J. D. (1985) Mineralization associated with the Mole Granite, Australia. In: Halls, C. (ed.) *High heat production granites (HHP), hydrothermal circulation and ore genesis*. London, Instn. Min. Metall. pp. 563 569
- Prichard J. (2013) The geochemistry and geochronology of cassiterite, NSW. Honours thesis, Research School of Earth Sciences, ANU. 84 pp.

# Tin-indium-silver-base metal polymetallic epithermal bonanza lodes from the Dover Castle district, Herberton tin-fields, NE Queensland

Nicholas H. S. Oliver<sup>1,2,3</sup>, Matthew Haindl<sup>2</sup>, Shane Mardon<sup>2</sup>, Paul Dirks<sup>3</sup>, Yanbo Cheng<sup>3</sup>, Craig Nettlebeck<sup>2</sup>, Carl Spandler<sup>3</sup>

<sup>1</sup>HCOVGlobal Consultants

<sup>2</sup>Dover Castle Metals Pty Ltd

<sup>3</sup>Economic Geology Research Centre, College of Science and Engineering, James Cook University, Townsville, QLD 4811, Australia

## Introduction

Renewed interest in strategic and 'hi-tech' elements for electric vehicles, robotics, renewable energy and nano-technology in general has driven rapid world-wide exploration in old tin districts, particularly tin and indium (anecdotally associated with the sensitivity of smartphone touch screens). This interest has also extended into elements previously regarded as 'deleterious' for zinc and gold production (e.g. arsenic, antimony, cadmium), for which modern and future demand is accelerating due to 21st century applications. Dover Castle is a historical tin-silver-zinc district near Petford in northern Queensland, that records an extraordinary diversity of metals in galena-sphalerite-dominant bonanza lodes. Although geochemical analysis of these rocks has proven quite difficult due to their very complex mineralogy, they provide an extraordinary opportunity to understand controls on this unusual polymetallic association. A recently released report from Geoscience Australia (Mudd et al., 2018) identifies some key problems: a) insufficient knowledge of critical minerals in Australian deposits and their behaviour during metallurgical processing, and b) few geological studies dedicated to assessing and facilitating the discovery of critical mineral resources in Australia. We present here initial results from a recent mapping, sampling and drilling campaign in this polymetallic base metal - tin system, compare our results with relevant ore deposits elsewhere in the world, and speculate on the nature of the unusual co-association of silver-lead-zinc-(arsenic-antimony-bismuth) with tin-indium-tungsten.

## Global context

Dover Castle contains ores that are particularly rich in lead, zinc, arsenic, silver, antimony, tin, tungsten and indium, with locally high copper and gold. In the broader Herberton - Chillagoe district, most of these metals are well represented, more commonly in separate associations largely considered to be intrusion-related, but locally overlapping in time and space (e.g. Baker et al., 2005; Chang et al., 2017), in skarns, peraluminous granite stockworks, breccias and pipes, and high-grade vein and fault systems. Few locations in the world have reported

co-associated, high grade, base metals, silver, and tin-indium-tungsten. Most prominent in the literature are the polymetallic vein systems from Freiberg in eastern Germany and surrounding Erzgebirge district, where indium was first identified historically. In that district, similar to north Queensland, the truly polymetallic veins at Freiberg lie within a broader district known for separate Sn-W-Mo, and Zn-Pb-Ag-Cu (Seifert & Sandmann, 2006). The host rocks in the Erzgebirge are core complex schists and gneisses, and the ore association is considered to reflect deep metal contributions to the upper crust via lamprophyres (Seifert & Sandmann, 2006). This host rock association is not the case for a similar polymetallic association from a district in Argentina, Pinguino, near the giant Cerra Laguardia low sulfidation epithermal Au-Ag deposit. Pinguino shows many characteristics similar to Dover Castle, with polymetallic sulphide-dominant veins controlled by faults and related veins, hosted by porphyries and volcanic rocks, and lie adjacent to but are cut by quartz-dominant epithermal veins with good evidence for boiling textures (Jovic et al., 2011).

## Dover Castle geology and mineralization

Host rocks are dominated by highly fractionated intrusive rocks of presumed mid-Carboniferous age (O'Briens Creek Supersuite) which intrude felsic to intermediate lapilli tuffs and flow banded rhyolites of the Old Featherbed Volcanics (Fig. 1). Although geochronology on the host rocks at the scale of the polymetallic mineral system are as yet lacking, the district around Dover Castle contains most of the region's large Sn-dominant deposits which are thought to have formed in the 330 to 315 Ma range (Cheng et al., 2018). With around 10 to 20% outcrop, and a very useful soil and rock chip geochemistry program that assisted rock classification, we produced the first detailed geological, structural and alteration map of the area (Fig. 2), as the basis for the developing 3D model utilizing drilling, the recent mapping and geophysical results including a detailed IP survey. Mineralization cuts all these intrusive and volcanic host rocks, and locally defines fault-related boundaries. Ore lodes are predominantly represented by steep, planar faults and planar- to irregularly bound

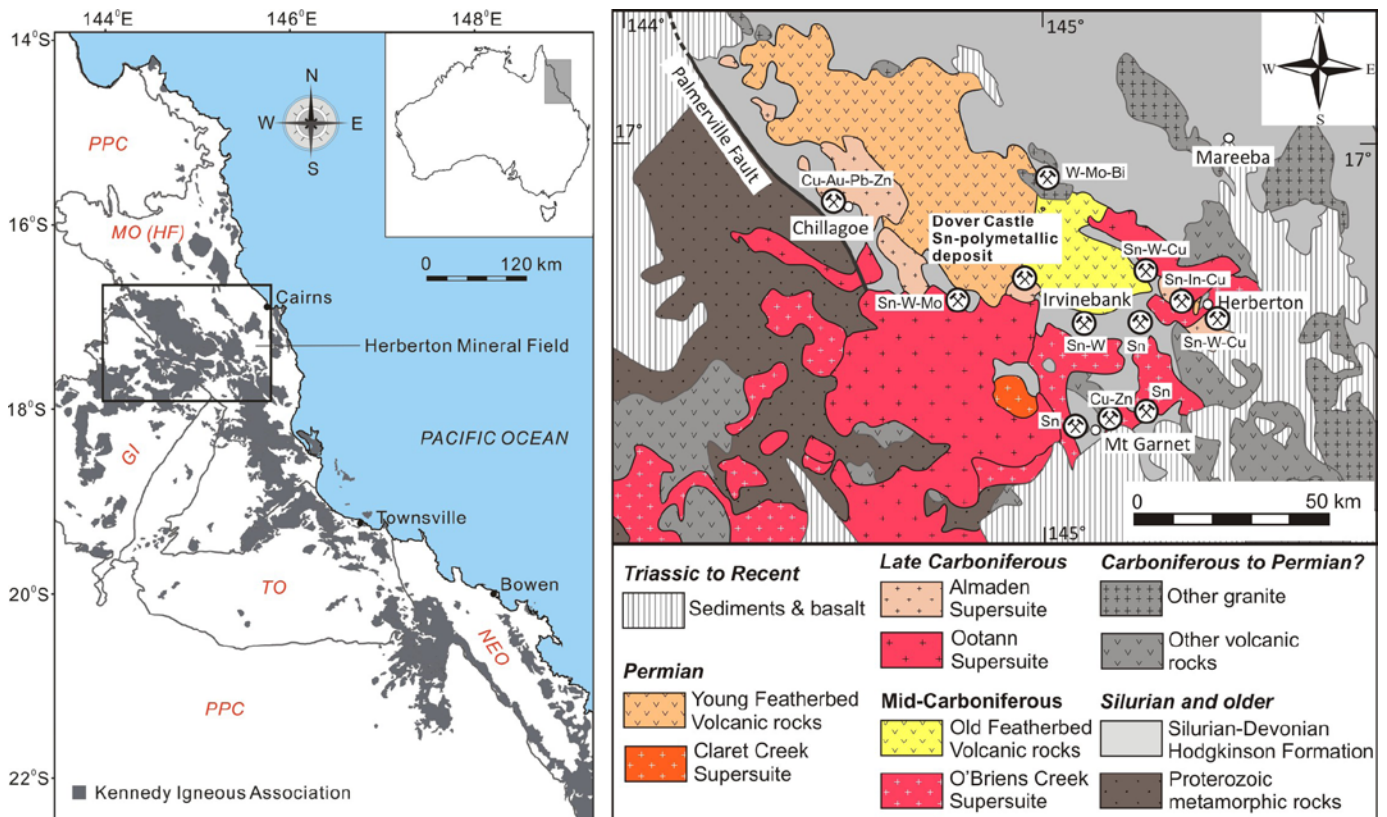


Figure 1. Location of Dover Castle relative to other Sn-W and base metal deposits of the Herberton mineral field, adapted from Cheng et al., 2018.

fault zone stockworks, dominated by sulphide-rich high-grade zones 0.3 to 5m wide, with strike lengths from 10s of metres to a few hundred metres or more (Fig. 2). On the basis of field observations and use of a portable XRF, ore lodes are inferred to be a mixture of dilatant shear veins and intensely altered fault rocks (Fig. 3), although detailed petrography has not been undertaken at the time of writing. Kinematic indicators on the faults are largely lacking but include shallow slickenlines on steep north-striking faults suggestive of a strike slip component late during the structural evolution. Most mineralized faults have steep to moderate east dips geometrically suggestive of normal faults; to date we have not observed clear sulphide-rich tension veins in outcrop that might assist with refining the kinematic understanding. Structural analysis of the gathered data is ongoing. Flanking the mineralized veins almost entirely around the km-scale ore system are very distinctive quartz-rich mosaic breccia veins, 0.2 to 1m across, which display “classic” boiling textures seen in many low sulfidation epithermal Ag-Au systems globally (Figs 2, 3). Locally in the north, these quartz-rich veins grade along strike into mineralized faults, and at least some of the boiling textured quartz appears intergrown with ore minerals in these transition zones.

Alteration and the metal associations are zoned at metre to ore-field scales (Fig. 2, 3). Around individual

or clustered ore lodes, proximal alteration is dominated by sulfidation and intense phyllic and/or argillic alteration (some of the latter may be supergene), at 0.1 to 10m scales. Locally, as at the Dover Castle hill, intense silicification, locally with drusy and/or boiling textured bladed quartz after calcite, lies above or adjacent to known mineralization, forming subvertical fault-related lozenges rather than sub-horizontal sheets that might be regarded as “lithocap”. At 1 to 50m scales around the lodes, there is common disseminated phyllic/silic alteration dominated by disseminated pyrite, local pyrrhotite and arsenopyrite, and varying proportions of secondary silica (fine grained quartz), and white mica. Epidote-chlorite propylitic alteration is typically more distal but also locally appears proximally around some lodes. The ores are zoned from more Sb-As-Ag-rich in the north, to Zn-Pb-Sn rich in the middle, and Cu-Zn rich in the south, suggesting a progressive increase in temperatures of ore precipitation to the south, a zonation also seen vertically. Extraordinary enrichments include up to 500ppm Ag, 6000 ppm Sb, > 5% Sn, all in association with rocks dominated by massive galena, sphalerite and local arsenopyrite (Fig. 4). The gold distribution has not yet been assessed systematically. Indium is strongly co-associated with both Sn and Zn in the drilling program results, and indium values in excess of 3000 ppm have been recorded, making this deposit one of the very richest in indium, globally.

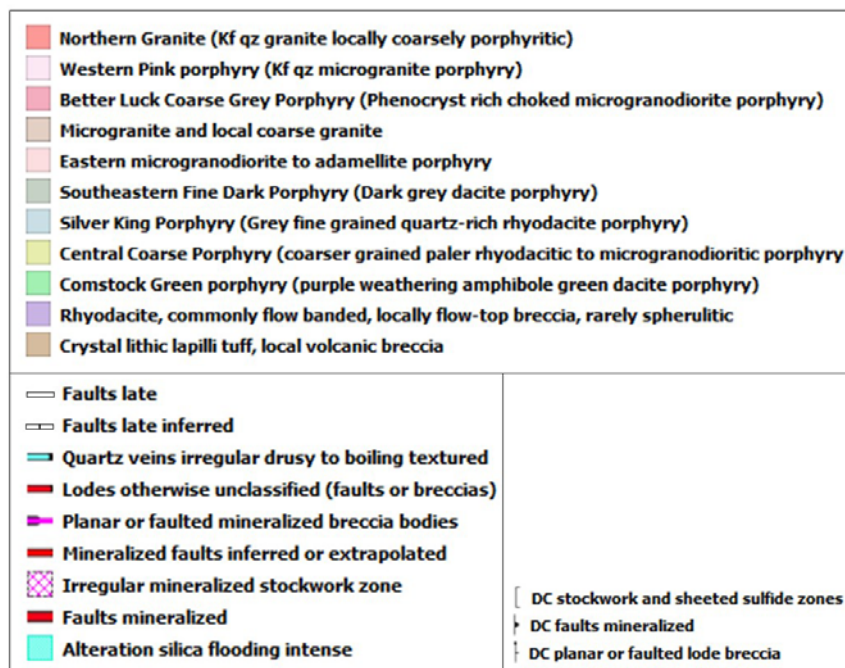
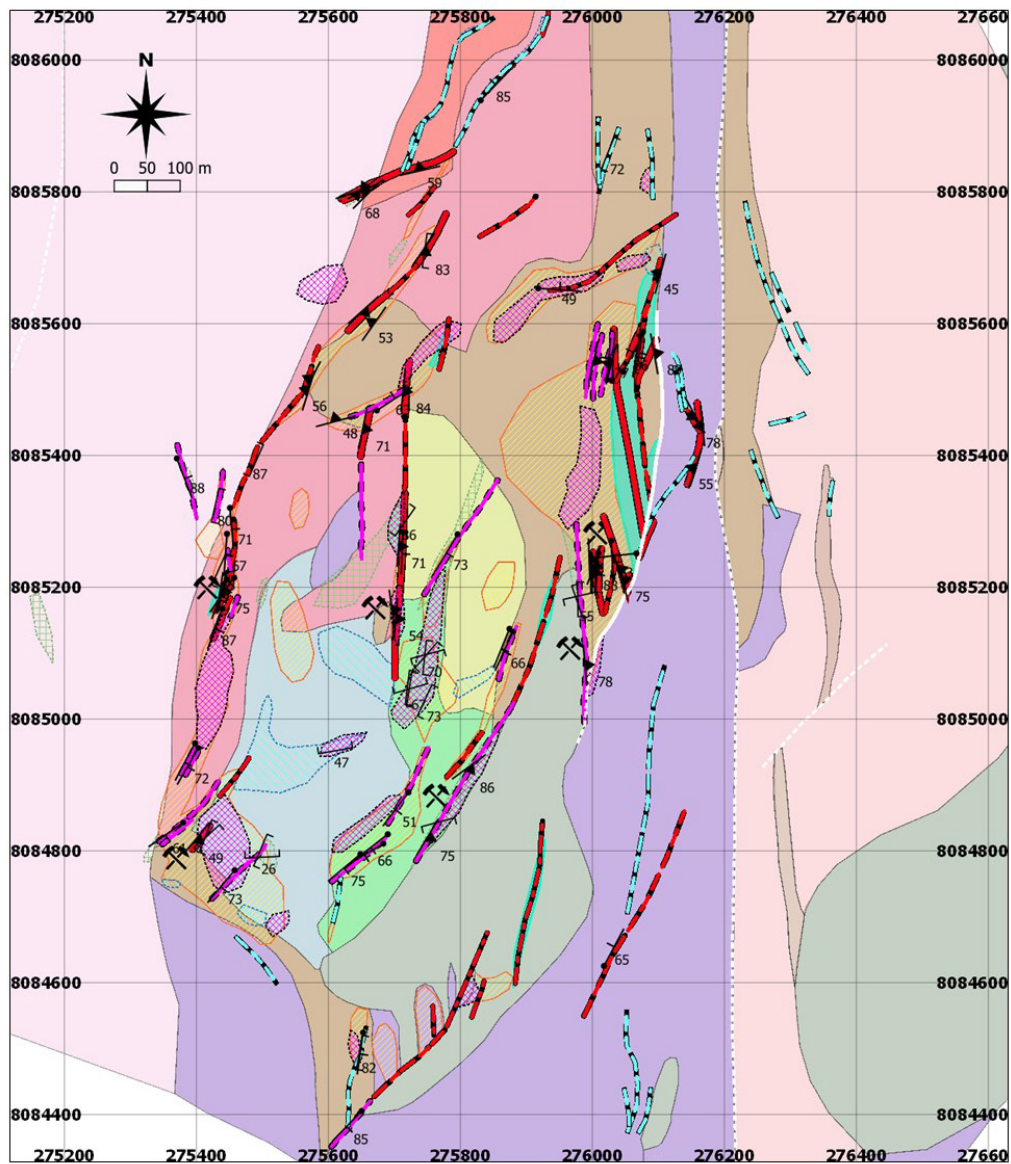


Figure 2. Geological map (this study) of rocks, lodes and structures at Dover Castle showing location of the main historic workings.

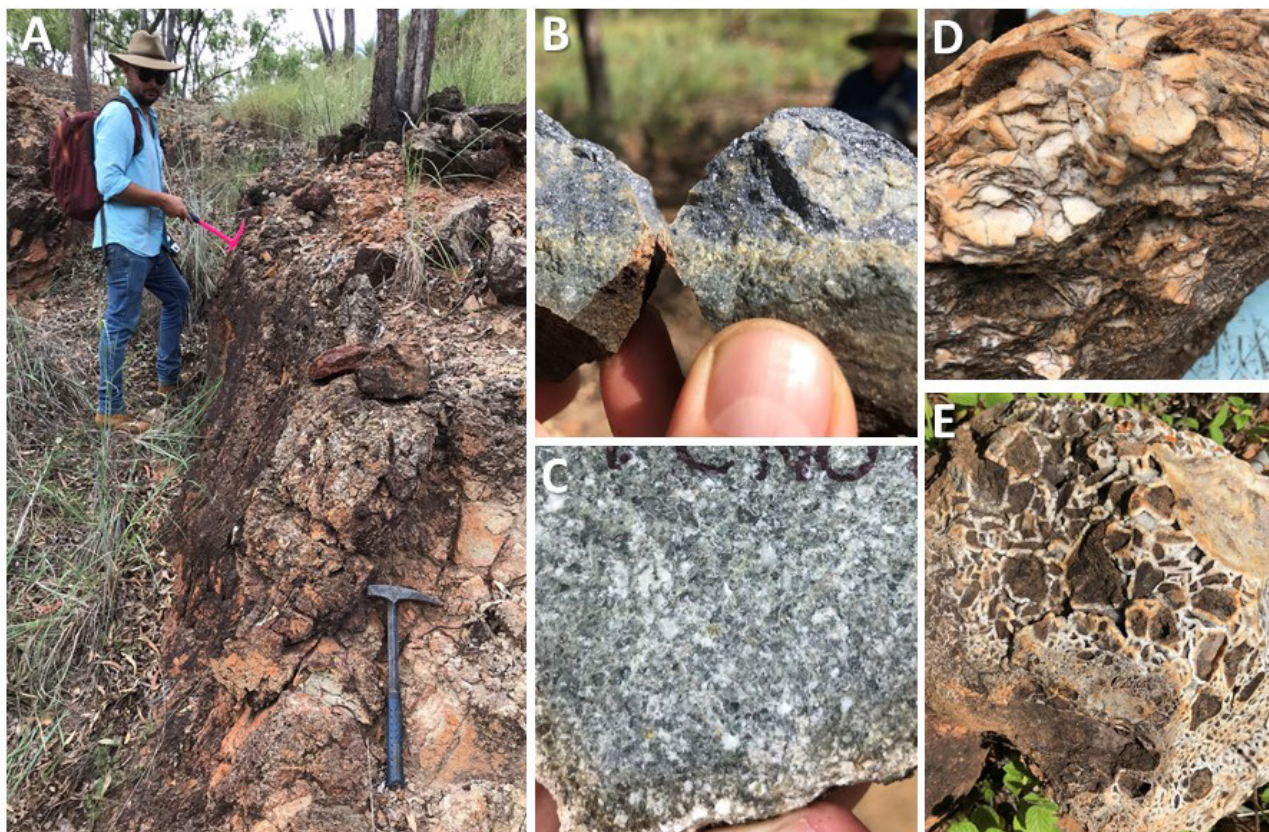


Figure 3. A) Typical high grade lode in the field is defined by fairly sharp-sided sulphide-rich fault zones with internal vein stockworks; B) Hand specimen of high-grade lode with intense quartz-sericite alteration adjacent; C) Little altered host rocks include these crystal-‘choked’ granodioritic to granitic porphyries; D) Epithermal boiling textures such as this quartz after bladed calcite are found in veins flanking the main lode area (Fig. 2); E) Bladed textures are found in association with this cockade quartz-cemented “hedgehog” mosaic breccia, also suggesting boiling.

Sample	Ag (ppm)	As (ppm)	Sb (ppm)	Cd (ppm)	Cu (ppm)	In (ppm)	Fe (%)	Pb (%)	Sn (%)	Zn (%)
DCWD01	64	289	<5	277	371	85	9.33	1.20	6.03	4.09
DCWD02	152	28	<5	9	1990	22	3.50	0.58	8.90	0.11
DCWD03	3	347	<5	8	134	67	8.13	0.10	56.90	0.12
DCWD04	144	257	<5	100	2490	67	6.29	0.85	12.10	1.45
DCWD05	2	27	<5	1	184	3	3.32	0.01	4.44	0.01
DCWD06	162	166000	111	60	9580	134	16.90	0.05	6.76	0.56
BLWD01	328	265	17400	2520	1440	45	2.49	11.45	0.11	36.50
BLWD02	145	1160	316	1650	552	286	3.69	4.83	0.04	21.30
CSWD01	2110	13850	2700	2050	946	781	5.37	42.40	0.01	22.00
DCRX0008	89	4900	19	1	409	9	3.18	2.09		0.03
DCRX0009	600	83	369	17	28	2	2.94	19.15		0.18
DCRX0010	538	35	369	62	79	27	2.23	17.20		0.76
DCRX0011	5030	783	4980	222	604	148	4.23	58.50		0.97
DCRX0012	767	59400	496	17	178	32	11.25	11.35		0.11
DCRX0016	72	663	123	1635	215	125	5.66	0.50		30.50
DCRX0017	316	1690	385	2570	695	398	8.20	5.74		36.50
DCRX0018	4	453	19	4	15	16	6.29	0.49		0.07
DCRX0019	95	172	102	91	199	79	6.01	4.11		1.02
DCRX0020	423	14250	894	1495	2680	3130	4.47	14.35		16.90
DCRX0021	1510	16500	1630	1565	5660	1920	4.73	32.20		17.05
DCRX0022	681	6410	497	847	655	811	3.17	13.60		8.94

Figure 4. Selected sample geochemistry focusing on high grade ores (ALS Orange, Brisbane and Townsville) with ultra-high grades highlighted by cell formatting.

## Discussion and ongoing work

Dover Castle is an example of the relatively scarce global category of Sn-In-W-Ag-bearing base metal polymetallic lodes, and has great potential to be at the forefront of Australia's drive into future strategic element production. Ore characterization and geometallurgy remains a major challenge in the short term, as well as the timing and geological setting of this deposit in the context of the broader Herberton mineral field. Many of these aspects are being addressed by a new collaboration between the organisations represented by the co-authors of this paper. The field associations, metal distribution, alteration and related quartz vein textures strongly suggest that this deposit is a Sn-In-W-Ag-bearing member of the intermediate to high sulfidation category of epithermal system. Mineralization most likely occurred across a 400 to 250°C temperature range at low pressures, and metals were most likely sourced ultimately from a deeper intrusion, probably by release upon boiling of fluids from highly fractionated parts of the I-type O'Briens Creek supersuite at ca. 320 Ma; dating of ore cassiterite is imminent.

## References

- Baker, T., Pollard, P.J., Mustard, R., Mark, G., Graham, J.L., 2005. A comparison of granite-related tin, tungsten, and gold-bismuth deposits: implications for exploration. *SEG Newsletter*, 61, 10-17.
- Chang, Z., Clarke, G., Cheng, Y., Poblete, J., Liu, K., 2017. Sn-W-Mo mineralisation in north-east Queensland. In *Australian Ore Deposits* (Phillips, G. N., ed.), AusIMM, Melbourne, p. 681 – 688.
- Cheng, Y., Spandler, C., Chang, Z., Clarke, G., 2018. Volcanic-plutonic connections and metal fertility of highly evolved magma systems: a case study from the Herberton Sn-W-Mo Mineral Field, Queensland, Australia. *Earth and Planetary Science Letters* 486, 84-93.
- Jovic, S., Guido, D., Schalamuk, I., Ríos, F., Tassinari, C., Recio, C., 2011. Pingüino In-bearing polymetallic vein deposit, Deseado Massif, Patagonia, Argentina: characteristics of mineralization and ore-forming fluids. *Mineralium Deposita*, 46, 257-271.
- Mudd G. M., Werner T. T., Weng Z.-H., Yellishetty M., Yuan Y., McAlpine S. R. B., Skirrow R., Czarnota K., 2018. Critical Minerals in Australia: A Review of Opportunities and Research Needs. *Geoscience Australia Record* 2018/51, 48 pp.
- Seifert, T., and Sandmann, D., 2006. Mineralogy and geochemistry of indium-bearing polymetallic vein-type deposits: implications for host minerals from the Freiberg district, Eastern Erzgebirge, Germany. *Ore Geol. Rev.*, 28, 1-31.

# The Watershed tungsten deposit, NE Queensland, Australia: An example of a Permian metamorphic tungsten upgrade after a Carboniferous magmatic-hydrothermal mineralisation event

Jaime Poblete<sup>1</sup>, Paul Dirks<sup>1</sup>, Jan-Marten Huizenga<sup>1</sup>, Zhaoshan Chang<sup>1,2</sup>

<sup>1</sup>Economic Geology Research Centre, College of Science and Engineering, James Cook University, Townsville, Queensland, 4811, Australia

<sup>2</sup>Colorado School of Mines, Department of Geology and Geological Engineering, 1516 Illinois St, Golden, Colorado, 80401, USA

Tungsten is considered a strategic metal by various countries, including Australia. Between 1998 and 2016 Australia has been steadily increasing its tungsten production, but it is still far smaller than those of the main producers (e.g., China, Russia). Watershed with its current resources of 49.2 Mt averaging 0.14% WO<sub>3</sub> is considered one of the biggest undeveloped tungsten deposits outside of China, and if developed would boost Australia's tungsten production. We will be presenting the geological, geochemical and structural characteristics of the Watershed deposit, as well as the timing, mineral paragenesis and fluid characteristics of the mineralizing system; with the main goal of improving our understanding of the Watershed tungsten deposit and how to explore for similar deposits in northeast Queensland.

## Geological context

The Watershed tungsten deposit lies within the Mossman Orogen (Fig. 1A), which comprises multiply deformed Silurian-Ordovician metasedimentary rocks of the Hodgkinson Formation intruded by Carboniferous-Permian granites of the Kennedy Igneous Association (Fig. 1B) (Champion and Bultitude, 2013; Henderson et al., 2013). The Hodgkinson Formation is host to tungsten, tin, copper and gold deposits (Fig. 1B). The Hodgkinson Formation in the Watershed area comprises skarn-altered conglomerate, psammite and slate units, which record at least four deformation events including early ductile folding and shearing events (D<sub>1</sub> to D<sub>3</sub>) and later brittle-ductile shear zones (D<sub>4</sub>) associated with mineralisation and the emplacement of scheelite-bearing tension veins, which record four separate stages of retrograde metamorphism/alteration (Retrograde Stages 1 to 4). Peak metamorphic assemblages (garnet, actinolite, quartz, clinopyroxene, titanite) in the host rocks to mineralisation formed during D<sub>1-2</sub>. Multiple felsic dykes intruded the metasedimentary rocks at Watershed and include: (a) Carboniferous, monzonite dykes (zircon U/Pb age of 350±3 Ma) emplaced during D<sub>1-2</sub>; and (b) Permian granite plutons and dykes (zircon U/Pb ages of 276±2 Ma, 275±2 Ma and 273±1 Ma), and diorite (zircon U/Pb age of 281±1 Ma) emplaced during D<sub>4</sub>.

## Mineralisation events and paragenesis

An early (syn-D<sub>1-2</sub>) mineralisation event involved the syn-tectonic growth of disseminated scheelite in monzonite dykes and adjacent skarn-altered conglomerate, and was associated with the emplacement of the monzonite, which appears to have enriched the Hodgkinson Formation in W-Be-B-Sc-Cu-Mo-Re. The bulk of the economic scheelite mineralisation formed in syn-D<sub>4</sub> shear-related, quartz-oligoclase veins and associated vein haloes (with a muscovite Ar-Ar age of 276±6 Ma). The veins developed preferentially in skarn-altered conglomerate, and they terminate abruptly where they encounter slate. Vein opening involved four stages, each associated with a characteristic retrograde alteration assemblage. The margins of the D<sub>4</sub> veins contain feldspar, scheelite and quartz, which represent Retrograde Stages 1 and 2. During Retrograde Stage 1 early sanidine (overgrown by plagioclase, An<sub>15-55</sub>) formed with minor quartz. Retrograde Stage 2 is characterised by intergrown scheelite and plagioclase (An<sub>3-43</sub>) overgrowing early plagioclase, phlogopite and trace apatite. Further vein opening during Retrograde Stage 3 infilled the central part of the vein with quartz, which is intergrown with muscovite, calcite and minor chlorite, tourmaline and fluorite. Fractures that formed during Retrograde Stage 4 cut textures belonging to the previous stages and contain pyrrhotite, arsenopyrite with lesser pyrite, chalcopyrite, and sphalerite.

## Scheelite trace element characteristics

Scheelite can incorporate small amounts of REE, and the origin of the scheelite grains (i.e. intrusion-related vs metamorphic) has been investigated using the relative abundance of contained LREE, MREE and HREE. Using ternary REE plots, early D<sub>1-2</sub> scheelite in monzonite coincides with the compositional field for scheelite that forms during magmatic-hydrothermal processes, whereas late D<sub>4</sub> vein-hosted scheelite is compositionally similar to pure hydrothermal scheelite. The Eu and Mo contents of scheelite, coupled with graphite inclusions in scheelite and the presence of pyrrhotite and arsenopyrite in scheelite-bearing veins, show that D<sub>1-2</sub> scheelite precipitated from a relatively oxidized fluid, while vein-hosted D<sub>4</sub> scheelite records a shift to more

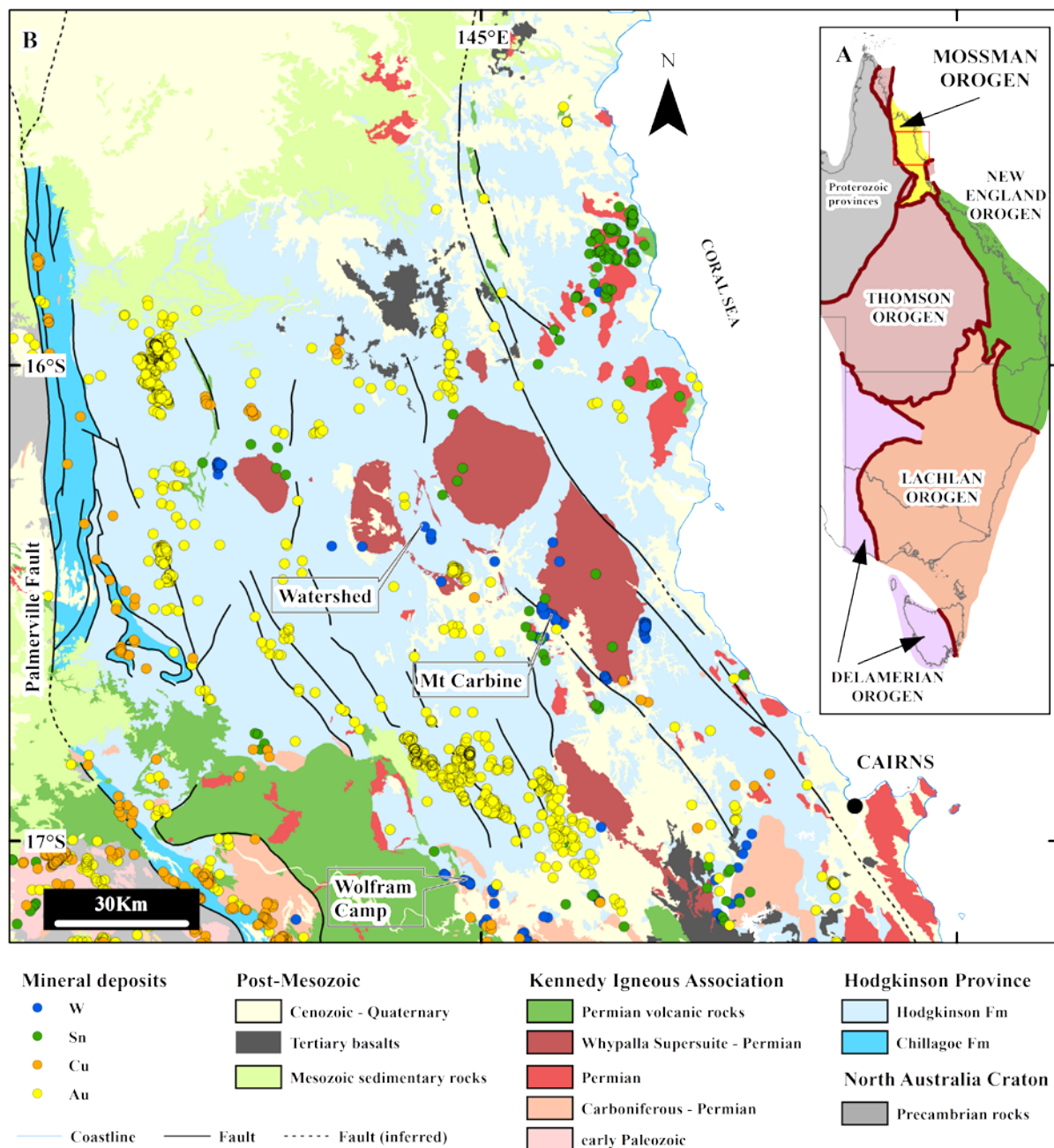


Fig 1. Regional geological setting of the Watershed tungsten deposit in northeast Queensland, Australia. The three largest tungsten deposits of the area are labelled: Mt Carbine (83,706 t WO<sub>3</sub>), Watershed (70,400 t WO<sub>3</sub>) and Wolfram Camp (12,260 t WO<sub>3</sub>). Other tungsten deposits are much smaller (Chang et al., 2017). Also gold, copper and tin deposits hosted in hard rock are shown in the map. Note the higher density of mineral occurrences in the Hodgkinson Formation compared with the rocks of the Kennedy Igneous Association. Mineral occurrences are those compiled by the Geological Survey of Queensland (2017).

reduced conditions as a result of fluid interaction with carbonaceous shale.

### Whole-rock geochemical pathfinders

Whole-rock geochemistry of the various rock types within the deposit indicates that the Watershed deposit is characterised by an enrichment of W-Be-B-Sc-Cu-Mo-Re. These elements were probably remobilised from the Hodgkinson Formation and introduced by hydrothermal fluids during D<sub>4</sub> veining. The fluid interacted with the skarn-altered conglomerate to leach REE, Y and Nb plus skarn-related elements (i.e., Ca-F-P-Fe-Sr), and add

Rb, Cs and Li in vein haloes. Whole-rock geochemistry of psammite units along a 2 km transect north of the deposit shows a regional footprint that is characterised by enrichment in W-Cu-Mo-Ca-Fe-Mn-Li.

### Fluid inclusions and stable isotope characteristics

Fluid inclusions in D<sub>4</sub> vein scheelite and quartz from Retrograde Stage 2 constrain *P-T* conditions during mineralisation to ca. 300°C and 1-1.5 kbar (i.e. depths of 3.5-6 km) indicating a high geothermal gradient, which has been linked to the emplacement of Permian granites.

The  $P$ - $T$  conditions are similar to those recorded in lode-gold deposits in the Hodgkinson Gold Field and elsewhere (Peters et al., 1990; Groves et al., 1998; Vos and Bierlein, 2006). The fluid inclusions preserve a low salinity  $H_2O$ - $NaCl$ - $CH_4$  fluid ( $X_{CH_4} < 0.01$ ) with evidence for fluid-fluid mixing between low- (close to 0 wt.%  $NaCl$ ) and medium-salinity (< 8 wt.%  $NaCl$ ) fluids. The oxygen fugacity was calculated at 0.6 to 0.8  $\log_{10}$  values below the FMQ buffer, consistent with the reduced mineralogy and geochemical signatures.  $\delta^{18}O_{VSMOW}$  values obtained for scheelite (+3.4 to +7.3‰), plagioclase (+7.0 to +11.8‰) and quartz (+12.6 to +15.5‰), which formed during Retrograde Stage 2, and  $\delta D_{VSMOW}$  (-73.4 to -62.7‰) and  $\delta^{18}O_{VSMOW}$  (+11.5 to +13.2‰) values for muscovite that formed during Retrograde Stage 3 are indicative of a metamorphic origin for the mineralising fluids, with a possible magmatic component. Sulphur isotope ( $\delta^{34}S_{CDT}$ ) values for sulphides formed during Retrograde Stage 4 in veins are consistent with the presence of seawater sulphate (i.e. basinal brine) in the system. Metamorphic fluids probably originated from prograde devolatilisation reactions during metamorphism of the Hodgkinson Formation.

### Main findings

Our findings indicate that tungsten was sourced from Carboniferous monzonite, which enriched the metasedimentary rock units of the Hodgkinson Formation during the early stages of deformation/ metamorphism. Continued ductile deformation and associated metamorphism during  $D_{1-3}$  caused devolatilisation reactions in the host rocks and remobilisation of tungsten. Permian scheelite mineralisation during  $D_4$  involved a metamorphic-hydrothermal fluid with minor magmatic input that deposited tungsten at 300°C and 1-1.5 kbar (<6 km depth). This tungsten was transported as  $NaWO_4^-$ ,  $HWO_4^-$  and  $WO_4^{2-}$  complexes (Wood and Samson, 2000) along extensional shear zones. Calcium was supplied by the skarn-altered conglomerate that hosts the scheelite-bearing veins. It is proposed that the precipitation of scheelite was promoted by the interaction between the relatively acidic hydrothermal fluids and the alkaline, carbonate-rich, skarn-altered conglomerate host rock, lowering the solubility of the tungsten complexes and co-precipitating scheelite and Na-rich plagioclase during Retrograde Stage 2.

The main controls on economic scheelite mineralisation at Watershed include: (a)  $D_4$  shear-zones that formed in response to N-S extension; (b)  $D_4$  tension veins (commonly E-W trending), that opened up in association with the shear-zones; (c) skarn-altered conglomerate units that supplied Ca as well as chemical (pH) and physical (localisation of tension veins) controls on mineralisation; (d) an extensional setting to allow fluid penetration; (e) high geothermal gradients driving fluid flow; and (f) the presence of ~350 Ma, scheelite-enriched monzonite dykes that appear to have prepared the ground. Thus, exploration should focus on the identification of ~350 Ma intrusions in association with skarn-altered units, and younger (i.e.  $D_4$ ) shear-zones that formed in an extensional regime. Considering a continuum model for this deposit type (i.e. mineralisation could form between 2-20 km depth) there is potential for mineralisation at depth.

### References

- 2017, Queensland Mineral Occurrence Data, in Greenwood, M., ed.: Brisbane, Queensland, Australia.
- Champion, D. C., and Bultitude, R. J., 2013, Kennedy Igneous Association, in Jell, P. A., ed., Geology of Queensland: State of Queensland, Geological Survey of Queensland, p. 473-514.
- Chang, Z., Clarke, G., Cheng, Y., Poblete, J., and Liu, K., 2017, Sn-W-Mo mineralisation in north-east Queensland, in Phillips, G. N., ed., Australian Ore Deposits: Melbourne, Australia, The Australasian Institute of Mining and Metallurgy, p. 481-488.
- Groves, D. I., Goldfarb, R. J., Gebre-Mariam, M., Hageman, S. G., and Robert, F., 1998, Orogenic gold deposits: A proposed classification in the context of their crustal distribution and relationship to other gold deposit types: *Ore Geology Reviews*, v. 13, p. 7-27.
- Henderson, R. A., Donchak, P. J. T., and Withnall, I. W., 2013, Mossman Orogen, in Jell, P. A., ed., Geology of Queensland: State of Queensland, Geological Survey of Queensland, p. 225-304.
- Peters, S. G., Golding, S. D., and Dowling, K., 1990, Melange- and Sediment-Hosted Gold-Bearing Quartz Veins, Hodgkinson Gold Field, Queensland, Australia: *Economic Geology*, v. 85, p. 312-327.
- Vos, I. M. A., and Bierlein, F. P., 2006, Characteristics of orogenic-gold deposits in the Northcote district, Hodgkinson Province, north Queensland: implications for tectonic evolution: *Australian Journal of Earth Sciences*, v. 53, p. 469-484.
- Wood, S. A., and Samson, I. M., 2000, The Hydrothermal Geochemistry of Tungsten in Granitoid Environments: I. Relative Solubilities of Ferberite and Scheelite as a Function of  $T$ ,  $P$ , pH, and  $mNaCl$ : *Economic Geology*, v. 95, p. 143-182.

# Magmatic and hydrothermal evolution of the Yichun Ta-Sn-Li deposit, south China

Peter J. Pollard

*Pollard Geological Services Pty. Ltd., 7 Jillinda Place, The Gap, Queensland, Australia 4061*

The Yichun Ta-Sn-Li deposit occurs within the 9.5 km<sup>2</sup> Yashan igneous complex (YIC), south China. The roof zone of extensive two-mica granite has been intruded by a sheet-like body of Li-mica granite which is overlain by a thin sheet of topaz-lepidolite granite and a marginal pegmatite at the upper contact. Ta-Sn-Li mineralization occurs predominantly in the topaz-lepidolite granite which is characterized by the presence of snowball textures in quartz, K-feldspar and topaz phenocrysts (Yin et al., 1995). Interstitial areas are composed mainly of lepidolite, albite and amblygonite, together with minor cassiterite, columbite-tantalite, microlite, monazite and pollucite.

Wu et al. (2018) interpret many of the petrographic and mineral chemical features of the topaz-lepidolite granite at Yichun as a resulting of post-magmatic alteration. In particular, they interpret snowball-textured quartz with zonally arranged albite laths to result from quartz alteration of pre-existing lepidolite because they believe some contacts between quartz and lepidolite near the margins of the snowball quartz indicate quartz alteration of lepidolite.

In reality, snowball textures at Yichun occur within quartz, K-feldspar and topaz phenocrysts, with the albite laths arranged parallel to crystallographic planes (growth zones) within these crystals. This must reflect simultaneous crystallization of quartz, topaz, K-feldspar and albite and replacement of pre-existing lepidolite is extremely unlikely. Progressive increase in the phosphorus content of albite inclusions from core to rim within a K-feldspar phenocryst (Huang et al., 2002) is also consistent with a magmatic origin due to progressive increase in the phosphorus content of the melt during formation of the snowball textured phenocrysts, followed by crystallization of amblygonite in the matrix.

Whole-rock geochemical data show a large compositional gap of >3.5 wt.% SiO<sub>2</sub> and 2.5 wt.% Al<sub>2</sub>O<sub>3</sub> between the Li-mica granite and topaz-lepidolite granite. Similarly, F, Li and P are very low in the Li-mica granite (F = 0.05-0.24 wt.%, Li<sub>2</sub>O = 0.02-0.11 wt.%, P<sub>2</sub>O<sub>5</sub> = 0.16-0.24 wt.%) compared to the strongly enriched the topaz-lepidolite granite (F = 1.09-2.30 wt.%, Li<sub>2</sub>O = 0.90-2.09 wt.%, P<sub>2</sub>O<sub>5</sub> = 0.43-0.54 wt.%). These compositional gaps are not easily explained by fractional crystallization models and other evolutionary mechanisms need to be considered.

Constitutional zone refining (London and Morgan, 2012) and melt immiscibility models (Thomas et al., 2006) have both been used explain the evolution of

rare-metal granites and pegmatites. The low F, Li and P contents of the Li-mica granite at Yichun indicate melt immiscibility is very unlikely as this typically requires F contents of >2 wt.%. Constitutional zone refining in the context of granitic magmas involves crystallization of mainly quartz, feldspar and mica in undercooled melt which leads to generation of a boundary layer melt depleted in SiO<sub>2</sub> and strongly enriched in flux and incompatible elements (London and Morgan, 2012). At Yichun, crystallization of the Li-mica granite may have led to separation of a boundary layer melt due to its very low viscosity compared with adjacent undepleted melt, allowing accumulation in the roof zone of the granite and leading ultimately to formation of the marginal pegmatite and topaz-lepidolite granite.

The marginal pegmatite at Yichun ranges up to 7 metres thick (Yin et al., 1995) and has been divided into core zone (upper contact), intermediate zone and wall zone (lower contact) (Wu et al., 2018). The intermediate zone contains nodules made up of minerals including columbite, uraninite, zircon, xenotime, monazite, lepidolite, molybdenite and bismuth (Wu et al., 2018). Nodules with similar mineralogy are thought to have crystallized from peralkaline melts formed by melt immiscibility in F-rich peraluminous magmas (Thomas et al., 2006). This peralkaline signature is also a feature of a minor quartz-lepidolite greisen zone formed at the top of the topaz-lepidolite granite which is enriched in K, Rb, Cs, Li, F, Ba, Sr, Ti, Zr, Nb, W, Th and REE compared with the adjacent granite.

## References

- Huang, X.L., Wang, R.C., Chen, X.M., Hu, H., Liu, C.S., 2002. Vertical variations in the mineralogy of the Yichun topaz-lepidolite granite, Jiangxi Province, southern China. *Canadian Mineralogist* 40, 1047-1068.
- London, D. and Morgan, G.B., 2012. The pegmatite puzzle. *Elements* 8, 263-268.
- Thomas, R., Webster, J.D., Rhede, D., Seifert, W., Rickers, K., Foster, H.J., Heinrich, W., Davidson, P., 2006. The transition from peraluminous to peralkaline granitic melts: evidence from melt inclusions and accessory minerals. *Lithos* 91, 137-149.
- Wu, M., Samson, I.M., Zhang, D., 2018. Textural features and chemical evolution in Ta-Nb oxides: Implications for deuteric rare-metal mineralization in the Yichun granite-marginal pegmatite, southeastern China. *Economic Geology* 113, 937-960.
- Yin, L., Pollard, P.J., Shouxi, H., Taylor, R.G., 1995. Geologic and geochemical characteristics of the Yichun Ta-Nb-Li deposit, Jianxi Province, south China. *Economic Geology* 90, 577-585.

# Influence of protolith chemistry on the regional distribution of Phanerozoic magmatic tin deposits

Rolf L. Romer<sup>1</sup>, Uwe Kroner<sup>2</sup>

<sup>1</sup>*Inorganic and Isotope Geochemistry, GFZ German Research Centre for Geosciences, Telegrafenberg, 14473 Potsdam, Germany*

<sup>2</sup>*Department of Geology, TU Bergakademie Freiberg, B. v. Cotta Str. 2, 09596 Freiberg, Germany*

Economically interesting Phanerozoic Sn mineralization occurs in belts that follow actual and former plate boundaries and is related to highly evolved granites, which are the local metal sources for Sn-greisen, Sn-vein and Sn-skarn type deposits. Although the relation between Sn belts and plate boundaries was taken as evidence for the importance of active subduction for the formation of Sn mineralization (Fig. 1), it is well-established now that Sn mineralization may form in a wide range of tectonic settings (Mitchell and Garson, 1981), such as subduction zones (e.g., Andes, Nova Scotia, SE China), continental collision zones (e.g. Erzgebirge), and rifting and extension zones (e.g., Cornwall). It is also well established that Sn mineralization within a particular Sn belt may have a wide range of different ages, may form on either side of the suture, and may have formed in different settings. These latter features indicate that the particular tectonic setting is not essential. Instead, the key features for the formation of Sn-specialized granites are the protoliths and the heat sources that permit melting of these protoliths. The protolith distribution eventually controls where tin belts may form and the availability of heat sources determines the age of mineralization.

The close relation of Sn mineralization with reduced (mainly ilmenite series), highly fractionated granites eventually formed the base for models for Sn mineralization, involving extreme magmatic fractionation followed by late-stage fluid-melt separation (e.g., Lehmann 1982).

Highly fractionated granites do not always show Sn mineralization, which implies that “highly evolved” is not a sufficient criterion for Sn mineralization. Sato (2012) highlighted the role of sedimentary protoliths to produce reduced melts and Sn mineralization, whereas Romer and Kroner (2015, 2016) highlighted the importance of intense chemical alteration of the sedimentary protolith for the formation of granite-bound Sn mineralization. The implicit key point of this latter statement is that the formation of Sn-specific granites involves a series of processes that occur in different settings, i.e., (i) intense chemical alteration (on the continent), (ii) sedimentary and tectonic accumulation (at the continent and plate margin, respectively) and (iii) high-temperature melting (at the plate margin). Each of these stages is necessary and they have to occur in the right order. They may be widely separated in time and bound to entirely unrelated event. The key implication of such a sequence of processes is that (i) the importance of each stage can be tested and

quantified and, (ii) the primary search target is not the presence of highly evolved granites, but whether the target area has the right geological history.

## Three stages on the way to Sn-specific granites

(i) Intense chemical alteration of silicate rocks occurs in tectonically stable areas with limited topography, as for instance in the interior of large continental masses. Especially, supercontinent assembly may represent ideal situations as the orogenic belts that formed during assembly provide copious amounts of sedimentary debris and the internal basins allow for multiple sediment redistribution, eventually leading to huge volumes of intensely altered sediments.

(ii) Source accumulation involves two separate processes; i.e., sedimentary and tectonic accumulation. (a) Sedimentary accumulation occurs when the chemically intensely altered sediments on “top” of the continent are redistributed to the margins of the continent, where they may form several thousand meter thick units of sediments carrying the chemical fingerprint of intense chemical alteration. Large-scale redistribution of intensely altered sediments may be caused by the fragmentation of supercontinents. The geochemical signature of intense chemical alteration is particularly prominent in the first sediments deposited in the newly formed basin, which may be particularly voluminous in deltas formed by major rivers. (b) Tectonic accumulation occurs when sedimentary packages deposited at a passive-margin are reworked in an active-margin setting. Source accumulation may be particularly important when delta deposits become tectonically stacked.

(iii) The nature of heat source controls the type of melting of the crustal source rocks and the partitioning of metals between melt and restite. Biotite-dehydration melting seems to be necessary to partition Sn preferentially into the melt. Internal heating of orogenically thickened crust only generates minimum-temperature melts (muscovite-dehydration melts). Biotite-dehydration melting requires external heat input from the mantle by (a) mantle-derived melts in subduction settings, (b) emplacement of ultrahigh-temperature metamorphic rocks that had been subducted to mantle depth during continental collision, and (c) mantle-derived melts in extensional settings. The age of mineralization reflects the event of heat input.

This three-stage process explains the distribution of Sn in belts at continent margins and the irregular distribution of Sn districts within these belts. Important Sn districts

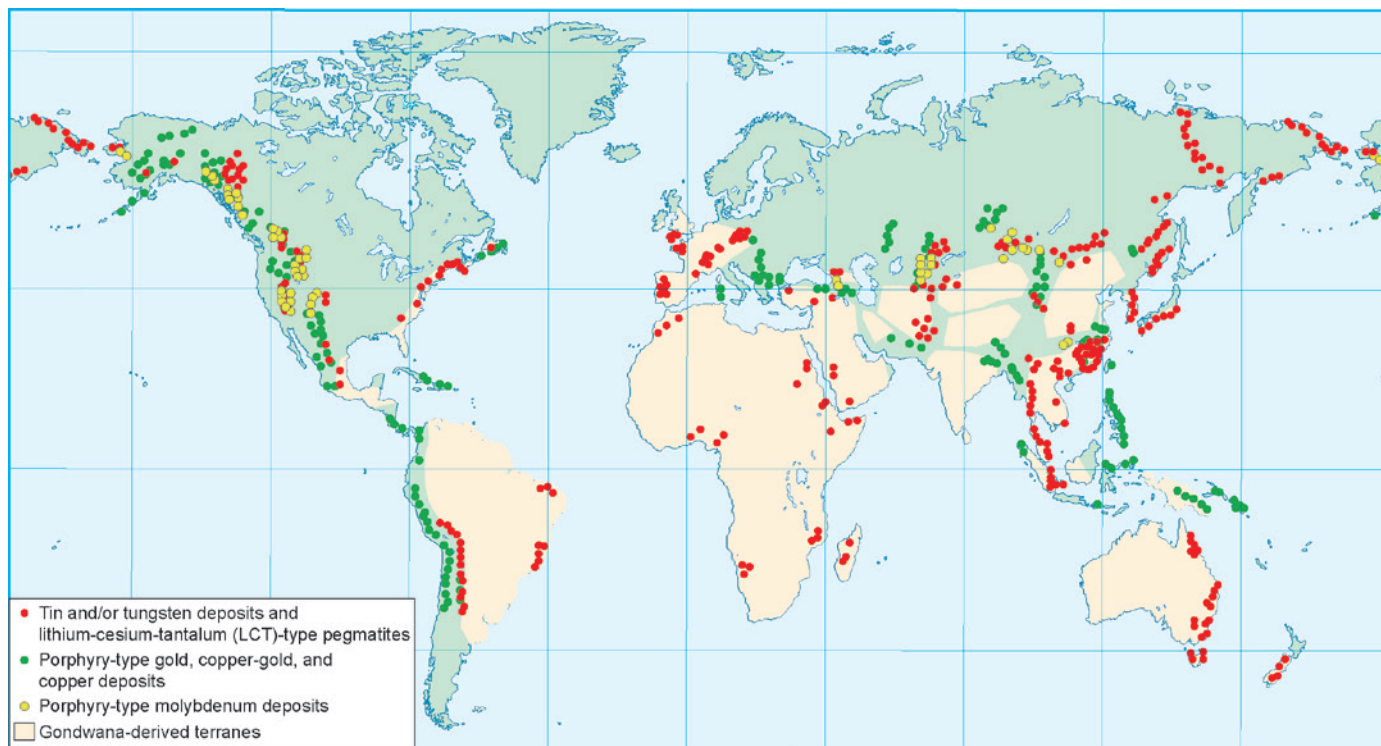


Fig. 1. Global distribution of Phanerozoic Sn-W deposits, LCT-type pegmatites, and Cu-Au and Mo porphyry-type deposits. The distribution is shown schematically to highlight the belts and to avoid crowding in major deposit provinces. The spatial separation of Sn-W and Cu-Au belts may host deposits of different age, reflecting that suitable Sn-W protoliths may have exposed to conditions favorable for metal mobilization in different segments of the belt at different time (for data sources see Romer and Kroner, 2016).

may correspond to areas with particularly voluminous packages of intensely-altered sedimentary protoliths, whereas areas without important packages of such protoliths are unlikely to develop Sn mineralization. Large volumes of suitable protoliths, however, are not sufficient for the development of Sn mineralization: The protoliths have to be exposed to high-temperature melting. The availability of heat sources inducing high-temperature melting determines the age of Sn mineralization. As different segments of a belt of suitable protoliths may melt during geologically entirely unrelated events, this model also explains the regionally variable age distribution within a Sn belt.

### The role of intense chemical alteration of the sedimentary protoliths on ore element partitioning during dehydration melting

Partial melting of metasedimentary rocks results in contrasting chemical (and isotopic) compositions of melt and restite. The major element composition of the melt is essentially buffered by the relative contribution and composition of the minerals taking part in the melting reaction. The trace element signature of this melt is the result of several processes: (i) The content of trace elements derived from melting of major phases may be modified by redistribution from the melt into the restite, largely depending on the mineral assemblage of the restite. (ii) Trace elements largely hosted in accessory phases will contribute to the extent these phases are dissolved in the melt, as for instance Zr or Ti saturation, which depends on temperature and melt chemistry.

Melting conditions and amounts of melt that may be produced by anhydrous melting largely depends on the mineralogy of the metamorphic protolith, which depends on the chemistry of the sedimentary protolith.

Intense chemical alteration of silicate rocks at the surface results in the preferential loss of most feldspar-bound elements (e.g., Na, Ca, Sr, and Pb) and in the residual enrichment of elements that are incorporated in or adsorbed on clay minerals and Fe-oxyhydroxides (e.g., Li, K, Rb, Cs, Sn, and W). Such sedimentary rocks are characterized by high K/Na, K/Ca, and Rb/Sr ratios. Thus, exogenic processes produce some of the geochemical hallmark signatures of Sn-specific granites, which generally are interpreted as evidence for extreme magmatic fractionation of granitic melts.

During progressive metamorphism, ore elements originally adsorbed on clay minerals and oxyhydroxides will be redistributed among silicate (e.g., muscovite, biotite, titanite) and oxide minerals (e.g., rutile, imenite). During partial melting, ore elements liberated from minerals contributing to the melt may remain in the melt or may be redistributed into stable restite mineral. The partitioning between melt and restite pairs depends on temperature and restite mineralogy (Fig. 2). In low temperature migmatites (metasedimentary protoliths), Sn, W, and REE preferentially remain in the restite, whereas Li, Cs, and Ta commonly concentrate in the melt. In contrast in high temperature migmatites (metasedimentary protoliths), Sn and W commonly fractionate into late melts that form by the consumption of the last biotite. There may be deviations from this

general behavior, as for instance if minerals that typically sequester Sn or W are absent at melting conditions. There also may be significant metal mobility before the onset of melting if the rocks is flushed by external fluids.

The maximum amount of melt that may be produced by dehydration melting of sedimentary rocks depends on the kind and amount of hydrous phases present. During prograde metamorphism of sedimentary protolith that have lost Ca and Na during intense chemical alteration, muscovite and biotite are the most important hydrous phases, whereas amphibole and plagioclase that are stabilized by the presence of Ca and Na are relatively rare. Therefore, muscovite and biotite both determine the condition of dehydration melting and the amount of melt produced. Early melts are low in Sn that becomes released during biotite dehydration melting. In a closed system, late melts with high Sn contents mix with early melts with low Sn contents. Thus, closed-system melts do not reach particularly high Sn contents even if they experience biotite dehydration melting. Melts with high Sn contents are only obtained if low-temperature melts are lost from the rock in one or several extraction steps before high-Sn melts form at high temperature. High contents of muscovite in the metamorphic rock allow to generate large amounts of low-temperature melts, which favors both multiple melt extraction and restite enrichment.

Thus, the important point about chemically intensely altered sedimentary protoliths is that metamorphism of

these rocks results in mineral assemblages that favor the generation of large amounts of low-temperature melts that may be lost from the system and support the residual enrichment of the protolith in Sn and other ore elements that are sequestered by biotite. Loss of low-temperature melts followed by late Sn-rich high-temperature melts also explains the typical association of Sn mineralization with small late intrusion rather than with the main intrusion. Furthermore, strongly Sn-enriched melts require only little fractionation to reach high Sn-levels.

## References

- Lehmann, B. (1982) Metallogeny of tin; magmatic differentiation versus geochemical heritage. *Economic Geology*, 77: 50–59.
- Mitchell, A.H.G., Garson, M.S. (1981) *Mineral Deposits and Global Tectonic Settings*. Academic Press, London, 405 pp.
- Romer, R.L., Kroner, U. (2015) Sediment and weathering control on the distribution of Paleozoic magmatic tin–tungsten mineralization. *Mineralium Deposita* 50, 327–338
- Romer, R.L., Kroner, U. (2016) Phanerozoic tin and tungsten mineralization – tectonic controls on the distribution of enriched protoliths and heat sources for crustal melting. *Gondwana Research*, 31: 60–95.
- Sato, K. (2012) Sedimentary crust and metallogeny of granitoid affinity: implications from the geotectonic histories of the Circum-Japan Sea region, Central Andes and southeastern Australia. *Resource Geology* 62, 329–351.
- Wolf, M., Romer, R.L., Franz, L., López-Moro, F.J. (2018) Tin in granitic melts: The role of melting temperature and protolith composition. *Lithos*, 310-311: 20–30.

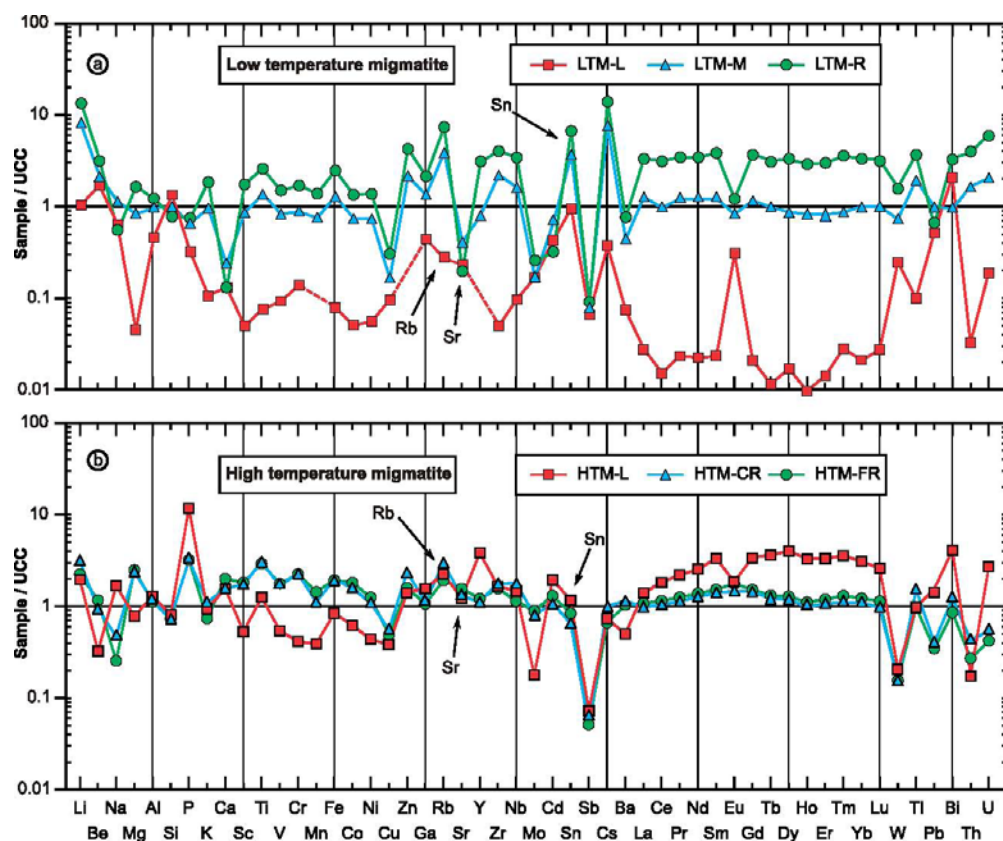


Fig. 2. Trace-element pattern (normalized to upper continental crust UCC) of melt and restite pairs. A. Low temperature migmatite (muscovite dehydration melting). B. High-temperature migmatite (biotite dehydration melting). Note the contrasting behavior of Sn, W and REE in the two migmatites (Wolf et al., 2018).

# Exogenic control on the distribution of endogenic Sn-W-Ta, Au, and U mineralization in the Appalachians and the Variscides

Rolf L. Romer<sup>1</sup>, Uwe Kroner<sup>2</sup>

<sup>1</sup>*Inorganic and Isotope Geochemistry, GFZ German Research Centre for Geosciences, Telegrafenberg, 14473 Potsdam, Germany*

<sup>2</sup>*Department of Geology, TU Bergakademie Freiberg, B. v. Cotta Str. 2, 09596 Freiberg, Germany*

Endogenic Sn-W-Ta, Au, and U mineralization result from the superposition of a series of exogenic and endogenic geochemical enrichment steps. Exogenic processes control (i) the enrichment of the ore elements in sedimentary protoliths (related in part to residual enrichment and in part to climatically or tectonically controlled redox traps), (ii) the spatial distribution of these enriched protoliths, and, thus, eventually (iii) the distribution of mineralization. Tectonic processes resulting in metamorphism and crustal melting control the mobilization of Sn/W, Au, and U from these enriched protoliths and, thus, control the age distribution of Sn/W and Au mineralization and of U-fertile granites. It is the coupling of exogenic and endogenic processes that eventually results in the formation of mineralization in particular tectonic zones. The Appalachian and Variscan orogenic belts host important mineralization of Sn-W-Ta, Au, and U (Fig. 1) and, therefore, represent an excellent region to demonstrate the interplay of exogenic and endogenic processes.

The Appalachian and Variscan orogenic belts formed during the assembly of Western Pangea by the closure of the Rheic Ocean between Gondwana and Laurussia. During most of the Paleozoic, the Laurentian part of Laurussia was in an active margin setting characterized by the accretion of magmatic arcs and the development of supra-subduction zone ophiolites in an overall transpressional setting. The subsequent collision with the East European Craton and Avalonia resulted in the formation of Laurussia that eventually collided with Gondwana.

In the early Paleozoic, peri-Gondwana is characterized by intracontinental rifting in northern Africa and South America, culminating in the opening of the Rheic Ocean and the separation of Avalonia. Fed by river systems draining mainland Gondwana (Stephan et al. 2019 and references therein), voluminous sedimentary packages were deposited on a vast shelf area. The Rheic Ocean closed diachronously between c. 400 Ma and c. 280 Ma. Initial collision occurred between the promontory of the extended W-African shelf, i.e., the Armorican Spur and Avalonia as part of Laurussia (Kroner and Romer 2013). The subsequent intracontinental subduction-accretion tectonics culminated in a final collision stage at c. 340 Ma that eventually resulted in high temperature metamorphism and the formation of voluminous migmatite-granite complexes. Plate tectonic

reorganization at 300 Ma caused the termination of the Variscan orogeny in Europe, the final closure of the Rheic Ocean, the concomitant Alleghany-Mauretania orogeny and the opening of the Neo-Tethys (Kroner et al. 2016).

The mobilization of metals is closely related to the tectonic development of the Appalachian and Variscan orogens: Large-scale processes determine the timing of mineralization and regional to local orogenic overprint (e.g., maximum metamorphic grade) determines whether metals are mobilized or not. Pre-orogenic processes, however, are of major importance for primary sedimentary accumulation of the particular ore elements. For example, Silurian black shales occur globally, but only those deposited on the peri-Gondwana shelf to the south of the Rheic Ocean served as source rocks for economic relevant U-mineralization. As the distribution of Ordovician and Silurian sediments on peri-Gondwana is similar, many Sn specific granites of the Variscan orogen also show enhanced U contents. The distribution of Ordovician and Silurian shelf sediments and their contrasting overprint during the orogenic events leading to the formation of Pangean eventually determine the irregular spatial distribution of the mineralization of Sn-W-Ta, Au, and U, most importantly (i) the regional separation of Sn and Au mineralization, (ii) the bipartite occurrence of W mineralization (without or together with Sn or Au, and (iii) the restriction of significant U mineralization to the south of the former Rheic Ocean.

## Enrichment of ore elements in the protoliths

Early Ordovician siliciclastic sedimentary rocks of northern Gondwana have the geochemical fingerprint of intense chemical alteration due to the decomposition of feldspar and the formation of secondary minerals. The rocks have very low Ca, Na, Sr, and Pb contents that are lost after feldspar decomposition and high contents of Al, K, and Rb, which are incorporated in secondary minerals. Sulfide-bound and redox-sensitive elements have been lost. Intense chemical alteration takes place on deeply eroded continental areas with long residence time of the sedimentary material and possible multiple redeposition from one basin to another one. In northern peri-Gondwana, these sedimentary units are characterized by slightly enhanced contents of Sn, W, and Ta (due to residual enrichment; Romer and Kroner, 2017) and variably enhanced Au contents (locally even forming paleo-placers; Romer and Kroner, 2018). For orogenic

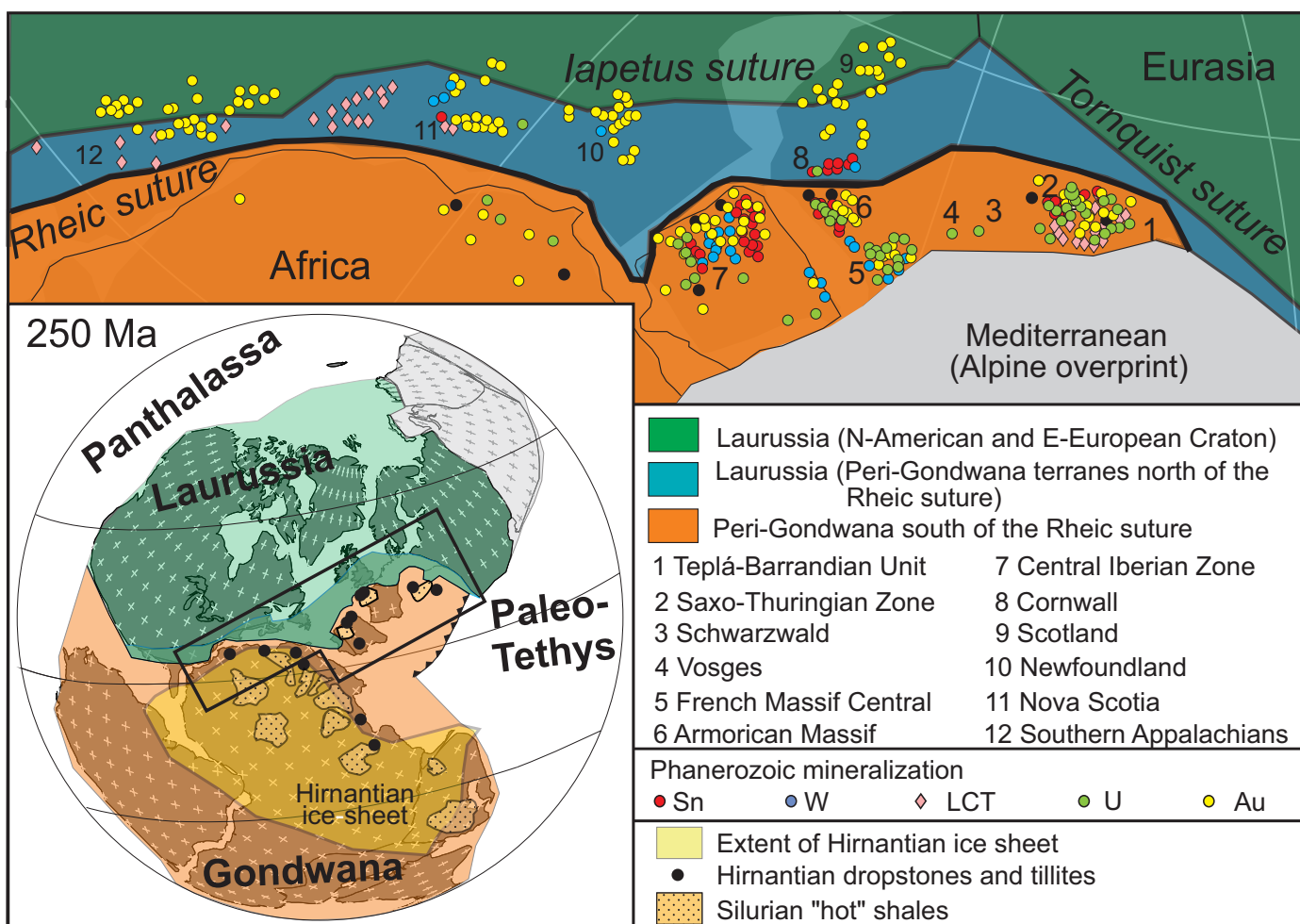


Fig. 1: Reconstruction of western Pangea for 250 Ma, showing the spatial distribution of Phanerozoic Sn, W, LCT (Li-Cs-Ta), Au, and U mineralization within the plate boundary zone between Laurussia and Gondwana. The distribution is controlled by protoliths rather than by tectonic setting; the timing of mineralization is controlled by tectonic processes (compiled from Romer and Kroner, 2016, 2018; Romer and Cuney, 2018).

Au mineralization within the Appalachian and Variscan orogens, there is an additional source-rock: magmatic arc that formed on old continental crust. The profound chemical alteration of near surface sedimentary rocks in the late Cambrian and Ordovician resulted in the loss of redox-sensitive elements, such as Mo and U.

Early Silurian black shales on northern Gondwana have unusually high contents of U that are much higher than U contents in earlier Silurian shales deposited on other continents. These high U contents are causally directly related to the Hirnantian glaciation: In the late Ordovician Gondwana was at the South Pole. The Hirnantian ice shield removed near surface rocks that previously had lost their U content during extensive chemical alteration and exposed rocks that had not lost their U yet. The melting of the ice sheet at the end of the Ordovician resulted in a global sea level rise, the inundation of vast shelf areas, and the development of reducing conditions on these shelves. Melting of the ice sheet made large land areas available to alteration, which in particular resulted in the leaching of U from metamict and readily oxidized minerals. Thus, the melting of the ice sheet both exposed the source rocks for U leaching

and produced the reduced trap to concentrate the leached U. As fresh source rocks only become available for leaching on glaciated continents, not all early Silurian shales are U rich.

Even the protoliths for Sn, Au, and U take entirely different paths of enrichment and form in completely different environments, they show broadly similar regional distribution in pre-Variscan northern Gondwana, as they were deposited at the same margin, but at different time. The intensely altered late Cambrian to early Ordovician sediments that originally formed on the deeply eroded cratonic areas of Gondwana were redeposited during the rifting of peri-Gondwana to marginal basins and the margin of peri-Gondwana. This redistribution of spatially extensive but thin deposits on the continent to thick deposits at the continent margin occurred in the early Ordovician. These sediments are overlain by late Ordovician (Hirnantian) tillites and by early Silurian U-rich black shales. Thus, the broadly similar distribution of Sn, W, Ta, U, and to some extent Au mineralization within the Variscan orogen (Fig. 1) reflects vertical superposition (i.e., in time) of suitable sedimentary source rocks.

## Tectonic stacking of the protoliths

During the closure of the Rheic Ocean, shelf sediments may have experienced extensive tectonic stacking in accretionary wedges. Such tectonic stacking increases the volume of suitable source rocks. Tectonic stacking seems to be a critical feature for the development of major tin provinces, such as Cornwall and the Erzgebirge within the Variscan orogen. It is important to be aware that tectonic stacking and melting of the protoliths may not be part of the same tectonic event. For instance within the Variscan orogen, tectonic stacking in the future Bohemian Massif and the Armorica/Cornwall region was related to the initial stages of closure of the Rheic Ocean at 400–380 Ma. The emplacement of Sn-specific granites, however, is much younger: In the Bohemian Massif, the c. 320 Ma old Sn-specific granites of the Erzgebirge formed after the c. 340 Ma continental collision, whereas the c. 290 Ma old Sn-specific granites of Cornwall are related to the post-Variscan development of the Central European Extensional Province.

## Mobilization of the ore elements during metamorphism and crustal melting

The behavior of ore elements during partial melting of sedimentary rocks strongly depends on restite mineralogy and melting conditions. During muscovite dehydration melting, Sn and W seem to partition into restite minerals, resulting in low-temperature melts with low Sn and W content. In contrast, during biotite dehydration melting, Sn and W are preferentially partitioned into the melt (Wolf et al., 2018). Melt with enhanced Sn and W contents are only generated during high-temperature melting and require multiple extraction of low-temperature melts (Wolf et al., 2018). The chemical composition of the sedimentary protolith strongly controls the melting behavior and, thus, the potential of these melts to eventually develop into Sn granites. Chemically intensely altered sedimentary rocks with low Ca and Na contents will form significant amounts of muscovite and biotite during prograde metamorphism, and, therefore, may produce larger volumes of low-temperature melts than comparable sedimentary rock with higher contents of Ca and Na. The loss of large volumes of low-temperature melts, however, is essential for enrichment of Sn and W in the restite (Wolf et al., 2018).

In contrast, Ta along with Li and Cs seem to concentrate in low-temperature melts. Contrasting mobilization conditions for Sn, W, and Ta provide a mechanism to separate these elements from each other and to result in regional contrasting mineralization types involving the same protoliths. Although Sn and Au occur in the same protolith, mineralization of these two elements commonly is regionally separated. The reason for this separation is the contrasting mobilization temperature of these metals. Whereas Sn generally requires high-temperature melting to become mobilized from the protolith, Au is mobilized at relatively low temperatures

by metamorphic fluids. Thus, Au is lost from the sedimentary protolith long before this protolith reaches conditions to mobilize Sn.

Enrichment of Sn during fractional crystallization requires relatively reduced melts. In the Variscan belt, the melting of intensely altered early Ordovician sedimentary rocks along with early Silurian black shales generates reduced melts that are enriched in Sn and U. The reducing conditions favor magmatic enrichment of Sn, whereas U forms uraninite and other U-rich phases that remain dispersed in the granite.

## Post-orogenic redistribution of ore elements

Post-orogenic crustal extension results in the formation of Sn-specific granites in Cornwall and coeval mobilization of Au (and locally W) in strike slip fault zones. Most importantly, however, the erosion of the orogen and the reactivation of fault zones allows for the leaching of U, in particular from the uraninite-bearing granites. This redistribution forms U mineralization, i.e., vein-type and episyenite U mineralization within and in the vicinity of granites and sediment-hosted U mineralization in Permian basins (Romer and Cuney, 2018). Later tectonic reactivation resulted in renewed redistribution of U, upgrading or destroying older deposits and forming new ones.

The erosion of the Appalachian and Variscan orogens started the next cycle of Au redistribution, forming placer deposits near areas hosting vein-type Au mineralization. The erosion of Sn-specific Variscan granites and their tin greisen and vein type mineralization may have produced local Sn placers.

## References

- Kroner, U., Romer, R.L. (2013) Two plates - many subduction zones: the Variscan orogeny reconsidered. *Gondwana Research* 24, 298-329.
- Kroner, U., Roscher, M., Romer, R.L. (2016) Ancient plate kinematics derived from the deformation pattern of continental crust: Paleo- and Neo-Tethys opening coeval with prolonged Gondwana-Laurussia convergence. *Tectonophysics* 681, 220-233.
- Romer, R.L., Cuney, M. (2018) Phanerozoic uranium mineralization in Variscan Europe – more than 400 Ma of tectonic, supergene, and climate-controlled uranium redistribution. *Ore Geology Reviews* 102, 474-504.
- Romer, R.L., Kroner, U. (2016) Phanerozoic tin and tungsten mineralization – tectonic controls on the distribution of enriched protoliths and heat sources for crustal melting. *Gondwana Research* 31, 60-95.
- Romer, R.L., Kroner, U. (2018) Paleozoic gold in the Appalachians and Variscides. *Ore Geology Reviews* 92, 475-505.
- Stephan, T., Kroner, U., Romer, R.L. (2019) The pre-orogenic detrital zircon record of the Peri-Gondwana crust. *Geological Magazine* 156, 281-307.
- Wolf, M., Romer, R.L., Franz, L., López-Moro, F.J. (2018) Tin in granitic melts: The role of melting temperature and protolith composition. *Lithos* 310-311, 20-30.

# Geology and ore genesis of the Yangibana LREE district, Western Australia

Paul Slezak<sup>1</sup>, Carl Spandler<sup>1</sup>, Andy Border<sup>2</sup>, Kieren Whittock<sup>2,3</sup>

<sup>1</sup>*Department of Geoscience, College of Science and Engineering, James Cook University, Townsville, QLD 4811, Australia*

<sup>2</sup>*Hastings Technology Metals Limited, Level 8 Westralia Plaza, 167 St. Georges Terrace, Perth, WA 6000, Australia*

<sup>3</sup>*Whittock Geological Pty Ltd., 7/3-5 Riverside Crescent Marrickville, NSW 2204, Australia*

## Introduction

Carbonatites are the most important primary sources for critical metals such as rare earth elements (REE) and high field strength elements (HFSE) (Chakhmouradian and Zaitsev, 2012). In many cases the economic viability of mining carbonatite deposits relies on post-magmatic enrichment processes, such as lateritisation, to concentrate Nb and REE to ore grades (Moreteani and Preinfalk, 1996).

Australia hosts a variety of different REE deposits, including several carbonatite deposits such as Mt. Weld, Cummins Range, and the Yangibana LREE district (Fig. 1). The Yangibana LREE district is hosted by the Gifford Creek Carbonatite Complex (GCCC) of Western Australia. It is owned by Hastings Technology Metals Ltd. and contains 21 million tonnes of ore grading 1.17% TREO (Hastings Technology Metals Ltd., 2019). The district comprises multiple deposits/prospects rich in Pr and Nd hosted mainly in monazite within ironstone dykes that we show are genetically related to the ankerite-siderite carbonatites of the GCCC.

## Regional Geology

The Yangibana LREE deposit is hosted by the GCCC in the Gascoyne Province of Western Australia. The Gascoyne Province comprises granitic rocks, gneisses, and metasedimentary rocks that have undergone a 1 b.y. history of terrane assembly and re-working related to several major orogenic events, creating multiple large-scale faults that delineate different crustal (Johnson et al. 2013).

The GCCC primarily intrudes the Durlacher Supersuite and Pooranoo Metamorphics in the region between the Lyons River Fault and the Bald Hill Lineament (Fig. 2). However, some small dykes are present south of the Lyons River Fault in the Edmund Group, and several different alkaline dykes and sills have been found immediately to the north of the Bald Hill Lineament (Fig. 2).

Seismic reflection shows that the Lyons River Fault extends down to – and offsets – the Mohorovičić Discontinuity (Johnson et al. 2013). The Lyons River Fault is a major shear zone, which sutured the Neoproterozoic Glenburgh Terrane with the Archean Pilbara Craton during the 2215 to 2145 Ma Ophthalmian Orogeny (Johnson et al. 2011).

The GCCC was emplaced at 1370 Ma (Zi et al., 2017; Slezak and Spandler, 2019). The region was subsequently subjected to multiple tectonomagmatic events, which are recorded in the GCCC by U–Pb dates from monazite and Sm–Nd isochron dates from monazite and apatite pairs (Zi et al., 2017; Slezak and Spandler, 2019). The events include the 1320 to 1170 Ma Mutherbukin Tectonic Event, the 1090 to 1040 Ma Giles Event, the 1030 to 950 Ma Edmundian Orogeny, and the 955 to 830 Ma Kuparr Tectonic Event.

## Rock types of the GCCC

The GCCC is made up of several different rock types: 1) the Lyons River Sills – fine-grained, calcite and dolomite carbonatite dykes; 2) magnetite-biotite dykes; 3) silica-rich alkaline veins; 4) ankerite-siderite carbonatites; and 5) alkaline amphibole-dolomite veins.

In addition, there are three rock types related to the primary units: 1) the Yangibana Ironstones, which host LREE mineralisation as monazite and are the weathered products of the ankerite-siderite carbonatites; 2) fenites – the altered wall rocks (mainly granite and metasediments) created through alteration by alkaline, carbonatite-related fluids; and 3) glimmerites – the alteration selvages related to ferrocarnatite reactions with granitic wall rocks.

## Ore deposit genesis

Monazite is the main ore mineral and is found in highest concentrations in the ironstones, but also occurs in significant amounts in the ankerite-siderite carbonatites. In the ironstones, it can comprise between ~1% and ~10% of the rock by volume. Monazite grains are often cream to peach colour in hand specimen and form large (~2 mm) clusters of subhedral to euhedral tabular crystals. Less commonly, monazite forms small, anhedral inclusions (~10 µm) in apatite, possibly produced by exsolution (Slezak et al., 2018). Some monazite grains are mantled by amorphous to acicular crystals identified as rhabdophane.

The ironstones are enveloped by fenite and glimmerite alteration styles analogous to those observed in the ankerite-siderite carbonatites. In addition, the ironstones have bulk-rock Nd isotope compositions ( $\epsilon_{\text{Nd}}^{\text{(t)}} = -2.24$ ) that are similar to other units of the GCCC

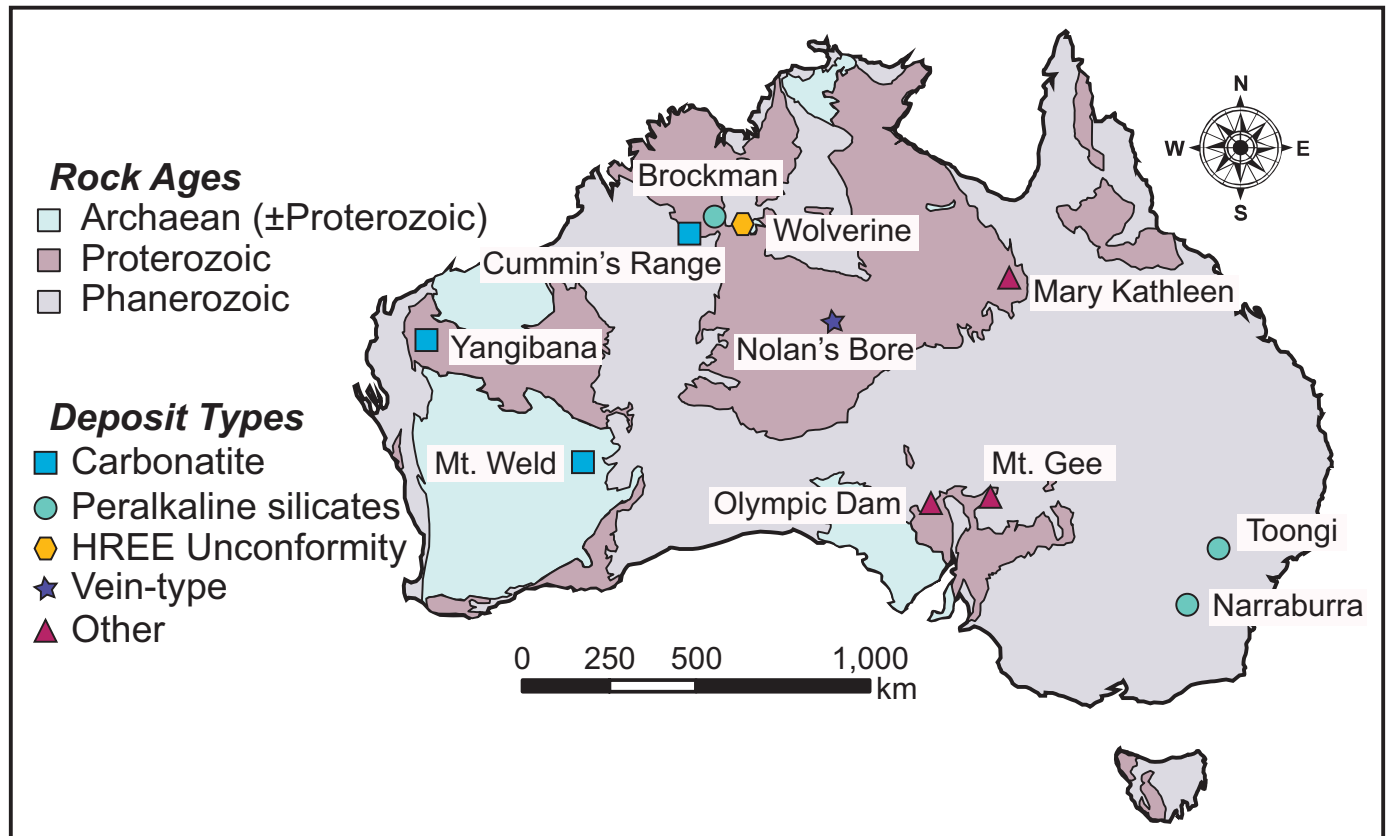


Figure 1. Map of major REE deposit types in Australia

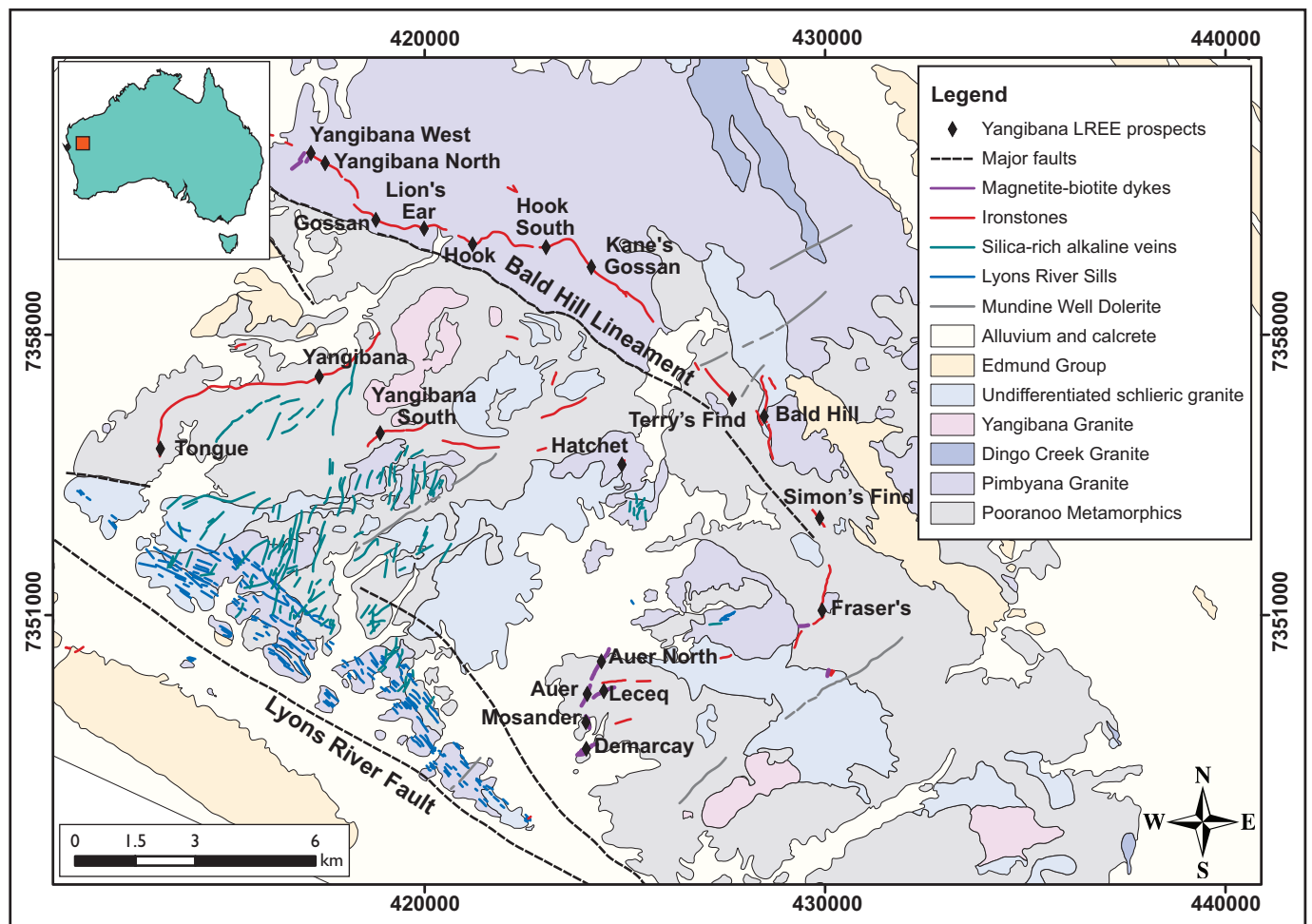


Figure 2. Geologic map of the Gifford Creek Carbonatite Complex (GCCC) with deposit/prospect locations, comprising the Yangibana LREE district (modified from Slezak et al. 2018)

( $\epsilon\text{Nd}_{(t1.37\text{Ga})} = -2.80$ ), indicating they have a common (enriched mantle) source.

At several ironstone outcrops, carbonate mineral dissolution cavities and Fe-oxides/hydroxides pseudomorphing carbonate minerals were observed. In drillcore, the ankerite siderite carbonatite is partially altered and oxidised to a porous, hematite-rich rock similar to the ironstones observed at surface. These field observations suggest the ironstones are likely the product of carbonate mineral dissolution through low temperature (i.e., meteoric) fluids. Other processes such as rødberg-style alteration have been suggested by Pirajno and González-Álvarez (2013), who noted hematite development along carbonate lamellae and hematite veins cross-cutting other textures, both of which were interpreted as higher temperature reactions. However, these distinct, euhedral crystalline features were rarely observed in this study. It is speculated these higher temperature features have been overprinted by later, botryoidal hematite, which along with the observed boxwork textures and vuggy nature of the ironstones, indicates additional low temperature alteration.

Weathering and laterite formation are important processes for improving the ore tenor of carbonatite deposits. The largest Nb deposits in the world include the pyrochlore-rich carbonatite deposits Araxá, Catalão, and Morro do Seis Lagos (Brazil), all of which have undergone extensive lateritisation (e.g., Mitchell, 2015) and weathering, which has increased the ore tenor through eluvial enrichment. At the Mount Weld REE deposit, primary REE-bearing minerals (e.g., monazite and apatite) were broken down, liberating REE to form REE-bearing oxyhydroxides, secondary monazite, churchite, cerianite, and a suite of REE-rich hydrated aluminophosphate (plumbogummite group) minerals. This lateritisation has enriched LREE concentrations by ~5 to 200 times compared to the average carbonatite LREE contents (Lottermoser, 1990).

Comparison of the Yangibana ironstones with likely precursor rocks indicates an average upgrade in ore tenor of ~3 to ~17 times during supergene alteration (Fig. 3). Overall the ankerite-siderite carbonatites and the ironstones have comparable normalised REY patterns, which is consistent with their genetic relationship and indicative of an environment involving little fractionation between REE. The ironstones of the Yangibana LREE district demonstrate that some monazite has been altered and remobilised to form rhabdophane and likely REE-bearing Fe-oxides/hydroxides, similar to the processes at Mount Weld. However, this REE-remobilisation has occurred on a much smaller scale since primary monazite and apatite remain the predominant REE-bearing minerals in the district. The significant amount of remnant primary REE-bearing phosphate minerals suggest the ironstones were upgraded through supergene processes similar to those involving pyrochlore concentration at the carbonatite deposits in Brazil, as opposed to the complete breakdown and remobilisation of primary REE-bearing phases.

The West Australia Craton has episodically undergone subaerial exposure since the late Proterozoic, though much of it underwent extensive regolith development from the Paleogene until the mid-Miocene (Pillans, 2007). The extended length of subaerial exposure of the GCCC has provided ample time for meteoric waters to infiltrate and alter the dykes, forming the present day ironstones (Fig. 4). This is supported by ankerite-siderite carbonatite altering to ironstone in core samples, and ankerite-siderite carbonatite only occurring in drillcore from depths of 40 metres below the immediate region where ironstone crops out at the surface. The depth of meteoric fluid infiltration was likely controlled and/or enhanced by internal structures (e.g., joints, faults) in the carbonatite and porosity generation by carbonate dissolution.

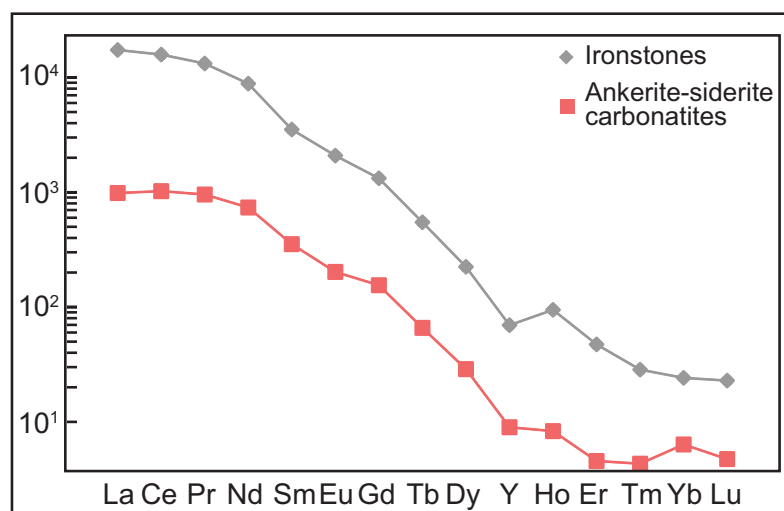


Figure 3. Chondrite normalised REY patterns for the average ankerite-siderite carbonatites (at Yangibana North) and the average Yangibana North ironstones.

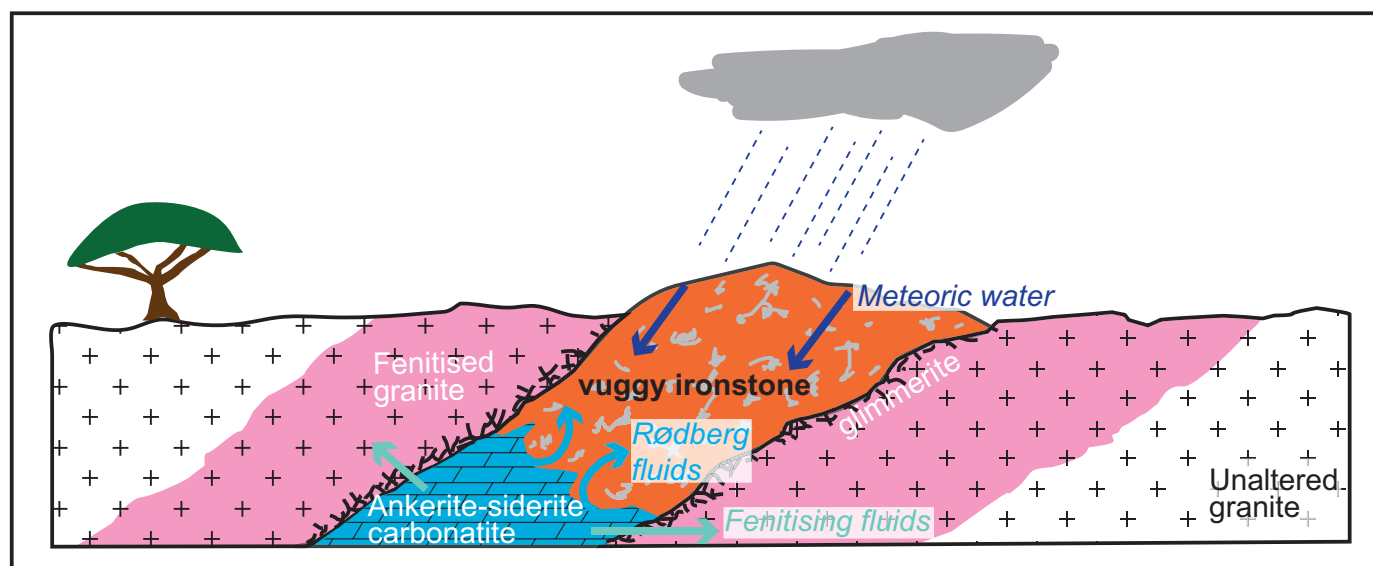


Figure 4. Schematic of the creation of vuggy ironstone through alteration of the ankerite-siderite dykes by rødberg and meteoric fluids.

## References

- Chakmouradian AR, Zaitsev AN (2012) Rare earth mineralization in igneous rocks: sources and processes. *Elements* 8:347-353 <https://doi.org/10.2113/gselements.8.5.347>
- Hastings Technology Metals, (2019) Yangibana JORC Ore Reserves. Retrieved from <https://hastingstechmetals.com/projects/yangibana/yangibana-jorc-resource/> on February 22, 2019
- Johnson SP, Sheppard S, Rasmussen B, Wingate MTD, Kirkland CL, Muhling JR, Fletcher IR, Belousova EA (2011) Two collisions, two sutures: punctuated pre-1950 Ma assembly of the West Australian Craton during the Ophthalmian and Glenburgh Orogenies. *Precambrian Research* 189(3-4):239-262. <https://doi.org/10.1016/j.precamres.2011.07.011>
- Johnson SP, Thorne AM, Tyler IM, Korsch RJ, Kennett BLN, Cutten HN, Goodwin J, Blay O, Blewett RS, Joly A, Dentith MC, Aitken ARA, Holzschuh J, Salmon M, Reading A, Heinson G, Boren G, Ross J, Costelloe RD, Fomin T (2013) Crustal architecture of the Capricorn Orogen, Western Australia and associated metallogeny. *Australian Journal of Earth Sciences* 60(6-7):681-705. <https://doi.org/10.1080/08120099.2013.826735>
- Lottermoser BG (1990) Rare-earth element mineralisation within the Mt. Weld carbonatite laterite, Western Australia. *Lithos* 24:151-167. [https://doi.org/10.1016/0024-4937\(90\)90022-S](https://doi.org/10.1016/0024-4937(90)90022-S)
- Mitchell RH (2015) Primary and secondary niobium mineral deposits associated with carbonatites. *Ore Geology Reviews* 64:626-641. <https://doi.org/10.1016/j.oregeorev.2014.03.010>
- Morteani G, Preinfalk C (1996) REE distribution and REE carriers in laterites formed on the alkaline complexes of Araxá and Catalão (Brazil). In: Jones AP, Wall F, Williams CT (eds) *Rare Earth Minerals: Chemistry, Origin and Ore Deposits*, Chapman and Hall, London
- Pillans B (2007) Pre-Quaternary landscape inheritance in Australia. *Journal of Quaternary Science* 22(5):439-447. <https://doi.org/10.1002/jqs.1131>
- Pirajno F, González-Álvarez I (2013) The ironstone veins of the Gifford Creek ferrocyanatite complex, Gascoyne Province: Geological Survey of Western Australia, Record 2013/12, p 19
- Slezak P, Spandler C (2019) Carbonatites as recorders of mantle-derived magmatism and subsequent tectonic events: an example of the Gifford Creek Carbonatite Complex, Western Australia. *Lithos* 328-329:212-227. <https://doi.org/10.1016/j.lithos.2019.01.28>
- Slezak P, Spandler C, Blake K (2018) Ghosts of apatite past: using hyperspectral cathodoluminescence and micro-geochemical data to reveal multi-generational apatite in the Gifford Creek Carbonatite Complex, Australia. *The Canadian Mineralogist* 56:773-797. <https://doi.org/10.3749/canmin.1800021>
- Zi JW, Gregory C, Rasmussen B, Sheppard S, Muhling JR (2017) Using monazite geochronology to test the plume model for carbonatites: The example of Gifford Creek Carbonatite Complex, Australia. *Chemical Geology* 463:50-60. <http://dx.doi.org/10.1016/j.chemgeo.2017.05.007>

# Geology and tectonic setting of the Toongi rare metal deposit, central NSW

Carl Spandler, Caitlin Morris

*Economic Geology Research Centre, James Cook University, Townsville, Qld, Australia*

## Geology of the Toongi deposit

The Toongi deposit (also known as the Dubbo Zirconia Project) contains over 73 Mt of mineral resources (measured and inferred) grading at 1.96 wt.% ZrO<sub>2</sub>, 0.04 wt.% HfO<sub>2</sub>, 0.45 wt.% Nb<sub>2</sub>O<sub>5</sub>, 0.03 wt.% Ta<sub>2</sub>O<sub>5</sub>, 0.14 wt.% Y<sub>2</sub>O<sub>3</sub> and 0.75 wt.% REE<sub>2</sub>O<sub>3</sub> (Alkane Resources Ltd. 2015). The deposit is entirely contained within a 0.3 km<sup>2</sup> elliptical trachyte laccolith located approximately 20 km south of Dubbo in central NSW (Fig. 1a). This mineralised laccolith is one of a number of small alkaline igneous bodies (most trachytic plugs, flows and laccoliths that are >2 km<sup>2</sup>) that collectively form a region known as the Toongi Alkaline Magma Field (TAMF; Fig. 1b).

The TAMF lies at the boundary between the Permo-Triassic Gunnedah Basin to the north and Cambrian to Carboniferous Lachlan Fold Belt to the south (Fig. 1a). TAMF magmatism is of late Triassic to Early Jurassic age. The field is distinguished in regional geophysics as a zone of anomalously high gravity and relatively high Th and U (Spandler and Morris, 2016). The geological units in the region (Fig. 1b) include the Late Silurian to Devonian Cudal, Toongi and Gregra Groups of the Lachlan Fold Belt, which are unconformably overlain by Early-Middle Triassic sandstones and siltstones of the Napperby Formation, of the Gunnedah Basin. All of these sedimentary units are host to TAMF igneous bodies (Fig. 1b). Subsequent Cenozoic magmatism includes extensive basalt lava flows now preserved to the north and south of Dubbo city (Zhang and O'Reilly, 1997).

The intrusion hosting the Toongi deposit outcrops at the surface and extends between ~50 and 150 m in depth. The deposit largely consists of fine-grained (<0.5 mm) trachyte that may be weakly porphyritic and/or vesicular. Most of the groundmass and phenocrysts (up to 1 mm) are composed of feldspar that is either near end-member albite or pure K-feldspar in composition (Fig. 2a). The phenocrysts are commonly oscillatory zoned, with albite rim zones of variable thickness. Aegirine occurs as occasional micro-phenocrysts and as fine (<0.1 mm) acicular crystals as part of the trachytic matrix of the rock (Fig. 2a). All of the rock mass has undergone variable degrees of post-magmatic hydrothermal alteration, with the most altered samples pervasively altered to sericite, chlorite and goethite, with only the albitic cores of phenocrysts and aegirine micro-phenocrysts remaining free of alteration.

Assay data and sample petrography reveal a remarkable level of homogeneity in ore grade, and in the mineralogy

and textural setting of the ore minerals across the deposit (Spandler and Morris, 2016). The ore minerals are always sub-mm in size and are distributed throughout the rock mass. The bulk of the ore metals are hosted in complex Na-Ca-Zr silicate phases (REE-rich eudialyte, vlasovite and catapleiite) that mainly occur as sub-spherical to irregular shaped blebs that are dispersed throughout the rock matrix (Fig. 2a). These phases comprise between 5% and 10% of the rock volume. These blebs are interstitial to feldspar and aegirine phenocrysts, and in many cases wrap or include phenocrysts. They are also characterized by an abundance of fine tabular to acicular inclusions of albite, K-feldspar and aegirine that are similar to the rock matrix. These inclusions, or clusters of inclusions, are commonly aligned, and often define spiral or circular forms (Fig. 2b) that do not parallel the trachytic flow foliation of the rock matrix. This texture henceforth labelled 'snowball texture'. The dominant Nb and Ta mineral is lueshite/natroniobite (NaNbO<sub>3</sub>) that is found as small (<40 μm) irregular grains that also formed in the interstices between matrix feldspar and aegirine grains (see Spandler and Morris, 2016, for more details).

A secondary ore mineral assemblage of irregular REE fluoro-carbonates and Ca-Na-Zr-silicates is found associated with sericite and chlorite alteration in micro-fractures in the rock or as infill to vesicles (Fig. 2c). The other major vesicle-filling phases are quartz and a Y+REE-rich variant of milarite with the approximate formula KCa(REE,Y)BeSi<sub>12</sub>O<sub>30</sub>.

## Tectonic setting of the Toongi deposit

The timing of TAMF magmatism coincides with the emplacement of extensive volumes of mafic magma along a belt extending from southern Africa, across the Transantarctic Mountains, into Tasmania and southern Australia: This belt is now recognized as the Karoo-Ferrar-SE Australia large igneous province that formed during continental extension related to the breakup of Pangaea in the early Jurassic (Veevers et al., 2012; Fig. 3). Plate reconstructions to this time place the Dubbo region at the northern extent of this magmatic belt (Fig. 3), so we suggest that the alkaline magmatism of TAMF and nearby areas (e.g. Garrawilla Volcanics) represents the northern termination of the Karoo-Ferrar-SE Australia large igneous province. The site of the magmatism overlies a pronounced step in lithospheric thickness from ca. 100 km in the east, to ca. 140 kms in the west, as defined from seismic tomography models (Rawlinson et al., 2017). The timing of formation of this lithospheric step is unknown,

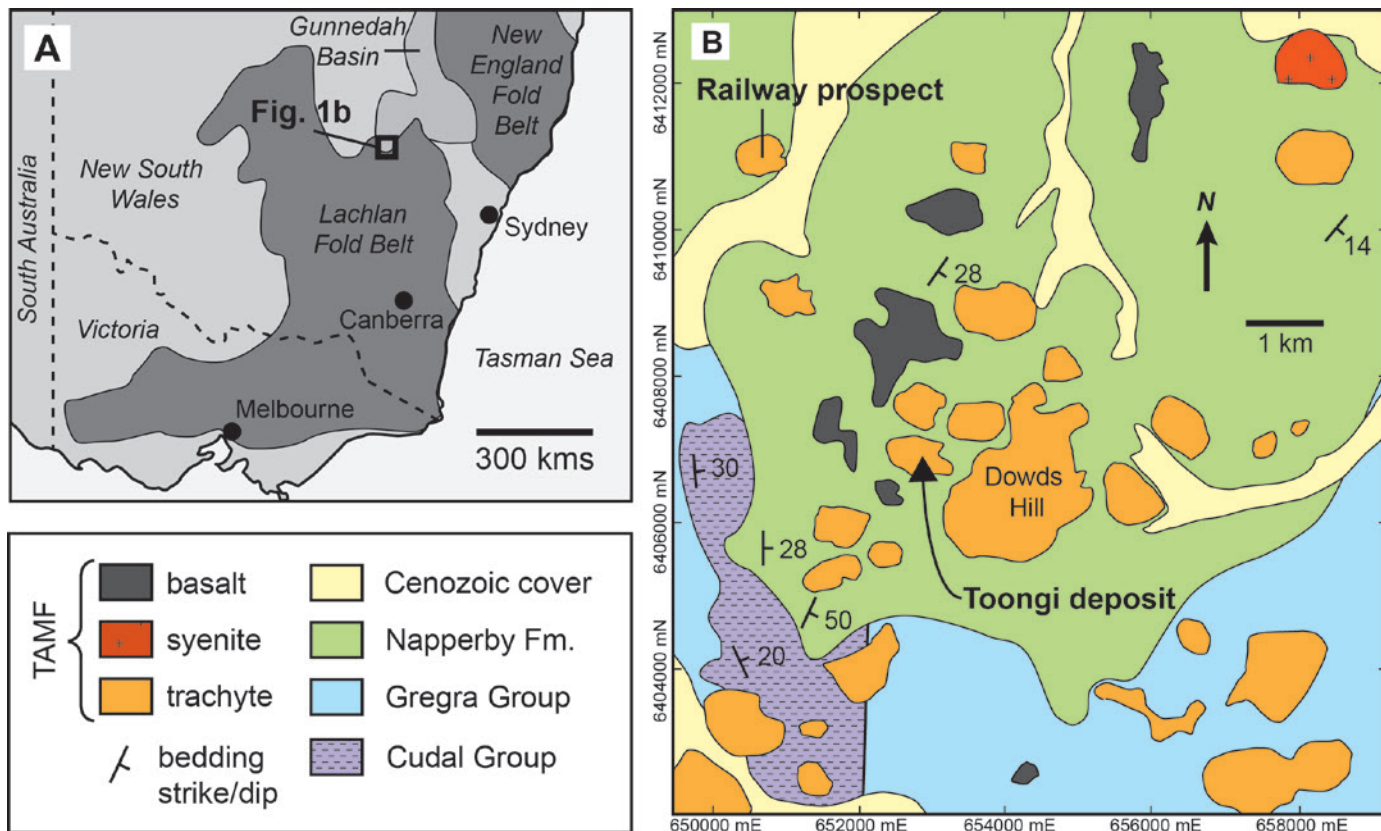


Figure 1. A. Relevant basement geology of southeast Australia, with location of Toongi Deposit. B. Geological map of the Toongi Deposit region.

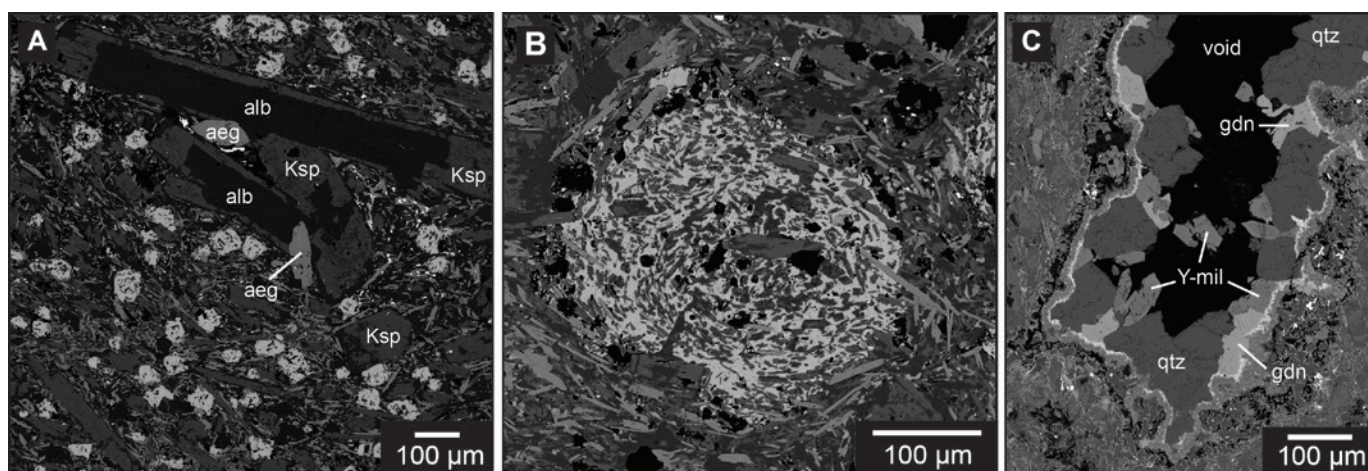


Figure 2. Backscatter electron images of ore minerals of the Toongi Deposit. A. Overview of inclusion rich blebs of Na-Zr silicate within the trachytic matrix. Note the aegirine and zoned feldspar phenocrysts. B. Snowball eudialyte with irregular grain boundaries and spiral/swirling clusters of feldspar and aegirine inclusions. C. Partially infilled vesicle lined with fine colloform REE carbonates (white), prismatic quartz, gaidonnayite and yttrian milarite. Mineral abbreviations; aeg = aegirine; alb = albite; Ksp = K-feldspar; qtz = quartz; gdn = gaidonnayite; Y-mil = yttrian milarite.

but most conceivably developed during the Permian extension phase that formed the Surat and/or Gunnedah Basins (Korsh and Totterdell, 2009), and hence would have existed during the late Jurassic. We therefore favour a model of mantle melting and melt focusing due to edge-driven convection of asthenosphere (e.g., King and Anderson, 1998) along this lithospheric step. This lithospheric step was again a focus of magmatism during the Cenozoic (Zhang and O'Reilly, 1997), possibly due to

mantle plume activity, or due to renewed mantle flow or asthenosphere shear.

The boundary between the Lachlan Fold Belt to the south, and Gunnedah Basin to the north (Fig 1a), may represent a crustal-scale structure that allowed mantle-derived magma to traverse the crust towards the surface. Most of the TAMF, however, consists of intermediate-composition rocks, which means the magmas evolved significantly prior eruption or emplacement at, or near,

the surface. Detailed petrographic, bulk geochemical and Sm-Nd isotope analysis combined with thermodynamic modelling of magma fractionation have been used to show that the majority of the TAMF igneous bodies formed from intermediate composition alkaline magmas that evolved via extensive (~90%) crystal fractionation at mid crustal levels of mantle-derived olivine tholeiite parental magma (see Spandler and Morris, 2016, for full details). The large gravity high that directly underlies the TAMF is interpreted to represent the remnant mafic/ultramafic differentiates of this fractionation process.

### Genesis of the Toongi Deposit

The Toongi Deposit Trachyte is geochemically distinct from other TAMF bodies; it is enriched in Na and incompatible trace elements, depleted in Al, and strongly peralkaline in composition. Modelling work indicates that the intrusion formed after extensive (>90%) polybaric (i.e., mid crustal and shallow crustal stages) fractionation of alkali olivine basalt parental magma with relatively low activity of H<sub>2</sub>O and under low fO<sub>2</sub> conditions (Spandler and Morris, 2016). Under these conditions, Zr+Nb+Y+REE may reach ore grade concentrations,

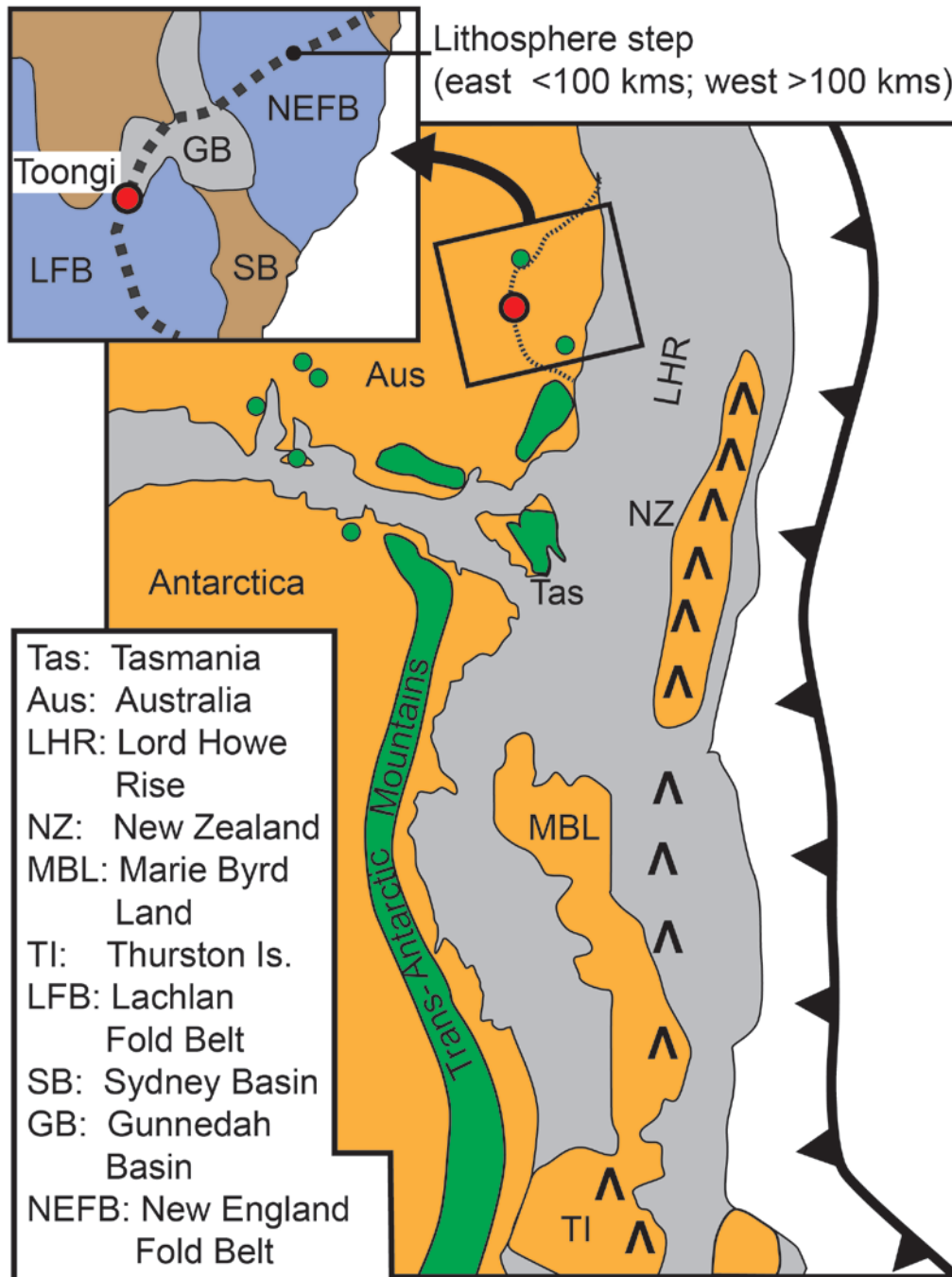


Figure 3. Early Jurassic tectonic setting of eastern Gondwana, with the Karoo-Ferrar-SE Australia large igneous province shown in green. Note, the Toongi Deposit lies at the northern end of the large igneous province, above the pronounced lithospheric step of eastern Australia (Rawlinson et al. 2017), and along the boundary between the Lachlan Fold Belt (LFB) and Gunnedah Basin (GB).

as they have high solubilities in sodic peralkaline melts, and the low  $H_2O$  activity would limit volatile loss that may otherwise deplete the magma of ore metals or their complexing agents, such as Cl and F (Markl et al., 2010). A magmatic origin for mineralisation is also consistent with the ore mineralogy and textures, and homogenous distribution throughout the intrusion. Therefore, key features that distinguish the Toongi Deposit trachyte from other TAMF trachytes, such as the peralkaline composition and extreme degree of fractionation, were also critically important for producing the ore grade mineralization that is unique to the Toongi Deposit.

A distinctive feature of the Toongi ore is the globular or snowball texture of the Na-Zr-silicates (Fig. 2) and their near uniform distribution throughout the trachyte. These textures resemble liquid immiscibility textures (e.g. Kjarsgaard and Hamilton, 1988), and we suggest that the snowball Na-Zr-silicates precipitated from a liquid phase that was present within the rock during formation of the igneous matrix minerals, but this liquid was a separate phase to that which crystallized the matrix minerals. In this case the clusters of matrix minerals included in the snowball Na-Zr-silicates (Fig. 2b) were entrained into the liquid, rather than crystallized from it. We tentatively imply that two immiscible liquids were present in the rock; one aluminosilicate melt that crystallised the feldspar and aegirine, and one Na-Zr silicate liquid that crystallized the bulk of the ore minerals of the Toongi Deposit. If silicate liquid unmixing did occur during low-pressure fractionation, then separation and concentration of the metal rich liquid fraction into the laccolith structure that now represents the Toongi Deposit may have been an important process in producing the high metal grades of the deposit.

The secondary ore mineral assemblage of REE fluorocarbonates, Na-Zr silicates and yttrian-milarite are interpreted to have formed via post-magmatic hydrothermal alteration. Based on the composition of secondary minerals, alteration was caused by Ca-bearing  $CO_2$ - $H_2O$  fluids that were derived either via fluid exsolution from the crystallizing and cooling laccolith, or from localized devolatilisation of country rocks due to intrusion of the Toongi trachyte. Trachyte alteration by these fluids led to localized redistribution of ore metals into vesicles and microfractures in the rock, but this redistribution was likely limited to the cm scale.

The only other volcanic-hosted rare metal deposits/prospects we are aware of are the Brockman deposit

of WA (Ramsden et al., 1993), and the Peaks Ranges of Queensland (Chandler and Spandler, this volume). The Brockman deposit is similar to Toongi in that mineralization consists of unusual Zr silicates (so-called 'zircon gel'; Ramsden et al., 1993) niobate minerals and REE carbonates, and is hosted in peralkaline rocks of trachyte to rhyolite composition. However, Brockman differs from Toongi in that the Brockman ore is very fine grained ( $<20 \mu m$ ) and was probably extensively remobilized by F-rich hydrothermal fluids, which now manifests as abundant fluorite, and extensive zones of Na depletion, in the volcanic sequence (Ramsden et al., 1993). Toongi also differs from the rare-metal enriched volcanic rocks of the Peaks Ranges, in that Peaks Ranges is rhyolitic in composition (Chandler and Spandler, this volume), and Toongi is of trachytic composition.

## References

- Alkane Resources Limited (2015). Annual report. <http://www.alkane.com.au/index.php/reports/annual-reports>.
- King SD, Anderson DL (1998). Edge-driven convection. *Earth and Planetary Science Letters* 160, 289-296.
- Kjarsgaard BA, Hamilton DL (1988). Liquid immiscibility and the origin of alkali-poor carbonatites. *Mineralogical Magazine* 52, 43-55.
- Korsch RJ, Totterdell JM (2009). Subsidence history and basin phases of the Bowen, Gunnedah and Surat Basins, eastern Australia. *Australian Journal of Earth Sciences* 56, 335-353.
- Markl G, Marks MA, Frost BR, (2010). On the controls of oxygen fugacity in the generation and crystallization of peralkaline melts. *Journal of Petrology* 51, 1831-1847.
- Ramsden AR, French DH, Chalmers DI (1993). Volcanic-hosted rare-metals deposit at Brockman, Western Australia. *Mineralium Deposita* 28, 1-12.
- Rawlinson N, Davies DR, Pilia S, (2017). The mechanisms underpinning Cenozoic intraplate volcanism in eastern Australia: Insights from seismic tomography and geodynamic modeling. *Geophysical Research Letters* 44, 9681-9690.
- Spandler C, Morris C, (2016). Geology and genesis of the Toongi rare metal (Zr, Hf, Nb, Ta, Y and REE) deposit, NSW, Australia, and implications for rare metal mineralization in peralkaline igneous rocks. *Contributions to Mineralogy and Petrology*, 171, 104.
- Veevers JJ (2012). Reconstructions before rifting and drifting reveal the geological connections between Antarctica and its conjugates in Gondwanaland. *Earth Science Reviews* 111, 249-318.
- Zhang M, O'Reilly SY (1997). Multiple sources for basaltic rocks from Dubbo, eastern Australia: geochemical evidence for plume—lithospheric mantle interaction. *Chemical Geology* 136, 33-54.

# The Tellerhäuser tin-zinc-indium deposit – new geological insights unlocking value

Antony Truelove  
*Anglo Saxony Mining Ltd*

## Introduction

The Tellerhäuser tin-zinc-indium deposit is a skarn hosted polymetallic deposit located in the Erzgebirge district of the state of Saxony in south-eastern Germany, close to the border with the Czech Republic. Erzgebirge translates as “Ore Mountains” and is a well-known mining district with written historical mine records dating from 1178AD and which has estimated production of over 10,000t silver, 300,000t tin and 250,000t uranium as well as significant zinc, lead, tungsten and nickel. Much of the world’s silver was sourced from this district during the early part of the last millennium.

Exploration and mining of uranium during the German Democratic Republic (GDR) era, between 1946 and 1991, was largely undertaken by the company SDAG Wismut, a Soviet/GDR joint venture whose main remit was uranium exploration and mining with a lesser focus on non-ferrous metals exploration and mining. Significant tin production during the GDR era came from the Altenberg, Sadisdorf and Ehrenfriedersdorf greisen deposits.

In the Tellerhäuser district, Wismut discovered and mined uranium at the Pöhla mine between the early 1960s and 1991 and explored a skarn hosted tin-zinc-indium deposit that was intersected in regional scale drilling and through which the main adit for mining of the uranium mineralisation passed. Wismut extensively drill tested this mineralisation (>141,000m drilling) and outlined three skarn seams containing tin-zinc-indium mineralisation as well as significant (20-30%) magnetite.

It was interpreted that these are typical skarn style tin deposits and extensive mineralogical investigations and mineral processing testwork was undertaken based on that assumption. After a considerable amount of investigation, it was concluded that good recoveries of tin could be obtained but that concentrate grades were low. The final conclusion was that 60-70% recovery could be obtained into a concentrate grading between 5% and 10% Sn.

The deposit was abandoned in 1991 after German reunification, the Soviets sold their interest in SDAG Wismut to the German government for a nominal sum. Wismut was then re-badged as Wismut GmbH, whose sole task was rehabilitation of all the old uranium mines in the country.

After a long period of quiescence, the area was recognised as having potential by an Anglo Saxony Mining Ltd (ASM) precursor company who pegged the ground in

2011. Since then ASM has conducted extensive data compilation, digitisation and assessment; underground mapping; underground channel and bulk sampling; and mineralogical and mineral processing testwork. ASM also worked collaboratively with several research projects, in particular FAME and AFK (see references) to characterise the mineralisation and investigate mineral processing options.

## Geological setting

The Tellerhäuser deposit is located within the Erzgebirge district which is part of the Saxo-Thuringian domain of central Europe in the Hercynian-Variscan orogen. The Erzgebirge district consists of a sequence of metamorphosed Palaeozoic (Cambrian to Ordovician) sediments consisting of shale, siltstone-sandstone and occasional limestone lenses overlying late Precambrian metamorphic (schist and gneiss) basement.

The Variscan orogeny (collision between Gondwana and Laurasia) deformed the Palaeozoic sedimentary sequence during the late Devonian to early Carboniferous. Early granitoids are deformed by this orogeny and affected by the regional metamorphism, whereas the later, mineralising granitoids (Permian) are generally undeformed and are classed as post tectonic.

## Local geology, alteration & mineralisation

Within the immediate Tellerhäuser project area, the geology consists of a mica schist sequence with several calc-silicate/skarn seams. These seams contain significant gneiss zones characterised by quartz and feldspar but it is unclear whether these are intrusions or part of the calc-silicate package (possibly originally tuffaceous sediments).

The calc-silicate/skarn seams consist of garnet-pyroxene-amphibole-magnetite-skarn with various proportions of the individual minerals, plus quartz-feldspar gneiss. Previous work attempted to define several types of skarn based on dominant mineralogy but it appears from recent work that this may be unrealistic, with mineralogy varying rapidly over small intervals.

In broad terms, the calc-silicate/skarn package can be thought of as having three distinct alteration/mineralisation events:

Stage 1: the main prograde garnet-pyroxene+/-amphibole (hornblende) stage (Figure 1) that is weakly tin mineralised (0.1% to 0.2% Sn). Tin is generally present in silicate form (e.g. stokesite) and in the lattice of, or as fine inclusions within, other silicate minerals

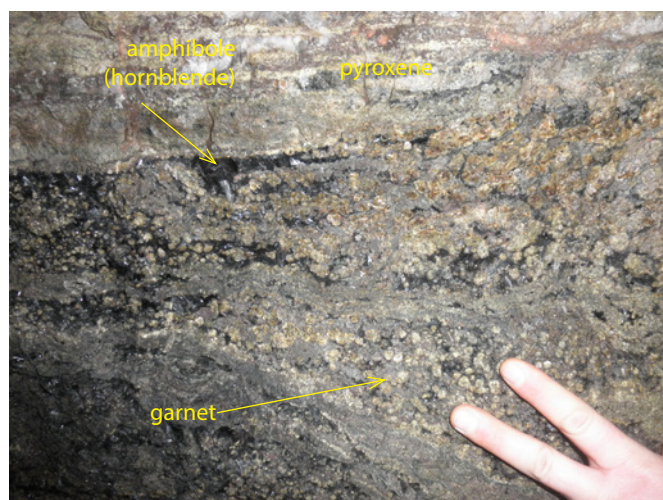


Figure 1. Stage 1 mineralisation - prograde garnet-pyroxene-amphibole(hornblende) skarn. Low grade tin occurs as silicates and tin-iron oxides.



Figure 3. Stage 3 mineralisation - late hydrothermal overprint comprising quartz - chlorite - fluorite - amphibole (tremolite)-cassiterite. Note coarse grained cassiterite in centre.

(e.g. titanite, epidote, amphibole, garnet and rutile) or in tin-iron-oxides. It is also occasionally present as ultra-fine cassiterite crystals (<10 micrometres). This event is probably related to the regional metamorphism.

Stage 2: the introduction of magnetite-sphalerite-(amphibole?) plus or minus other sulphides (Cu, As, Fe) in varying proportions (Figure 2). Magnetite occurs as massive beds and lenses up to several metres in thickness consisting of massive magnetite, partly altered to haematite (martitisation). Zinc occurs as coarse sphalerite crystals in massive seams/lenses up to one metre thick. It is often associated with magnetite and appears contemporaneous. Chalcopyrite and arsenopyrite occur as patches and veins within the skarn and magnetite. Interestingly, significant quantities of indium were also deposited at this time in the form of minute roquesite grains formed as a result of coupled substitution between sphalerite and chalcopyrite. Roquesite generally occurs in association with fine sphalerite grains within larger chalcopyrite grains. Tin occurs as ultrafine cassiterite inclusions within magnetite and other iron oxides.

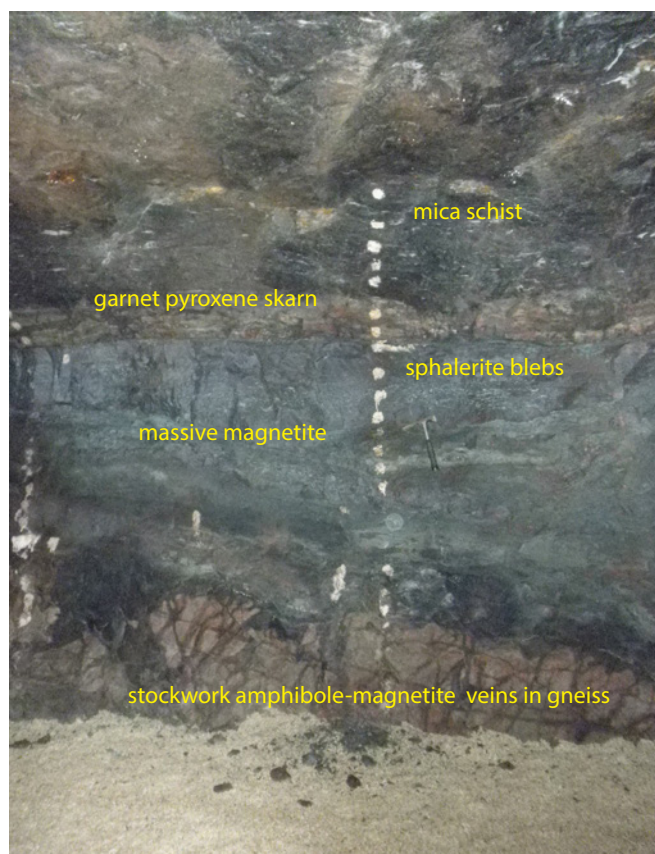


Figure 2. Stage 2 mineralisation - magnetite-sphalerite-amphibole (hornblende) overprint. Zinc-copper-indium-magnetite+/-tin introduced.

Stage 3: a late, retrograde hydrothermal overprinting event which is comprised largely of chlorite-amphibole (tremolite)-quartz-fluorite-cassiterite (Figure 3). Tin appears to occur largely in the form of relatively coarse grained cassiterite crystals ranging from 100 micrometres up to several centimetres across and as clumps of cassiterite up to several decimetres across (Figure 3). This forms the high grade tin mineralisation (generally plus 0.5% Sn, often plus 1-2% Sn) and the majority of what is now considered to be the potentially mineable part of the deposit. This was introduced by the late, undeformed, Permian granites and recent dating suggests this could be up to 20 million years later than the skarn formation.

The Stage 3 overprint appears to be structurally controlled and related to a dominant northeast trending structure and several less well defined, subsidiary, northwest trending structures. This assemblage is restricted to the skarn package but does not totally replace it, instead occurring as alteration fronts, patches and veins within the package, in a pseudo stockwork type arrangement. However, the overprint “zone” has well defined edges and once out of the zone, little or no overprint is seen and tin grade drops dramatically.

A third style of tin mineralisation consisting of quartz-cassiterite+/-tourmaline+/-feldspar occurs as sub-horizontal and rarely sub-vertical veins within the underlying schist package.

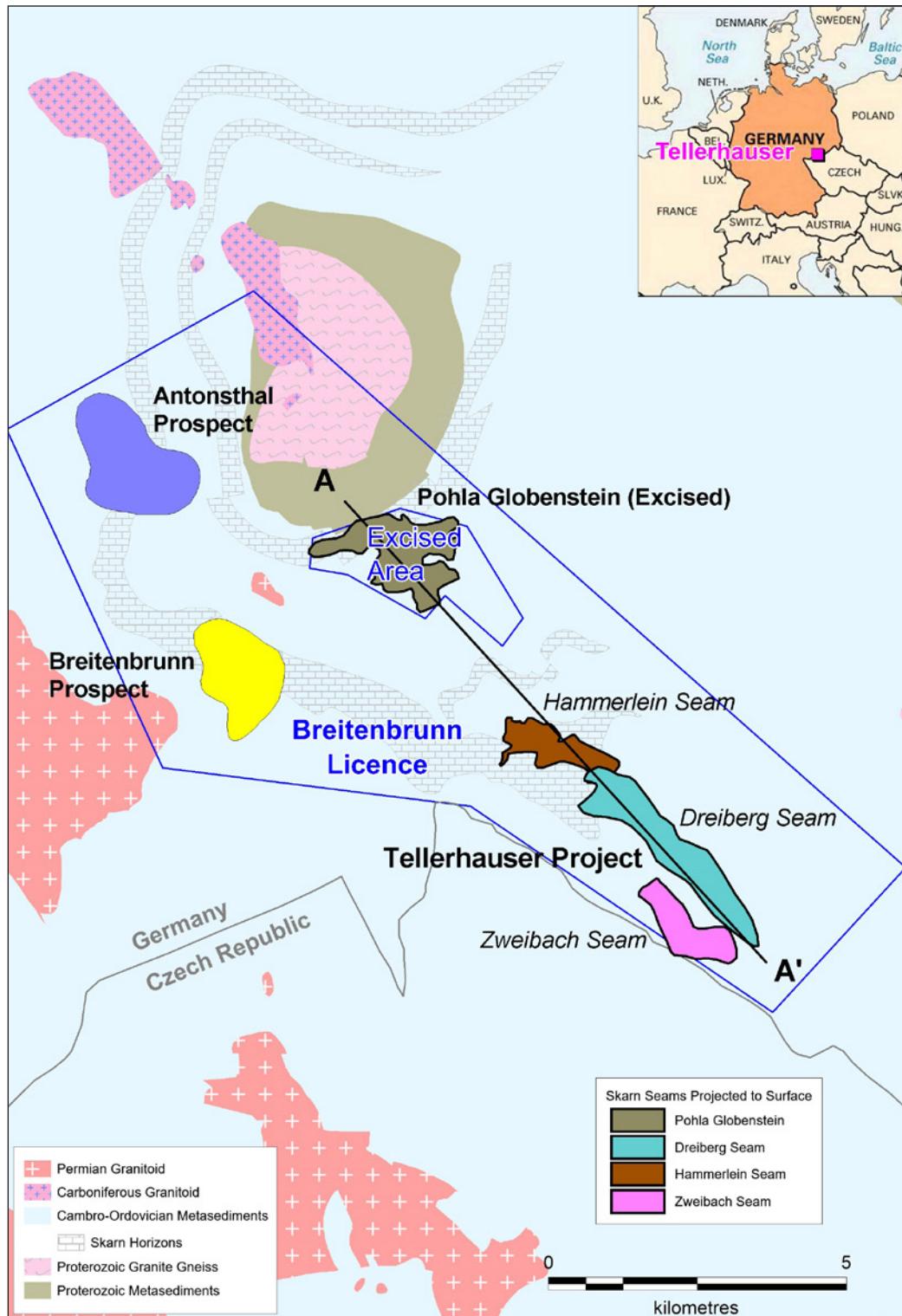


Figure 4. Simplified geology of the Tellerhäuser area showing the current licence area and surface projection of skarn seams.

## Resources

The main mineralisation at Tellerhäuser is hosted within three calc-silicate/skarn packages or seams over a strike length of more than 6km: Hämmerlein, Dreiberg and Zweibach seams (Figures 4 & 5).

The main mineralisation of interest occurs as well defined zones of hydrothermal overprint that occur in several structurally controlled parts of the skarn packages. These tend to form discrete zones in the order of 200-500 metres by 100-200m.

Total resources have recently been estimated and reported according to JORC 2012 guidelines as:

- Indicated 6.1Mt @ 0.48% Sn (29,500t tin)
- Inferred 16.1Mt @ 0.46% Sn (74,500t tin)
- Total 22.2Mt @ 0.47% Sn (104,000t tin)

Using a higher grade cut-off of around 0.4% Sn can be used as a proxy for estimating the overprint mineralisation as it is very rare to get values higher than this in the non-overprinted skarn mineralisation.

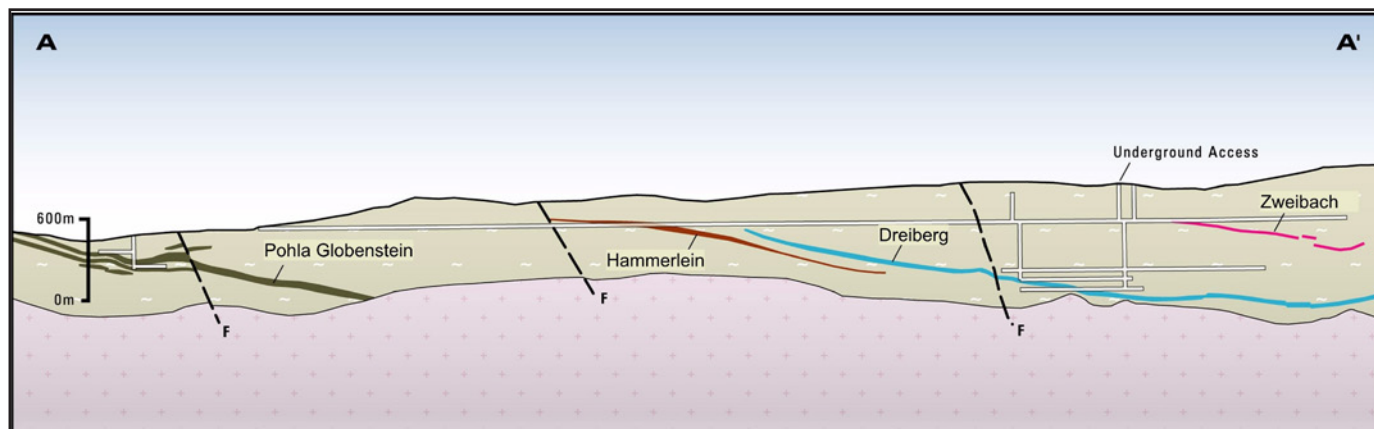


Figure 5. Schematic cross-section showing the calc-silicate / skarn seams (location shown on Figure 4).

This provides an estimate of around 7.4Mt @ 0.84% Sn (61,900t tin). Hence tonnage is reduced by around 65% while tin contained is only reduced by about 40%. This has very beneficial impacts on both mining and processing economics.

### Mineral processing ramifications

Based on the new geological interpretation, it is now recognised that there is a constant background of between 0.1% Sn and 0.2% Sn in the skarn that is associated with silicates and iron oxides and which is not recoverable. This is shown best by a re-examination of the old mineral processing data which shows a very good correlation between acid soluble tin (tin in silicates and iron-oxides) and tin occurring as cassiterite (total tin minus acid soluble tin) for proposed mining blocks which gives an excellent correlation and a constant 0.18% acid soluble tin.

This has been confirmed by mineralogical investigations by the FAME and AFK research projects which show a constant 0.1% to 0.2% tin content in minerals other than cassiterite.

If this background tin is taken into account when assessing the results of the previous metallurgical testwork it can be seen that good recoveries of tin as cassiterite were achieved and that the low tin grade of the concentrates was due to recovery of the tin in silicates and iron-oxides to the concentrates.

Based on this, ASM conducted new mineral processing testwork, including the building of a pilot plant treating 700kg/hr of skarn mineralisation. This has shown that good recoveries of cassiterite tin (plus 65%) can be obtained to a saleable tin concentrate (plus 50% Sn).

It has also been demonstrated that a bulk sulphide concentrate can be obtained via standard sulphide flotation and a saleable zinc concentrate extracted from this. The remaining mixed sulphide concentrate is currently being examined as a source of indium. Preliminary work suggests a good recovery of indium

(plus 50%) can be obtained via leaching using an organic acid in an autoclave and then electrowinning the pregnant solution. This could be a very significant source of indium and one of the few that is not a by-product of, or tied up in the lattice of, sphalerite.

### Conclusion

A revised understanding of the geology of a well-known but unloved old deposit, long thought of as being un-processable, has resulted in the recognition of two overprinted styles of tin mineralisation. The first, associated with a prograde skarn assemblage, is considered as background due to the form in which the tin occurs (silicates and iron-oxides) and its low grade (0.1-0.2% Sn). The second, associated with a significantly later hydrothermal overprint, brought in much more tin (generally over 0.5% and up to several percent tin) mostly in the form of coarse cassiterite. This new understanding has resulted in the recognition that the second stage of mineralisation is actually quite simple to treat and has changed the perception that this is an untreatable tin deposit.

The prograde skarn mineralising event resulted in the formation of significant quantities of iron as magnetite, zinc as sphalerite and indium as roquesite. These form good by-product credits, with some occurring within the tin mineralisation and some outside which may be mineable in their own right.

ASM is currently proceeding with a Prefeasibility Study on the mineralisation and early indications are positive. This is expected to be completed late 2019.

### References

- FAME – Flexible and Mobile Economic Processing Technologies, Deliverable D5.7, Grant Agreement 641650, Horizon 2020
- AFK – “Aufbereitung feinkörniger polymetallischer heimischer In/W/Sn-Komplexerze”; Helmholtz Institute Freiberg for Resource Technology; TU Bergakademie Freiberg; UVR FIA GmbH Freiberg; Grant number: 033R128, BMBF

# Magmatic and hydrothermal evolution of the tin-mineralisation at the Groenfontein Tin Mine in the Lebowa Granite Suite, South Africa

L.C. Vonopartis<sup>1</sup>, P.A. Nex<sup>1</sup>, J.A. Kinnaird<sup>1</sup>, L.J. Robb<sup>1,2,3</sup>

<sup>1</sup>University of the Witwatersrand, Johannesburg

<sup>2</sup>Oxford University, United Kingdom

<sup>3</sup>University of Johannesburg, Johannesburg

## Introduction

The Lebowa Granite Suite in the northern limb of the Bushveld Complex is known for its tin mineralisation, which is associated with the Bobbejaankop and Lease granites. These granites form the “Zaaipplaats Tin fields”, along the Makapansberg escarpment, 35 km northwest of Mokopane (Fig 1) (Robb, et al., 2000; Crocker, et al., 2001; Bailie & Robb, 2004). The petrogenesis and mineralisation of the stanniferous Bobbejaankop and Lease granites and their inter-relationships in the Zaaipplaats Tin field have long been contentious issues (Robb, et al., 2000; Crocker, et al., 2001; Bailie & Robb, 2004). The present study utilises detailed mapping, petrography and geochemistry coupled with ASTER image interpretation, and field based portable XRF geochemical mapping, to shed light on the geological relationships between the two granites and the distribution of tin mineralisation within them.

## Granite petrography

The Bobbejaankop Granite is an equigranular, coarse-grained, miarolitic granite that is primarily composed of red alkali feldspar, quartz, chloritised biotite with minor fluorite, chlorite and tourmaline. The Bobbejaankop Granite at the old Zaaipplaats Tin Mine is economically mineralised with disseminated cassiterite, however in the bounds of the adjacent Groenfontein Tin Mine it is barren and only the overlying Lease granite is mineralised (Strauss & Truter, 1944; Coetzee, 1984; Crocker, et al., 2001). Miarolitic cavities are a prominent feature, typically filled with clusters of tourmaline, quartz, calcite and fluorite, surrounded by haloes of silicification. Toward the stratigraphic middle of the intrusion, anastomosing swarms of tourmaline rich pipe-like structures appear to radiate upwards from its centre into the overlying Lease Granite. These pipe-like structures contain minor cassiterite, scheelite and sulphides compared to the corresponding, well-endowed pipes mined at Zaaipplaats. Although there is a sharp contact between the Bobbejaankop and Lease granites there are regions of interfingering and the Bobbejaankop granite begins to exhibit features of the overlying Lease Granite closer to the contact, such as an increase of fluorite, and more prominent microclinisation, chloritisation, sericitisation, saussuritisation and granophyric intergrowths.

The Lease granite is a thin lenticular body found

peripherally along the roof margin of the Bobbejaankop facies as fine-grained, miarolitic granite with extensive pegmatitic margins beneath the roof contact with the Rashoop Granophyre Suite. Swarms of dykes of Lease granite extend upwards from the centre of the Bobbejaankop towards the roof contact and feed into the overlying Lease Granite. The Lease Granite is typically composed of quartz, alkali feldspar and altered biotite. Within the Lease, perthite becomes more prominent as the main alkali-feldspar, with an increase in hydrothermal-related microclinisation and sericitisation. The biotites experience variable chloritisation and later sericitisation.

At Groenfontein, tin mineralisation occurs primarily within the Lease Granite. Pipe-like ore bodies are well endowed with cassiterite which is associated with intense, localised greisenisation, while disseminated cassiterite is confined to zones of pervasive alteration. These pipe-like ore bodies are extensions of pipes from the Bobbejaankop Granite below, yet in contrast to Zaaipplaats, are only economic once within the Lease Granite. These pipe-like ore bodies terminate into large greisenised lenticular ore bodies which are highly enriched in cassiterite.

## Mapping

Detailed geological mapping of the Groenfontein Tin Mine was last published by Strauss (1954) and since then little or no updating has been done on the granites outside of the Zaaipplaats Tin Mine. Therefore a lithological discrimination of the Lease and Bobbejaankop granites was completed in addition to targeting zones of intensely altered granite using multispectral ASTER data. This work was validated by extensive field mapping and ground truthing. By isolating signatures related to hydrothermal alteration from surrounding rocks using band ratios B8/B2 and B8/B4, while specifically enhancing the chlorite signature using B2/B4, regions of increased hydrothermally induced chloritisation were identified (Fig 2). These regions correspond with known regions of disseminated cassiterite and zones around greisenised pipes (Fig 2).

Coupling the space borne remote sensing with elemental isopleths of incompatible elemental ratios, generated from portable XRF field analysis, allowed for the discrimination of various granites and regions of increased fractionation (Fig 3). The Rb/Ba ratio

is a proxy for an increase in fractionation and volatile saturation of the granites, and corresponds to known zones of mineralisation (Fig 3). Thus, utilising both ASTER and portable XRF mapping, may provide a first order exploration technique, for the targeting of potential mineralisation within A-type granites (Fig 3).

### Whole-rock geochemistry

The Nebo, Bobbejaankop and Lease granites show little variation in their major element abundances. The A-Type granite classification diagrams proposed by Frost et al., (2001), categorise these as ferroan, calc-alkali granites, within the defined A-Type granite field (Fig 4) (Frost, et

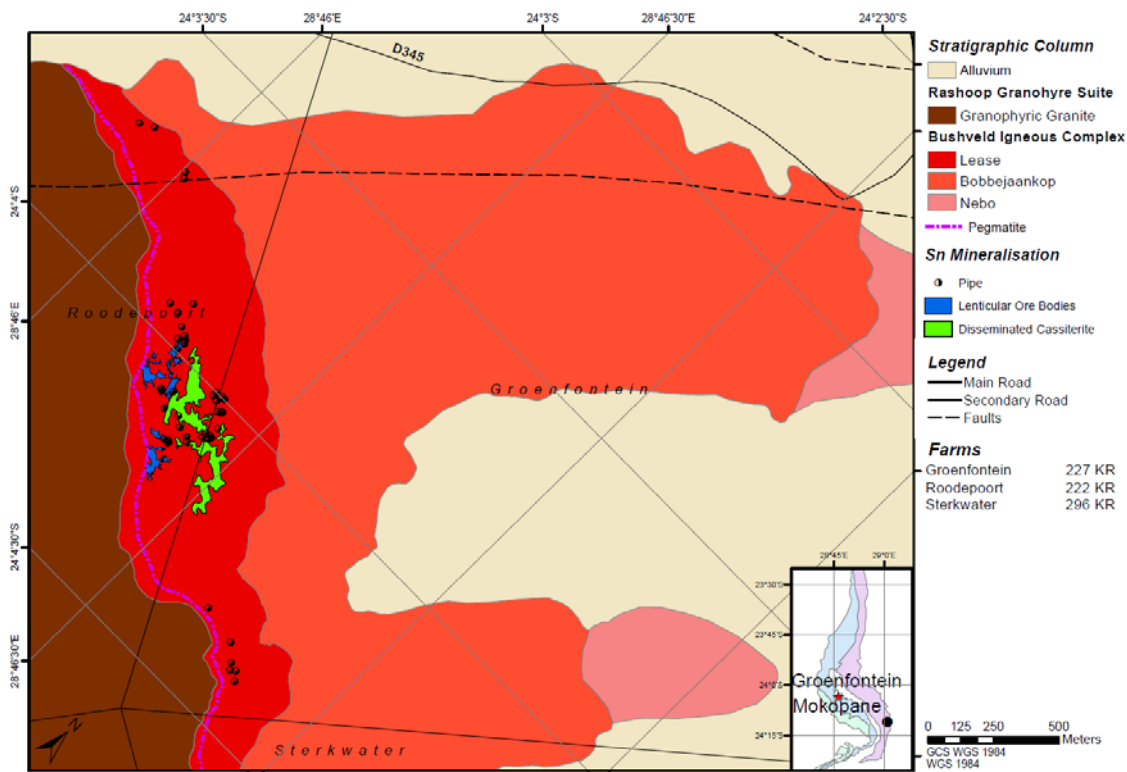


Fig 1: Revised Geological map of the Groenfontein Tin Mine. The zones of disseminated mineralisation, mineralised pipes and lenticular ore bodies were determined by the integration of extensive field mapping and published maps. Original base maps were revised, refined and added to from Strauss (1954) & Coetzee (1984). Lithological boundaries were defined by published maps and by the ground validation of remotely sensed data. Nomenclature for the lithological units displayed is taken from SACS (1980).

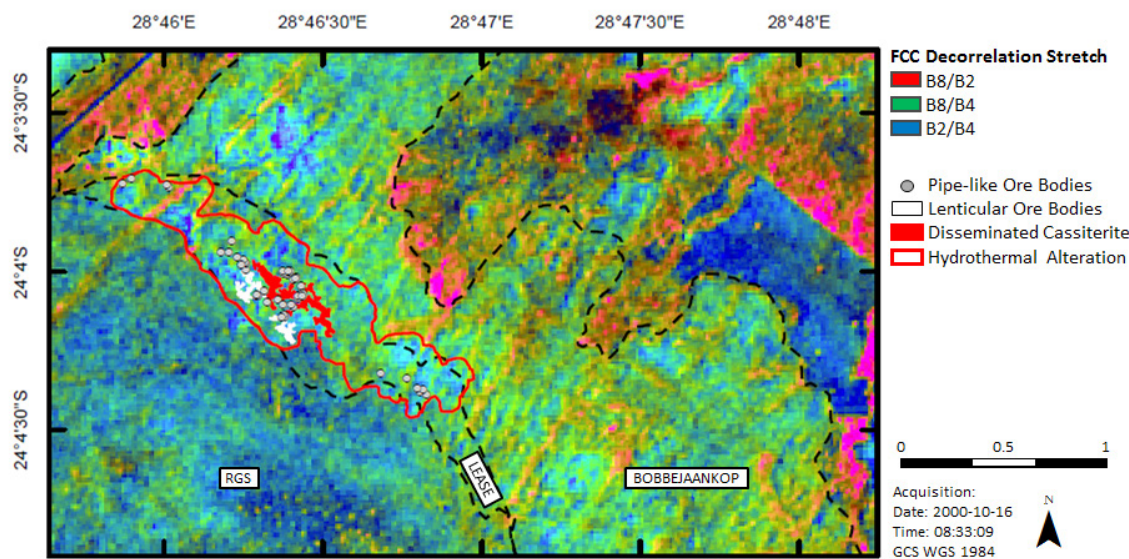


Fig 2: ASTER false colour composite band ratio RGB 8/2, 8/4, 2/4 after decorrelation stretching. The Nebo Granite, Bobbejaankop Granite, Lease Granite and Rashoop Granophyre Suite (RGS) are delineated. The region of chloritised hydrothermal alteration is outlined in red.

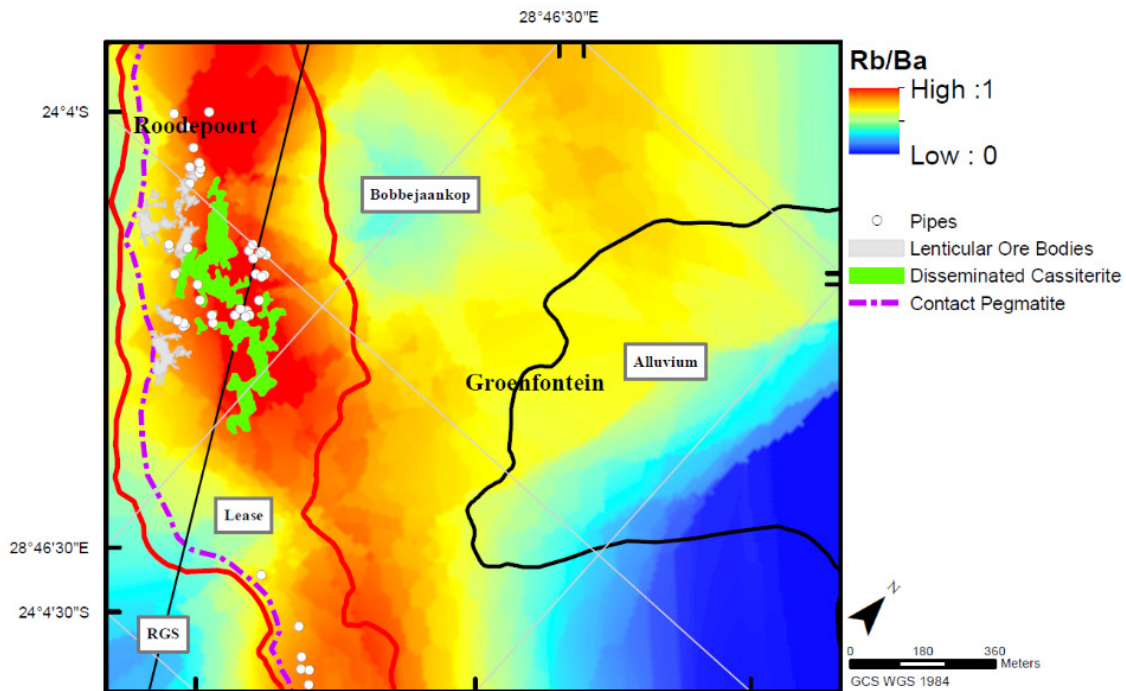


Fig 3: Handheld XRF produced Rb/Ba isopleths over the Groenfontein Tin Mine. Superimposed regions of mineralisation are determined from field mapping and literature (Strauss (1954) & Coetzee (1984)).

al., 2001; Frost & Frost, 2011). When plotted on the A/KNC vs A/NK diagram, the three lithologies fall within the ranges of other global mineralised and unmineralised A-type granites (Fig 4). The Bobbejaankop and Nebo granites exhibit the weakly peraluminous characteristics of A-type granites with an A/CNK (molar  $\text{Al}_2\text{O}_3 / (\text{CaO} + \text{Na}_2\text{O} + \text{K}_2\text{O})$ ) ranging from 0.90 – 1.23 (Fig 4) (Maniar & Piccoli, 1989; Gao, et al., 2016). However, the Lease Granite exhibits a more peraluminous trend (Fig 4). The Lease Granite from Groenfontein appears to plot within the same region as the Bobbejaankop Granite from Zaaipiaats and the Lease Granite from Zaaipiaats extends further into the peraluminous sector beyond the region of global A-Type granites (Fig 4).

Trace element compositions of these granites reveal distinct variations of the incompatible element ratios between the three granite types. The Rb/Sr ratio shows a trend of sequential fractionation from the Nebo Granite to the Bobbejaankop and then the Lease Granite (Fig 5a) (McCarthy & Hasty, 1976). When plotted using Zr/Hf vs  $\text{SiO}_2$ , all the granites plot within the mineralised greisen granite zone, however the lithologies from Zaaipiaats appear to be further evolved than the equivalent ones from Groenfontein (Fig 5b) (Zaraisky, et al., 2009).

The negative correlation between Nb/Ta and K/Rb proposed by Dostal & Chatterjee, (2000), suggests an influence of fractionating and mineralising fluids in highly evolved rocks. There is a separation of the Lease and Bobbejaankop granites from Zaaipiaats and Groenfontein evident by a decrease in the Nb/Ta ratio of Zaaipiaats (Fig 5c). This difference coupled with a positive correlation between Ta and Li suggests that internally derived magmatic auto-metasomatism preceded greisenisation (Fig 5c) (Dostal & Chatterjee, 2000). The

Lease and Bobbejaankop granites from Zaaipiaats show a greater involvement of these fluids (Fig 5d).

The concentration of Sn within the granite is positively correlated with the apparent extent of fractionation experienced, as the Lease Granite shows the most Sn enrichment (fig 6a). Additionally, the Sn content of the Lease Granite appears to be associated with an increase in chloritisation and greisenisation, yet is depleted when greisenisation is the dominant alteration (fig 6b). Three types of Lease have been described at Groenfontein. Type 1 & 2 which exhibit chloritised biotites with minor greisenisation are more enriched in Sn and associated with disseminated mineralisation and the highly greisenised Type 3 Lease, which exhibits a depletion of Sn, is typically unmineralised and surrounds pipe-like ore bodies.

## Conclusions

According to the available data, a modification of the current models of tin mineralization is suggested. The fractionation and formation of the volatile enriched Bobbejaankop Granite at the roof of the Nebo Granite is followed by concentration of an incompatible element and volatile enriched fluid-saturated phase in the middle of the Bobbejaankop Granite. Subsequent fracturing of the Bobbejaankop carapace allowed for upward movement and formation of the Lease Granite at the upper contact. Inward crystallisation of the Lease and Bobbejaankop resulted in further concentration of incompatible constituents, alteration of biotite and liberation of Sn, allowing for the crystallisation of cassiterite. The movement of magmatic fluids from the Bobbejaankop below resulted in these fluids greisenising and scavenging the surrounding granite of Sn, and the precipitation of cassiterite within the greisenised pipe and lenticular ore bodies.

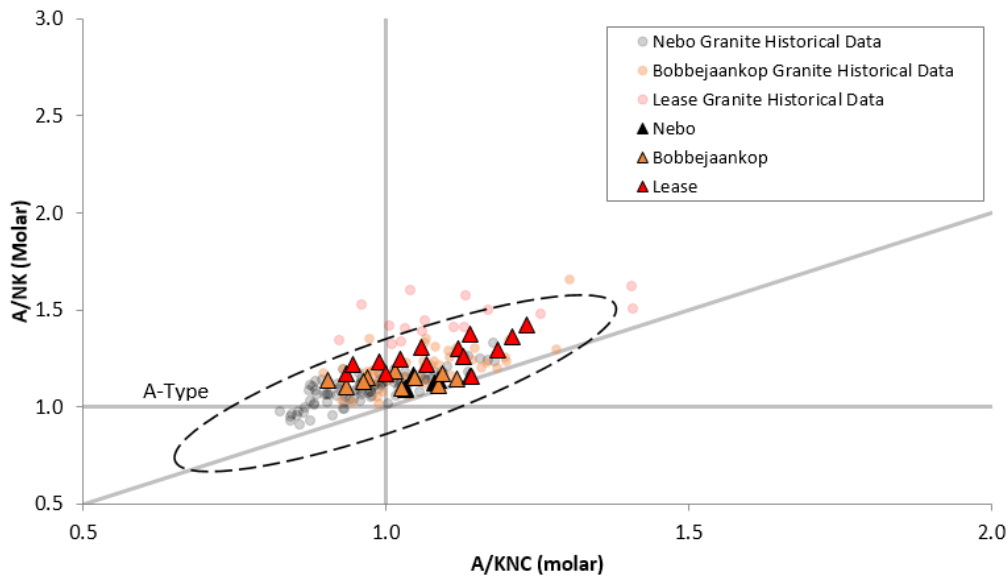


Fig 4: A/KNC vs A/NK discrimination diagram. Range of A-Type granites shown within the dashed ellipse, compiled from data collected from Juniper & Kleeman, 1979; Zhou et al., 2017 Jiang, et al., 2014; Li et al., 2014; Singh & Vallinayagam, 2012; Frost & Frost, 2011. Shaded areas and circular data points represent the range of literature geochemical analyses; Nebo Granite (grey), Bobbejaankop Granite (orange) and Lease Granite (red) (Kleemann & Twist, 1989; Pollard, et al., 1991; Hill, et al., 1996; Labuschagne, 2004).

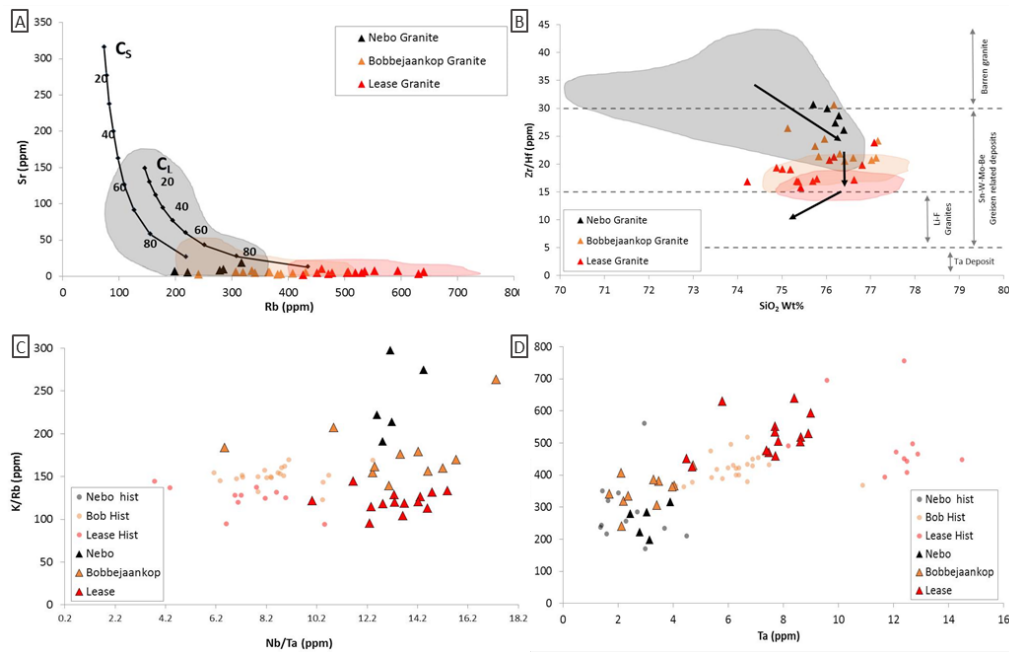


Fig 5: (A) Rb/Sr graph describing the fractionation relationship between the Nebo (black), Bobbejaankop (orange) and Lease (red) granites. Percentage of crystal fractionation indicated on the trend lines; concentration in solid (Cs), concentration in liquid (CL). (B) Plot of Zr/Hf vs SiO<sub>2</sub> indicating the correlation between fractionation and mineralisation in felsic magmas (adapted from Zraisky et al., 2009). (C) Plot of Li vs Ta showing extent of fractionating fluid. (D) Plot of K/Rb vs Nb/Ta shows influence of internally derived fluids. Shaded areas and circular data points represent the range of literature geochemical analyses (historical data = hist); Nebo Granite (grey), Bobbejaankop Granite (orange) and Lease Granite (red) (Kleemann & Twist, 1989; Pollard, et al., 1991; Hill, et al., 1996; Labuschagne, 2004).

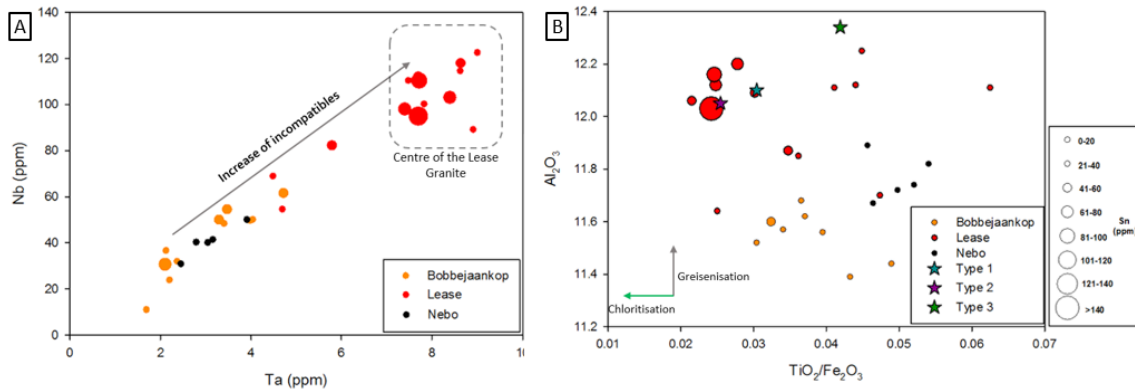


Fig 6: The relationship of Sn concentration relative to fractionation and hydrothermal alteration. (A) Bubble plot of Nb vs Ta vs Sn indicates the concentration of Sn with increase in fractionation of the granites. (B) Bubble plot of  $\text{Al}_2\text{O}_3$  vs  $\text{TiO}_2/\text{Fe}_2\text{O}_3$  vs Sn compares the tendency for Sn to be associated with chloritisation (decrease in  $\text{TiO}_2/\text{Fe}_2\text{O}_3$ ) or greisenisation (increase in  $\text{Al}_2\text{O}_3$ ). Bubble size is representative of the amount of Sn in ppm.

## References

- Bailie, R. H. & Robb, L. J., 2004. Polymetallic mineralization in the granites of the Bushveld Complex - examples from the central southeastern lobe. *South African Journal of Geology*, 107, pp. 633-652.
- Coetzee, J., 1984. A Geochemical and Petrographical Investigation of the Low-Grade Tin Deposits in the Bobbejaankop Granite at the Zaaipplaats Tin Mine. Unpub. M.Sc dissert., Univ. Pretoria, p. 126.
- Crocker, I. T., Eales, H. V. & Ehlers, D. L., 2001. The Fluorite, Cassiterite and Sulphide Deposits Associated with the Acid Rocks of the Bushveld Complex. Pretoria: Council for Geoscience.
- Dostal, J. & Chatterjee, A. K., 2000. Contrasting behaviour of Nb/Ta and Zr/Hf ratios in a peraluminous granitic pluton (Nova Scotia, Canada). *Chemical Geology*, 163, pp. 207-218.
- Frost, B. R. et al., 2001. A geochemical classification for granitic rocks. *Journal of Petrology*, 42(11), pp. 2033-2048.
- Frost, C. D. & Frost, B. R., 2011. On Ferroan (A-type) Granitoids: their Compositional Variability and Modes of Origin. *Journal of Petrology*, 52(1), pp. 39-53.
- Gao, P., Zheng, Y. F. & Zhao, Z. F., 2016. Experimental melts from crustal rocks: A lithochemical constraint on granite petrogenesis. *Lithos*, pp. 133-157.
- Hill, M., Barker, F., Hunter, D. & Knight, R., 1996. Geochemical Characteristics and Origin of the Lebowa Granite Suite, Bushveld Complex. *International Geology Review*, 38, pp. 195-227.
- Jiang, H. et al., 2017. Geochronological, geochemical and Sr-Nd-Hf isotopic constraints on the petrogenesis of Late Cretaceous A-type granites from the Sibumasu Block, Southern Myanmar, SE Asia. *Lithos*, pp. 32-47.
- Juniper, D. N. & Kleeman, J. D., 1979. Geochemical Characterisation of some Tin-Mineralising Granites of New South Wales. *Journal of Geochemical Exploration*, 11, pp. 321-333.
- Kleemann, G. J. & Twist, D., 1989. The Compositionally-zoned Sheet-like Granite Pluton of the Bushveld Complex: Evidence Bearing on the Nature of A-type Magmatism. *Journal of Petrology*, 30, pp. 1383-1414.
- Labuschagne, L. S., 2004. Evolution of the ore-forming fluids in the Rooiberg tin field, South Africa. *Memoir- Council for Geoscience*.
- Lenthall, D. H. & Hunter, D. R., 1977. The Geochemistry of the Bushveld Granites in the Potgietersrus Tin-Field. *Precambrian Research*, 5, pp. 359-400.
- Li, H., Watanabe, K. & Yonezu, K., 2014. Geochemistry of A-type granites in the Huangshaping polymetallic deposit (South Hunan, China): Implications for granite evolution and associated mineralization. *Journal of Asian Earth Sciences*, 88, pp. 149-167.
- Maniar, P. D. & Piccoli, P. D., 1989. Tectonic discrimination of granitoids. *Geological Society of America Bulletin*, 101, pp. 635-643.
- McCarthy, T. S. & Hasty, R. A., 1976. Trace element distribution patterns and their relationship to the crystallisation of granitic melts. *Geochimica et Cosmochimica Acta*, 40, pp. 1351-1358.
- Pollard, P. J., Taylor, R. G., Taylor, R. P. & Groves, D. I., 1991. Petrographic and Geochemical Evolution of Pervasively Altered Bushveld Granites at the Zaaipplaats Tin Mine. *Economic Geology*, 88, pp. 1401-1453.
- Robb, L. J., Freeman, L. A. & Armstrong, R. A., 2000. Nature and longevity of hydrothermal fluid flow and mineralisation in granites of the Bushveld Complex, South Africa. *Earth Sciences*, 91, pp. 269-281.
- SACS, 1980. Stratigraphy of South Africa. Part 1 In: L.E. Kent (Compiler), *Lithostratigraphy of the Republic of South Africa. Handbook of the Geological Survey of South Africa*, 8, p. 690pp.
- Singh, L. G. & Vallinayagam, G., 2012. Petrological and Geochemical Constraints in the Origin and Associated Mineralization of A-Type Granite Suite of the Dhiran Area, Northwestern Peninsular India. *Geosciences*, pp. 66-80.
- Strauss, C. A., 1954. The geology and mineral deposits of the Potgietersrus tin fields. *South African Geological Survey Memoirs*, 46, p. 241.
- Strauss, C. A. & Truter, F. C., 1944. The Bushveld Granites in the Zaaipplaats Tin Mining Area. *Transactions of the Geological Society of South Africa*, 47, pp. 47-77.
- Zaraisky, G. P. et al., 2009. The Zr/Hf Ratio as a Fractionation Indicator of Rare-Metal Granites. *Petrology*, 17, pp. 25-45.
- Zhou, G. et al., 2017. Petrogenesis of the Huashanguan A-type granite complex and its implications for the early evolution of the Yangtze Block. *Precambrian Research*, 292, pp. 57-74.

# Intensive Mesozoic Li-Be-Nb-Ta mineralization in the Kelumute-Jideke pegmatite field, Chinese Altai

Chun-Long Wang<sup>1,2,3</sup>, Shao-Yong Jiang<sup>1</sup>, Ke-Zhang Qin<sup>2,3</sup>

<sup>1</sup>State Key Laboratory of Geological Processes and Mineral Resources, Collaborative Innovation Center for Exploration of Strategic Mineral Resources, Faculty of Earth Resources, China University of Geosciences, Wuhan 430074, China

<sup>2</sup>Xinjiang Research Center for Mineral Resources, Xinjiang Institute of Ecology and Geography, Chinese Academy of Sciences, Urumqi 830011, China

<sup>3</sup>Key Laboratory of Mineral Resources, Institute of Geology and Geophysics, Chinese Academy of Sciences, Beijing 100029, China

The Chinese Altai is located in the central part of the southern Central Asian Orogenic Belt (CAOB), within which more than 100,000 granitic pegmatite dykes are exposed and comprise the well-known Altai pegmatite province (Zou and Li, 2006). The Kelumute-Jideke pegmatite field (KJPF) is located in the central portion of the Chinese Altai. More than 400 pegmatite dykes and at least 10 rare-metal deposits are developed in the KJPF (Fig. 1), which is one of the most important rare-metal and gemstones ore-clusters in the Chinese Altai. Moreover, great advances in rare-metal exploration have been achieved in the Kukalagai and Qunkuer ore districts in recent years, which has led to this pegmatite field being the regional focus for the study of rare-metal pegmatites.

## Regional zonation of pegmatites in KJPF

Besides important rare-metal reserves, the rare-metal pegmatites of the KJPF show an uncommon regional zonation around the Jideke granite (Fig. 1). According to the pegmatite classification of Černý and Ercit (2005), the regional zonation pattern of pegmatite groups surrounding the Jideke granite, including barren feldspar-muscovite pegmatites close to or within the pluton, to beryl-columbite sub-type (Be-Nb-Ta), then to albite-spodumene type (Li-Be-Nb-Ta), and finally to albite type and lepidolite sub-type (Li-Ta-Cs and gemstones) away from the parental granite (Zou and Li, 2006; Wang, 2017).

## Important rare-metal deposits in KJPF

Corresponding to the regional zonation of rare-metal pegmatites, important rare-metal deposits in the KJPF include the Azubai Be-gemstone deposit, the Qunkuer Be-Nb-Ta deposit, the Kelumute and Kukalagai Li-Be-Nb-Ta deposits, and the Jiamukai Li-Nb-Ta-gemstone deposit.

### Azubai Be-gemstone deposit

Eight pegmatite dykes are exposed in the Azubai ore district. These pegmatites are dominated by a graphic zone that represents relatively low degrees of fractionation, and late albite, quartz and coarse-grained muscovite enriched units that occur as nests or veins. Beryl is the main Be-bearing mineral in this deposit, and is distributed in both the graphic zones and late units,

although it is more abundant in the latter. High quality aquamarine has been discovered in several pegmatites, especially in the No. 328 and 528 pegmatites. One beryl bearing muscovite-quartz-albite pegmatite gave a zircon U-Pb age of  $191.6 \pm 2.1$  Ma (Zhang et al., 2016).

### Qunkuer Be-Nb-Ta deposit

Due to significant advances in prospecting for underground rare-metal ores, the Qunkuer ore district, has developed to be the only large-scale Be-dominated deposit in the KJPF. The distribution of pegmatites are mainly controlled by orogen-parallel NW-striking faults. The rare-metal reserves are mainly hosted by the Qunkuer No. I and II pegmatites. Both horizontal and vertical internal zonations have been observed in the No. I pegmatite. Internal zones in this pegmatite include an aplitic border zone, a beryl-quartz-microcline zone (Fig. 2A), a blocky microcline zone and a massive quartz zone. Late fine-grained platy albite, muscovite-quartz-albite and muscovite-quartz units occur as nests or veins. Columbite group minerals are dominantly enriched in the late units, and these occasionally show intimate intergrowth relationships with beryl. Zircon U-Pb dating yielded a time range of 206.8 to 194.1 Ma for this pegmatite (Ren et al., 2011; Zhou et al., 2016).

### Kelumute Li-Be-Nb-Ta deposit

The Kelumute Li-Be-Nb-Ta deposit has been regarded as the second largest rare metal deposit in the Chinese Altai. Approximately one hundred pegmatite dykes are exposed in the ore district; that are mainly hosted by late Ordovician granitic rocks. Albite-spodumene sub-type pegmatites, such as No. 112, 116 and 228, have attracted much attention due to their large sizes and rare metal reserves.

The No. 112 pegmatite is the largest and most representative pegmatite in the Kelumute deposit. This pegmatite can be further divided into six textural zones, including a fine-medium grained quartz-albite zone, a blocky microcline zone, a quartz-spodumene-albite zone (Fig. 2B), a muscovite-quartz-albite zone, a saccharoidal albite zone, and a massive quartz zone. Field and petrographic evidence reveals that the Kelumute No. 112 is an albite-spodumene sub-type pegmatite that has experienced a two-stage evolution. The lanthanide tetrad effect and non-chondritic Y/Ho and Zr/Hf ratios

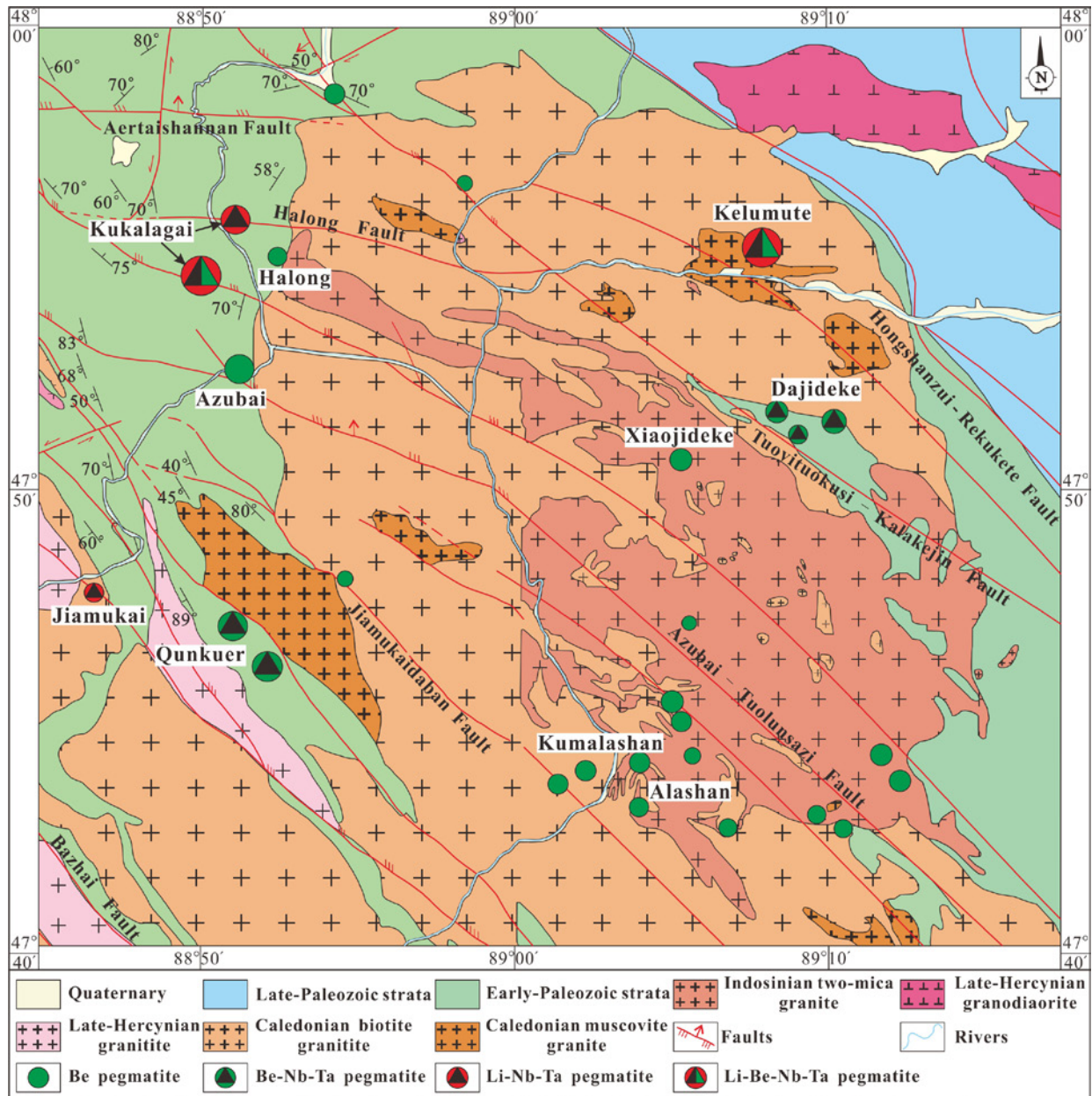


Figure 1. Geological sketch map of Kelumute-Jideke pegmatite field.

have been observed in columbite-tantalite and zircon from different zones (Wang, 2017). These extreme fractionation signatures did not enhance or diminish during internal evolution of the pegmatitic system, thus can be ascribed to the intrinsic features of the highly evolved initial melt. Highly concordant columbite-tantalite U-Pb ages reveal a time range of 207.9–202.2 Ma for timing of emplacement and internal evolution of pegmatites in this ore district (Wang, 2017).

### **Kukalagai Li-Be-Nb-Ta deposit**

The Kukalagai Li-Be-Nb-Ta deposit is another large Li-enriched rare metal deposit of the KJPF, and is located in the outer zone of the regional zonation sequence about 5 km northeast from the Jideke granite (Fig. 1). With the recent discovery of the No. 804, 806 and 807 pegmatites with abundant lithium reserves, the Kukalagai becomes the largest remaining lithium resource in the Chinese Altai.

The No. 650 pegmatite located in the southern part of the ore district is the earliest discovered rare-metal pegmatite. This pegmatite is conformably hosted by Silurian andalusite-biotite-quartz schists. Three internal zones have been observed in this pegmatite, including a muscovite-quartz-albite zone, a lepidolite-muscovite-quartz-albite zone (Fig. 2C), and a quartz-spodumene-albite zone. Spodumene dominated nests are widely developed in the central part of the pegmatite, within which columbite group minerals are enriched as well. The No. 807 pegmatite is the largest rare-metal pegmatite among the newly-discovered pegmatites. This pegmatite shows a characteristic vertical internal zonation, including a muscovite-lepidolite-quartz-albite zone at surface and a spodumene-quartz-albite zone with much more abundant Li-Nb-Ta mineralization (Fig. 2D) at depth.

Despite the distinct ore-controlling structures and internal zonation of rare metal pegmatites in the Kukalagai

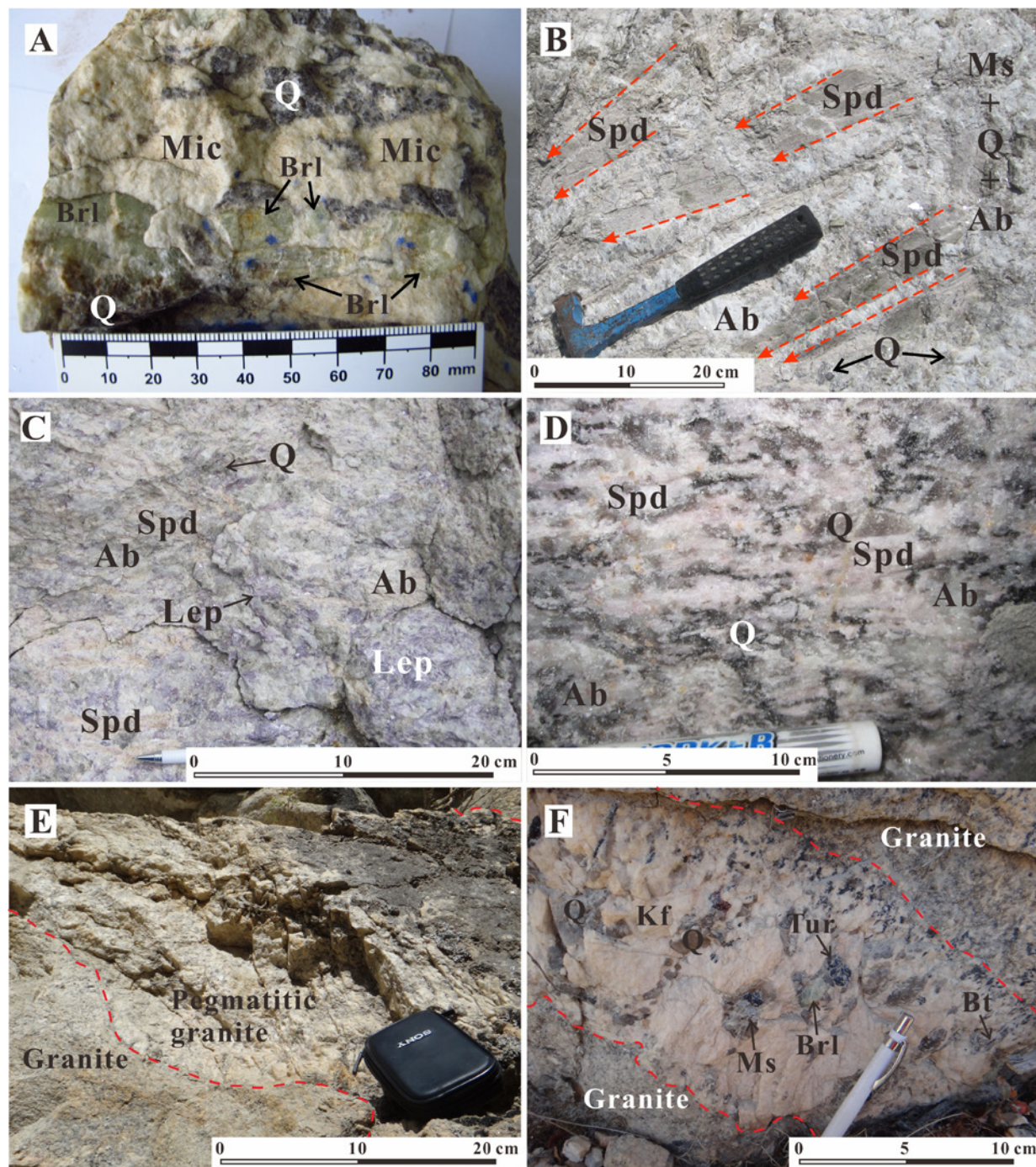


Figure 2. Photographs of internal zones of typical pegmatites and the parental granite. A. beryl-quartz-microcline zone in the Qunkuer No. 1 pegmatite; B. quartz-spodumene-albite pegmatite in the Kelumute No. 112 pegmatite with oriented spodumene megacrystals; C. lepidolite-spodumene-quartz-albite pegmatite with abundant lepidolite aggregations in the Kukalagai No. 650 pegmatite; D. spodumene-enriched nests in the Kukalagai No. 807 pegmatite with oriented spodumene crystals perpendicular to pegmatite-wallrock contact; E. pegmatitic granite in the outer portion of the Jideke granite; F. beryl and tourmaline enriched schlieren in the Jideke granite. Abbreviations: Ab-albite; Brl-beryl; Bt-biotite; Kf-potassium feldspar; Lep-lepidolite; Mic-microcline; Ms-muscovite; Q-quartz; Spd-spodumene; Tur-tourmaline.

ore district, these pegmatite dykes are dominated by the quartz-spodumene-albite zone, which covers over 70 vol.% of these dykes. Thus, internal zonation and mineral assemblages indicate that these pegmatites belong to the highly fractionated albite-spodumene sub-type. Mineral chemistry of microcline, micas, columbite-tantalite and zircon from representative rare metal pegmatites indicates high and identical fractionation degrees for

these rare metal pegmatites (Wang, 2017). In addition, relatively homogeneous internal structure of columbite-tantalite and micas from primary zones of these pegmatites indicate near-equilibrium crystallization during the primary magmatic stage. A time span of 206.8–202.4 Ma has been implied by columbite-tantalite U-Pb ages for emplacement and internal evolution of different pegmatites in the district.

### Jiamukai Li-Nb-Ta and gemstone deposit

Lepidolite sub-type pegmatites are mainly exposed in the Jimukai ore district, which is located in the southeastern extent of the KJPF and at a distance of 10 km from the Jideke granite (Fig. 1). Tens of east-west trending pegmatite dykes are developed in the ore district, and these are mainly hosted by biotite-quartz schists of the Silurian Kulumuti Group. Rare-metal pegmatite is represented by the No. 87 pegmatite, which consists of a fine-grained muscovite-quartz-albite border zone, a spodumene-quartz-cleavelandite zone, a lepidolite-albite zone, and a blocky albite core zone. The lepidolite-albite zone constitutes the main part of the pegmatite, and features giant lepidolite crystals and abundant gemstones (e.g. aquamarine, tourmaline and moonstone) in miarolitic cavities. One columbite-group mineral bearing sample from the muscovite-quartz-albite zone yielded a zircon U-Pb age of  $192.0 \pm 2.3$  Ma (Zhang et al., 2016).

### Jideke granite—the parental granite for the pegmatite field

Field observation reveals the highly heterogeneous nature of the Jideke granite. Three different lithologies, including equigranular two-mica granite, two-mica potassium feldspar granite and fine-grained two-mica granite, have been identified (Wang, 2017), with pegmatitic granite and accessory and rare-metal mineral enriched units developed locally (Fig. 2E, F). Major element features indicate peraluminous leucogranitic composition for various petrographic facies of the granitic stock, which are consistent with typical parental granites of rare-metal pegmatites globally (Černý, 1991). Trace element features combined with mineralogy of muscovite and microcline indicate a high degree of fractionation of the granite, which is capable of generating pegmatitic melts. Zircon U-Pb dating results reveal that the formation of different petrographic facies in the Jideke granite were between 207.8 and 203.4 Ma. This time range nearly overlaps with the time span of columbite-tantalite U-Pb ages for rare-metal pegmatites in the different ore districts. The majority of zircon U-Pb ages for pegmatites overlap with this time span as well. Several younger ages (196.2–191.1 Ma) are also reported possibly due to the metamict nature of the dated zircon (Lv et al., 2012; Wang, 2017).

Consequently, the highly fractionated nature of the Jideke granite, combined with the spatial and temporal consistency of granite and pegmatite, suggest that the Jideke granite is the parental granite for the Kelumute-Jideke pegmatite field.

### Petrogenesis of the granite-pegmatite system in the KJPF

Rare-metal pegmatites in the KJPF show close proximity to the Jideke granite as mentioned above. Highly-evolved

pegmatitic melts with exceptional enrichments of rare-metal elements and fluxes, are most probably derived from very extensive differentiation of the parental granite. Available zircon and columbite-tantalite U-Pb ages reveal that major rare-metal pegmatites in the KJPF are emplaced during the early Mesozoic. Despite the variable zircon Hf isotopic data of the Jideke granite and related rare-metal pegmatites (Lv et al., 2012; Wang, 2017), negative  $\epsilon_{\text{Hf}}(t)$  values and Mesoproterozoic Hf model ages (TDMC) of the majority of analysed zircons indicate an ancient crust-dominated source for the granite-pegmatite system. Consequently, these early Mesozoic granites and related rare-metal pegmatites are likely generated in an intraplate anorogenic or post-collisional setting (Wang et al., 2014), and most probably resulted from decompression melting of thickened crust, as is typical of LCT granite-pegmatite systems worldwide (Černý, 1991; Černý and Ercit, 2005).

**Acknowledgements:** This study is financially supported by the National Key R&D Program of China (no. 2017YFC0602405).

### References

- Černý P (1991) Rare-element granitic pegmatites. II: Regional to global environments and petrogenesis. *Geosci Can* 18:68–81.
- Černý P, Ercit TS (2005) The classification of granitic pegmatites revisited. *Can Mineral* 43:2005–2026.
- Lv Z-H, Zhang H, Tang Y, Guan S-J (2012) Petrogenesis and magmatic-hydrothermal evolution time limitation of Kelumute No. 112 pegmatite in Altai, Northwestern China: Evidence from zircon U-Pb and Hf isotopes. *Lithos* 154:374–391.
- Ren BQ, Zhang H, Tang Y, Lv ZH (2011) LA-ICP-MS U-Pb zircon geochronology of the Altai pegmatites and its geological significance. *Acta Mineral Sin* 31(3):587–596 (in Chinese with English Abstract).
- Wang CL (2017) Li-Be-Nb-Ta mineralization in the Kelumute-Jideke ore deposit cluster, Chinese Altai. PhD Thesis, Xinjiang Institute of Ecology and Geography, Chinese Academy of Sciences, 238pp (in Chinese with English Abstract).
- Wang T, Jahn B-M, Kovach VP, Tong Y, Wilde SA, Hong D-W, Li S, Salnikova EB (2014) Mesozoic intraplate granitic magmatism in the Altai accretionary orogen, NW China: Implications for the orogenic architecture and crustal growth. *Am J Sci* 314:1–42.
- Zhang X, Zhang H, Ma Z-L, Tang Y, Lv Z-H, Zhao J-Y, Liu Y-L (2016) A new model for the granite-pegmatite genetic relationships in the Kaluan-Azubai-Qiongkuer pegmatite-related ore fields, the Chinese Altai. *J Asian Earth Sci* 124:139–155.
- Zhou QF, Qin KZ, Tang DM, Wang CL, Sakyi PA (2016) LA-ICP-MS U-Pb zircon, columbite-tantalite and  $40\text{Ar}-39\text{Ar}$  muscovite age constraints for the rare-element pegmatite dykes in the Altai orogenic belt, NW China. *Geol Mag* 155(03):707–728.
- Zou TR, Li QC (2006) Rare-elements and REE Deposits in Xinjiang, China. Geological Publishing House, Beijing, 284p (in Chinese).

# Geological features of the Jiaoxi tungsten deposit in the western Bangong-Nujiang metallogenic belt, Tibet, China

Yong Wang<sup>1</sup>, Juxing Tang<sup>2</sup>, Liqiang Wang<sup>2</sup>, Jan Marten Huizenga<sup>3</sup>

<sup>1</sup>School of Earth Sciences and Resources, China University of Geosciences, Beijing, China

<sup>2</sup>Institute of Mineral Resources, Chinese Academy of Geological Sciences, China, Beijing

<sup>3</sup>Economic Geology Research Centre, College of Science and Engineering, James Cook University, Townsville, Qld, Australia

## Introduction

The Tibetan Plateau includes two important metallogenic belts, the Gangdese metallogenic zone in southern Tibet and the newly delimited Bangong-Nujiang metallogenic belt in central Tibet (Geng et al., 2016). The Bangong-Nujiang metallogenic belt is considered to be a Fe-Cu-Au metallogenic belt since the discovery of the Tiegelongnan giant porphyry-epithermal Cu-Au deposit (Tang et al., 2014), the Duobuza large porphyry deposit (Li et al., 2012) and the Ga'erqiong-Galale large skarn Cu-Au deposit (Zhang et al., 2015). The Jiaoxi quartz vein-type tungsten deposit ( $WO_3$ : 39,000 t, Wang et al., 2018) is the first quartz-vein type tungsten deposit found in this belt.

## Geological features

The Jiaoxi deposit is located in the Shiquanhe-Nam Tso Mélange Zone. The strata exposed in the district includes the Early Cretaceous Shiquanhe ophiolite mélange of sandstone, shale and sheet of ophiolite. Sandstones and shales in the deposit area have been locally metamorphosed, due to the emplacement of the granites in this area. Intrusions in the deposit includes biotite monzogranite porphyry, granite porphyry and muscovite monzogranite. Muscovite monzogranite has only been found in drill core at a depth of 402 to 415 m.

Tungsten-bearing quartz vein is the main mineralization type in this deposit. The extensional veins are subvertical and strike approximately north-south. Wolframite and scheelite coexist with chalcopyrite, pyrite, molybdenite, galena, sphalerite, quartz, beryl, lepidomelane, fluorite, ankerite and topaz (Fig. 1a). So far, around 70 tungsten orebodies have been discovered at surface. The orebodies are mainly hosted in the sandstone and shales (Fig. 1b, c, d). However, drill core inspection revealed that the biotite monzogranite porphyry and the muscovite monzogranite also host some orebodies (Fig. 1g, h).

Three stages of mineralization have been identified. The first, prominent, oxide stage is characterized by the development of the following vein types:

- rare quartz + molybdenite ± feldspar (in the biotite monzogranite only) veins (Fig. 2f),
- quartz + wolframite + lepidomelane veins (Fig. 2h);
- quartz + wolframite veins (Fig. 2c);
- quartz + wolframite + fluorite veins (Fig. 1b);
- quartz + pyrite + wolframite + lepidomelane veins (Fig. 1d), and
- quartz + lepidomelane + beryl + topaz veins.

The second sulfide stage is characterized by different types of sulfide-bearing veins, including ;

- quartz + pyrite + chalcopyrite + galena + sphalerite veins (Fig. 2i), and

- quartz + pyrrhotite + chalcopyrite veins and the quartz + lepidomelane + pyrite + chalcopyrite veins.

The final fluorite-carbonate stage is characterized by pure fluorite veins, pure ankerite veins, fluorite + lepidomelane veins, quartz + pyrite veins, lepidomelane + scheelite veins and minor quartz + calcite veins.

## W-Nb-Ta mineralization potential

The discovery of Ta-Nb oxides-containing pegmatite in the northeast of Jiaoxi deposit (Fig. 3a, b), indicates the potential for W-Nb-Ta mineralization in this district. Field data indicate that this pegmatite is exposed at a large scale in this district.

## References

- Geng, Q.R., Zhang, Z., Peng, Z.M., Guan, J.L., Zhu, X.P., Mao, X.C., 2016, Jurassic-Cretaceous granitoids and related tectono-metallogenesis in the Zapug-Duobuza arc, western Tibet. *Ore Geology Reviews* 77, 163-175.
- Li, G.M., Li, J.X., Qin, K.Z., Duo, J., Zhang, T.P., Xiao, B., Zhao, J.X., 2012, Geology and hydrothermal alteration of the Duobuza gold-rich porphyry copper district in the Bangongco metallogenetic belt, Northwestern Tibet: *Resource Geology* 62, 99-118.
- Tang, J.X., Wang, Q., Yang, C., Ding, S., Lang, L.H., Liu, H.F., Huang, Y., Zheng, W.B., Wang, L.Q., Gao, Y.M., Feng, J., Duan, J.L., Song, Y., Wang, Y.Y., Lin, B., Fang, X., Zhang, Z., Yang, H.H., 2014, Two porphyry-epithermal deposit metallogenetic subseries in Tibetan Plateau: practice of "absence prospecting" deposit metallogenetic series. *Mineral Deposits* 33, 1151-1170 (in Chinese with English abstract).
- Wang, L.Q., Wang, Y., Fan, Y., Danzhen, W.X., 2018, A Miocene tungsten mineralization and its implications in the western Bangong-Nujiang metallogenic belt: Constraints from U-Pb, Ar-Ar, and Re-Os geochronology of the Jiaoxi tungsten deposit, Tibet, China. *Ore Geology Reviews* 97, 74-87.
- Zhang, Z., Yao, X.F., Tang, J.X., Li, Z.J., Wang, L.Q., Yang, Y., Duan, J.L., Song, J.L., Lin, X., 2015, Lithochemical, Re-Os and U-Pb Geochronological, Hf-Lu and S-Pb Isotope Data of the Ga'erqiong-Galale Cu-Au Ore-Concentrated Area: Evidence for the Late Cretaceous Magmatism and Metallogenetic Event in the Bangong-Nujiang Suture Zone, Northwestern Tibet. *Resource Geology* 65, 76-102.

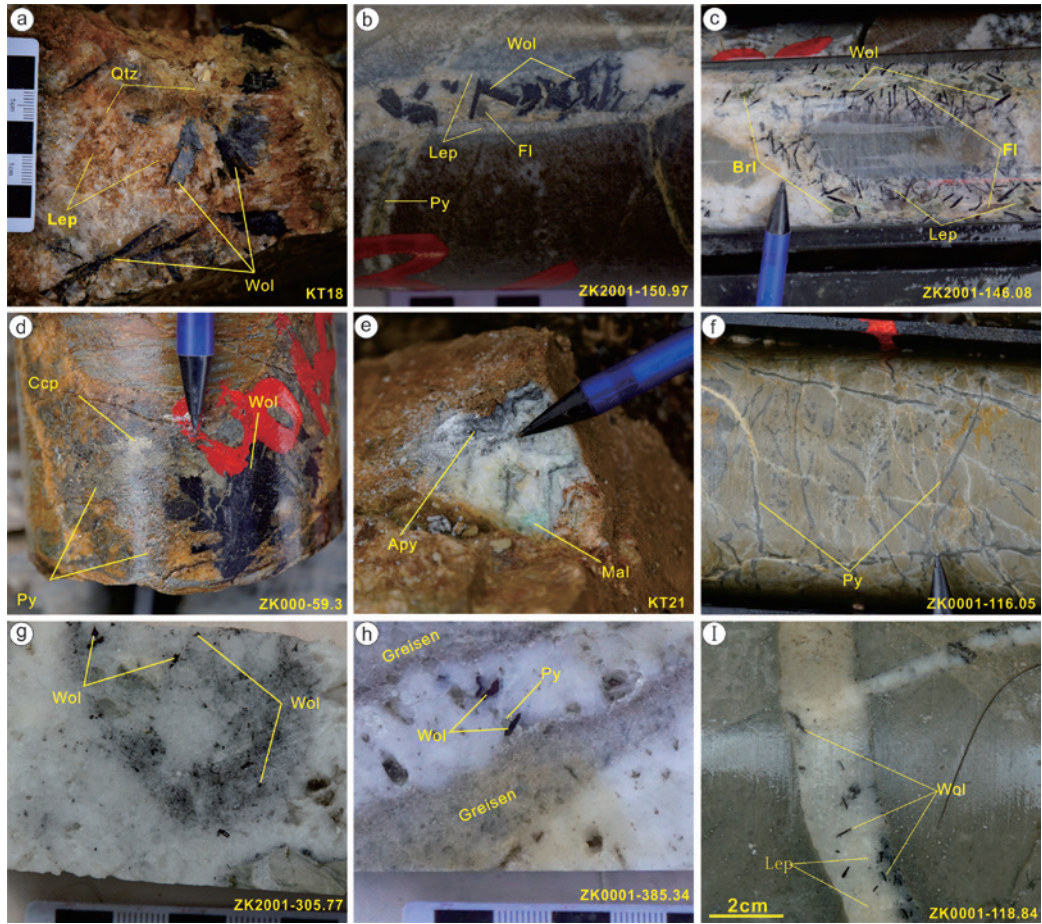


Figure 1. Photographs of mineralization features in Jiaoxi deposit. Apy = arsenopyrite; Brl = beryl; Ccp = Chalcopyrite; Fl = fluorite; Lep = lepidomelane; Py = pyrite; Mal = malachite; Qtz = quartz; Wol = wolframite.

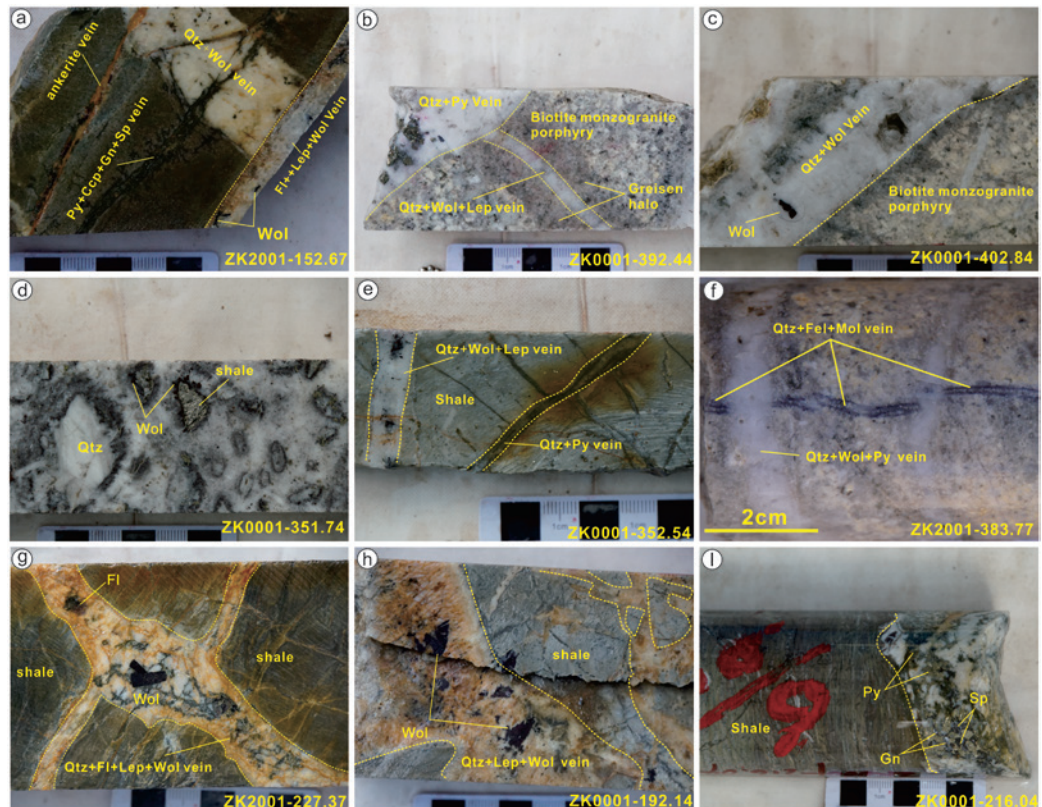


Figure 2. Illustration of different types of veins in Jiaoxi deposit. Ccp = Chalcopyrite; Fl = fluorite; Fe = feldspar; Gn = Galena; Lep = lepidomelane; Py = pyrite; Qtz = quartz; Wol = wolframite.

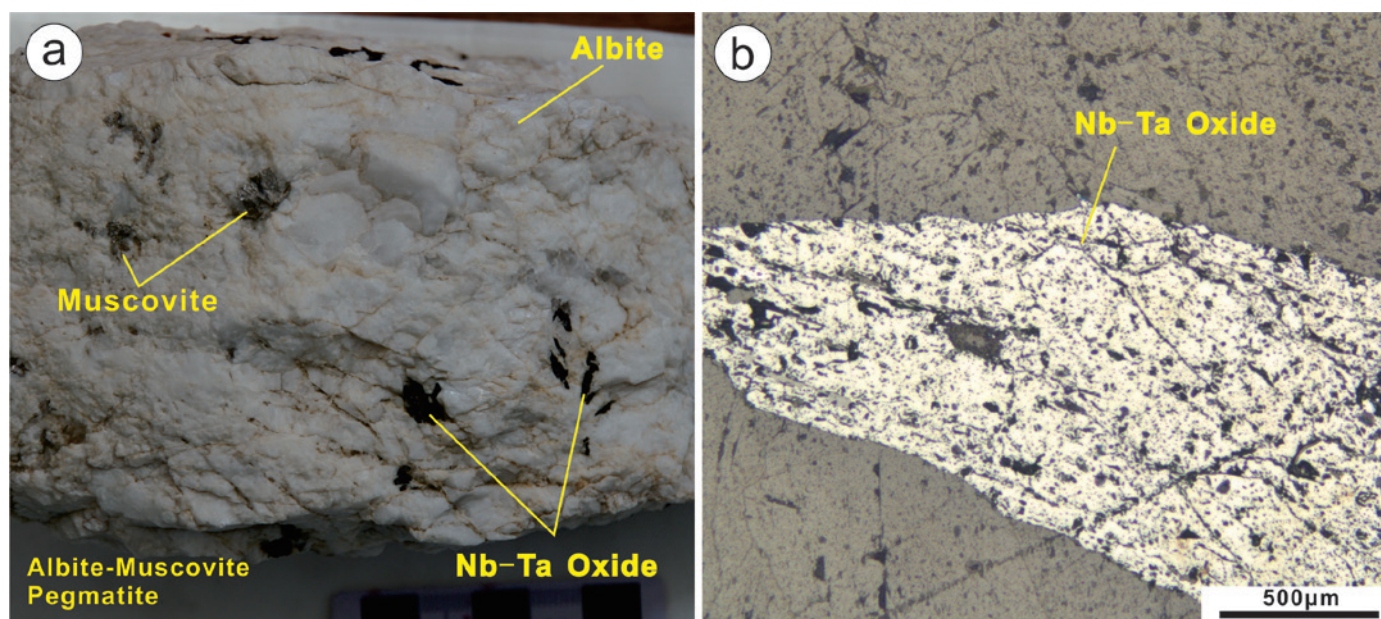


Figure 3. Hand specimen photograph (a) and microphotograph (b) of Nb-Ta oxide-containing pegmatite in the Jiaoxi district.

# Redox controls on granite related hydrothermal ore deposits

Jo Ward<sup>1</sup>, John Mavrogenes<sup>1</sup>, Nick Tailby<sup>2</sup>

<sup>1</sup>Research School of Earth Science, ANU, Bldg 142, Mills Rd, Acton, 2601

<sup>2</sup>American Museum of Natural History, New York, USA 10024-5192

It has long been recognized that the reduced “S-type” granites are associated with Sn-W deposits while the oxidized “I-type” granites are linked to Cu ( $\pm$  Au or Mo) porphyry deposits. Given that no direct link exists between the igneous and hydrothermal realms, it has been difficult to definitively explain these associations. In an effort to track chalcophile element behaviours in granitic systems pre-fluid exsolution, pyrite was extracted from seven I- and six S- type granites from the Lachlan Fold Belt (LFB) for in situ analyses. LA-ICPMS analysis of trace elements and SHRIMP-SI sulfur isotopic analyses of these pyrite grains are the purpose of this report.

Pyrite is the ideal sulfide to track chalcophile element budgets because it is stable only <750 °C (Kullerud and Yoder, 1959), assuring its formation late in the process. The pyrite crystals studied herein all occur within fine-grained groundmass and were not observed as inclusions in phenocrysts, confirming their place in the late stages of crystallization. This monomineralic phase tracks chalcophile elements directly, thus avoiding the pitfall of dilution inherent in bulk analyses (e.g. XRF).

## Redox

LFB granites have been characterized by bulk Fe<sup>2+</sup>/Fe<sup>tot</sup> (Chappell and White, 2001) and Ce/Ce\* (Trail et al., 2015) of zircon. Both techniques confirm that I-type granites are more oxidized than S-type granites.

## S isotopes

LFB pyrites are clearly delineated by sulfur isotopes, with pyrite from reduced granites yielding  $\delta^{34}\text{S} > 3\text{‰}$  and oxidized (I-type) pyrites yielding  $\delta^{34}\text{S} < 3\text{‰}$ . This is consistent with S-type granites involving heavy sulfur-rich sediments (Sasaki and Ishihara, 1979) and their reduced nature. This trend of more reduced sulfides containing more negative sulfur has been shown in many hydrothermal deposits. The current study confirms this relationship in an igneous setting, and reaffirms the redox difference between these two granite types.

## Trace elements

While sulfur isotopes discriminate granite types, when combined with trace elements the distinction becomes even clearer. Trace elements show redox dependent differences between pyrites from the two populations. In general, pyrites from I-type granites contain lower concentrations of trace elements than their reduced counterparts. This is likely due to reduction being a more general saturation trigger than oxidation, an observation that holds for hydrothermal ores as well. I-type pyrites

have higher median concentrations of Ni (1074 vs 236 ppm) and Co (2936 vs 135 ppm) relative to S-type pyrites. S-type pyrites, on the other hand, yield higher median concentrations of Zn (9 vs 2 ppm) Mn (19 vs 3 ppm), Sn (3 vs 0.01 ppm), Sb (3 vs 0.09 ppm), Pb (168 vs 7 ppm), Au (0.2 vs 0.02 ppm) and Bi (11 vs 6 ppm) relative to I type pyrites.

Oxidised pyrites have higher concentrations of Co and Ni and lower concentrations of Sb, As and Au than reduced pyrites; however, given the overall higher concentrations in reduced pyrites, relative differences are best observed via ratios. Pb/W and As/Ni categorize most samples into granite types. The highest Au concentrations are found in reduced granites (average 0.9 ppm) and the highest individual Au concentration was found in the most reduced granite sampled, Jilamatong (1.2 ppm).

Higher Pb/W is found in oxidized pyrites due to higher average Pb concentrations (19 vs 604 ppm respectively). Arsenic is lower in I -type pyrites than in S-types, likely due to redox controlled partitioning. This is similar to the Wallaby gold deposit (Western Australia) where As and Sb concentrate into pyrite under reducing conditions (Ward et al., 2017) Conversely, Mn concentrations in pyrite are similar in both granite types.

## Cu-Mo versus Sn-W bearing granites

Blevin et al. (1996) used redox to explain this link, which the sulfur isotopes reported herein supports. Sn<sup>4+</sup> in oxidized magmas substitutes into Ti<sup>4+</sup> sites in opaque minerals, such that high Sn concentrations are only seen in reduced systems. Both I- and S-type pyrites contain similar W concentrations, yet Sn/W distinguishes granite types, with an average Sn/W of 3.7 in I-type pyrites and an average Sn/W of 344 in S-type pyrites. This clear redox sensor, seen in individual pyrite grains, is obscured in whole rock analyses.

Trends observed in pyrites from the reduced Hatapang granite suite of Sumatra are similar to those identified here. These granites, associated with Sn-W deposits, contain pyrites rich in Pb, As, Zn and Bi (Clarke and Beddoe-Stephens, 1987). This contrasts with the Hongshan Cu-Mo deposit of China (Wang et al., 2014), which is associated with oxidised granites, and contains pyrites rich in Mo, Ag and Co. Thus these key chalcophile elements clearly distinguish oxidized from reduced pathways.

Chappell and White (2001) established the link between Cu-Mo porphyries and I-type granites, and we have found this same relationship in pyrite that can be used

to delineate granite types. This potentially assesses the fertility of any given granite to have associated economic concentrations of Cu and Mo. S-Type pyrites have on average a higher Cu/Mo (188) compared to I-Type (33). This suggests, regardless of concentration that I-Type Cu and Mo are closer to unity relative to reduced systems. This difference relies on the concentration of Mo in pyrite during fractionation, as Mo prefers pyrite under oxidizing conditions (Candela and Holland, 1984). This is consistent with oxidized systems forming Cu-Mo deposits (Frikken et al., 2005; Rowins, 2000).

Orogenic Au deposits are often linked to oxidized granite suites. The Hill End Trough gold deposits in New South Wales are considered associated with oxidized granites (Downes et al., 2008). Given that trace gold is found in higher concentrations in S-Type (0.9 ppm) compared to I-type granite (0.03) pyrites, it seems likely that bisulfide complexed gold partitions into pyrite while chloride complexed (oxidized) gold partitions into hydrothermal fluids. This could explain why the Braidwood (I-Type) pyrites contain low average Au (0.3ppm) while the hydrothermal fluids that formed the Major's Creek gold deposit efficiently scavenged gold from the melt (Wake and Taylor, 1988).

## Conclusion

We have shown that sulfur isotopes of paragenetically late pyrites independently sense redox, and discriminate S- from I-type granites. We have also shown that redox sensitive trace elements in pyrite reflect this. When combined, sulfur isotopes and trace elements of pyrite show remarkable trends, as follows;

- S-type pyrites, precipitated under reducing conditions, contain high concentrations of As, Sn, Bi, Zn and Au.
- I-type pyrites, precipitated under oxidizing conditions, are concentrated in Co and Ni and have low gold concentrations despite being associated with hydrothermal gold deposits.

We assert that absolute trace element concentrations are higher in pyrite formed under reducing conditions than those that formed under oxidizing conditions. The As-Au affinity observed in economic gold deposits is also seen in S-type non-economic granites. This suggests a universal control on partitioning of elements of economic interest

in sulfides. We also suggest that despite the gamut of trace elements available within melts or fluids, semi-transition metals most obviously substitute for Fe or S in the pyrite structure. Since redox controls oxidation states and therefore size, the idea of an over-arching redox control on ore deposition is plausible for both magmatic and hydrothermal deposits.

## References

- Blevin, P.L., Chappell, B.W., Allen, C.M., 1996. Intrusive metallogenic provinces in eastern Australia based on granite source and composition. *Geological Society of America Special Papers* 315, 281-290.
- Candela, P.A., Holland, H.D., 1984. The partitioning of copper and molybdenum between silicate melts and aqueous fluids. *Geochimica et Cosmochimica Acta* 48, 373-380.
- Chappell, B., White, A.J.R., 2001. Two contrasting granite types: 25 years later. *Australian Journal of Earth Sciences* 48, 489-499.
- Clarke, M., Beddoe-Stephens, B., 1987. Geochemistry, mineralogy and plate tectonic setting of a Late Cretaceous Sn-W granite from Sumatra, Indonesia. *Mineralogical Magazine* 51, 371-387.
- Downes, P., Seccombe, P., Carr, G., 2008. Sulfur-and lead-isotope signatures of orogenic gold mineralisation associated with the Hill End Trough, Lachlan Orogen, New South Wales, Australia. *Mineralogy and Petrology* 94, 151.
- Frikken, P.H., Cooke, D.R., Walshe, J.L., Archibald, D., Skarmeta, J., Serrano, L., Vargas, R., 2005. Mineralogical and isotopic zonation in the Sur-Sur tourmaline breccia, Rio Blanco-Los Bronces Cu-Mo deposit, Chile: Implications for ore genesis. *Economic Geology* 100, 935-961.
- Kullerud, G., Yoder, H.S., 1959. Pyrite stability relations in the Fe-S system. *Economic Geology* 54, 533-572.
- Rowins, S.M., 2000. Reduced porphyry copper-gold deposits: A new variation on an old theme. *Geology* 28, 491-494.
- Sasaki, A., and Ishihara, S., 1979. Sulfur isotopic composition of the magnetite-series and ilmenite-series granitoids in Japan. *Contributions to Mineralogy and Petrology* 68, 107-115.
- Trail, D., Tailby, N.D., Sochko, M., Ackerson, M.R., 2015. Possible biosphere-lithosphere interactions preserved in igneous zircon and implications for Hadean Earth. *Astrobiology* 15, 575-586.
- Wake, B., Taylor, G., 1988. Major's Creek, NSW, Australia - A Devonian epithermal gold deposit. *Mineralium Deposita* 23, 239-246.
- Ward, J., Mavrogenes, J.A., Murray, A., Holden, P., 2017. Trace element and sulfur isotopic evidence for redox changes during formation of the Wallaby Gold Deposit, Western Australia. *Ore Geology Reviews* 82, 31-48.

# Structural controls and geochronology constraints on the metallogenesis of the Lame Zn-Cu-Sn polymetallic skarn deposit, Guangxi Province, China

Changhao Xiao

*Institute of Geomechanics, Chinese Academy of Geological Sciences, Beijing 100081, China*

The Youjiang Basin, the superimposed part of Tethyan Domain and Western Pacific Domain (Fig. 1a; Cai and Zhang, 2009; Nevolko et al., 2017), is a Devonian-Triassic rift basin on the southwestern margin of South China, at the junction of the Cathaysia, the Yangtze and Indochina blocks (Fig. 1b; Wang et al., 2018; Xiao et al., 2018a, b). It hosts numerous large tin-polymetallic deposits and large gold deposits, such as Dachang and Gejiu Sn-polymetallic orefields and Nibao, Lannigou, and Shuiyindong gold deposits (Fig. 1c). The world-class Dachang tin-dominant polymetallic orefield at the eastern margin of the basin is located in the central of the NW-trending Danchi fold-and-thrust belt (Cai et al., 2007) (Fig. 1b). The economic deposits in the Dachang orefield include the Tongkeng-Changpo, Bali and Gaofeng polymetallic Sn deposits (western belt), the Lame Zn-Cu-Sn polymetallic skarn deposit and the Chashan Sb deposit (central ore belt), and the Dafulou, Huile and Kangma polymetallic vein Sn deposits (eastern ore belt) (Fig. 2). The strata consist of the Mid-Devonian Nabiao and Luofu Groups, Upper-Devonian Liujiang, Wuzishan and Tongchejiang Groups, and Carboniferous Shimen and Huanglong Groups (Cai et al., 2007). The main structures are the parallel NW-trending Longxianggai anticline and Longxianggai fault and the Dachang anticline and Dachang fault (Cai et al., 2007) (Fig. 2). The most important outcrop of the Yanshanian intrusions is the Longxianggai pluton.

The Lame Zn-Cu-Sn deposit is situated in the central ore belt close to the outcrops of the Longxianggai pluton. Four types of Zn-Cu-Sn mineralizations are recognized and the structural controls on the four mineralization were analysed:

(i) The stratiform orebodies ( $242^{\circ}/48^{\circ}$ ) formed in the lithologic interface and/or fracture, such as hosted in Upper Devonian limestone and siliceous rocks. The striations on the roof of the orebody plunge to  $308^{\circ}$  and  $332^{\circ}$ , respectively; calculated orientations of the principle stresses ( $\sigma_1$ ) plunge to the directions of  $69^{\circ}$  and  $180^{\circ}$  at the angles of  $48^{\circ}$  and  $57^{\circ}$ , respectively, suggesting two phases of fault sliding. Thickening at the hinges of the skarn implies a shortening event. The kinematics determined from the geometry of the secondary intralayer folds indicates a late-phase extensional event. The principle stress ( $\sigma_1$ ) determined from the NW- and SE-trending echelon conjugate veins (tension gashes) plunges to the direction of  $69^{\circ}$  at an angle of  $48^{\circ}$ . These observations indicate that stratiform orebodies were deposited in the

veins, which were first generated as tension gashes during intralayer sliding and connected via following extension;

(ii) The steeply-dipping large vein orebodies form in the exoskarn, such as No. 11 to No. 14 orebodies. For instance, the No. 14 orebodies are composed of two sets of conjugate veins trending  $100^{\circ}$  and  $260^{\circ}$ , respectively, with the same steep dip angles of  $80^{\circ}$ . The principle stress is calculated N-plunging at an angle of  $45^{\circ}$ .

(iii) The veinlet orebodies are commonly observed in the Lame deposit with the overall trend of N-S, forming crosscutting networks with stockwork and steep dipping large veins locally. Wall-perpendicular growth of the sphalerite indicates that the fluid activity is syntectonic with the opening of the veins (Fig. 3). Reconstruction of the stress field shows that the principle stress is normal to the regional bedding of strata, implying that the veins or tension gashes are produced via a magmatic diapirism and filled through upwelling of the magmatic fluids.

(iv) The stockwork orebodies formed in the shallow part of the Upper Devonian Longxianggai pluton, composed of conjugate vein sets with the orientations of  $300^{\circ}/74^{\circ}$  and  $195^{\circ}/65^{\circ}$ , respectively. Results of stress analysis indicates that the principle stress plunges to the direction of  $69^{\circ}$  at an angle of  $48^{\circ}$ , suggesting that the early NW- and SW-trending conjugated veins developed during the formation of the anticline were used as the ore-deposit spaces. Structural controls on the four mineralization types suggest that all four types were formed in the same magmatic-hydrothermal system.

The evolution of the Longxianggai pluton can be divided into porphyritic biotite granite, biotite granite, and aplite (Fig. 4a). The porphyritic biotite granite was trapped by the biotite granite and both were cut by the aplite. The ores are generally related with the skarn which contact with the biotite granite. Ore-bearing granite are muscovitization. La-ICP-MS zircon U-Pb dating constrains the porphyritic biotite granite, biotite granite, and aplite at  $92.47 \pm 0.54$  Ma (MSWD=1.16, n=20),  $91.21 \pm 0.26$  Ma (MSWD=0.78, n=20), and  $92.44 \pm 0.94$  Ma (MSWD=2.4, n=17), respectively (Figs. 4b, c, d). They have the same ages as each other within errors, suggesting they are magmatism coevally emplaced during the Later Cretaceous. The  $^{40}\text{Ar}/^{39}\text{Ar}$  age of the muscovite from the altered biotite granite yields a weighted plateau age of  $92.97 \pm 0.13$  Ma (Fig. 5a). This age is comparable to the age of Longxianggai pluton. Two types of molybdenite

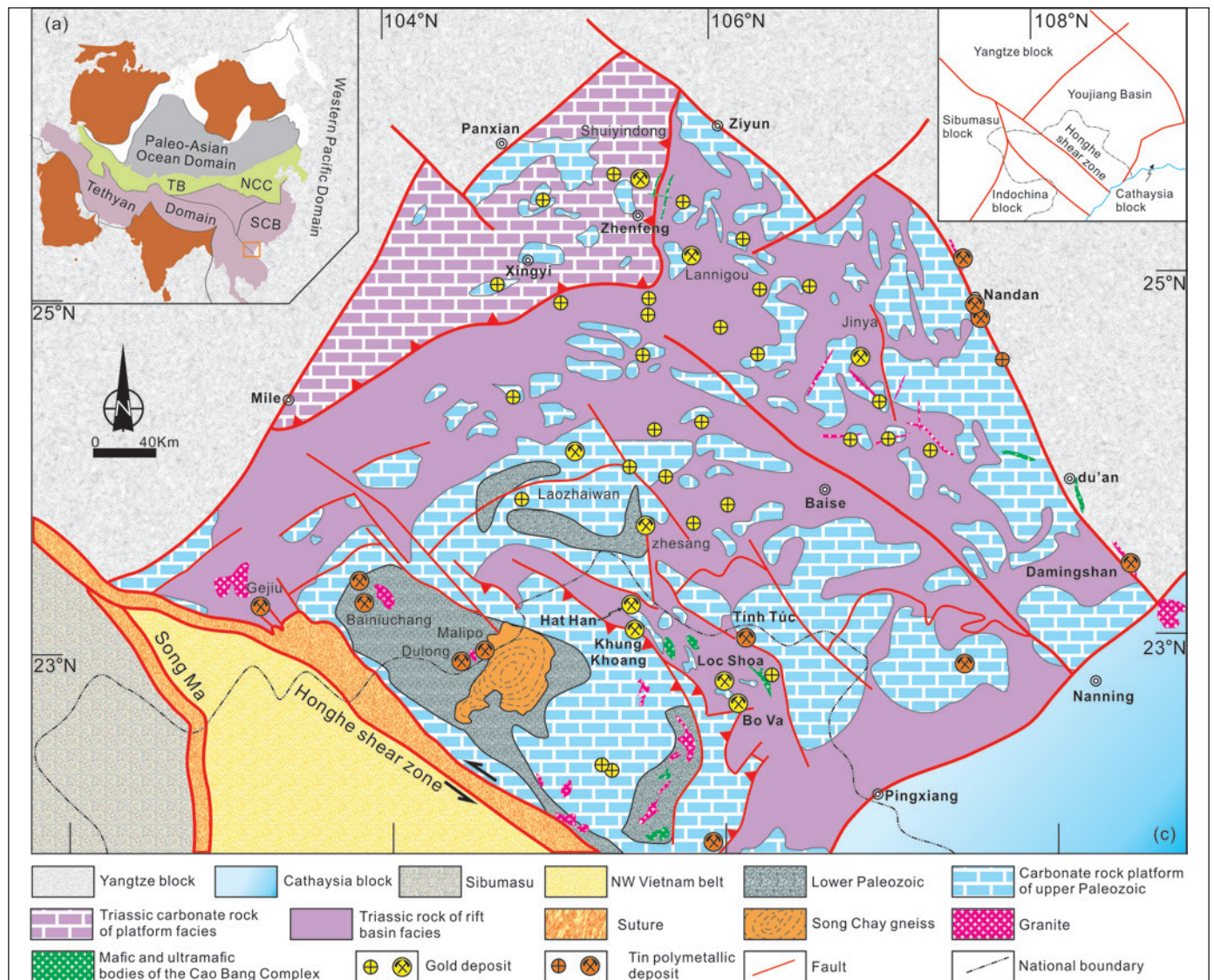


Figure 1. Simplified geology and distribution map of tin-gold-polymetallic deposits in the Youjiang Basin, Southwestern China.

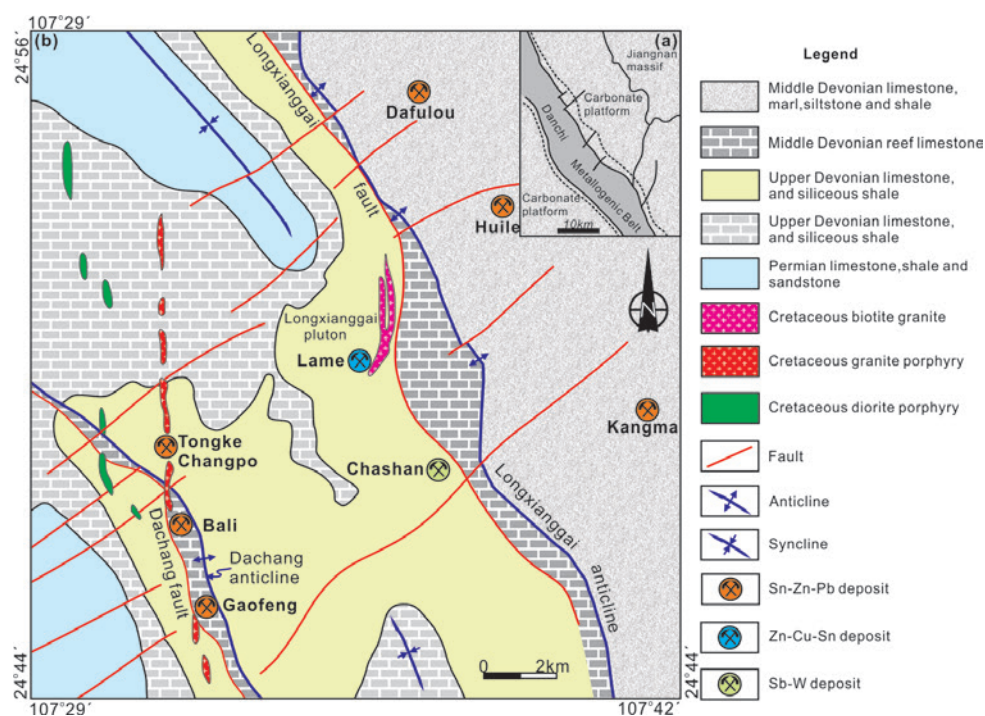


Figure 2. Geological map of the Dachang district in the east of Youjiang Basin.

were first found in the Lame deposit. The skarn-type molybdenite was found in the stratiform orebodies. One skarn-type molybdenites yield a Re-Os age of  $90.97 \pm 1.74$  Ma. The sulfides occur as disseminated aggregates in aluminosilicate minerals. The minerals are mainly molybdenite, chalcopyrite, wollastonite, and diopside. The quartz vein type molybdenite formed in the steep dip angles vein-type orebody. The minerals are mainly molybdenite, wolframite, chalcopyrite, sphalerite, and quartz. Three quartz vein type molybdenite have

a narrow range of  $91.36 \pm 1.47$  Ma to  $92.23 \pm 1.54$  Ma. Four molybdenite samples give a Re-Os isochron age of  $91.55 \pm 0.67$  Ma (MSWD=0.92) (Fig. 5b). It suggests that the stratiform and vein orebodies formed at the same time. The mineralization age is consistent with previous data (Guo et al., 2018; Wang et al., 2015). We interpret the Lame deposit was formed in a granite-related magmatic-hydrothermal system controlled by the Longxianggai pluton.

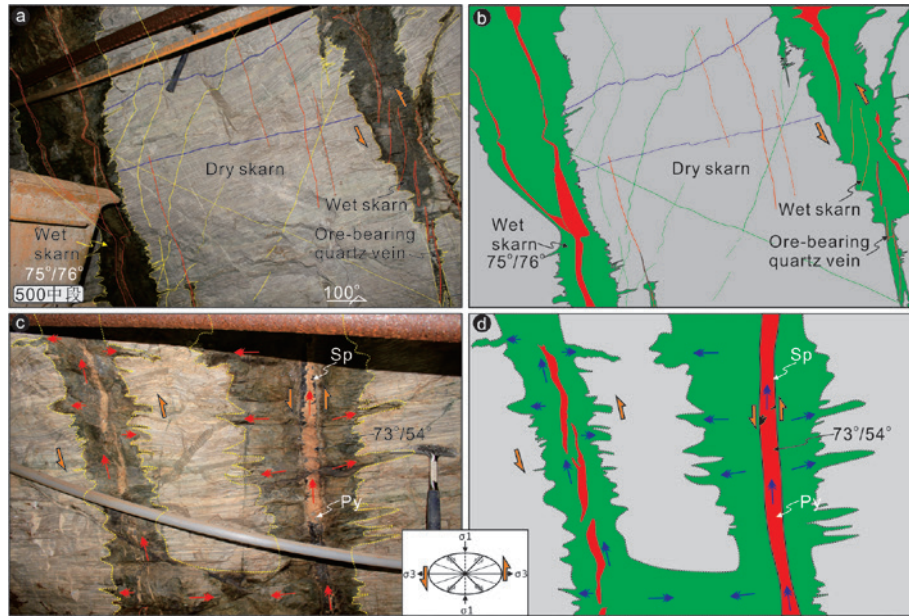


Figure 3. characteristics of the structure-alteration-mineralization in the Lame Zn-Cu-Sn polymetallic deposit

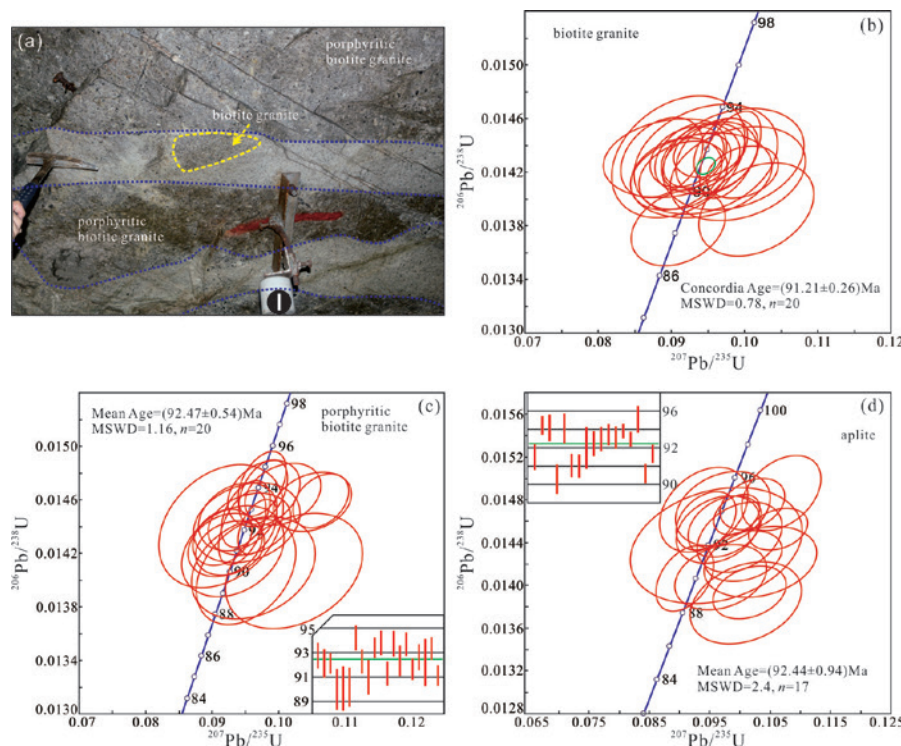


Figure 4. Magmatic evolution and U-Pb Concordia and weighted mean ages for the Longxianggai pluton from Lame Zn-Cu-Sn polymetallic deposit.

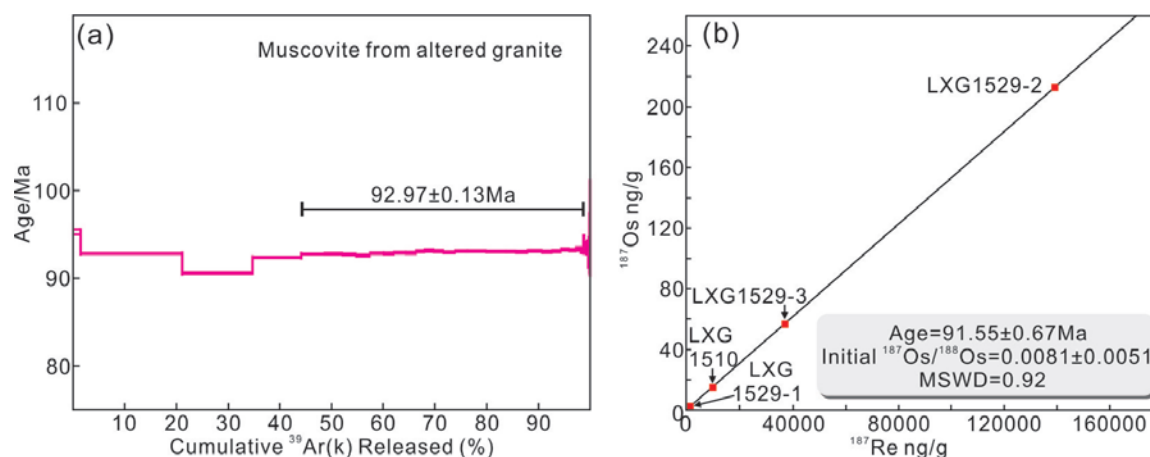


Figure 5.  $^{40}\text{Ar}/^{39}\text{Ar}$  age of muscovite and Re-Os age of molybdenite from the Lame Zn-Cu-Sn polymetallic deposit.

## References

- Cai, M.H., Mao, J.W., Liang, T., Pirajno, F., Huang, H.L., 2007. The origin of the Tongkeng-Changpo tin deposit, Dachang metal district, Guangxi, China: clues from fluid inclusions and He isotope systematics. *Mineralium Deposita* 42, 613–626.
- Cai, J.X., Zhang, K.J. 2009. A new model for the Indochina and South China collision during the Late Permian to the Middle Triassic. *Tectonophysics* 467, 35–43.
- Guo, J., Zhang, R.Q., Sun, W.D., Ling, M.X., Hu, Y.B., Wu, K., Luo, M., Zhang, L.C. 2018. Genesis of tin-dominant polymetallic deposits in the Dachang district, South China: Insights from cassiterite U–Pb ages and trace element compositions. *Ore Geology reviews*, 95, DOI: 10.1016/j.oregeorev.2018.03.023.
- Nevolko, P.A., Hoa, T.T., Redin, Y.O., Anh, T.T., Phuong, N.T., Ly, V.H., Dultsev, V.F., Dung, P.T., Huong, N.T. 2017. Geology, mineralogy, geochemistry and  $\delta^{34}\text{S}$  of sedimentary rock-hosted Au deposits in Song Hien structure, NE Vietnam. *Ore Geology Reviews* 84, 273–288.
- Tanelli, G., and Lattanzi, P. 1985. The cassiterite-polymetallic sulfide deposits of Dachang (Guangxi, People's Republic of China). *Mineralium Deposita* 20, 102–106.
- Wang, Q.F., Groves, D. 2018. Carlin-style gold deposits, Youjiang Basin, China: tectono-thermal and structural analogues of the Carlin-type gold deposits, Nevada, USA. *Mineralium Deposita* 53, 909–918.
- Wang, X.Y., Huang, H.W., Chen, N.S., Huang, X.Q., Wu, X.K., Hao, S., Li, H.M., 2015. In-situ LA-MC-ICPMS U-Pb Geochronology of cassiterite from Changpo-Tongkeng tin-polymetallic deposits, Dachang orefield, Guangxi. *Geological Review* 61 (4), 892–900 (in Chinese with English abstract).
- Xiao, C.H., Shen, Y.K., Liu, H., Wei, C.S., Le, X.W., and Fu, B. 2018a. Oxygen isotopic compositions and geological significance of zircons from the Yanshanian felsic intrusions in the Xidamingshan cluster, southeastern margin of the Youjiang fold belt, South China: In situ SHRIMP analysis. *Acta Petrologica Sinica*, 34(5) 1441–1452 (in Chinese with English abstract).
- Xiao, C.H., Shen, Y.K., Wei, C.S., Su, X.K., Le, X.W., Zhang, L. 2018b. LA-ICP-MS zircon U-Pb dating, Hf isotopic composition and  $\text{Ce}^{4+}/\text{Ce}^{3+}$  characteristics of the Yanshanian acid magma in the Xidamingshan cluster, southeastern margin of the Youjiang fold belt, Guangxi. *Geoscience*, 32(2) 289–304 (in Chinese with English abstract).





# EGRU

Economic Geology Research Centre  
Geoscience  
College of Science and Engineering  
James Cook University  
Townsville, QLD 4811, Australia  
T: +61 7 4781 4726 E: [egruc@jcu.edu.au](mailto:egruc@jcu.edu.au)  
W: [jcu.edu.au/egruc](http://jcu.edu.au/egruc)

For more than 35 years EGRU has been connecting researchers, students, industry, and government organisations, and building productive working relationships by:

- › promoting collaborative research;
- › providing applied research services;
- › delivering professional development training;
- › hosting industry-relevant conferences.